Synthèse des travaux
présentée à l'Université Paris-Sud

pour obtenir le

Diplôme d'Habilitation à Diriger des Recherches

par

Esther Ferrer Ribas

Commissariat à l'Énergie Atomique et aux Énergies Alternatives
IRFU/SEDI

Contribution to the search of solar axions

with Micromegas detectors

Soutenue le 4 avril 2014, devant le jury composé de:

Rapporteurs	Denis Bernard	LLR, Ecole Polytechnique
	José Busto	CPPM, Université de Marseille
	Klaus Desch	University of Bonn
Examinateurs	Axel Lindner	DESY, Hambourg
	Michel Mur	IRFU/SEDI, CEA
Président	Patrick Puzo	LAL, Université Paris-Sud

.

Résumé

Ce mémoire présente une synthèse de mes travaux de recherche effectués depuis mon recrutement au SEDI en octobre 2002. Mon travail a été consacré en grande partie au développement de détecteurs Micromegas pour la détection des événements rares, en particulier dans le cadre de l'expérience CERN Axion Solar Telescope (CAST). Le contexte de l'expérience CAST a donné lieu à l'optimisation d'une nouvelle technologie de détecteurs Micromegas, les détecteurs microbulks. Par leur grande radiopureté intrinsèque et leur excellente résolution en énergie, les détecteurs microbulks combinés à des techniques d'expériences souterraines (étude du bruit de fond et blindage), se sont révélés très adaptés à la recherche des axions solaires. L'évolution des détecteurs Micromegas au sein de l'expérience CAST et l'amélioration du bruit de fond de plus de deux ordres de grandeur seront présentées. Enfin, des développements qui ont découlé de ce travail en dehors du contexte de l'expérience CAST seront également exposés.

Abstract

This manuscript presents a synthesis of my research activities since October 2002. My work has been dedicated to the development of the Micromegas detectors for the detection of rare events in particular in the context of the CERN Axion Solar Telescope (CAST). The environment of the CAST experiment has resulted in the optimisation of a new technology of Micromegas detectors, the microbulk detectors. Thanks to their good intrinsic radiopurity and their excellent energy resolution, the microbulk detectors combined to underground experiment techniques (study of background and shielding), have proven to be very appropriate for the search of solar axions. The evolution of Micromegas detectors within the CAST experiment and the improvement of the background level by more than two orders of magnitude are presented. In addition, related developments beyond the context of the CAST experiment are also exposed.

Remerciements

C'est un grand honneur que m'ont fait Denis Bernard, José Busto, Klaus Desch, Axel Lindner, Michel Mur et Patrick Puzo d'accepter de faire partie de ce jury de thèse d'habilitation. Je veux les remercier ici pour leur lecture critique et attentive de mes travaux. Les lecteurs de cette thèse leur seront reconnaissants pour toutes les fautes en moins et les clarifications en plus.

Je voudrais remercier les chefs de service du SEDI, Philippe Rebourgeard et Michel Mur, pour m'avoir donné l'opportunité d'accomplir ce travail dans d'excellentes conditions et avec une grande liberté. Un grand merci à Eric Delagnes, mon chef de laboratoire, pour son soutient et sa confiance depuis mon arrivée.

Ce manuscrit est consacré à mon activité après mon post-doctorat. Mais il y a eu bien des personnes qui ont compté pour moi auparavant ! Un grand merci à Achille Stocchi, directeur de stage lors de ma première venue en France en tant qu'étudiante Erasmus puis directeur de thèse, pour m'avoir transmis son enthousiasme et sa façon particulière d'aborder la physique. Je voudrais également remercier Bruno Mansoulié qui, en me faisant découvrir lors de mon post-doc le monde de l'instrumentation, m'a convaincue que la construction et la mise au point d'un détecteur étaient un sujet passionnant.

Je remercie vivement ici Yannis Giomataris, pour la confiance et la liberté qu'il m'a accordées depuis mon recrutement en 2002 au SEDI. Il sait faire règner dans son équipe une atmosphère particulièrement stimulante, et travailler à ses côtés est une grande aventure !

J'ai eu la grande chance de débuter dans le monde de Micromegas accompagnée de Fabien Jeanneau et de Julien Pancin, et je veux les remercier ici pour tout ce qu'ils m'ont apportés, mais aussi pour les bons moments passés ensemble. Je dois beaucoup à Alain Delbart, Jacques Derré et Paul Colas pour m'avoir transmis leur vision pour les développements futurs de ce détecteur. Merci à Arnaud Giganon pour avoir partagé les secrets du placage de grille, et à Stéphan Aune pour savoir toujours trouver des solutions simples à des problèmes compliqués. Merci à Marc Riallot et à Jean-Philippe Mols pour les designs des différents détecteurs. Merci à Daniel Desforge pour sa grande disponibilité et pour toutes les mesures et photos avec le Mitutoyo, et à Didier Jourde pour en avoir enfin fini avec nos problèmes de bruit. Un grand merci à Mariam Kebbiri pour sa compétence et sa participation active aux différents sujets de R&D. Et enfin merci à Alan Peyaud, pour son énergie et son dynamisme, ainsi qu'à David Attié qui, ne sachant jamais dire non, se trouve régulièrement embarqué dans de nouveaux projets avec moi.

Une grande partie du travail présenté ici a été effectué au sein de l'expérience CAST. Merci à tous ses membres, et en particulier aux deux capitaines Konstantin Zioutas et Martyn Davenport, qui mènent à bon port cette jolie expérience. Merci également à Biljana Lakić pour sa disponibilité et son aide lors des présentations au SPSC. Et merci évidemment à Thomas Papaevangelou, pour sa creativité et sa précieuse intuition, et sans qui CAST ne serait pas CAST.

Maria, 3 ans

Pablo, 7 ans

Carla, 10 ans

Contents

Appendix: Publications 97

Bibliography 161

Introduction

This manuscript presents a synthesis of my research activities since October 2002. My work has been dedicated to the development of the Micromegas detectors for the detection of X-ray events in particular in the context of the CERN Axion Solar Telescope (CAST). The environment of the CAST experiment has resulted in the optimisation of a new technology of Micromegas, the microbulk detectors. Thanks to their good intrinsic radiopurity and their excellent energy resolution, the microbulk detectors combined to underground experiment techniques (study of background and shielding), have proven to be very appropriate for the search of solar axions. The evolution of Micromegas detectors within the CAST experiment and the improvement of the background level by more than two orders of magnitude will be presented. In addition, related developments beyond the context of CAST are also exposed.

The document is organised as follows: the first chapter is dedicated to a description of the context of the axion search with a brief description of the theoretical motivations and the search strategies. In the second chapter, the CAST set-up is described as well as the main physics results. The third chapter is devoted to a concise review on the state of the art of Micromegas detectors followed by the fourth chapter where the evolution and performance of the CAST Micromegas detectors is outlined. IAXO, the International AXion Observatory, the next generation helioscope experiment, with Micromegas detectors as the baseline for its X-ray detectors is described in the fifth chapter. The sixth chapter is devoted to the development of detectors for rare-event detection like in the case of the MIcro-tpc MAtrix of Chambers (MIMAC) Collaboration and to upstream R&D efforts (small gap microbulks, segmented mesh microbulk and Piggyback Micromegas) that could be of use for these types of experiments in the future.

In addition, this introduction gives me the opportunity to acknowledge my closest collaborators. It is obvious that without their contribution this work would not exist.

Before the SEDI

After my PhD defense in 2000 at the Laboratoire de l'Accélerateur Linéaire on the search of the Higgs Boson with the DELPHI experiment at LEP [83] with Achille Stocchi as supervisor, I was recruited as a post-doc in the "Service de Physique de Particules" (SPP/DAPNIA/CEA) on the validation and characterisation of the Tower Builder Board for the Level 1 trigger of the electromagnetic calorimeter of the ATLAS experiment [37] for 2000-2002. This work was done under the supervision of Bruno Mansoulié and in collaboration with Pierre Borgeaud, Xavier de la Broise, Alain Le Coguie and José Pasqual. It was my first contact with instrumentation and then I got to like detector physics. These studies are not described here.

The CAST experiment

Yannis Giomataris participated in the design of the CAST experiment and proposed the Micromegas detectors for X-ray detection. It was the first application of Micromegas detectors for a rare-event experiment. In October 2002, when I arrived at "Service d'Electronique des Détecteurs et d'Informatique" (SEDI/DAPNIA/CEA) recruited with a permanent position, a prototype existed and had already been successfully tested in the PANTER X-ray facility. I participated in the commissioning of the detector during installation in the CAST experiment in the last months of 2002. Arnaud Giganon showed me the art of coupling the Micromegas mesh to the readout plane by controlling the screwing of the mechanical frame of the micromesh. Not an easy task especially on top of the LHC dipole! The coupling of the detector with a thin transparent window and the magnet vacuum environment presented some problems and Stephan Aune (SEDI) proposed a solution with differential windows that solved the problem. The design of the detector in these first years was realised by Marc Riallot (SEDI) and the detectors were manufactured, as it has been ever since, by Rui de Oliveira, Antonio Teixeira and recently Serge Ferry from CERN. The gassiplex electronics were implemented by Philippe Abbon (SEDI) and the acquisition was developed by George Fanourakis and Theodoros Geralis from Demokritos (DMK). An important upgrade of the electronics was done at the end of 2003 when the micromesh signal was sampled with a VME digitizing board, the MATACQ (MATrix for ACQuisition) thanks to Eric Delagnes (SEDI). The main results of the first Micromegas detectors used in CAST can be found in [2].

The first test of Micromegas with a passive shielding, showing an impressive background reduction, was done in 2005 with the help and advice of the Zaragoza's group, in particular of Igor G. Irastorza. It was the start of a fruitful collaboration that is still continuing today and has lead to many of the results that are presented here.

In view of these results, a completely new line was designed in order to accomodate the shielding and an X-ray telescope. The design of the new line was coordinated by Stephan Aune with the support of the Service d'Ingénierie des Systèmes (SIS/IRFU). Moreover the CAST collaboration was convinced to replace the ageing Time Projection Chamber (TPC) by two Micromegas detectors. In 2006, we decided to replace the conventional Micromegas detectors by the novel emerging microbulk technology. The design of the Micromegas detector was realised by Jean-Philippe Mols (SEDI).

With Thomas Papaevangelou (post-doc at that time in our group) and the Zaragoza group we commissioned the first set of these kind of detectors for the 2007 data taking. The manufacturing technique evolved and Ziad Abou Haidar, internship for 6 months in 2009, contributed to the characterisation and optimisation of these detectors. Paco Iguaz, post-doc from 2009 to 2011, contributed to the data analysis and studied in particular the improvement of upgrading the Gassiplex electronics by the more performant T2K ones.

In the Zaragoza group, different bench tests have been developed at ground and in the underground Laboratory of Canfranc to test different shielding configurations. In addition, the intrinsic radiopurity of different detector components have also been measured with germanium detectors showing that the microbulk are very radiopure objects [48, 49]. These results have been essential inputs for the different shielding upgrades that have been performed in the last two years and the understanding of the background that have allowed us to collectively design and manufacture a new generation of microbulk detectors, representing the state of the art of our knowledge, installed in CAST in autumn 2013 [20, 21]. In IAXO, a proposed fourth generation axion helioscope, these microbulks are the baseline technology for its X-ray

detectors [104, 63, 64].

The success of the Micromegas detectors in the CAST experiment is very much due to all the students from different institutes that have contributed with dedication to the simulation, design, installation, commissioning, operation and analysis for more than a decade of CAST operation. It is worth mentioning them: Thomas Papaevangelou, Theopisti Dafni, Kostas Kousouris, Berkol Dogan, Javier Galán, Theodoros Vafeaidis, Alfredo Tomás, Cenk Yildiz, Juan Antonio García, Javier G. Garza, Inaki Ortega[1]. I have had the chance to host in Saclay a few of them for at least a couple of weeks during their PhD: the first Javier, Theodoros, Alfredo and Juan Antonio.

The MIMAC Collaboration

In 2007, through the national french agency of research (ANR-07-BLANC-0255-03 funding) we started a collaboration for the development of a directional Time Projection Chamber with a Micromegas readout for the detection of dark matter. Our closest collaborators were Daniel Santos and Olivier Guillaudin from the Laboratoire de Physique Subatomique et Cosmologie (Grenoble). I was in charge of the design, characterisation and validation of the $10 \times 10 \, cm^2$ Micromegas readout planes. Jean Philippe Mols realised the design and supervised the production of the two dimensional readout planes that were manufactured outside CERN. Fréderic Druillole and Denis Calvet (SEDI) assisted us for the implementation of the T2K electronics and the characterisation tests were performed by Paco Iguaz during his post-doc [98] (2010-2012).

Micromegas for the ATLAS New Small Wheel

In 2007, we started to be involved in Muon ATLAS MicroMegas Activity (MAMMA Collaboration) that was defending the Micromegas detectors as an option for the replacement of the muon forward chambers for the High Luminosity Large Hadron Collider (HL-LHC). The first efforts of the Saclay group were dedicated to test different types of resistive anodes in order to decrease the secondary effects of the spark rate that Micromegas detectors would suffer in the HL-LHC context [121]. I co-directed Séphora Kirsch (Master M2 Paris Diderot University), for an internship of 6 months on this activity as well as Faruk Diblen (Master M2 Gaziantep University, Turkey) for 4 months. In addition we were also involved in the ageing tests (X-rays and thermal neutrons) of the resistive detectors [85]. This effort was lead by Fabien Jeanneau (SEDI). In 2012 the Micromegas detectors were chosen officially as one of the technologies to replace the present forward muon chambers in the New Small Wheel (NSW) becoming an official ATLAS project. The Technical Design Report of the small wheel was written in July 2013 and the first version of the MoU in October of the same year. At present, IRFU has several responsibilities in the NSW: definition of the layout design; construction and validation tests of one third of the $1200 \, m^2$ of detector to be produced involving the construction of a clean room. The production of the readout planes will be made by an industrial partner and the modules assembled in house. Final characterisation tests will take place at CERN before integration in the ATLAS wheels.

In order to cope with all these responsibilities the IRFU group has grown with a project team gathering forces from SEDI, SPP and SIS. This effort is coordinated by Fabien Jeanneau

---

[1]Special thanks to Spain and Greece for their constant efforts! ($> 90\%$ of students).

(SEDI), Patrick Ponsot (SIS) and Philippe Schune (SPP). I have participated to the design of an operational prototype that will be commissioned and tested in the next months and I will be particularly involved in the test of different prototypes for the final modules. My participation to this activity is not described here.

Generic Research and Development of Micromegas detectors

Microbulk

Since 2006 I have been involved in the development of the microbulk technology. In collaboration with the University of Zaragoza and particularly with the various internships of Paco Iguaz and Alfredo Tomás during their PhDs (2007-2009) we explored the feasibility of using microbulk detectors for a double beta decay experiment. These first tests were very encouraging [71]. I participated with Jean Philippe Mols to the design of a large microbulk ($30\,cm^2$ diameter) that has been developed and commissioned by the Zaragoza's group in the context of the R&D of Micromegas for the NEXT experiment [65] producing interesting results [51, 67, 66].

In order to optimise the operation of microbulks at high pressure, Laura Seguí during her internship in 2011, started studying small gap microbulks. With Mariam Kebbiri (SEDI) and Thomas Papaevangelou, we pursued these studies and the results have been compiled in a recent publication [19].

The microbulk technology is also interesting for its low mass budget and little interference for instance with neutron beams. In this context microbulk detectors have been extensively used in the NTOF experiment for neutron flux monitors and neutron beam profilers. In order to push the technology further we are developing ultra thin 2-dimensions microbulk by segmenting the micromesh in one direction and the readout anode in the other direction. The RD51 collaboration has funded this R&D project between Demokritos, CERN, the University of Zaragoza and SEDI. This work is being mainly done in collaboration with Mariam Kebbiri, Thomas Papaevangelou (SEDI) and Theopisti Dafni (UZ), Theodoros Geralis (DMK) and Rui de Oliveira, Serge Ferry and Martyn Davenport (CERN). Recently P2IO Labex funded this R & D to develop specifically such a detector for the NTOF experiment. The development is carried out with Thomas Papaevengelou, Marc Riallot (SEDI) and Frank Gunsing (IRFU/SPhN).

In addition, segmented mesh detectors are of interest for rare-event detection as the low mass budget might provide a more radiopure detector. Moreover the manufacturing process of these detectors, once completely mastered, will be simpler than the standard $x - y$ microbulk and seems a promising option, coupled with autotriggered electronics [31], to cover large surfaces with high radiopurity.

Piggyback Micromegas

Piggyback is a new type of Micromegas detector that has been developed recently. It is called Piggyback Micromegas as it can be placed "on the back" of any readout plane with a granularity that can be adapted easily. A resistive anode is deposited on a thin ceramic substrate and in this way the active region is dissociated from the readout plane providing full spark protection by the resistive layer. Due to the detector materials used, it exhibits excellent

properties making it appropriate for sealed operation, opening up new windows of applications. The radiopurity of this new structure has to be measured but it could be interesting for large rare-event detection experiments. In particular the use of the resistive coating limits the number of electronics channels to be implemented: a coarser strip segmentation can be used as the charge is spread over a large number of channels keeping a high spatial resolution. Moreover the dissociation of the amplification plane from the readout plane gives versatility on the electronics to be used.

The first prototypes were designed by Dominique Durand and Daniel Deforges (SEDI) and manufactured by Rui de Oliverira and Antonio Teixeira at CERN. The initial characterisation tests were realised at SEDI in collaboration with David Attié, Javier Galán, Yannis Giomataris, Alexi Gongadze, Paco Iguaz, Fabien Jeanneau, Thomas Papaevangelou and Alan Peyaud [17, 18]. The internship of Ludovic Boilevin-Kayl from September 2013 to February 2014 has materialised the idea of coupling a Micromegas detector with ultra low noise Caliste electronics initiating a collaboration with Olivier Limousin (IRFU/SAP) specialised in micro spectro-imaging polarimeters with CdTe semiconductors detectors.

After this general overview, the next chapters describe in more detail my research activities.

In addition, at the end of this document, are included five papers that I consider to be the most representative of my research. The list of these publications is given here:

- P. Abbon *et al.*, "The Micromegas detector of the CAST experiment", *New J. Phys*, (2007) **9**, 170 [2].

- S. Andriamonje *et al.*, "Development and performance of Microbulk Micromegas detectors", *JINST* (2010) **5**, P02001 [6].

- F. J. Iguaz *et al.*, "Micromegas detector developments for Dark Matter directional detection with MIMAC", *JINST* (2011) **6**, P07002 [98].

- I. G. Irastorza, E. Ferrer Ribas and T. Dafni, "Micromegas in the rare event searches", *Mod. Phys. Lett. A* (2013) **28**, 1340026 [102].

- D. Attié *et al.*, "Towards small gap Microbulks", *JINST* **9** (2014) C04013 [19].

Chapter 1

Axions: a brief overview

The Standard Model (SM) of particle physics is a very successful theory that explains with a high level of accuracy the fundamental constituents of matter and their interactions, especially since a Higgs Boson has been discovered at the Large Hadron Collider (LHC) in 2012. Yet the SM is not a complete theory as there are still a number of unanswered questions among them the origin of Dark Matter (DM) and Dark Energy (DE) and of the matter-antimatter asymmetry of the universe, why gravity can not be included in this theory and explanations for the values of its many parameters... In a large number of more general theories, embedding the SM, low mass and very weakly interacting particles, the so called WISPs (Weakly Interacting Slim Particles) are predicted. Axions and axion-like particles (ALPs) are salient examples of WISPs. In this chapter the motivations for axions and their phenomenological properties are briefly reviewed. The limits derived from astrophysical and cosmological bounds are also exposed in order to understand the relevant constraints in the ALP space. The last section is devoted to the search strategies to detect ALPs.

1.1 Axion motivations

1.1.1 The strong CP problem

The axion was introduced as an elegant solution of the strong charge conjugation (C) and parity (P) problem, so called CP problem. CP-violation by quantum chromodynamics (QCD) originates from two sources which are of perturbative and non-perturbative origins and have no reasons to cancel (magnitude, phase). One of the consequences is that the neutron should have a large electric dipole moment which is not the case in the experimental measurements [28].A solution was proposed by Peccei and Quinn (PQ) in 1977 who postulated a new global U(1) symmetry that is spontaneously broken at some large energy scale, allowing for the dynamical restoration of the CP symmetry. Weinberg [162] and Wilczek [163] proposed the particle interpretation of this mechanism, the axion. The axion is the Nambu-Goldstone boson of the Peccei-Quinn symmetry with zero spin, zero electric charge and negative intrinsic parity. This concept has been generalised to other, axion-like particles (ALPs) which may arise as (pseudo) Nambu Goldstone bosons from the breaking of other global symmetries such as, for example, family symmetries.

The relation between the mass of the axion, m_a, and the axion decay constant, f_a, can be
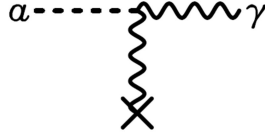
Figure 1.1: Axion photon conversion in the presence of an external electric or magnetic field.

written as follows:

$$m_a = \frac{f_\pi m_\pi}{f_a} \cdot \frac{\sqrt{m_u m_d}}{m_u + m_d} \approx 0.6\,\text{eV}\left(\frac{10^7\,\text{GeV}}{f_a}\right) \tag{1.1}$$

The energy scale f_a is the scale at which the new symmetry U(1) is broken. It can have any value up to the Planck scale.

The two-photon interaction is exploited in most of the experimental searches and is expressed as follows:

$$\mathcal{L}_{a\gamma} = -g_{a\gamma}\,\mathbf{E}\cdot\mathbf{B}\,a. \tag{1.2}$$

In this expression $\mathbf{E}$ and $\mathbf{B}$ are the electric and magnetic fields, a is the axion field and $g_{a\gamma}$ is the axion-photon coupling constant. The mechanism is shown in figure 1.1 and is a particular case of the Primakoff effect where there is resonant production of neutral pseudo-scalar mesons by high energy photons. These pseudo-scalars, like neutral pions, have the same triangular diagram interaction with photons. This coupling results in observable consequences from processes involving large electromagnetic fields. This can occur in astrophysical environments and can also be produced in laboratory experiments. The coupling constant is inversely proportional to f_a and is expressed as:

$$g_{a\gamma} = \frac{\alpha}{2\pi f_a}\left(\frac{E}{N} - \frac{2}{3}\frac{4+z}{1+z}\right), \tag{1.3}$$

where E and N are parameters (related to the anomaly of the axial current associated with the axion field) and $z = 0.56$ is the mass ratio of the up and down quarks. Axions couplings change depending on the models. In the original hadronic KSVZ model [111, 145], couplings are minimal in the sense that generic axion interactions with hadrons and photons derive from mixing with the pseudoscalar mesons. In these models $E/N = 0$, the interactions with leptons are usually negligible. In Grand Unified Models, axions couple to quarks and leptons as in the non hadronic DFSZ model [167, 77]($E/N = 8/3$). This lepton coupling results in a variety of axion-production channels in stars which are much more effective than the Primakoff process: electron-ion bremsstrahlung, electron-electron bremsstrahlung, Compton, axio-recombination and, to a lesser extent, axio-deexcitation of ions [32]. This coupling to electrons is most efficient in young stars like the sun, low-mass red giants and white dwarfs stars.

Generally E/N is not known, so for fixed f_a, a broad range of $g_{a\gamma}$ values is possible. The fact that the mass of the axion and the coupling constant $g_{a\gamma}$ are both inversely proportional to f_a make axion models lie in a diagonal band called the "axion band" in the $g_{a\gamma}$–m_a parameter space. The overall spread of axion models resulting from the possible values of E/N is represented by the width of the yellow band of figure 1.2. In more general models of ALPs, m_a and $g_{a\gamma}$ are not related and thus the whole parameter space is available.

Early accelerator axion searches discarded "standard axions" where f_a was of the order of the electroweak scale, f_{EW}. "Invisible axion" models with $f_a \gg f_{EW}$ were soon adopted and experimentally searched. These models were called "invisible" as m_a is inversely proportional to f_a and for arbitrarily high f_a, the mass m_a will be arbitrarily small and the coupling of the axion to the photon very small.

1.1.2 Dark Matter

Today the composition of the overall density of the universe is known to be 4.9% of ordinary matter and 26.8% of DM and 68.3% of DE (latest Planck results [130]). DM is weakly interacting and non-baryonic. Beyond the SM, the most evoked candidates are the Weakly Interacting Massive Particles (WIMP) appearing in supersymmetric extensions of the SM. WIMPs have been searched for in dedicated underground experiments exploring a fair part of the phase parameter space without success. Moreover the LHC has shown no sign of supersymmetry up to now. There are recent theoretical advances that define a generic category of light particles, WISPs. These particles appear in extensions of the SM, like string theory.

The axion, that has been introduced independently of the DM problem, could however account for part of the DM of the universe. There are scenarios where mixed WIMP-axion DM are theoretically viable [26, 23].

Axions are produced in the early universe by a number of different process. When they are produced thermally by collisions of particles in the primordial plasma, like WIMPs, they contribute to the hot DM component. This production is more important at large values of m_a and results in a limit on $m_a \leq 0.9\,\mathrm{eV}$ [93, 11] shown in figure 1.2. In addition axions could also have been produced in the very early universe by non-thermal production resulting in non-relativistic axions and therefore contributing to the cold DM. In this case axions could account for the totality of the cold DM. However as details about the primordial axion production mechanism remain uncertain, a wide range of axion models are possible giving rise to a "classic axion window", $m_a \sim 10^{-5} - 10^{-3}\,\mathrm{eV}$ [160]. The QCD axion with masses above the classical window can still solve the DM problem in non-standard cosmological scenarios. Some fine-tuned models, so called "anthropic axion models" allow much lower masses [118, 95].

1.2 Summary of Astrophysical and Cosmological bounds

A summary of the astrophysical and cosmological bounds in the axion/ALP parameter space $(m_a, g_{a\gamma})$ is given in figure 1.2 [63]. The limit derived from constraints on the population of low mass horizontal-branch stars in globular clusters [134, 136] is depicted. The hot DM [93, 11] limits discussed in the previous section are also shown. Limits resulting from searches of decay lines in radio telescopes appear at high mass [36]. The yellow band represents a range of realistic axion models. The green line refers to the KSVZ model. In the yellow band different regions are distinguished: CDM1 corresponds to the region corresponding to the anthropic window below $1\,\mathrm{meV}$ with no limit at low mass; CDM2 represents the models where the axion represent the totality of the DM while CDM3 are models where axions are just a fraction of the DM. Constraints derived from the long standing cooling anomaly of white dwarfs and attributable to axions are also depicted [133, 107, 106]. Another astrophysical case that has invoked axion production is the excessive transparency of the intergalactic medium to very (VHE) photons [123, 147]. The universe should be opaque to distant VHE due to the probability of interaction via e^+e- pair production. However different measurements show

that the degree of transparency of the universe is too high. These observations could be easily explained by photon-ALP oscillations in the cosmic magnetic fields. The HESS collaboration uses its data to excluded couplings of $\gtrsim 10^{-11}\,\mathrm{GeV}^{-1}$ in the mass region invoked for this effect [62].

1.3   Search strategies

Depending on the considered source of ALPs, the search is cosmological, astrophysical or laboratory based. Sikivie in the early 80's was the first to propose an experimental search of the axion [146] by proposing to look for axions from the galactic halo and axions originating from the sun. Today there are three main strategies: microwave cavity search looking for halo axions, laboratory experiments searching for axions produced by means of a laser and helioscopes looking for solar axions. We describe briefly the first two and we focus on the helioscope technique that is the most relevant for this study. For a detailed and comprehensive review of all the different experimental approaches, the reader is referred to recent documents prepared for roadmapping events in Europe [29, 79] and in the US [96, 46].

1.3.1   Haloscopes based on microcavities searches

Under the hypothesis that the axions are the predominant form of cold dark matter, masses of a few to tens of μeV are assumed. The detection concept to detect these relic axions is based on dark matter axions going through a microwave cavity embedded in a strong magnetic field where the axions can resonantly convert into photons when the cavity frequency matches the axion mass. First feasability tests were carried out at Brookhaven National Laboratory and at the University of Florida achieving sensitivities an order of magnitude above the sensitivity needed to reach plausible axion couplings. The Axion Dark Matter eXperiment (ADMX) [129, 15] is the follow up of these first experiments. It consists of a large 8 T superconducting solenoid magnet of a diameter of 0.5 m and a length of 1 m. The power resulting from axion to photon conversion was initially measured with low noise High Electron Mobility Transistor (HEMT) preamplifiers coupled to the cavity [129]. The sensitivity was upgraded in replacing the HEMTs by Superconducting QUantum Interference Device (SQUID) operating at low temperature (100 mK) to improve the temperature noise [15]. Figure 1.2 shows the exclusion limits obtained with the ADMX runs, excluding at 90% C.L axion masses ranging 1.9 μeV to 3.53 μeV. Improvements are foreseen to extend the sensitivity of the experiment to higher m_a values [15].

1.3.2   Laboratory searches

The main technique to look for laboratory produced axions is the light-shining-through-wall experiments (LSW). This type of experiments makes use of high power lasers and strong magnetic fields to produce ALPs and relies on the possibility that photons could be converted into axions in the presence of a magnetic field. They could then be transmitted through a wall and converted back into detectable photons. This approach does not depend on any astrophysical or cosmological assumption.

The most advanced implementation of this technique is the ALPS experiment [81] in DESY. The first phase of ALPS has achieved the best laboratory limits on axion like particles
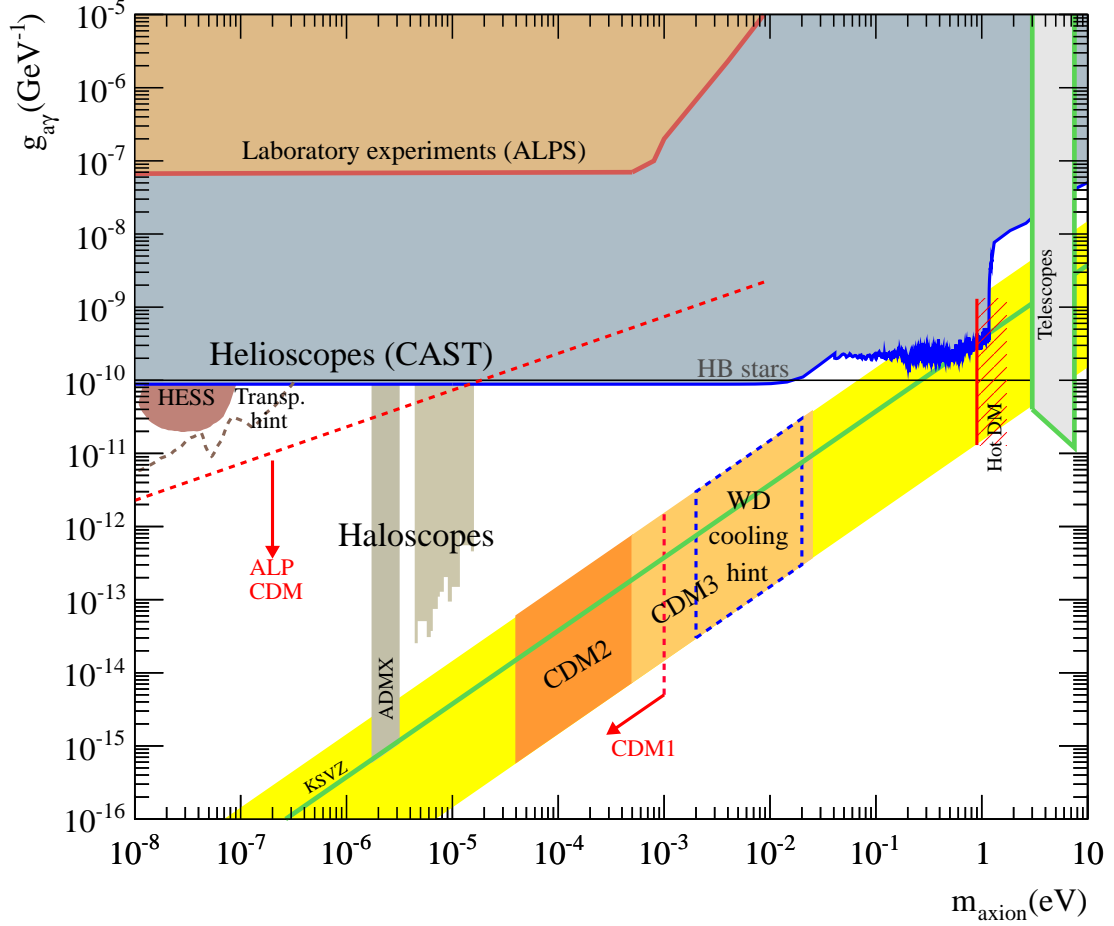
Figure 1.2: Parameter space for the axion-photon coupling $g_{a\gamma}$ versus axion mass m_a showing relevant cosmological and astrophysical constraints as well as experimental bounds [63]. The yellow axion band represents a range of realistic axion models with the green line referring to the KSVZ model. Constraints from the horizontal branch (HB) stars [134, 136] and the hot DM (HDM) [93, 11] are also shown. Limits derived from searches of decay lines in telescopes are shown at high mass. Regions referring to cosmological favoured models are depicted by CDM1 [118, 95], CMD2 [160] and CDM3 [26, 23]. Also shown the region invoked for the WD cooling anomalus [133, 107, 106] as well as in the transparency of the universe. The brown region is excluded by the HESS experiment [62]. The experimental constraints of dedicated axion searches (ALPS [81], ADMX [129, 15] and CAST [1, 8, 12, 13, 14]) are also included.
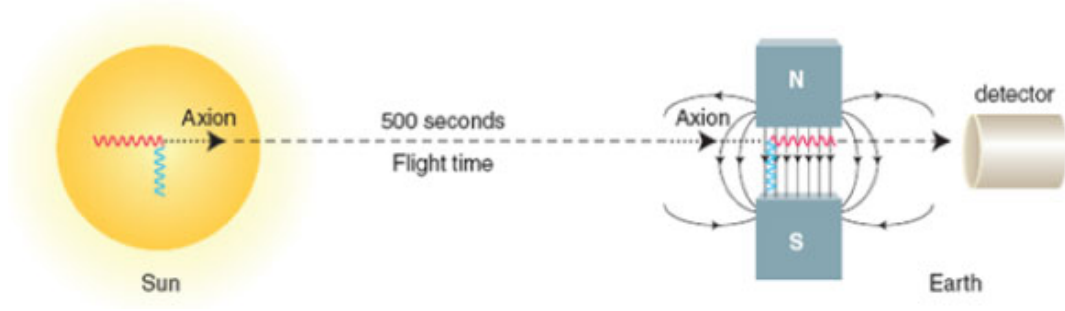
Figure 1.3: Illustration of the principle of an axion helioscope.

shown in figure 1.2. ALPS-II [27] aims to use 24 HERA straightened dipole magnets with an upgraded laser and a regeneration cavity to increase WISP-photon conversions.

Another way of producing axions in the laboratory is by the so called photon polarisation experiments. In these experiments the dichroism and birefrigence of the beam through a transverse magnetic field is measured. In 2006 a polarisation experiment, PVLAS, reported a signature of magnetically induced vacuum dichroism that could be interpreted as the effect of a pseudoscalar with $m_a = 1 - 1.5\,\mathrm{meV}$ and $g_{a\gamma} = 1.6 - 5 \times 10^{-6}\mathrm{GeV}^{-1}$ [165]. However this effect was later attributed to an instrumental artifact [166]. In any case, this claim triggered different experiments, among them BMV [139], GammeV [56] as well as ALPS. All of them ruled out the PVLAS result.

1.3.3   Helioscopes for solar searches

The idea of detecting solar axions was first proposed by Sikivie [146] in 1983. Solar axions produced in the solar core would escape and could be possibly detected on earth by means of a helioscope by conversion into low energy X-rays as they go through a strong magnetic field as is shown in figure 1.3.

The expected flux of axions on Earth is given by [8]:

$$\Phi = g_{10}^2\, 3.75 \times 10^{11}\mathrm{cm}^{-2}\mathrm{s}^{-1} \tag{1.4}$$

with $g_{10} = g_{a\gamma} \times 10^{10}$. The solar flux spectrum assuming only Primakoff conversion of plasma photons into axions is shown in figure 1.4. The average energy of solar axions is $4.2\,\mathrm{keV}$. The probability of conversion of a solar axion into a photon when passing through a magnet of field strength B and length L is given by:

$$P_{a\gamma} = 2.6 \times 10^{-17} \left(\frac{B}{10\,\mathrm{T}}\right)^2 \left(\frac{L}{10\,\mathrm{m}}\right)^2 \left(g_{a\gamma} \times 10^{10}\mathrm{GeV}\right)^2 F \tag{1.5}$$

where F can be written as:

$$F = \frac{2(1 - \cos qL)^2}{qL} \tag{1.6}$$

and q is the photon-axion momentum transfer. The factor F reflects how axion and photon waves remain in phase over the length of the magnet, i.e it is a measure of the coherence of the process. For very low masses, q tends to 0 and F tends to 1, so that the maximum conversion probability is reached. For more massive axions, the axion and photons waves are out of
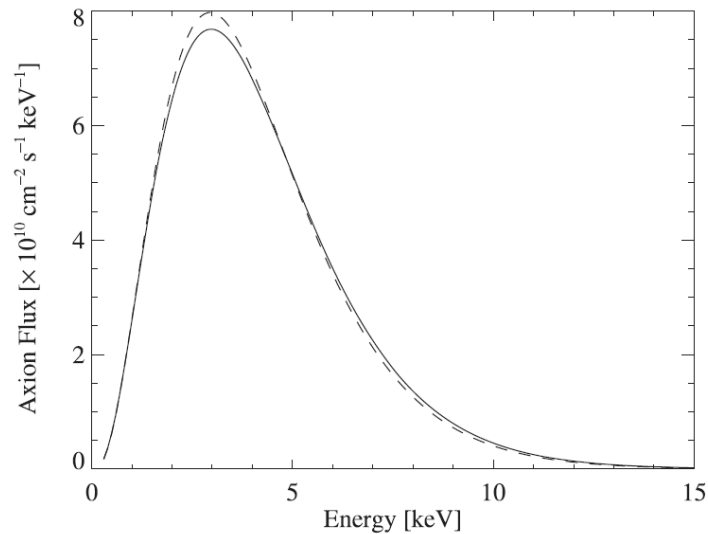
Figure 1.4: Solar axion flux at Earth assuming Primakoff conversion of plasma photons into axions. The two lines correspond to two different solar models. A $g_{a\gamma}$ of $10^{-10}\,\mathrm{GeV}^{-1}$ has been assumed [8].

phase and the conversion probability decreases quickly. The coherence of the process can be extended [157] to higher axion masses by filling the conversion region with a buffer gas[1] like helium, attributing an effective mass to the photons which can then match the axion's mass, m_a. In this manner the conversion probability can be restored to its theoretical maximum for any specific axion mass. A scan of the gas pressure will result in a scan of the axion mass.

The first implementation of the axion helioscope was built at Brookhaven using a 2.2 T dipole magnet of 1.8 m length oriented at the sun with a proportional chamber for X-ray detection [117] in 1992. The experiment took two hours of data as the magnet was fixed. However they exploited the two running modes of the present helioscopes: with vacuum in the magnetic field region for the lower axion mass region and with a buffer helium gas in the magnetic field region of up to 13 mbar for the higher mass region. In 1995 the Tokyo axion helioscope started its construction developing a second generation helioscope concept by including a rotating platform that allows a movement of $\pm 30^{\circ}$ vertically and 360° horizontally, enabling the tracking of the sun. A few years later the first results were published using vacuum in the conversion region for low masses [125]. The second and third phase of the experiment enabled to scan heavier masses up to 1 eV [101, 100].

The CERN Axion Solar Telescope (CAST) is a third generation experiment that started data taking in 2003. The CAST experiment is using a decommissioned dipole prototype of the LHC with a magnetic field of 9 T over a length of 9.3 m and a 14.5 cm^2 cross sectional area. With these parameters the axion-photon conversion probability is larger by a factor 100 with respect to the Tokyo helioscope. The description of the CAST experiment and of the main physics are the subject of chapter 2. Here we only want to underline that the operation of the CAST experiment has led to one of the most competitive experimental bounds on the

---

[1]"Buffer gas" is a terminology used since the first paper where this technique was described in 1989 [157]. According to one of the authors, a more suited wording would be "dispersion-relation-matching gas" [156] describing better its function. However this wording was not adopted due to its length and complexity.

Weakly Interacting Sub-eV Particles (WISPs)

Axion Like particles (ALPs)

Hidden Photons (HPs)

**Stringy axion
Arion
Majoron**

Mini Charged Particles

Axions

Chameleons
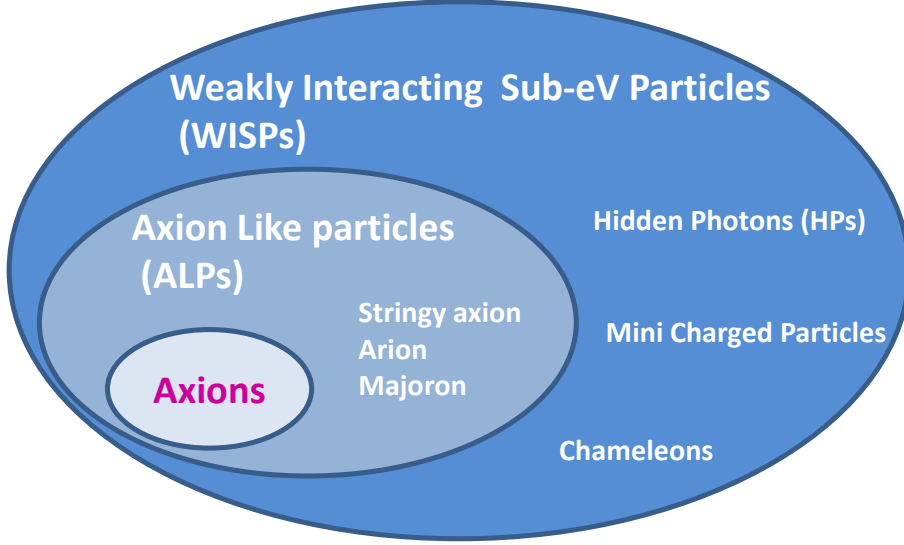
Figure 1.5: Diagram illustrating the WISPs families.

axion mass and on the axion couplings as can be seen in figure 1.2.

1.4   Conclusion

Many extensions of the SM predict new heavy particles. Some of these particles such as neutralinos are natural candidates for the constituents of cold DM in the form of WIMPSs. However, extensions of the SM often also imply the existence of new low mass particles, very weakly coupled to the standard model, that we call in general WISPs. ALPs are a subfamily of WISPs. Figure 1.5 shows a simple diagram to illustrate these various families[2]. One of the most prominent candidates are the axions that have been introduced to provide a solution to the longstanding strong CP problem. As WISPs are light and very weakly interacting particles they could contribute to the DM and DE of the universe. Some cosmological and astrophysical hints could indicate the existence of WISPs. The detection strategies of the axion are based on the coherent interaction of an axion and a photon in a strong magnetic field. The relevant parameter space, $g_{a\gamma}$ versus m_a, has been discussed with the pertinent bounds derived from cosmology and astrophysics. The current experimental panorama has been briefly exposed invoking the principle search techniques: haloscopes, laboratory experiments and helioscopes.

An attractive feature of ALPs experiments is that in case of a positive signal, the experiment is in a strong position to claim or disclaim the discovery quickly (for instance by observing the signal amplitude as a function of magnetic field).

---

[2]Thanks to Javier Redondo and Biljana Lakić for fruitful discussions on this representation.

Chapter 2

The CAST experiment

2.1 Introduction

The CERN Axion Solar Experiment (CAST) was proposed in 1999 [1], seven years after the first implementation of the helioscope technique. CAST added several innovations with respect to previous helioscopes that are listed here:

- the LHC dipole magnetic field and length allow a gain in sensitivity of a factor 100 ($B \times L = 91$ Tm compared to 9.2 Tm for the Tokyo helioscope);

- the use of X-rays optics to focus the parallel beam of incoming photons to a small spot in order to increase the signal-to-noise ratio;

- the implementation of low background techniques for the X-ray detectors to reach the lowest possible backgrounds.

In the next sections the experimental set-up is briefly described. The physics program accomplished up to now is depicted as well as the perspectives for the near future.

2.2 Experimental set-up

A detailed description of the experimental set-up can be found in [1, 168]. Here we will only give a concise overview of the experiment. The refurbished LHC test magnet ($L = 9.26$ m, $B \sim 9.0$ T) is mounted on a moving platform that allows following of the sun for about 1.5 h both at dawn and at dusk. In order to reach such a high magnetic field, the magnet is operated at a temperature of 1.8 K. The movement of the magnet is controlled by a dedicated tracking system software [86]. This system is checked periodically in order to verify that the magnet is following the sun core with the required precision (1 arcmin). The tests consist in measuring deviations (laser measurements and geometric survey measurements) with respect to reference points defined in an absolute position measurement campaign that was achieved before the start of the 2002 data taking campaign. In addition the accuracy is measured by "sun filming" by means of a CCD camera that has been placed on top of the magnet aligned with the magnet axis. Thanks to the window that was built especially for this purpose in the CAST hall, the magnet is able to directly observe the sun twice per year in March and September during about 5 min. A sun filming software has been developed to determine the

Figure 2.1: Picture of the CAST experimental hall.

position of the sun centered at the CCD camera. The measurements are done twice per year and are often limited by weather conditions.

To enable smooth operation of the magnet essential slow control systems are required: cooling and vacuum systems. These systems will not be discussed here but are described in detail in [86].

2.2.1 Upgrades and strategy for buffer gas operation

The CAST experiment went through two major upgrades in the experimental set-up motivated by the extension of the sensitivity to larger masses. The sensitivity that can be obtained with operation in the vacuum mode applies only for axion masses $m_a \leq 0.02\,\text{eV}$. This is due to the fact that the conversion probability is written as follows:

$$P_{a \to \gamma} = \left(\frac{g_{a\gamma} B L}{q} \right)^2 \frac{\sin^2(x)}{x^2}, \tag{2.1}$$

where $x = qL/2$, q being the momentum transfer in vacuum that can be written as $m_a^2/2E$ and L the length of the magnet. The sensitivity to $g_{a\gamma}$ is degraded at high masses due to the x^{-2} suppression of the conversion probability when $x \gg 1$. Considering the CAST magnet length $L \simeq 9.26$ m and the typical $4\,\text{keV}$ energy of solar axions, the sensitivity will be reduced for $x \gtrsim 1$ i.e $m_a \gtrsim \sqrt{4E/L} \approx 0.02\,\text{eV}$. The sensibility can be restored for higher masses if the conversion region is filled with a suitable buffer gas. In this way the photons acquire an effective mass m_γ and the momentum transfer becomes $q = (m_a^2 - m_\gamma^2)/E$. If m_γ is chosen near m_a values the maximum sensibility is restored. The strategy consists in changing the gas density by steps in order to scan a wide range of m_a as m_γ can be written as:

$$m_\gamma(\text{eV}) = \sqrt{\frac{4\pi \alpha N_e}{m_e}} \approx 28.9 \sqrt{\frac{Z}{A} \rho \left(\frac{\text{kg}}{\text{m}^3} \right)} \tag{2.2}$$

where N_e is the electron density of the buffer gas, Z is the atomic number and A is the atomic weight. This technique was realised by the first helioscope [117] at Brookhaven. When using a buffer gas in the conversion volume the conversion probability is then written as follows:

$$P_{a \to \gamma} = \left(\frac{g_{a\gamma} B}{2} \right)^2 \frac{1 + e^{-\Gamma L/2} - 2e^{-\Gamma L/2} \cos(qL)}{q^2 + \Gamma^2/4}, \tag{2.3}$$
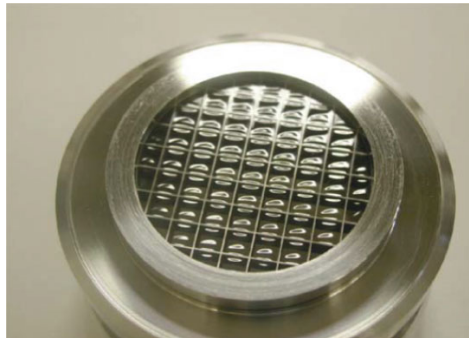
Figure 2.2: Transparent X-ray window.

where Γ is the attenuation coefficient of the photon in the buffer gas. The use of a buffer gas allows to recover the conversion probability for axion masses $m_a \geq 0.02\,\text{eV}$ by changing the pressure of the gas in steps.

The first upgrade was done to enable operation with ^{4}He buffer gas in the cold magnet bore. This system was operational from November 2005 to December 2006 with around 10 months of data taking. The density of the gas was changed in daily steps equivalent to $0.08\,\text{mbar}$ covering equivalent pressures up to $13.4\,\text{mbar}$ at $1.8\,\text{K}$. This is the maximum pressure obtainable at this temperature because for higher pressures the gas condensates. This is the reason why ^{3}He was used to scan at higher masses. During 2007, a more sophisticated and complex gas system was installed and commissioned to operate with ^{3}He. This system required a pressure-limiting safety system and a more complex monitoring system in order to ensure that the ^{3}He would not be lost. One key element of the two systems was the use of *cold windows* to support the pressure difference due to the increasing amount of gas inside the cold bores with a tight confinement of the gas with no leaks and with resistance to quenches. In addition the windows allow good transmission for X-rays in the axion energy range and work at cryogenic temperatures without degradation of performance. In order to fulfill these requirements dedicated windows were designed with a stainless steel grid structure (strongback electropolished) with a polypropylene foil of $15\,\mu\text{m}$. A picture of one of these windows is shown in figure 2.2.

2.2.2 X-Ray Detectors

At both ends of the magnet, in each magnet bore of $14.52\,\text{cm}^2$, the locations for four X-ray detectors are available. These detectors aim to search for excesses of X-rays from axion conversion inside the magnet when pointing to the sun. Initially a conventional time projection chamber (TPC) was looking for X-rays from "sunset" axions covering both bores of one of the magnet side. At the other end in one of the bores, facing "sunrise" axions, a charge coupled device (CCD) was coupled to a focusing X-ray mirror telescope. In the other bore, an unshielded conventional Micromegas detector was installed. This configuration was changed in 2007 where the sunrise Micromegas detector and the TPC were replaced by second generation Micromegas detectors (the so-called microbulk Micromegas) with passive shielding. In 2012 the sunset shielding was improved. In 2013 new state-of-the-art Micromegas detectors were installed and the CCD detector was replaced by another type of Ingrid Micromegas detectors [112, 113], making CAST a 100% Micromegas experiment. In the following sections only

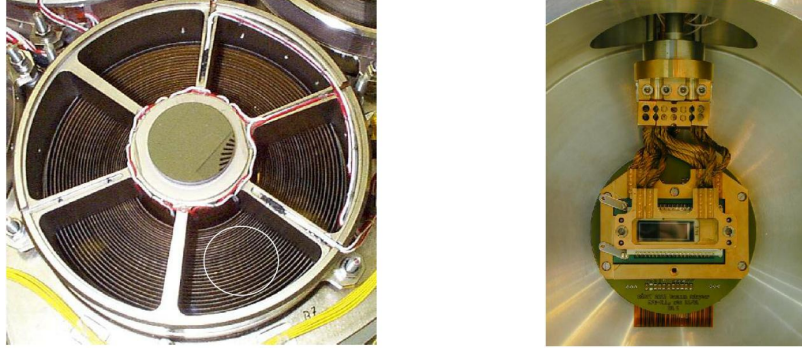Figure 2.3: Left: Front view of the X-ray telescope. The individual mirror shells and the supporting spoke structure are shown. One of the six sectors is illuminated through the magnet bore, the approximate size of the magnet bore is indicated by the white circle. Right: The focal plane pn-CCD detector inside the CAST telescope without the internal Cu/Pb shielding.

the CCD system and the TPC is described. Chapter 4 is devoted entirely to the Micromegas detectors where they are described in detail.

The pn-CCD detector and the X-ray telescope

The photons issued from axion conversions can be observed directly with a detector covering the magnet bore, as in the case for the Micromegas detectors and the TPC of CAST, or it can be focused with X-ray optics onto a focal plane with a high spatial resolution. The main advantage of focusing the potential signal from the magnet acceptance area of $14.5\,\mathrm{cm}^2$ to a small spot of a few mm^2 is that the background is decreased by a factor more than 100. This is the case for the pn-CCD detector that is installed in one of the locations of the sunrise side of the experiment and is coupled to a Wolter1 type X-ray mirror system [115].

In addition, thanks to the imaging capability of the CCD, an axion image can be acquired and by taking simultaneously signal and background events, systematic effects can be reduced. The CAST X-ray telescope is based on the concept of a Wolter 1 mirror optics and is a spare module which was originally built for the X-ray mission ABRIXAS [84]. In the focal plane of the telescope, the pn-CDD detector installed is of the same type of the one used in the X-ray satellite XMM-Newton [80]. The telescope consists of 27 nested, gold coated, and con-focally arranged parabolic and hyperbolic nickel shells with a focal length of $1600\,\mathrm{mm}$. Since the diameter of the bore of the CAST magnet ($d = 43\,\mathrm{mm}$) is much smaller than the diameter of the outermost mirror shell ($163\,\mathrm{mm}$), the telescope is mounted off-axis such that only one of the six mirror sectors is used for imaging as can be seen in figure 2.3. The overall combined efficiency of the mirror system and the pn-CCD detector for X-rays from axion conversion varies between 25 and 46%.

The pn-CCD is a $280\mu\mathrm{m}$ thick fully depleted with a quantum efficiency $\geq 95\%$ in the entire photon energy range of interest (1–$7\,\mathrm{keV}$). The pn-CCD has a sensitive area of $2.88\,\mathrm{cm}^2$ divided into 200×64 pixels with a size of $150 \times 150\,\mu\mathrm{m}^2$ each. This surface makes it possible to have a sensitive area that is larger than the expected axion image of the sun. The detector is installed in a cooling system and is hosted inside a vacuum vessel surrounded by a $10\,\mathrm{mm}$ of copper and $20\,\mathrm{mm}$ of lead. The back of the detector has an additional lead shielding to
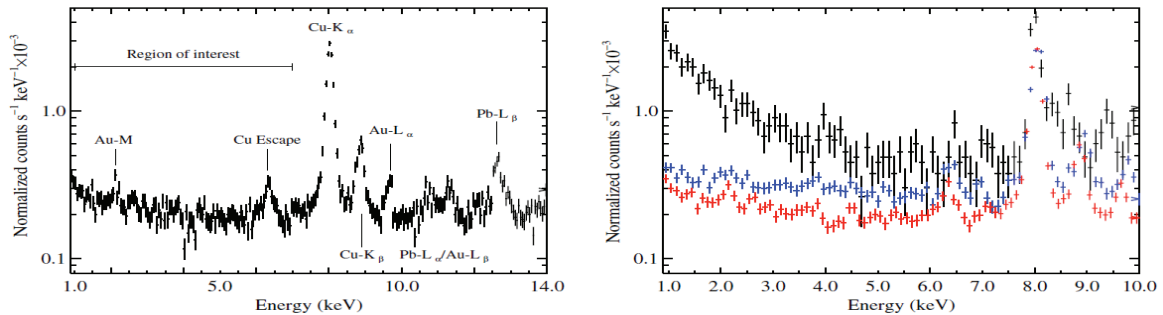
Figure 2.4: Left: Background spectrum during background data taking in 2004. Right: Background spectra for different background configuration. From top to bottom: background observed with the internal copper shielding (black) and with the internal lead and copper shielding (blue). The lowest spectrum (red) represents the observed background with the final shield configuration, which consists (from the outside to the inside) of an external lead shield followed by the evacuated detector vessel, and the internal lead and copper shield [115].

reduce the γ background from the concrete wall.

The typical performance of the pn-CCD detector is shown in figure 2.4. The count rate over the full detector area is 2.21×10^{-4} counts s^{-1} keV^{-1} corresponding to a mean differential flux of 8.00×10^{-5} counts keV^{-1} cm^{-2}s^{-1} corresponding to a count rate of 0.16 counts hour^{-1} in the $9.4\,\mathrm{mm}^2$ solar spot. The background spectrum is characterised by the fluorescent emission lines from materials close to the pn-CCD chip (copper, gold and lead). Below $7\,\mathrm{keV}$ the background is dominated, besides the Si escape peak from the copper line, by an almost flat continuum of predominantly Compton scattered photons and secondary electrons. The CCD background was modeled and it was shown that, in the CAST region of interest, the background is dominated by the external gamma background due to natural activities at the experimental site, while radioactive impurities in the detector itself and cosmic neutrons contribute with a smaller fraction [47].

The X-ray telescope and the pn-CCD detector were operated in the CAST experiment till 2013 when the pn-CCD detector was dismounted to be replaced by an InGrid Micromegas detector [112].

The Time Projection Chamber

A full description of the Time Projection Chamber (TPC) of CAST can be found in [22, 35, 141]. The TPC was lead out with a multi-wire proportional chamber (MWPC) optimised to have low threshold (at the keV level), relatively high gain and pattern recognition for background rejection, good efficiency and stable operations over long periods of data taking. The conversion volume of the TPC was of $10 \times 15 \times 30\,\mathrm{cm}^3$. The $10\,\mathrm{cm}$ drift direction was parallel to the magnet beam pipes, and the section of $15 \times 30\,\mathrm{cm}^2$ was perpendicular to that direction, covering both magnet bores. The TPC was operated with a mixture of Ar(95%)+CH$_4$(5%) at atmospheric pressure. The conversion probability of photons of $6\,\mathrm{keV}$ is greater than 99%. The TPC entrance is covered by two thin X-rays windows to allow photons coming from the magnet bores to enter the detector without being absorbed. Another feature of the detector design was a differential pumping system to couple the chamber (at

1 bar) to the magnet (at mbar) without diffusion of gas in the magnet bore pipes.

The TPC was surrounded by shielding in order to reduce the level of background seen by the detectors but also to homogenise the dependence of background with position. The design of the shielding had to take into account size and weight considerations imposed by the lifting screws and the existing support structure. From inside to outside, the shielding is composed by: a copper box of 5 mm thick to reduce electronic noise and to stop low energy X-rays; 2.5 cm thick lead bricks to reduce low and medium energy γ radiation; a 1 mm thick cadmium layer to absorb thermal neutrons slowed down by the 22.5 cm polyethylene wall that followed; a PVC bag covered the whole shielding to be able to flow N_2 gas in order to expel radon out from this environment. This is shown in figure 2.5. This shielding configuration offered CAST a test bench for later shielding configurations for the Micromegas detectors.

The TPC was active during the data taking campaigns of 2003 and 2004. However in 2003 the TPC operated with a reduced shielding configuration consisting only of the copper cage and the N_2 flow. The background level, in this uncomplete configuration, suffered from a strong dependence on magnet position. To avoid this systematic effect, the background data was selected by only considering the background data taken in magnet positions where sun tracking had been performed. This data was then weighted accordingly by the tracking time spent in each position. The TPC background level between 1 and 10 keV was 4.10×10^{-5} counts cm^{-2} s^{-1} keV^{-1}, a factor of ~4.3 below the level reached by the TPC with no shielding. The observed background energy spectra for 2003 data and 2004 are shown in figure 2.6. In figure 2.6 the final configuration is shown as well as two intermediate configurations with only the copper box and N_2 flux. The TPC was replaced in 2006 by two Micromegas with improved background discrimination. The background studies based on Monte Carlo simulations [119] were a precursor of the studies that later were extended to the other X-ray detectors.

2.3   Axion search: results and perspectives

The CAST physics program started in 2003. In 2003 and 2004 the experiment operated with vacuum inside the magnet (CAST phase I) and set the best experimental limit on the axion-photon coupling constant in the range of axion masses up to 0.02 eV [168, 8]. Beyond this mass the sensitivity is degraded due to coherence loss. By changing the pressure of the buffer gas in steps, one can scan an entire range of axion mass values. The CAST experiment started this gas program entering its phase II at the end of 2005. From 2005 to 2007, the magnet bore was filled with ^{4}He gas extending the sensitivity to masses up to 0.4 eV [12]. From March 2008 onwards the magnet bore was been filled with ^{3}He. With the end of the 2011 data taking in July, the CAST experiment has covered axion masses up to 1.18 eV surpassing the initial goal of the phase II which was to reach 1.16 eV [13, 14]. A summary table describing the CAST physics program is given in figure 2.1. The final results of the ^{3}He phase are given in figure 2.7. The black-red line corresponds to the current helioscope limits, dominated by CAST for all axion masses. Also shown are the constraints from the last Tokyo helioscope "Sumico" [125, 101, 100] the horizontal branch (HB) stars [135] and hot DM (HDM) [93, 11]. The yellow "axion band" represents the range of realistic axion models. In 2012 the data program was dedicated to revisit with improved sensitivity and longer exposures, a narrow part of a theoretically motivated range of axion masses around 0.4 eV using ^{4}He as a buffer gas. A preliminary exclusion plot is given in figure 2.8 [59]. In 2013 and 2014 CAST aims to significant increase of its sensitivity by important changes in the X-ray detectors. The current
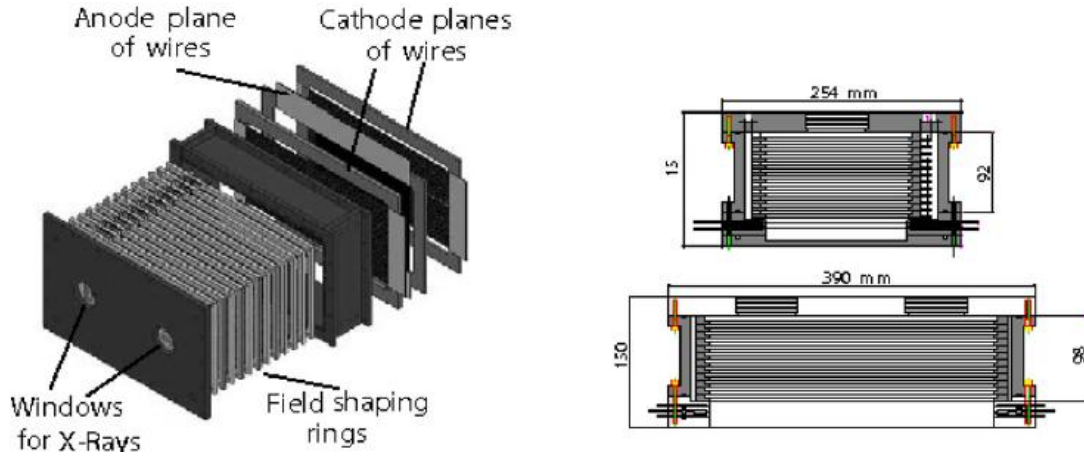
Figure 2.5: Left: Exploded view of the TPC. Right: Side view of the TPC showing the dimensions in mm.
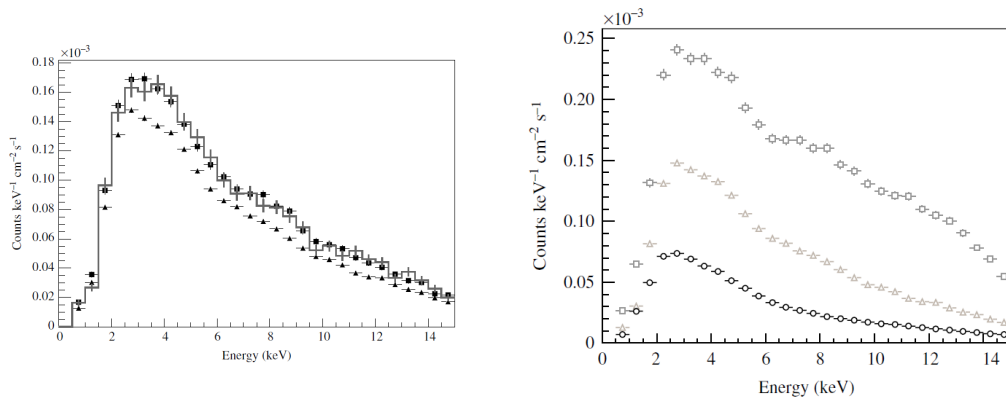
Figure 2.6: Left: Background spectra for the TPC detector measured during 2003. The triangles correspond to the total measured spectrum, the weighted background spectrum is shown with the squares and finally the solid line is showing the tracking spectrum. Right: Background spectra for the TPC detector measured during 2004 with two incomplete shielding configurations [22].
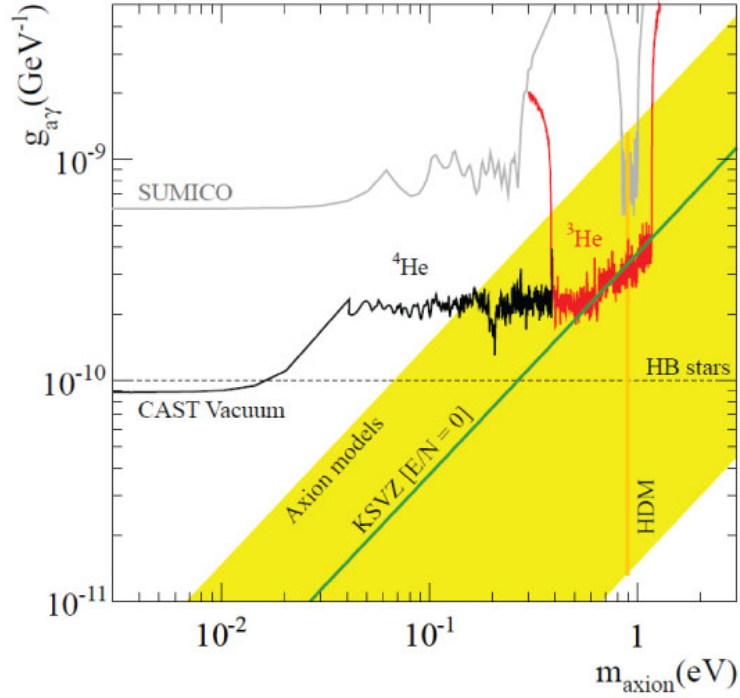
Figure 2.7: Exclusion regions in the $m_a - g_{a\gamma}$ parameter space achieved by CAST in vacuum [168, 8], in ^{4}He [12] and ^{3}He phase [13, 14]. We also shown constraints from Sumico [125, 101, 100], horizontal branch (HB) stars [135] and the hot DM (HDM) bound [93, 11]. The yellow band represents typical theoretical models with $E/N - 1.95 = 0.07 - 7$. The green solid line corresponds to $E/N = 0$ (KSVZ model).

sunset detectors will be conserved only upgrading the muon veto scintillator. On the sunrise side, the currently installed pn-CCD chip will be replaced by a new shielded InGrid detector, after it has successfully passed acceptance tests. For the sunrise Micromegas, a new detector and shielding system is designed to be coupled to a new X-ray optic device. Details will be given in chapter 4.

The collaboration has performed by-product analysis of the data taken, to look for other axion scenarios to which CAST would also be sensitive. Indeed CAST was mainly focused on hadronic axions which were appealing as hot Dark Matter candidates. In hadronic models, the bulk of the solar axion flux comes from Primakoff production. Lately, non-minimal axion models are also considered. In these models other couplings intervene, in particular axions couple to electrons at tree level opening axion-production channels in stars which are much more effective than the Primakoff process leading to larger axion fluxes from stars than the coupling to photons. The sensitivity of CAST to non-hadronic axions has been studied [32] and has made it possible to set a bound on the product of both coupling constants $g_{a\gamma}g_{ae} < 8.1 \times 10^{-23}\,\mathrm{GeV}^{-1}$ for $m_a < 10\,\mathrm{meV}$.

In addition, the TPC phase I data has been reanalysed to look for 14 keV axions coming from M1 transitions [9]. Moreover data taken with a calorimeter during the phase I were used to search for high energy (MeV) lines from high energy axion conversion [10]. Furthermore a few days of data were taken with a visible detector coupled to one end of the CAST
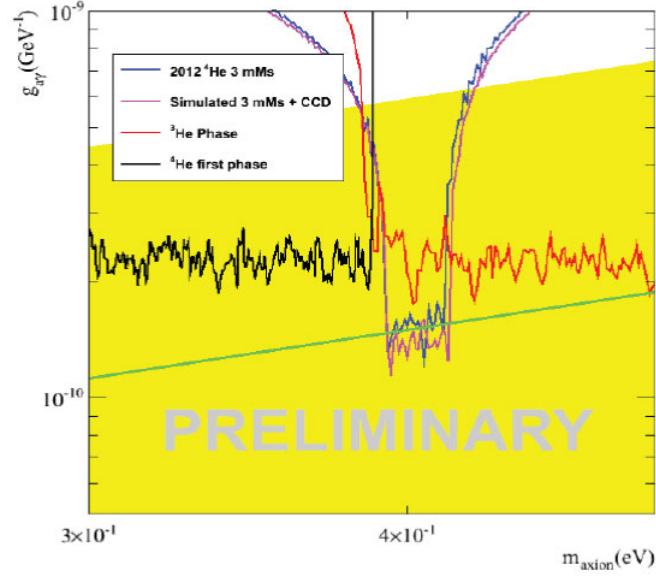
Figure 2.8: Preliminary results of the ^{4}He data taking of 2012 with improved performance detectors with respect to the 2006 run [59].

magnet [45], to search for axions with energy in the "visible" range. A permanent setup has been installed in the experiment in order to take data without interfering with the standard program of CAST.

Lately there has been increasing interest in some non standard scenarios that predict the emission of solar chameleons [41, 40] in the sub-keV energy range. These models have been proposed in the context of particle interpretations of the nature of DE. Similar to axions, they are expected to be created via the Primakoff effect in the magnetised inner sun, and they can be detected by the inverse Primakoff process, provided at least one CAST X-ray detector is sensitive in the sub-keV range. The InGrid detector with its very low energy threshold will be able to explore this low energy region and provide interesting competitive results in 2014. Meanwhile, for the 2013 data taking, a Silicon Drift Detector has also been installed and tested during the data campaign as it has a good resolution at low energy (65 eV at 500 eV) [59]. However it does not have any imaging capabilities.

2.4 Conclusion

The CAST experiment is providing experimental limits on the axion-photon coupling at a level of $10^{-10}\,\mathrm{GeV}^{-1}$ for m_a up to $\sim$ eV as explained in the first sections of this chapter. These limits are the most stringent experimental limits in most of this axion mass range. This achievement has been possible thanks to the use of the LHC magnet, the use of an X-ray telescope and the implementation of low background techniques for its X-ray detectors. In about 10 years of operation, the CAST experiment has undergone major modifications of its apparatus in order to extend the sensitivity towards higher masses. The construction and commissioning of the gas system have taken some months, see table 2.1 but these shutdown

Mode of operation	Period	Sensitivity	Background level Micromegas/ CCD/TPC (counts keV^{-1} cm^{-2}s^{-1})
Vacuum	2003–2004	$m_a \leq 0.02$ eV	$5 \times 10^{-4}/8 \times 10^{-5}$ $/17 \times 10^{-4}$
Preparation of ^{4}He gas system	2005		
^{4}He	2006–2007	$0.02\,\text{eV} \leq m_a \leq 0.39$ eV	$5 \times 10^{-5}/8 \times 10^{-5}$ $/17 \times 10^{-4}$
Preparation of ^{3}He gas system	2008		
^{3}He	2009–2011	$0.39\,\text{eV} \leq m_a \leq 1.18$ eV	$6 \times 10^{-6}/8 \times 10^{-5}$ /-
Revisit ^{4}He	2012	$0.3\,\text{eV} \leq m_a \leq 0.4$ eV	$1 \times 10^{-6}/8 \times 10^{-5}$ /-
Revisit vacuum	2013–2014	$m_a \leq 0.02$ eV	$7 \times 10^{-7}/$-/-

Table 2.1: Summary of the CAST program. The background level for the three type of detectors is given when appropriate. The background level of the CCD takes into account the focalisation of the X-ray telescope. The detail of the the evolution of the Micromegas background level is given in chapter 4.

periods have also been profitable in order to conceive, optimise, build and commission X-ray detectors with improved performance. In particular, Micromegas detectors have been in constant evolution in order to optimise their performance to the axion search. The detectors installed in the experiment today are very different from the detectors installed 11 years ago. In chapter 4 the evolution of the Micromegas detectors is described in detail.

Chapter 3

The Micromegas detectors

3.1 Introduction

In 1968, the invention of the Multiwire Proportional chamber (MWPC) by George Charpak revolutioned the world of radiation detectors moving from optical readout devices (cloud chambers, bubble chambers)[1] to the electronics era. The main breakthrough was the good spatial resolution achieved before the introduction of silicon trackers with energy loss measurement and time resolution. The limiting factor was the minimum distance between wires of the order of 1 mm due to mechanical and electrostatics forces [152]. Six years later, with the advent of the Time Projection Chamber (TPC) by David Nygren and the implementation of fast enough electronics to the MWPC wires allowing to measure time differences and therefore the full three dimensional reconstruction of a track.

MWPC were succeeded by Micro-Pattern Gas Detectors (MPGD) when the wires were replaced by a readout implemented by means of printed circuit board techniques allowing much better spatial resolution, faster signals and higher counting rates. The first example of MPGD was the Micro Strip Gas Chamber (MSGC) [127] in 1986 where metallic strips were printed on a glass base. The main vulnerability was that the thin metal layers were damaged by discharges. In addition a degradation of the gain with time appeared due to charge accumulation. In the 90's, different families of MPGD detectors were developed in order to overcome the drawbacks of the MSGC. Today the most used devices are Gaseous Electron Multipliers (GEM) and Micro MEsh GAseous Structure (Micromegas). MPGDs are well established technologies that are used in a very wide range of applications in the High Energy Physics community but also in astroparticle and neutrino physics. These technologies are now mature enough to transfer the production of crucial detector components to industry in order to be able of supplying a very large quantity of detectors in the coming years [72]. Another sign of the level of maturity is the fact that there are applications outside our communities, like for screening for homeland security or muon radiography for geological studies, that are emerging.

In the next sections, I focus on the Micromegas technologies to which I have been contributing since 2002. GEM detectors will also be described for completeness.

---

[1]Exceptions are the nuclear emulsions for which the resolutions that can be achieved are at the level of microns, $1\,\mu$m being the size of the sensitive grains [149].
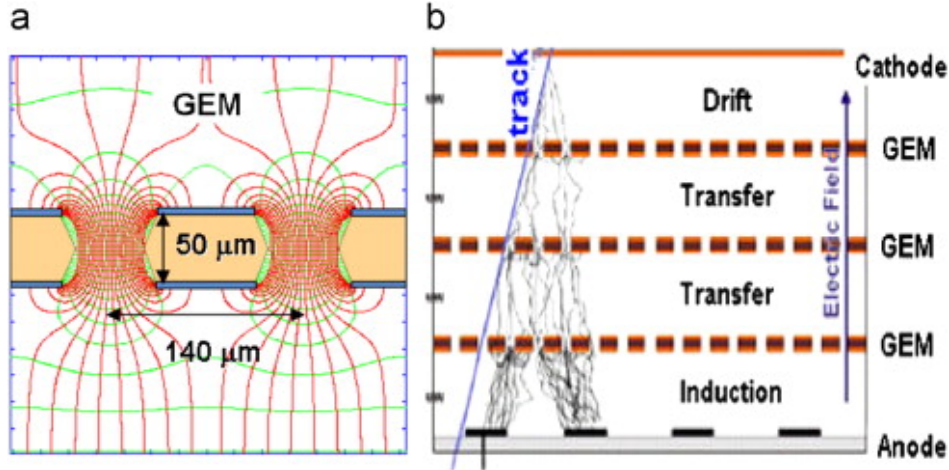
Figure 3.1: Left: Schematic view of a GEM cell with the electric field configuration. Right: Schematic view of a triple GEM [152].

3.2 Modern Micro Pattern Gaseous Detectors: GEM and Micromegas

MPGDs can be divided into two categories [152]: Strip and hole structure giving rise to the Gaseous Electron Multiplier (GEM) type of the detectors and its declinations (THGEM, REGEM...) and micromesh based structures developing in the Micromegas type detectors (classical, bulk, microbulk, ingrid).

3.2.1 GEM

The GEM [143] was introduced in 1996. It consists of a thin copper clad film, i.e. copper, insulator, copper and the insulator being often $50\,\mu$m kapton, that has been chemically etched to obtain a high density of holes. A schematic view can be seen in figure 3.1 left. When applying a potential difference between the two sides of the GEM, the electric field generated concentrates the field lines through the holes to work as amplification regions, shown on the right of figure 3.1. When placing a drift electrode above the GEM foil, the electrons released by the primary ionisation drift into the holes where amplification takes place in the high electric field (50-$70\,$kV/cm). The avalanche electrons will be transferred into the gap below the GEM. Normally several (2 or 3) GEMs are used together in order to distribute the gas gain over several gaps reducing the risk of discharges. The hole diameter is typically of the order of 25-$150\,\mu$m with a distance between holes of 50-$200\,\mu$m.

COMPASS is the first high luminosity experiment using GEM (and Micromegas) at large scale reaching a flux of $25\,$kHz/mm^2 with large triple-GEM ($30{\times}30\,$cm^2) with an excellent tracking efficiency and no degradation in performance after an accumulated charge of a few mC/mm^2 [151]. GEMs are also used in TOTEM, a set-up integrated into the CMS experiment to measure the total proton-proton cross-section [24]. In LHCb, GEMs are being used as the first station of the muon detector in the most inner region [4]. Furthermore GEMs have been used in KLOE [25] as a tracking system composed of four tracking layers each realised as a cylindrical triple-GEM.
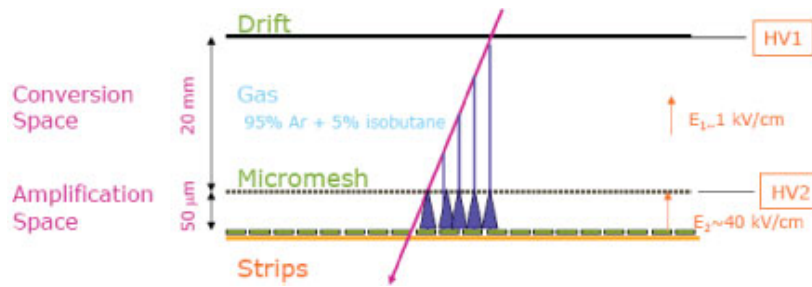
Figure 3.2: Transverse view of the main elements of a Micromegas detector.

3.2.2 Micromegas

Micromegas (MICRO-MEsh-GAseous Structure) is a two-stage avalanche chamber with a narrow amplification gap defined by the anode plane and a thin micromesh [88, 87], and a drift region with dimensions that range between a few mm and a few meters depending on the application. A sketch of the structure is given in figure 3.2. The parallelism between the micromesh and the anode is maintained by insulator spacers that are normally layed down by means of conventional lithography. Figure 3.3 shows the typical funnel shape of the electric field around the holes of the micromesh due to a much larger electric field in the amplification gap than in the drift region ($E_{\mathrm{amp}} \gg E_{\mathrm{drift}}$). When a charged particle enters the drift region, the primary electrons produced by ionisation drift towards the amplification gap thanks to the constant electric field, E_{drift}. In the amplification gap an avalanche process takes place due to the large amplification electric field, E_{amp}. The advantages of Micromegas detectors have been described extensively elsewhere [88, 87]. Here we mention briefly the most important:

- The relative small amplification gap (20-128 μm) is an advantage as locally small variations due to the mechanical imperfections will not produce gain fluctuations [87] resulting in a very stable behaviour.

- Micromegas detectors have been tested in a large variety of gases and can reach high gains. The standard mixture for 50 μm gaps is Argon + 5% Isobutane where gains of 10^5 can be easily achieved.

- The charge signal is mainly due to the positive ions drifting to the micromesh depending on the amplification gap and the gas mixture. With fast enough electronics, the electron signal (much faster than the ions signal) can be detected with a rise times of less than 1 ns.

- Spatial resolutions better than 50 μm can be obtained by optimisation of the gas mixture and the anode readout plane.

- The rate capability of Micromegas detectors has been tested in different environments [53, 87]. Fluxes of X-rays and charged particles as high as $10^7/\mathrm{mm}^2/\mathrm{s}$ do not present a problem [74].

- The radiation resistance of Micromegas detectors was extensively proven in the early days [33, 150] and has recently been demonstrated again with more recent detectors [85, 121].
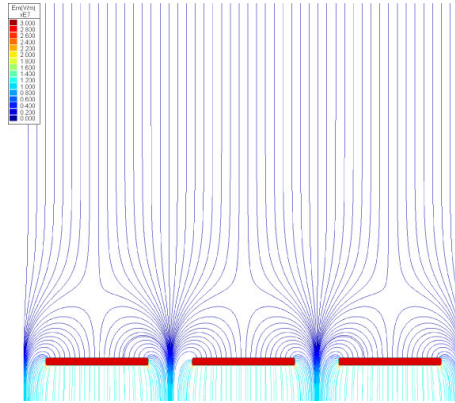
Figure 3.3: Electric field configuration of a Micromegas detector.

- Single electron detection capability has been measured in photodetector mode [75] and with neutrons [97]. In these configurations time resolutions better than nanoseconds have been achieved.

- Micromegas detectors can be manufactured from very radiopure materials like copper and kapton resulting in extremely radiopure detectors [48, 49].

- The Micromegas micro-mesh has the intrinsic property to naturally stop a large fraction of the secondary positive ions created in the avalanche. Ion feedback is reduced to the percent level [57].

Having described the GEM and Micromegas technologies, it might be of interest to underline the main differences[2] [159]:

- The charge development in Micromegas happens within a few tens of microns while in GEM, due to the diffusion in the space transfer, takes place in hundreds of microns.

- The signal development in GEM is only due to electrons while for Micromegas there is a fast contribution from electrons and the main contribution is due to the ions.

- The amplification of GEM is rather low for one single GEM electrode but it is possible to use several GEM foils resulting in an amplification that is comparable to the one obtained with a single Micromegas detector. GEM, being a preamplification structure, needs at least a third electrode (collection) to get a signal. Exceptions are the Thick-GEM (THGEM) [42] where large gains can be easily obtained. Moreover depending on the collection field only part of the charge cloud is collected while in Miromegas the full charge is recovered, i.e there is no ballistic deficit. In addition, the efficiency to primary electrons in Micromegas is larger than 95% while for GEM is much smaller.

- In Micromegas, the ion back flow can be controlled rather well with the field ratio and the mesh transparency. In standard conditions, the Micromegas ion back flow is at the few percent level. However with special configurations, levels down to the 10^{-6} can be reached [109].

---

[2]A GEM fan would probably not express these differences in the same way. The reader is invited to visit [76] in order to build his/her own opinion.

- At fixed total gain, the spark rate of 3 GEM foils compared to the one in Micromegas is lower. However recent solutions with resistive anodes used in Micromegas, discussed in the next sections, can overcome this effect.

- Dead zones can be minimised more easily with Micromegas detectors and coverage of large areas is simpler.

- GEMs are more sensitive to cleanliness during their lifetime than Micromegas. The user needs to develop the know-how, the tooling and the appropriate conditions to operate GEMs in clean conditions and often results in an increase of operation cost.

- The cost of the Micromegas detectors, specially the bulk technology with a metallic industrial mesh described in the next sections, is low compared to 3 GEM foils manufactured with a more delicate and expensive manufacturing procedure involving copper and kapton etching.

- Finally, operation with Micromegas is simpler as usually only one high voltage is needed while in GEM the number of voltages needed is twice the number of GEM foils to be used (normally 3 GEMs are needed for operation so 6 high voltages are required).

In the next sections we concentrate on the different Micromegas technologies. A classification is made related to the type of mesh that is used and the manner that the insulator spacers are manufactured and disposed. We also cite the development of resistive Micromegas, initially in the aim of charge sharing and latter for spark protection.

3.3 The Micromegas technologies

3.3.1 Standard

In the first Micromegas the spacers were glued on the anode plane and the micromeshes were suspended on top of them. A type of spacers that was first used were fishing lines of $100\,\mu$m diameter. Later, spacers were layed down by standard techniques of lithograhy on the anode plane or electroformed micromeshes were produced with pillars attached to them. The parallelism between the anode and the mesh depended greatly on the manufacturing of the mechanics of the detector and on the expertise of the user. The first Micromegas applications in the 2000's were using this technology. Examples are the NTOF experiment installed in 2001 for neutron flux monitoring [128] and the COMPASS [114] experiment at CERN using chambers of 40×40 cm^2 since 2002. The first CAST detectors [2] used from 2002 to 2006 were also using this type of Micromegas.

These standard Micromegas were more or less abandoned after the advent of bulk and microbulk technologies in 2006-2007 described in the next subsections. In the more recent technologies instead of having two separate components (mesh and anode plane) the amplification structure is manufactured in a single entity. This classical technology will have a new life with the future production of $1200\,$m^2 with the upgrade of the muon chambers of the ATLAS New Small Wheel [58] for the upgrade of the luminosity of the LHC, High Luminosity HLC (HL-LHC), in 2018. It has been shown that this classical technology seems to be the most favorable and optimised for the production of the required large size and large number of detectors [58, 164].
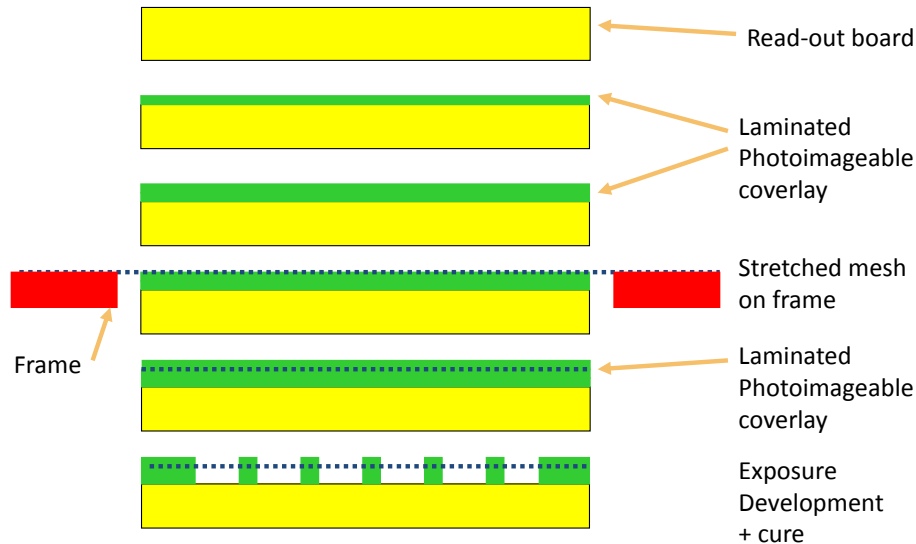
Read-out board

Laminated
Photoimageable
coverlay

Stretched mesh
on frame

Frame

Laminated
Photoimageable
coverlay

Exposure
Development
+ cure

Figure 3.4: Manufacturing process of the bulk Micromegas detectors [73].

3.3.2 Bulk technology

In bulk Micromegas [89] a commercial woven mesh is encapsulated in insulators pillars by a standard printed circuit board (pcb) process. A summary of the process is given in figure 3.4. The main steps consist in placing a stretched mesh between layers of insulator (often two on bottom and one on top) directly on a readout plane. A mask with the pattern of the pillars is placed on top of this stack and is illuminated by ultraviolet light. The parts that are illuminated stay when going through a chemical bath that removes the non-illuminated regions. The final structure is a readout plane with an encapsulated mesh between insulator pillars giving very robust and easy to manufacture Micromegas detectors. These types of detectors were developed by IRFU/SEDI and Rui de Oliveira's CERN workshop. They are presently produced at CERN and at the IRFU bulk workshop. Moreover there is an ongoing effort to industrialise this manufacturing process and good progress has been achieved with two european companies, ELVIA in France and ELTOS in Italy.

The typical amplification gap of a bulk detector is $128\,\mu$m but multiples of $64\,\mu$m (the raw material of insulator has this thickness) are possible and 64, 192, 256, $512\,\mu$m have already been manufactured with a $35\,\mu$m thick woven mesh. These detectors achieve high gains and have reasonable energy resolutions (20% FWHM at $5.9\,$keV) for gaseous detectors. They are used in many different applications. For instance, bulk Micromegas cover the largest MPGD TPC ($9\,\text{m}^2$) in the T2K [82] experiment and survived without problem the Japan tsunami in 2011. Another example of Micromegas TPC is the MINOS TPC [126] tested successfully in 2013. Bulk Micromegas have also been used in the MIMAC collaboration, an R&D effort

to build a directional gaseous TPC for dark matter search that is discussed in more detail in chapter 6. The CLAS12 [131, 52] experiment is also finalising the design and construction of bulk Micromegas detectors to operate them in the near future in a magnetic field. These bulk detectors are for the first time of cylindrical shape for the following reasons [132]:

- optimise the hermeticity of the detector;

- reduce the volume occupied;

- minimise the number of electronic channels, as this number is proportional to the number of tiles which is much larger in the case of polygonal tiles.

3.3.3 Microbulk technology

The microbulk technology resembles the bulk technology in the sense that the final structure is a single entity with the micromesh and the anode plane in one single entity. However the main constituents are different: the raw material is a thin flexible kapton foil (of 50, 25 or even $12.5\,\mu$m thickness) with a 5 μm copper layer on each side (figure 3.5 step 1). The manufacturing process is based on lithography and is skteched in figure 3.5. A thin photoresistive film is laminated on top of the kapton foil and it is illuminated by UV light to produce the required mask (figure 3.5 step 2). The copper is then removed by a standard lithographic process and the non-illuminated regions produce a pattern of a thin mesh. The kapton is then etched and partially removed in order to create tiny pillars in the shadow part below the copper mesh. The holes are of a typical diameter of $40\,\mu$m with a pitch of $100\,\mu$m. A microscope picture of the top layer is shown in figure 3.6.

Thanks to their thin mesh and to the homogeneity of the gap, the achieved energy resolutions are extremely good for a gaseous detector,~11% (FWHM) at $5.9\,$keV in an Argon + %5 Isobutane mixture, close to the theoretical attainable statistics-limited value of 10.8%. This will be discussed in more detailed in chapter 6. Microbulk detectors are less robust to sparks than bulk detectors. However they have been used with remarkable stability in the case of the CAST experiment (see chapter 4) for long data taking periods and in the NTOF experiment as a neutron beam profiler [34, 7, 92]. Microbulk detectors are currently being developed by the NEXT Micromegas R&D line where energy resolutions of 7.3% (9.6%) FWHM at 1(10) bar at $22\,$keV are obtained [51, 67, 66]. This extrapolates to very competitive values at the two-electron energy end point $Q_{\beta\beta}$ of Xe, opening very good prospects for double beta decays experiments.

3.3.4 Resistive anode Micromegas: charge dispersion and spark protection

The first Micromegas with a resistive coating were developed in the context of the R&D for the ILC-TPC. The idea was to increase the charge dispersion by means of a resistive coating in order to decrease the total number of electronics channels keeping a good spatial resolution while reducing the total cost of the detector. This was demonstrated in [78]. It was soon realised that with this strategy the sparks limit was surpassed and sparks were aborted. For high flux environments, where the consequences of sparking need to be reduced, resistive Micromegas detectors are an interesting solution. In the last years an active program of R&D has been developed for resistive strip readout in particular in the frame of the upgrade of the muons detectors of the New Small Wheel (NSW) for the High Luminosity LHC (HL-HLC)
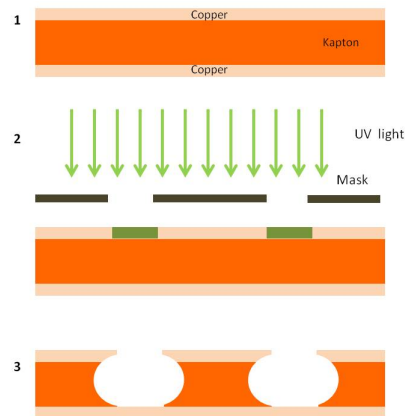
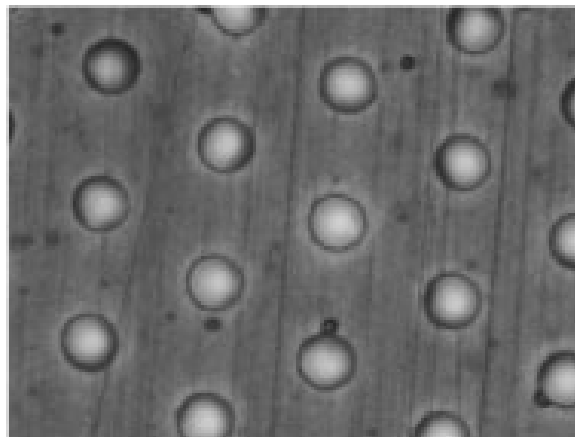Figure 3.5: Manufacturing process of the microbulk detectors.

Figure 3.6: Photo of the surface of a Microbulk detector. The holes diameters are usually of $40\,\mu$m while the pitch is $100\,\mu$m.
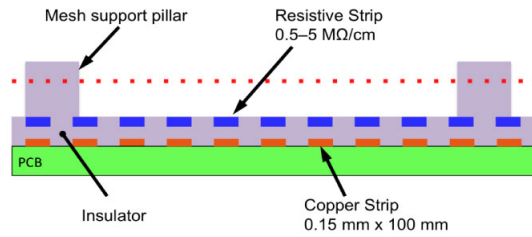
Figure 3.7: Sketch of the resistive Micromegas detectors to be used in the upgrade of the ATLAS New Small Wheel for the HL-LHC.

that is expected to start in 2018 [3]. The luminosity upgrade is expected to be in two stages: first by a factor of three in collision rate then by a factor of ten for the nominal HL-LHC phase-II. In this environment, the high flux of hadrons can produce highly ionizing events that leads to large energy deposit and an increasing probability for sparks in Micromegas detectors. The main concern is the induced dead time (few ms) to recover the nominal voltage after the discharge of the mesh. The solution that has been adopted is to use resistive strips embedded on an insulator on top of the copper strips as shown in figure 3.7. The required surface is $1200\,\mathrm{m}^2$ representing more than 2 millions electronic channels for a surface integration in 2017. Resistive Micromegas detectors will also be used for the forward tracker of the CLAS12 tracker [131].

3.3.5 Gridpix technology

Gridpix is a detector integrating a Micromegas grid with a pixel readout chip as the signal collecting anode manufactured by microelectronics techniques [54]. This technique has been developed by the MESA institute and the University of Twente. The precision of the Micromegas grid (InGrid) on silicon wafers (holes controlled to $1\,\mu$m precision and gaps varying less than 1%) results in an excellent resolution $\sim$12% (FWHM) at 5.9 keV in an Ar+10% Isobutane mixture with high enough gains to detect single primary electrons and to observe Auger and photo-electrons.

The first tests were done with a thin mesh built on top of a Medipix-2 chip [158]. The structure was designed in such a way as to completely minimise the dead space due to the Micromegas pillars as the grid holes are perfectly aligned with the pixel input pads and the pillars aligned with in inter-pad space. The main problem that limited the lifetime of the structure to only of a few minutes were the discharges that are unavoidable in gaseous proportional detectors. In order to protect the chips, a high resistivity layer was deposited on top of the chip as described in the previous section. Different materials and thickness were tested and a 4-8 μm of Si-rich Silicon Nitride proved to be ideal.

Gridpix is being developed for the readout of large TPC for the future linear collider. Low cost Gridpix chips will need to be developed to build large area readout panels. The extreme sensitivity of this detectors can suggest applications such as the detection of photon polarisation [16]. Another possible application is the developing of gaseous vertex detectors by using a small drift gap of the order of 1 mm on top of the Gridpix the so called Gas On Slimmed Silicon Pixels (Gossip). Recently a Gridpix detector is being developed and optimised to be implemented in the CAST experiment for the 2014 data taking run coupled
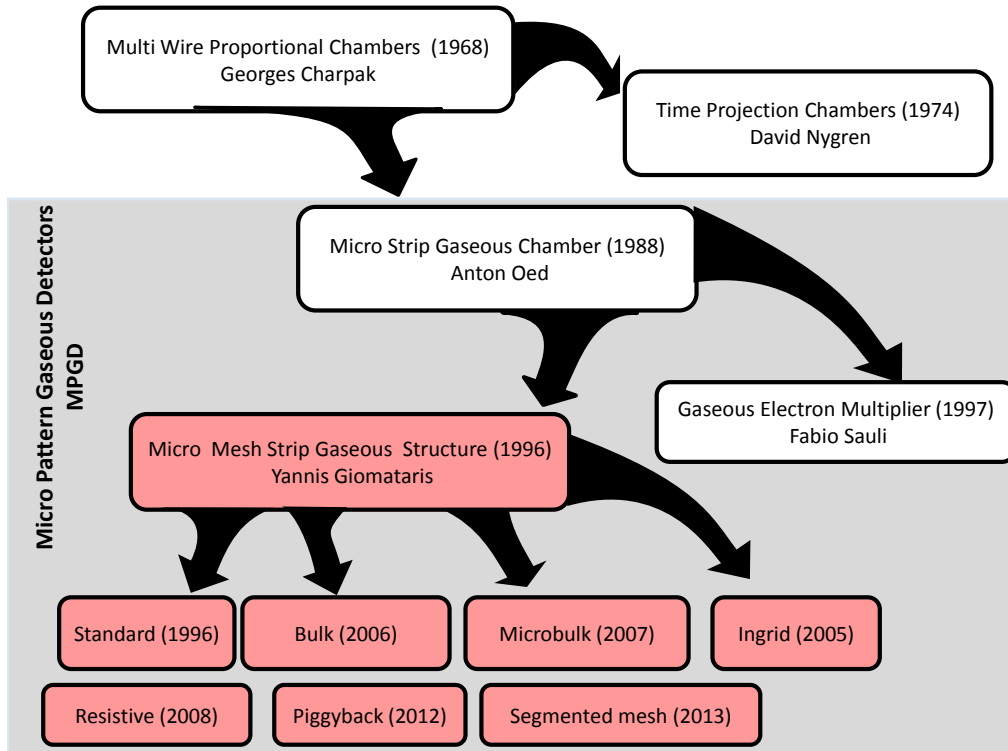
Figure 3.8: Micromegas genealogical tree and present technologies from [108].

with the XMM X-ray telescope [110].

3.4   Conclusions and outlook

The Micromegas detectors are used in a large variety of High Energy Physics, Astroparticles and Nuclear Physics experiments in very different contexts thanks to the adaptability of the different technologies depicted in figure 3.8. A summary of the main advantages of each technology is given in figure 3.9. The technology has arrived at a level of maturity that makes the large production of robust detectors possible by industrial partners. Novel recent structures, the Piggyback and the segmented mesh microbulk detectors, will be described in more detail in chapter 6.

Apart from the academic context, Micromegas detectors have been used or are being currently developed for a growing number of societal applications such as the detection of forest fires, geological characterisations, oil search, and homeland security.
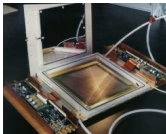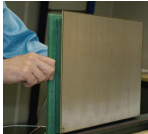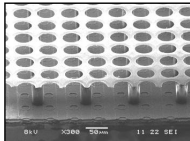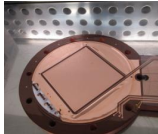
	STANDARD 1996	BULK 2003	INGRID 2005	MICROBULK 2006
Mesh Readout plane	TWO mechanical entities	INTEGRATED: ONE single entity		
Type of mesh	Any type	30 µm Stainless steel	1 µm Aluminium	5 µm Copper
Advantages	Demontability Large Surface	Robust Industrial manufacturing process (PCB)	Excellent energy resolution Single electron efficiency	Intrinsically Flexible Low mass Radiopure

Figure 3.9: Summary of the advantages of the different Micromegas technologies.

Chapter 4

Evolution and performance of Micromegas detectors in the CAST experiment

4.1 Introduction

In order to detect the photons from axion conversions, the sensitivity of the CAST detectors needs to be optimised for low-energy X-ray photons (1–10 keV). The possible signal must be distinguished from sources of background like cosmic rays and natural radioactivity. Gaseous detectors present the advantage of being able to reconstruct tracks and at the same time they can access both the energy and the track properties. With the advent of Micropattern gaseous detectors, the possibility to design and to build precise readout planes making possible the reconstruction of low-energy (few keV) tracks of a few mm length is simpler and easier than with conventional wire planes. In particular, the advantages of Micromegas detectors for rare event searches, like the ones required for the CAST experiment, were first suggested in [68]. These advantages include sensitivity in the keV and sub-keV energy region where a good energy resolution can be achieved, good spatial resolution, one-dimensional or $x - y$ readout capability, stability, construction simplicity and low cost. In addition, the proper choice of construction materials can lead to a detector appropriate for low-background measurements.

In the lifetime of the CAST experiment, the Micromegas group has improved constantly the performance of its detectors reducing the background level by more than two orders of magnitude with respect to the first detector used in 2003 as is shown in figure 4.1.

This chapter reviews the path followed to achieve this performance. The first section describes the first unshielded classical detectors used from 2003 to 2007. Section 2 is devoted to the microbulk detectors used up to 2012. The third section summarises briefly the underground and background simulations studies that conducted to the design of new shielding configurations, that are reported in section 4. The latest microbulk detector representing the state-of-the-art that has been installed recently in CAST is described in section 5.
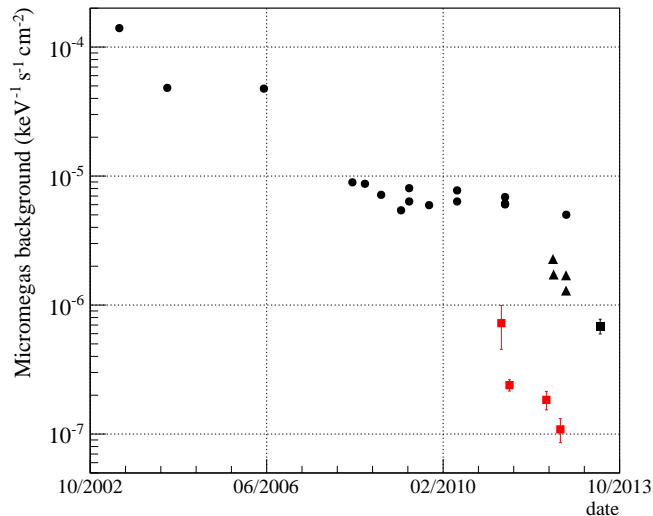
Figure 4.1: Micromegas background history. The (round and triangle) black points correspond to the values obtained with the different detectors in the CAST experiment while (square) red points correspond to different shielding configurations in the Canfranc Underground Laboratory. The first three points, with background levels above 10^{-5}, were obtained with non-shielded standard Micromegas detectors. The rest of the points correspond to data obtained with shielded Microbulk detectors.

4.2   Standard unshielded Micromegas: 2003-2007

4.2.1   Detector description

The first Micromegas detector in the CAST experiment was mounted on one of the two west superconducting magnet apertures looking for "sunrise" axions converted into X-ray photons entering the detector active volume perpendicularly to the $x - y$ strip plane. A sketch of the set up is given in figure 4.2.

The novelties with respect to other Micromegas detectors existing at the time were the following:

- **The selection of construction materials.** The detector was made out of selected low radioactivity materials: plexiglass for the body and the support of the readout plane, kapton for the readout plane and copper for the micromesh.

- **Bidimensional readout used for the first time.** The charge collection strips were made out of a $x - y$ structure on a copper double faced kapton foil. The x strips were on one side of the kapton film and the y strips were connected on the other side of the film by metallised holes depicted in figure 4.3. The total active area was of $45\,\mathrm{cm}^2$ largely exceeding the $14.55\,\mathrm{cm}^2$ of the projection of the magnet bore, with two hundred strips per direction with a pitch of $350\,\mu\mathrm{m}$.

- **The signal of the micromesh was used as the trigger.** At the same time the
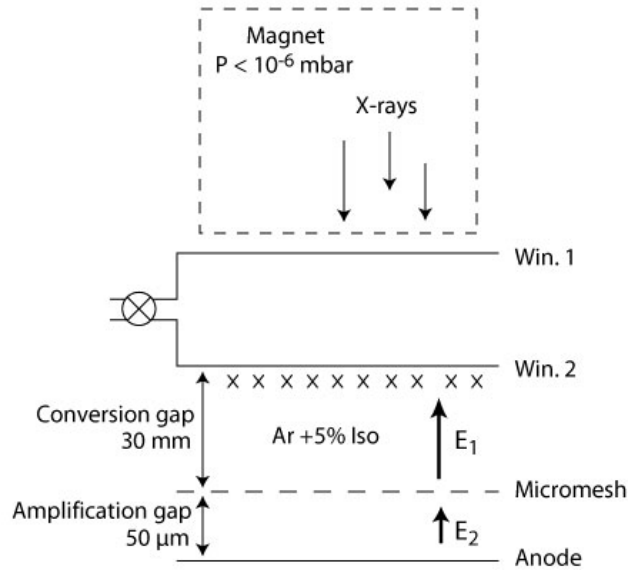
Figure 4.2: The coupling of the CAST Micromegas detector to the magnet bore. Transparent X-ray windows are needed in order to couple the gaseous volume of the Micromegas detectors with a vacuum environment maintaining maximal transparency and minimal vacuum leak.

pulse characteristics were exploited for background discrimination.

- **A differential window system.** Such a system was necessary in order to couple the Micromegas gaseous volume with a vacuum environment, keeping the maximum transparency to X-ray photons and a minimum vacuum leak. The solution of two $4\,\mu$m polypropylene windows with a differential pumping was adopted.

A detailed description of this detector can be found in [2]. The readout strips were read by front end cards developed in house based on the Gassiplex chip [142] while the mesh signal was recorded by the MATACQ (MATrix for ACQuisition) [43] board allowing a sampling frequency of $1\,$GHz and an acquisition window of $2.5\,\mu$s per event. The data acquisition and monitoring system was based on LabView software and was developed by the Demokritos group.

4.2.2 Calibration

Before the installation in the CAST experiment, one detector was characterised in the PAN-TER X-ray facility of the Max-Planck-Institut für extraterrestrische Physik (MPE) in Munich in spring 2002. The simulated efficiency of the detector was validated with experimental data at different energies and could serve as a basis for later configurations with different parameters. Moreover the detector was mounted in the focal plane at the X-ray focusing telescope that would be later installed in CAST. For the first time the $x-y$ position determination capability was shown. A remarkable agreement with the beam shape expected from the focusing properties of the X-ray telescope was exhibited [5].

In order to control the stability and performance of the detector during data taking campaigns a calibrator system was developed. The system consisted on an automatic mechanism

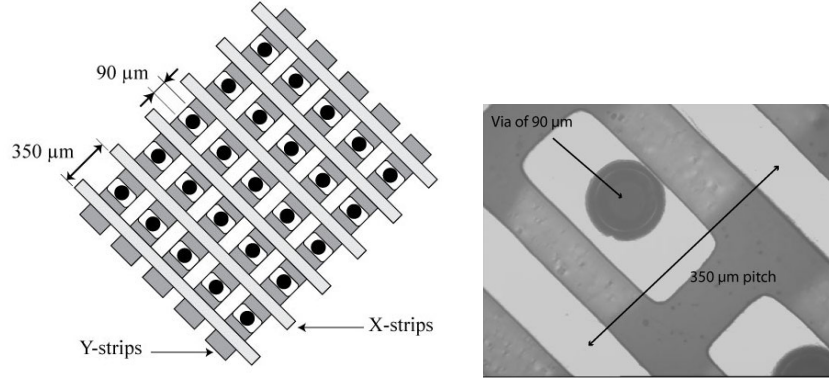Figure 4.3: The readout plane of the first CAST Micromegas detectors. On the left a schematic of the 2D design. On the right a picture of one of the detectors. The metallised holes (vias) can be observed.

controlled by the acquisition that placed an ^{55}Fe source at the back of the detector daily. The source was housed inside a lead shielding the rest of the day. The daily calibration is also useful to evaluate the efficiency of the detector: the 5.9 keV peak due to the k_α (5.9 keV) and k_β (6.5 keV) emissions of the ^{55}Fe source in the ratio of 8.5/1[91]. This energy is well in the region of interest for the axion-photon conversions. In fact we profit from two other peaks: the 3 keV Argon escape peak and the 8 keV Copper fluorescence peak due to the copper present in the mesh and in the readout strips. These peaks serve to estimate the efficiency of the discrimination algorithms. The Micromegas detector was calibrated daily. "Tracking" occurred at sunrise and during the rest of the day background data was recorded.

The calibration strategy has not changed since then. In addition, since 2007, the CAST experiment has set up a dedicated "detector laboratory" [155, 90] where the detectors can be tested at different energies with an electron beam based on PIXE (Particle Induced X-ray Emission).

4.2.3   Detector Performance

Strategies for background rejection and performance

The signal events, from axion conversions into photons of energies 2-8 keV, have a well defined signature. The main sources of background are due to cosmic rays and natural radioactivity. Figure 4.4 shows schematically the difference between an "axion-like" event and a typical cosmic ray event. The signals induced on the mesh and on the strips are shown on the left side for the axion like events and on the right side for cosmic rays. It is observed that the signal events have a localised energy deposition while background events are more dispersed. In addition the pulse signals for the two types of events are topologically different.

These pictures are the basis of the background rejection strategies. The analysis has been refined during the years, but the discrimination is always based on cluster topology and mesh pulse characteristics. The selection procedure is focused on the following points:

- **Localised energy deposition in the strips for signal events:** leading to restrictions on the cluster size.
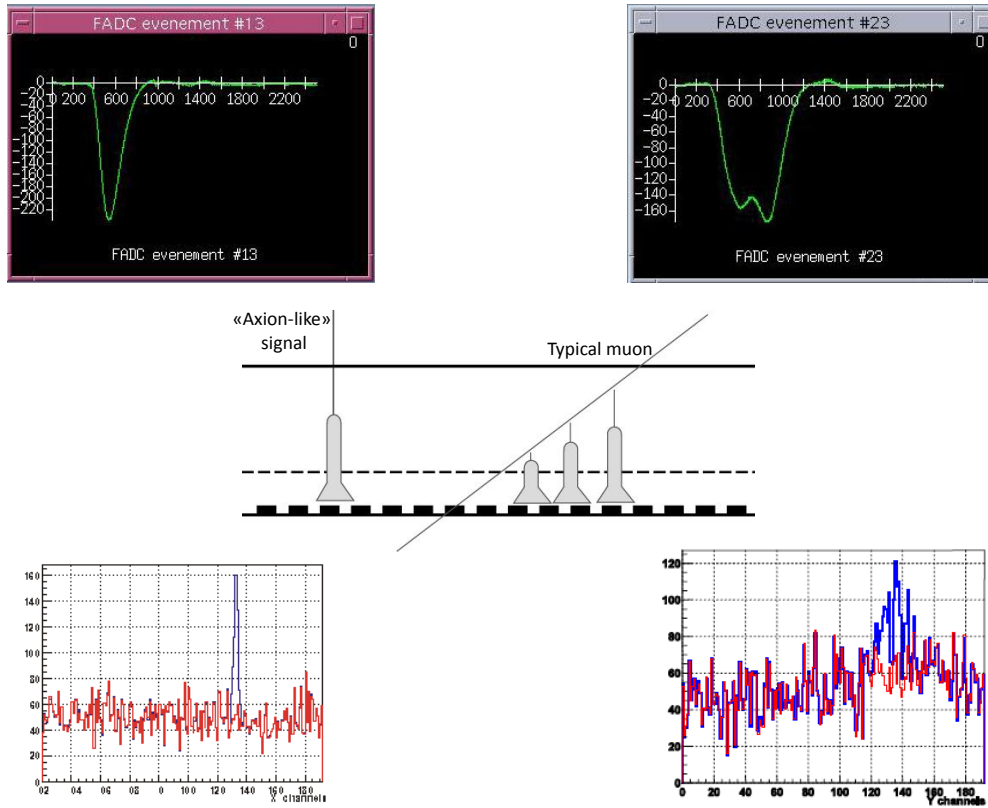
Figure 4.4: Topological differences between a "signal-like" event and a cosmic ray. The induced signals on the mesh and on the strips of the anode plane are represented.

- **Balance between $x-y$ energy depositions:** for signals events the energy deposition in the two readout directions is equivalent resulting in the same number of fired strips.

- **Pulse characteristics of the mesh signal:** leading to selection cuts on rise time and amplitude.

- **Correlation of the energy measured in the strips and in the mesh.**

In figure 4.5 the background spectra after the selection cuts are shown. The first averaged background obtained in 2003 with a sequential cut analysis was of 1.4×10^{-4} counts $\mathrm{keV}^{-1}\,\mathrm{cm}^{-2}\mathrm{s}^{-1}$ with an efficiency of 95% for 5.9 keV. The strip cluster information could not be completely exploited due to crosstalk between strips caused by residual copper left on the kapton pillars of the micromesh. This effect was not present in the new detector used for the 2004 data taking campaign where the background obtained was of 4.8×10^{-5} counts $\mathrm{keV}^{-1}\,\mathrm{cm}^{-2}\mathrm{s}^{-1}$ with an efficiency of 92%. The detector was slightly different: the amplification gap was of 100 μm instead of 50 μm; the pillars were made out of kevlar instead of kapton and a micromesh was suspended on top (instead of "plotted" micromesh used in 2003). The selection analysis used in 2004 was based on a discriminant method instead of on sequential cuts. Despite these differences, the common main characteristic of these spectra is the peak at 8 keV. This peak,

as mentioned before, comes from the fluorescence due to the copper present mainly in the anode plane and in the copper strips. The background origin is discussed in more detailed in the following sections. The level of background, obtained with an unshielded detector in 2004, was comparable to the level obtained with the shielded TPC.

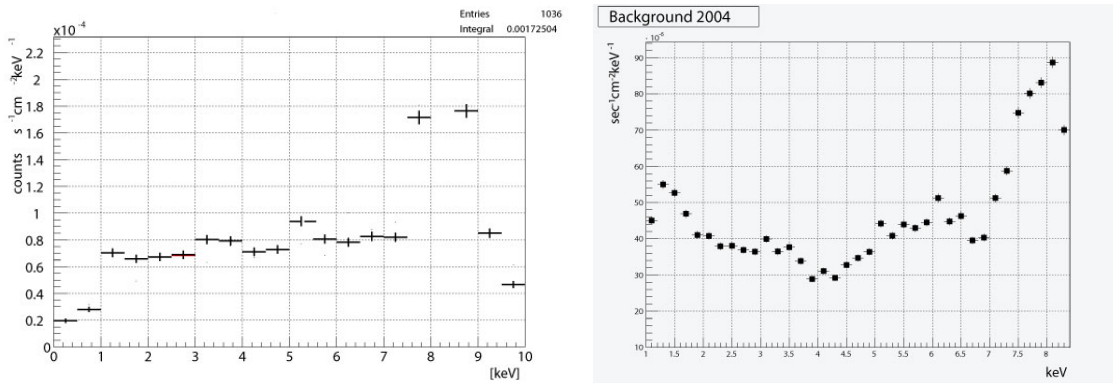Figure 4.5: Spectra obtained after the selection cuts for the 2003 and 2004 data taking periods. The detectors used were different and the analysis selection was sequential for 2003 and for 2004 a discriminant method was used.

Test with shielding

The reduction of background observed by the CAST TPC due to the insertion of shielding motivated the Micromegas team to also test the effect of shielding. In 2005, profiting from the shutdown for the adaptation of the magnet to operate with a buffer gas, the sunrise Micromegas detector was dismounted and covered by "bricks" of 5 cm of lead. The effect is shown in figure 4.6. The background reduction in the region of interest is more than 50%. After this result, it was decided to design a new detector that would make possible the insertion of shielding in the so much reduced space that was available due to the presence of the X-ray telescope in the neighbour line. Moreover contacts with a team of Lawrence Livermore National Laboratory (LLNL) were established in order to also include an X-ray focusing optics in the new sunrise Micromegas line that would allow a further improvement on the signal-to-noise ratio. The new sunrise Micromegas line will be the object of the next section. Furthermore, after this test, the CAST collaboration realised that the Micromegas detectors could potentially achieve much better backgrounds. The combined fact that the performance of the TPC covering the two locations of the sunset side was degraded by ageing together with the fact that a new Micromegas detector was being designed, convinced the CAST Collaboration to replace the sunset TPC by two new shielded Micromegas detectors.

Conclusions

The first Micromegas detectors used in the CAST experiment were standard Micromegas detectors. The use of the mesh signal for background discrimination resulted in an improvement of the background level. The first shielding test performed in 2005 motivated the design of a new more compact detector that could accommodate passive shielding. The results of this test incited the CAST collaboration to replace the existing sunset TPC by two Micromegas
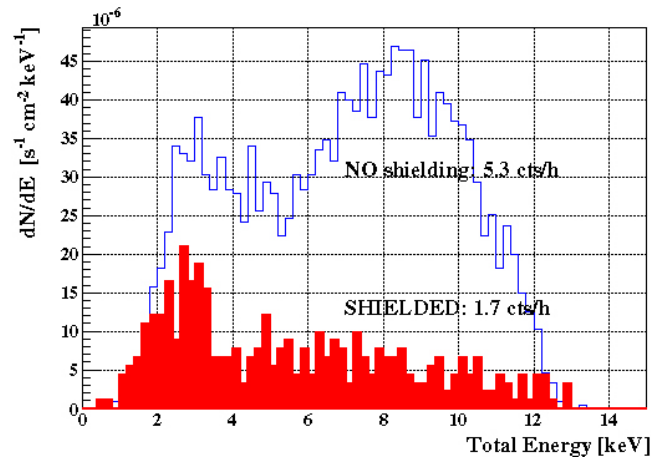
Figure 4.6: Effect of the copper shielding on the background reduction.

Period	Characteristics of the detectors Standard Micromegas	Background mean rate (10^{-5}counts keV^{-1} cm^{-2}s^{-1})
2003	Kapton plotted copper mesh $50\,\mu$m amplification gap Stainless steel cathode	14.0
2004	Copper mesh, kevlar plotted readout plane $100\,\mu$m amplification gap Aluminium cathode	4.8
2005	Same detector as in 2004 Shielding 5 cm lead	1.5

Table 4.1: Summary of the background levels achieved for the first Micromegas detectors installed during the 2003 and 2004. In addition the level of background achieved with lead and copper shielding is also given.

detectors. A summary table of the levels of backgrounds achieved during this period is given in table 4.1.

4.3   Shielded microbulk Micromegas: 2007-2012

The design of the detector was identical for the sunrise and for the sunset detectors. However the shielding geometry was different for the two locations even if the components and their thickness were the same. Moreover the sunrise side was designed to accommodate the X-ray optics. The design of the sunrise line is detailed in the following sections.

4.3.1   Sunrise Line design

The strategy for the new line was based on:

- the use of low radioactive construction materials;

- the design of a dedicated passive shielding;

- the use of focusing optics to concentrate the signal into a few mm diameter spot.

A sketch of the line is given in figure 4.7. The shielding configuration was limited by the available space on the magnet platform. From inside to outside, it consisted of 5 mm of copper to stop low-energy particles entering the detector, 2.5 cm of archaeological lead covered by polyethylene shielding of different thickness (up to 10 cm) depending on the space available for neutrons, followed by a cadmium shielding to absorb thermalised photons. These three layers were enclosed in a cylindrical plexiglass in order to flush nitrogen around the detector to limit radon concentrations.
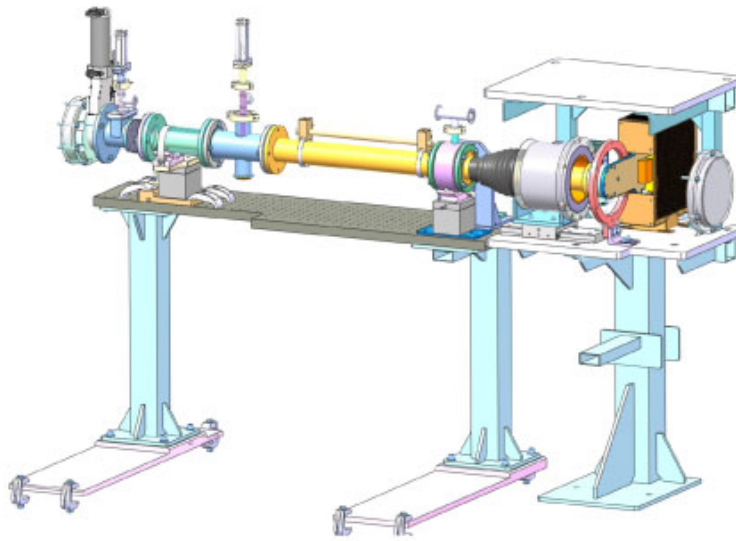
Figure 4.7: A sketch of the design of the new Micromegas line with the detector in the Faraday cage surrounded by the shielding.

The operation conditions of the detectors were modified slightly with respect to the conditions of the previous data taking campaigns. The percentage of Isobutane was decreased to 2.3% (instead of 5%) in order to be just below the inflammability threshold and ease safety requirements. Moreover the operation pressure was increased to 1.4 bar to increase the efficiency of conversion of photons, reaching 74% in the range of 2-7 keV convoluted with the axion spectrum. The gas system was designed to maintain a constant pressure with a regulated flow.

4.3.2 Optics

The purpose of the X-ray optics is to focus the potential X-ray signal to an as small as possible spot, and doing so, reduce the size of the detector required and, ultimately, the detector background. The performance of an X-ray optics can be characterised by three quantities: the shape of the focusing spot called the point spread function (PSF); the throughput that is the amount of incident photons properly focused by the optics; and the field-of-view (FOV), the extent to which the optics can focus off-axis photons. Optimising of these properties
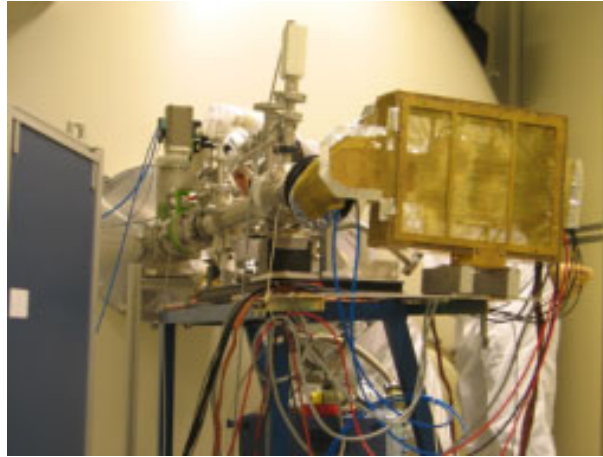
Figure 4.8: The Micromegas line in the Panter X-ray facility while tuning the alignment of the collimator. The detector is surrounded by its Faraday cage.

is a compromise between the focal length that should be the smallest possible in order to have the smallest spot area and the X-ray reflectivity that is enhanced with focal length. With these considerations and the space available in the CAST experiment hall the designed optics consisted in a concentrator with a 1.3 m focal length and a 47 mm diameter, allowing to increase the signal to noise ratio by a factor ~ 100 by focusing the photon flux to a 2 mm spot. This concentrator consisted of 14 nested polycarbonate shells, each 125 mm long and coated with iridium. The optics was designed to transmit $\sim 36\%$ of the 0.5 -10 keV flux emerging from the magnet bore. A new manufacturing method was developed by Lawrence Livermore National Laboratory using plastic substrates [144].

The detector with the integrated optics was tested at the PANTER X-ray test facility in Munich in September 2006. A picture of the set-up is shown in figure 4.8.

The aim of this test was first, to characterise the collimator measuring the focal length, the point spread function and the throughput (effective area). Secondly, to couple the collimator to the detector and measure the overall performance.

The test was very useful in providing experience in the alignment procedure and in giving hints for the improvements of the integration of the line. However the collimator did not meet the specifications. The focal length was measured to be 1.4 m, longer than expected due to manufacturing errors in the length of the shells. In addition the measured throughput was much lower than the simulated performance. This difference came from geometrical errors on the shells, larger than expected and higher roughness on the reflective coatings probably due to some contamination. The coating process performed by pulsed laser deposition, produced a hot localized spot at the end of the Iridium rod. When the Iridium rod was deposited on the plastic, the hot spot heated and slightly deformed the plastic substrate on an approximate 0.1-3 mm length scale. Those additional shape errors produced an unacceptable amount of scatter (lost light) and a too large spot.

Figure 4.9 shows a comparison of the measured data to the simulation of these effects. It can be observed that the behaviour of the optics is quite well understood. Due to the poor performance, the telescope was not installed in the Micromegas sunrise line.
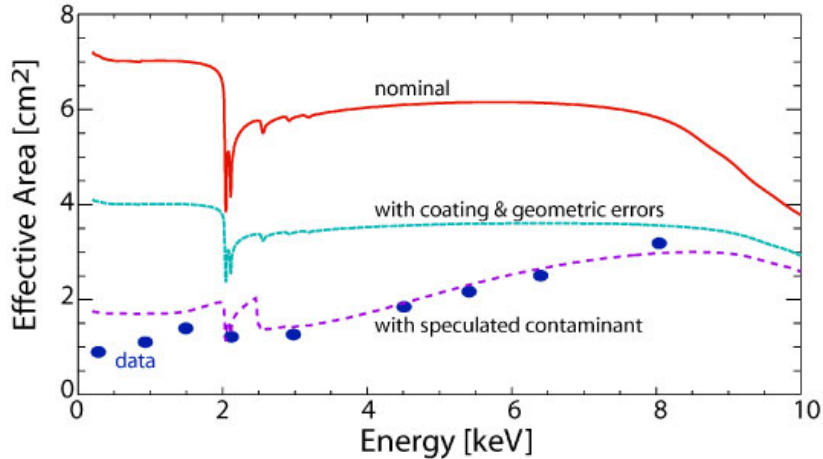
Figure 4.9: Effective area (throughput) as a function of energy. The red line shows the nominal effective area. The green line shows the throughput after accounting for geometrical and coating errors, while the purple curve shows the additional reduction that could result from a contamination layer on the optics.

4.3.3   Detectors: developing the microbulk technology

The first tests of the microbulk technology, described in chapter 3, were being developed at the same time. This technology seemed interesting for the needs of CAST as the manufacturing process would enable to further improve the uniformity and energy resolution of the detectors. Tests had been performed with a simpler single anode readout. For CAST, $x-y$ readout planes were needed. The first CAST microbulk detectors, manufactured in 2006, exhibited excellent energy resolutions however they were very fragile with respect to sparks. The manufacturing process needed to be optimised. The initial problem was that the mesh holes were covering the whole pixelised active area. It was found that the mesh hole etching could not be controlled well enough when the holes were above the isolation strip between pixels. Figure 4.10 shows a picture of the first CAST microbulk detectors as well as a picture of one of the detectors used today in CAST. The evolution of the manufacturing technique can be clearly seen in the quality and uniformity of the mesh holes. The manufacturing technique is described in detail in [6].

These microbulk detectors have been characterised in an Argon+5% Isobutane (the standard mixture to test Micromegas detectors) exhibiting gains higher than 10^4 with energy resolutions of 13-16% at 5.9 keV. Long term stability and reliability has been demonstrated by the fact that one of the detectors has been operated by more than 3 years [20].

4.3.4   Performance of microbulk detectors

The detectors showed a good stability and efficiency during long periods. Results are going to be illustrated by the performance of the detectors during the 2010 and 2011 data taking [60]. Figure 4.11 shows the gain stability with both the mesh and strip signals for one of the detectors. The stability is within $\pm5\%$. The abrupt changes correspond to modifications of the mesh voltage.
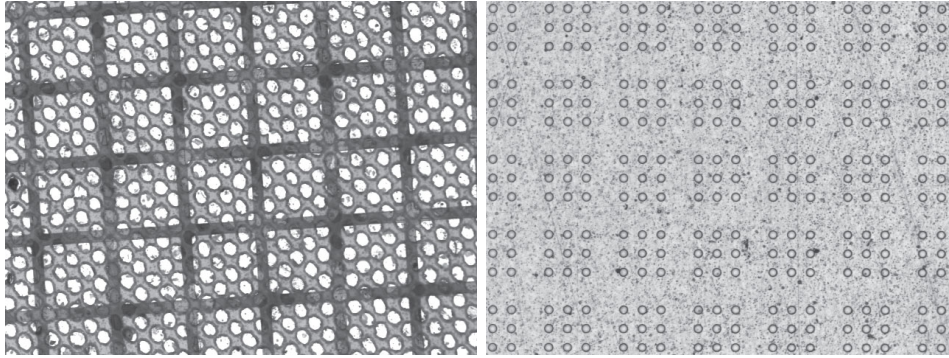
Figure 4.10: Pictures of the hole patterns for the microbulk micromesh. Left: Hole pattern of the one of the first microbulk 2D detectors manufactured for the CAST experiment. Right: Hole pattern of one of the microbulk detectors (M16) installed today in CAST. The holes have a diameter of $40\,\mu$m with a pitch of $100\,\mu$m inscribed into a pixel of size $400\,\mu$m.

The averaged level of background achieved is $\sim 6 \times 10^{-6}\,\mathrm{counts\,keV^{-1}\,cm^{-2}s^{-1}}$. A table with the detail of the background levels for 2010 and 2011 is given in table 4.2. The energy spectra for the three detectors is also given in figure 4.12. The spectra show the typical copper fluorescence peak. The differences in shape between the sunset and the sunrise detectors are due to the differences in shielding.
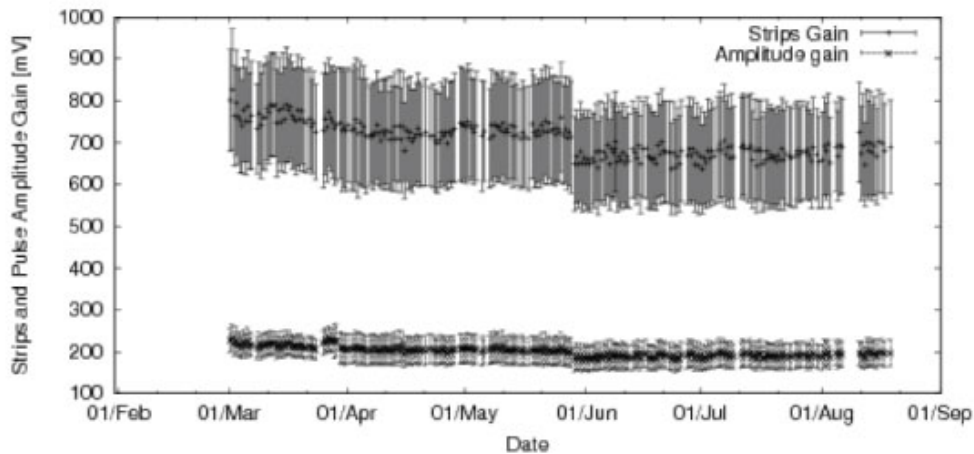
Figure 4.11: Gain evolution for one of the sunset microbulk detectors during the 2011 data taking campaigns.

4.4   Background simulation and underground studies

The CAST Micromegas detector has been carefully simulated by the Micromegas group at the University of Zaragoza in order to understand the dominant background contributions. These results will be treated here as they have been at the source of important upgrades in the Micromegas systems.

Background mean rate $(10^{-6}\text{counts keV}^{-1}\,\text{cm}^{-2}\text{s}^{-1}$)	2010	2011
Sunrise	6.39 ± 0.05	6.27 ± 0.10
Sunset 1	5.83 ± 0.07	5.53 ± 0.10
Sunset 2	7.11 ± 0.11	6.56 ± 0.11

Table 4.2: Summary of the background levels for the microbulk detectors installed during the 2010 and 2011 CAST data campaigns.
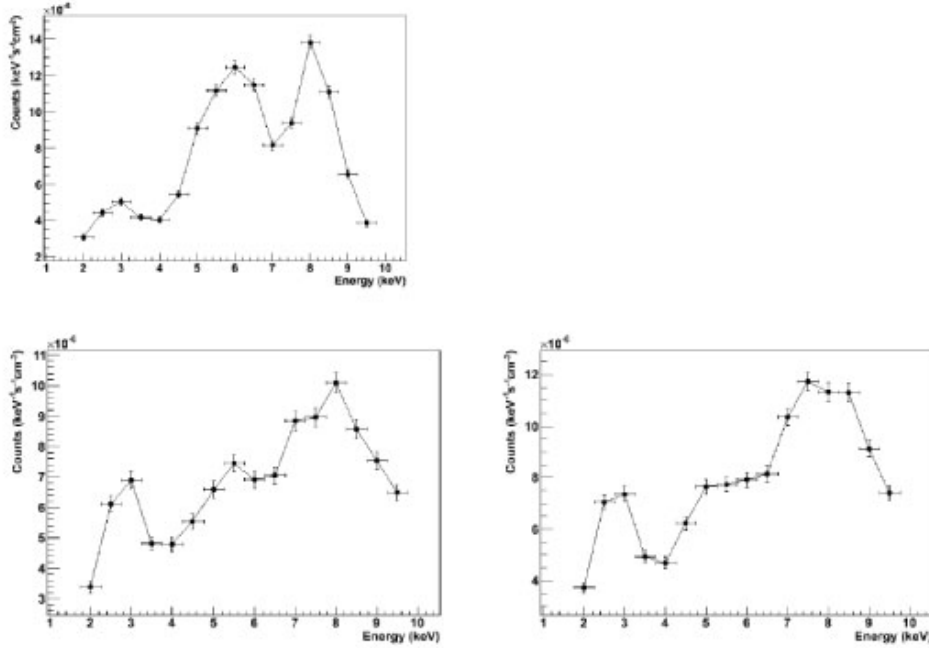
Figure 4.12: Background spectra obtained for the three spectra in the data taking of 2011.

The identification of the principal sources of background enables to target the shielding design to further improve the background level. The simulation chain has been developed from the generation of primary electrons, the drift of electrons to the Micromegas plane and the simulation of the avalanche size in the gas. In addition, the electronic chain is also simulated so the developed simulation makes possible to study the whole chain of process from primary electron generation to the electronic signals developed on the mesh and on the strips can be treated with the same analysis as is used in CAST. This simulation is described in detail in [153, 154]. The simulations have been confronted to measurements in the CAST experimental hall and in the underground laboratory of Canfranc to validate the accuracy of the MonteCarlo simulations and the relevance of the conclusions. In Canfranc different configurations of shielding have been studied to understand the various background contributions. The final results of these tests can be seen in figure 4.1 and are indicated by the red points. The lowest level, of 2×10^{-7} counts keV^{-1} cm^{-2}s^{-1} was achieved, by shielding the detector by 20 cm of lead and replacing the particular non radiopure elements (such has the aluminium cathode and the brass gas connectors by copper components). This level can

be attributed to the intrinsic radioactivity of the detector components or to the electronics close by. It represents an improvement of a factor 50 with respect to the level achieved in CAST. The main conclusions from these studies are listed here:

- More than 50% of the low-energy gammas remaining after the selection cuts correspond to primary or secondary gammas penetrating through the shielding weak points (magnet's bore, X-ray window, signal outlet) and populate mainly the 5-7 keV region.

- Cosmic muons are the most common events at surface but do not dominate the background level after the selection cuts.

- The gamma flux is the main contribution to the final background.

- Neutrons are not likely to be a dominant source as the addition of 20 cm of polyethylene shielding did not have any effect on the level of background.

- Microbulk detectors were measured with a high purity germanium spectrometer to determine the radiopurity of the samples. The results showed that the microbulk readout planes are currently manufactured with radiopurity levels below $30 \, \mu Bq/cm^2$ for Th and U chains and $\sim 60 \, \mu Bq/cm^2$ for ^{40}K, already comparable to the cleanest detector components of the most stringent low background experiments at present [49, 50]. It has to be noted that these results were obtained with standard microbulks where no special consideration of radiopurity was taken into account to optimise the manufacturing process. Obviously the production process could be further optimised concerning radiopurity issues.

These conclusions motivated the upgrade of the shielding. Modifications on the sunrise side were complicated due to the lack of space. It was decided that the modifications would be implemented in the sunset detectors where more space was available.

4.5 Upgrades of the sunset shielding

The conclusions from the previous sections indicate that the main source of background at surface for the installed detectors are the external gamma flux and in particular from fluorescence. In order to decrease this dominant contribution, the lead thickness was increased to 10 cm and the coverage of the general shielding was improved in the sunset side for the 2012 data taking. The copper shielding was equally increased from 0.5 to 1 cm. A further improvement was to replace the tube connecting the detector to the magnet bore by a copper pipe shielded with lead and with an inner teflon coating to shield the 8 keV copper fluorescence. With these modifications the performance of the sunset detectors is lower than $2 \times 10^{-6} \text{counts} \, \text{keV}^{-1} \, \text{cm}^{-2} \text{s}^{-1}$ which is about a factor 4 lower than the best result achieved with a detector in the CAST experimental hall.

The difference in background achieved at surface and in the underground laboratory of Canfranc indicate that there might be residual cosmic muons dominating the background. In order to improve further the background level, a cosmic veto in anti-coincidence with the Micromegas DAQ was installed. For this preliminary test the coverage was only of 44%. The result of this test was a background reduction of 25% as shown in figure 4.13 and the background levels achieved are detailed in 4.3.

Figure 4.13: Background reduction due to the implementation of a partial cosmic veto with only 44% coverage.

Background mean rate $(10^{-6}\text{counts}\,\text{keV}^{-1}\,\text{cm}^{-2}\text{s}^{-1})$	2012
Sunset 1	1.29 ± 0.07
Sunset 2	1.69 ± 0.07

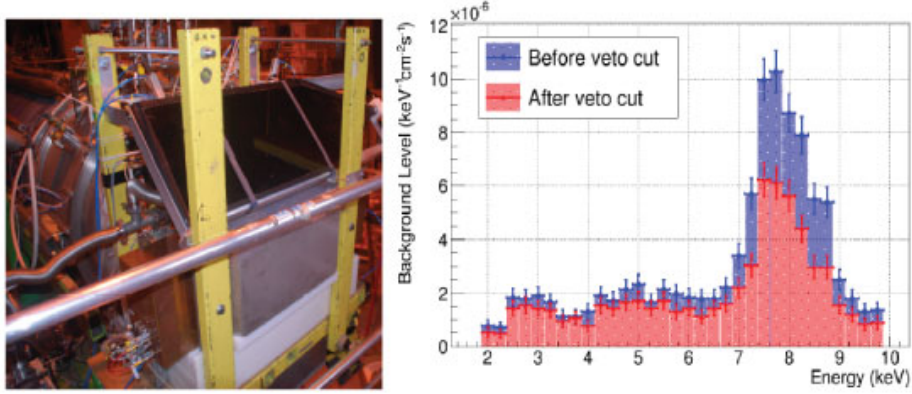Table 4.3: Summary of the background levels for the microbulk detectors installed during the 2012 CAST data campaigns.

In view of these results, an increased shielding coverage of 90%, was designed based on two plastic scintillators for the 2013 data taking. Once implemented the background reduction obtained was of 46% attaining a level of background below $10^{-6}\text{counts}\,\text{keV}^{-1}\,\text{cm}^{-2}\text{s}^{-1}$: $6.6 \times 10^{-7}\text{counts}\,\text{keV}^{-1}\,\text{cm}^{-2}\text{s}^{-1}$ as shown in figure 4.14. This result was obtained with the use of the AFTER electronics that is described in the next section. It is noteworthy to mention that this result was realised with aluminium cathodes installed in the detectors. Indeed they are known to be less radiopure than the copper ones. The use of a copper cathode will probably induce an improvement in the background level by an additional factor 2.

4.6 New detector for the 2013 and 2014 data taking campaign

For the 2013 and 2014 vacuum data taking a campaign, a new detector has been designed for the sunrise side with the accumulated knowledge from the background studies and the experience on the design and manufacturing of the detectors. The designed detector can be considered as a pathfinder for the detectors that are to be developed for IAXO. The novelties include a completely new design for the detector and shielding, new readout electronics and the coupling of the Micromegas detector with a dedicated X-ray focusing device for the sunrise side. The reader is referred to [90] for a detailed description.

4.6.1 Detector design

The body of the chamber as well as the support of the readout plane is made out of 18 mm of copper having a double function: gas container and shielding. Connections for mesh, drift and field shaper have been included in the printed circuit board to avoid any soldering near
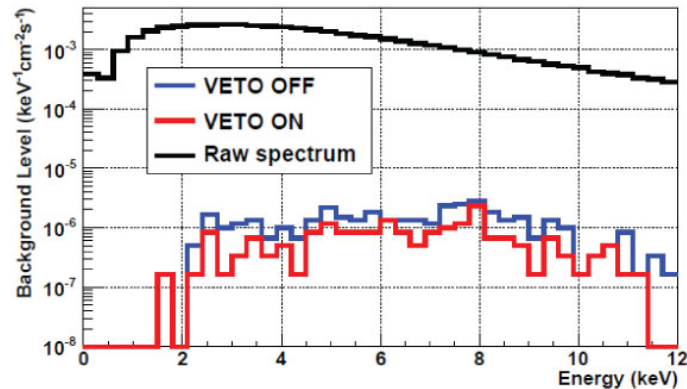
Figure 4.14: Background reduction due to the implementation of a cosmic veto covering 90% of sunset detectors and the use AFTER electronics.

the active area. The field shaper is printed on a flexible multilayer circuit with polyimide as substrate. The outer side of the circuit is used to bring the HV connections from the detector board to the field-shaper strips and to the drift cathode. An inner PTFE(teflon) foil blocks the fluorescence from these strips without disturbing the field lines. A general sketch of the mechanical mounting is shown in figure 4.15 left. The readout pattern of the microbulk has hardly been changed: the amplification gap is kept at $50\,\mu$m and the number of strips per direction has been slightly increased from 106 to 120 in an active area of $6\times6\,\mathrm{cm}^2$ (i.e a pitch of $500\,\mu$m). Figure 4.16 right shows a picture of the active area of the microbulk. The connection to the front-end electronics is done by a high density connector which is located away from the active area that is connected to an interface card that by means of flat cables that bring the strip signals to the front-end board.
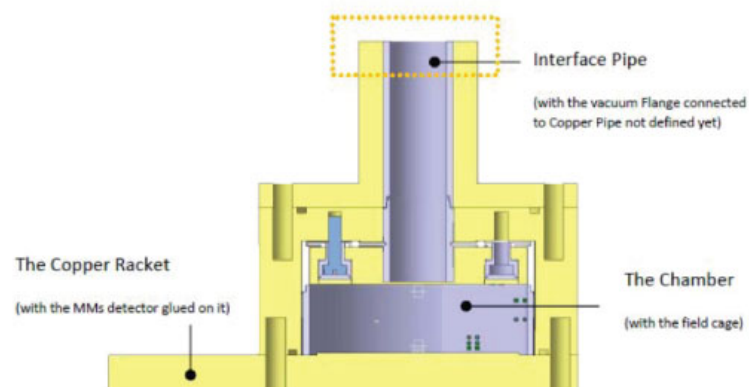
Figure 4.15: Cross-section of the detector, chamber, inner shielding and interface to cold bore.
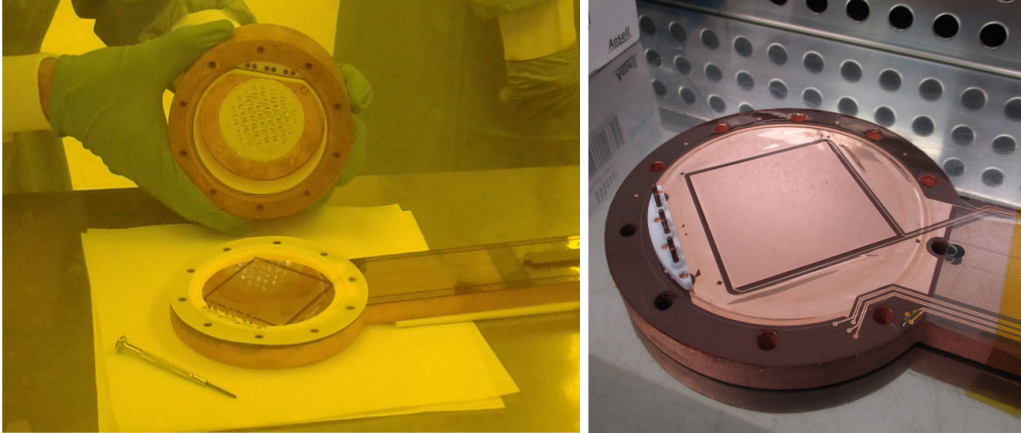
Figure 4.16: Left: Detector opened. The body and the cathode entrance window are visible as well as the readout plane on its copper support. The PTFE foil used to block the copper fluorescence can also be observed as well as the pins that connect the high voltage. Right: Close up of the microbulk active zone.

4.6.2   AFTER electronics

The Gassiplex electronics used up to 2012 could only provide the integrated charge per strip. Tests show that by the use of the AFTER electronics [30] developed for the T2K experiment, the background level as well as the energy threshold can be improved. The T2K electronics are based on the AFTER chip that allows to amplify and digitise the pulse signal of every strip. The chip allows sampling at $100\,\mathrm{MHz}$ with 511 samples recording for a time window of $5\,\mu\mathrm{s}$. The trigger, given by the mesh signal, is still recorded by the MATACQ card as in the past. The FEMINOS board [44] allows pedestal subtraction and zero-suppression. Three dimensional reconstruction is possible thanks to the identification of x and y position by the two dimensional readout and the relative z position is determined from the temporal position of the strip pulses allowing additional information that can be used in the selection criteria. As an example the xz and yz view of a background event and a calibration event using ^{55}Fe is shown in figure 4.17. In [90] it is shown that the AFTER electronics induce an improvement of the background level of 25%.
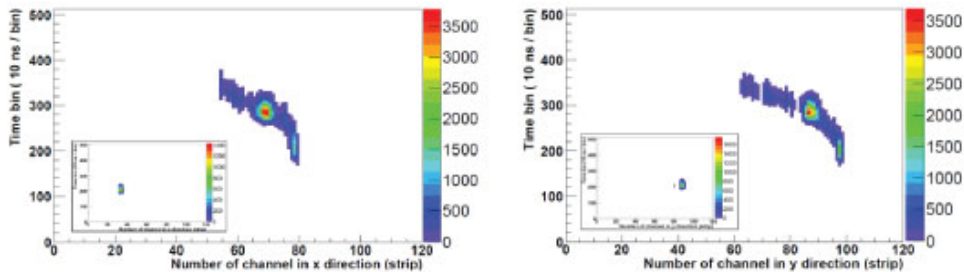
Figure 4.17: The xz (left) and yz (right) view of an electron acquired in a background run using the AFTER based electronics. In the embedded figures a typical ^{55}Fe event is shown.
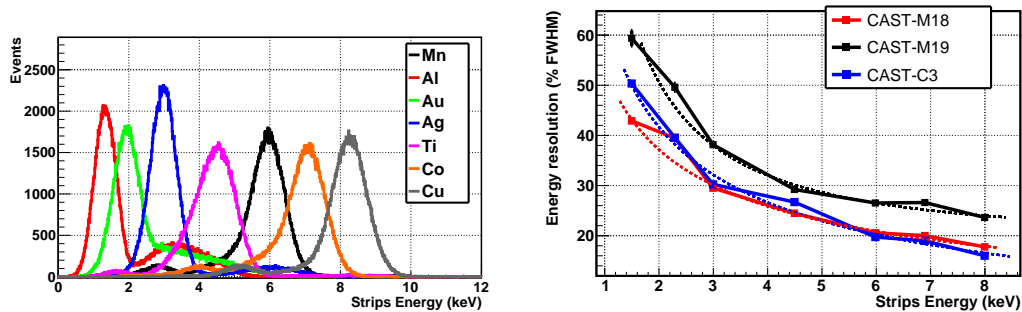
Figure 4.18: Left: Calibration energy spectra of the CAST-C3 detector. Right: Dependence of the energy resolution registered by the strips with the incident X-ray energy for three CAST-Micromegas detectors [90].

4.6.3 Characterisation

Three detectors were produced one month before the installation in the experiment. They were characterised in standard conditions with Argon+2.3% Isobutane at 1 bar pressure exhibiting normal behaviour: gains of 10^4 were reached and energy resolutions of 15-18% at operation gains were obtained.

The detectors were characterised in the CAST detector laboratory at CERN [155] with an electron beam based on PIXE (Particle Induced X-ray Emission) enabling calibrations from 1.5 to 9 keV. The detector response is given in figure 4.18. The experimental points show good agreement with the scaling given by the parametrization: $\frac{\sigma}{E} = \frac{a}{\sqrt{E}} + \frac{b}{E}$, where the first term represents the statistical fluctuation of the electrons generating the signal and the second is the calibration term. The measurements as well as the fit parameters are given in table 4.18 for this new detector (C3) and two older ones (M18 and M19). The first term being dominant, it can be noted that the latest detector, C3, achieves considerably better resolutions than M19 and similar ones to M18.

Detector	a	b
CAST-M18	49.3 ± 0.45	4.46 ± 0.82
CAST-M19	65.2 ± 0.94	2.13 ± 2.11
CAST-C3	37.4 ± 0.46	2.97 ± 0.81

Table 4.4: Fit parameters of the energy resolution versus energy for the C3 detector (newest microbulk) compared to two other CAST detectors.

4.6.4 X-ray telescope

The new X-ray telescope is designed and built by a collaboration between Lawerence Livermore National Laboratory (LLNL), Columbia University and the Danish Technical University Space (DTU-Space) based on their common experience for the Nuclear Spectroscopic Telescope Array (NuSTAR [94]) satellite X-ray optics launched in June 2012. The X-ray telescope for NuSTAR is based on a technology using float glass that is to be heated in the appropriate

shape for the substrate. The coatings to enhance reflectivity are deposited alternating layers of high and low atomic numbers materials. The CAST optics profits from all the existing facilities and tooling. The telescope consists of 15 nested shells (instead of the 133 for NuS-TAR) and a reduced size of the mirror sectors as the area to cover of the magnet bore is only $14.55\,\mathrm{cm}^2$. A schematic view of the X-ray optic is given in figure 4.19. More details on the construction and optimisation of this telescope can be found in [59]. The telescope was not ready for the 2013 data taking campaign. Once the coating and the assembly of the shells is finished, the telescope will be tested in the PANTER X-ray facility for a complete characterisation. The installation in the CAST experiment is foreseen for July 2014.
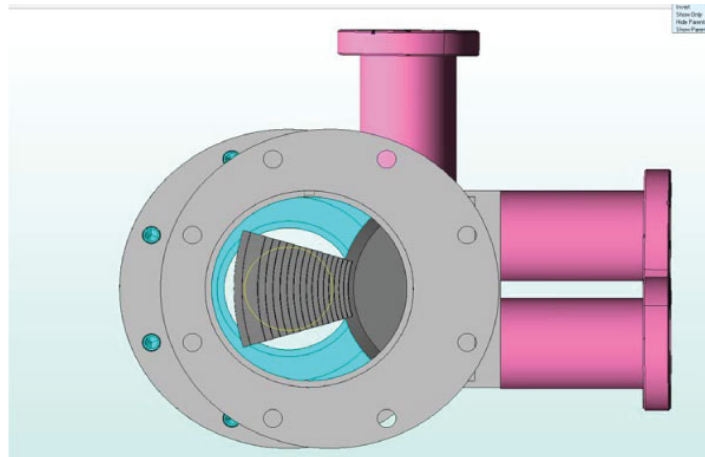
Figure 4.19: Schematic view of the new X-ray optic for CAST. The magnet bore is designated by the yellow circle.

4.6.5   Operation in 2013 data taking campaign

The detector was installed end of September 2013 in the experiment. Pictures during the installation can be seen in figure 4.20. The stability was not optimal due to different problems that will be corrected with a new detector production at the beginning of 2014 for the next data taking. The main concerns were related to the high voltage strip lines printed in the readout plane that could not stand in stable manner the required voltages and a problem with the interface card connector between the detector and the electronics. The new detector production should be available during February which gives enough time for testing the full system before the data taking due in June 2014.

4.7   Conclusion

At present CAST is a 100% Micromegas experiment with three microbulk detectors and one ingrid detector developed by Bonn University [112, 113] that will be installed in the experiment mid of 2014 replacing the CCD detector. The ingrid detector will then be coupled to the XMM-Newton and thanks to its sensitivity it will enable to decrease the energy threshold. This is specially interesting for the search of chameleons [41, 40].

The continuous development of Micromegas detectors since 2003 has achieved a reduction of background of more than two orders of magnitude with respect to the first unshielded
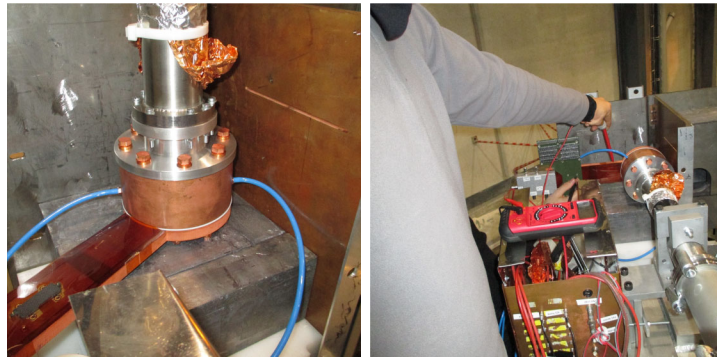
Figure 4.20: Pictures of the new microbulk detector taken during installation in autumn 2013.

detector. This has been possible thanks to the improvement of the Micromegas technology, to the understanding of the background and to the optimisation of the shielding and finally to the refinement of the selection criteria. This global approach has been realised in close collaboration with the Micromegas group of the University of Zaragoza and has been largely supported by the T-REX R&D project [103, 69, 70] funded by the European Research Council (ERC).

Chapter 5

The fourth generation helioscope: the International Axion Observatory (IAXO)

The concept of a new generation of helioscope was proposed in [104] with ultra-low background Micromegas detectors as the baseline option for the X-ray detectors. Recently a letter of intent was proposed to CERN [63] and the conceptual design is described in [64]. The next sections summarise the main ideas of these references.

5.1   Physics objectives

The aim of IAXO is to improve the sensibility in terms of axion-photon coupling, $g_{a\gamma}$, by a factor ~ 20 with respect to CAST, meaning about 4-5 orders of magnitude in terms of signal intensity. In order to justify the choices made for the different systems i.e. the magnet, the X-ray focusing optics and the X-ray detectors, the dependence of the sensitivity of IAXO with respect to each system is now discussed.

The discovery potential of the experiment depends on $N_\gamma / \sqrt{N_b}$ where the number of axion signal counts N_γ and background counts, N_b can be written as follows [104]:

$$N_\gamma \sim N^* \times g_{a\gamma}^4 = B^2 L^2 A \epsilon t \times g_{a\gamma}^4 \tag{5.1}$$

and

$$N_b = ba\epsilon_t t \tag{5.2}$$

where B, L and A concern the magnetic field, the length and the cross sectional area respectively. ϵ is the total efficiency $\epsilon = \epsilon_d \epsilon_o \epsilon_t$ taking into account the detector efficiency, ϵ_d, the optics throughput ϵ_o and the data taking efficiency ϵ_t, that is the amount of time where the magnet is following the sun. The background of the detector is denoted b and given in counts $\mathrm{keV^{-1}\,cm^{-2}s^{-1}}$, a is the total focusing spot area and t is the duration of the data taking. We can define a figure of merit that takes into account the contribution of the different systems to the total sensitivity:

$$f = \frac{N_\gamma}{\sqrt{N_b}} = f_M f_{DO} f_t \tag{5.3}$$

with

$$f_M = B^2 L^2 A; \ f_{DO} = \frac{\epsilon_d \epsilon_o}{\sqrt{ba}}; \ f_t = \sqrt{\epsilon_t t}. \tag{5.4}$$

These relations assume that the axion-photon conversion is fully coherent throughout the length of the magnet L and that background counts are in the Gaussian regime. From these expressions, one can see that the sensitivity of a helioscope is mainly driven by the magnet parameters. In order to surpass CAST performances, it does not seem feasible to build a dipole that would outperform the CAST LHC dipole parameters in a significant manner. Instead the toroidal configuration might enable to keep a BL close to the levels achieved by CAST while increasing significantly the cross sectional area. It is desirable to have X-ray focusing optics in most of the magnet bores with an entrance that fits the magnet bore and with a large throughput ϵ_o and a small spot area a. The background level of X-ray detectors should be below 10^{-7} counts keV^{-1} cm^{-2}s^{-1} or lower. With the present performance of the Micromegas detectors this should not be a problem specially after the 2014 data taking during which a new state-of-the-art microbulk detector will be tested. The tracking efficiency should be also improved with a platform that allows tracking the sun for at least 30 or 50% of the day.

With these considerations and after a preliminary study, a conceptual design has been proposed with a 8-coil toroidal magnet with 60 cm diameter bores and equipped with X-ray focusing optics into 0.20 cm^2 spots coupled to ultra-low background Micromegas X-ray detectors. The magnet would be on a platform that would allow solar tracking for 12 hours per day. A sketch of the conceptual design is given in 5.1 as well as possible implementation.

In the next sections the experimental set-up as well as the expected sensitivity are briefly described.

5.2   Experimental set-up

5.2.1   The magnet

After a prospective study on the available magnets on the various accelerators and experiments, the CERN magnet group concluded that a new magnet is required in order to achieve the required sensitivity. A well known proven engineering technology has been chosen, the NbTi technology. With this technology, the attainable peak magnetic field is 5-6 T. Therefore, in order to reach the required magnet FOM $f_m = L^2 B^2 A$, the aperture is the parameter that can be enlarged easily.

The first optimisation of the geometry of the IAXO superconducting magnet based on simulations have shown that the toroidal geometry, inspired by the ATLAS barrel and endcap toroids, is the preferred one [104]. These simulations have been realised within the CERN magnet group. The study has shown the optimal configuration is a toroid with 8 magnet bores each 1 m large and 25 m in length reaching a peak magnetic field of 5.4 T and an averaged field in the bores of 2.5 T (critical magnetic field 8.8 T). The study of the magnet is taking into account implementation options of the rest of the systems. For instance, the optimisation of the different parameters will not be the same whether the optics are positioned as close as possible to the inner radius of the the toroid ("field dominated") or between each pair of racetrack coils ("area dominated"). The study also shows that is better to have an increased fraction of the aperture of the optics exposed to X-rays favouring the "area dominated" options.
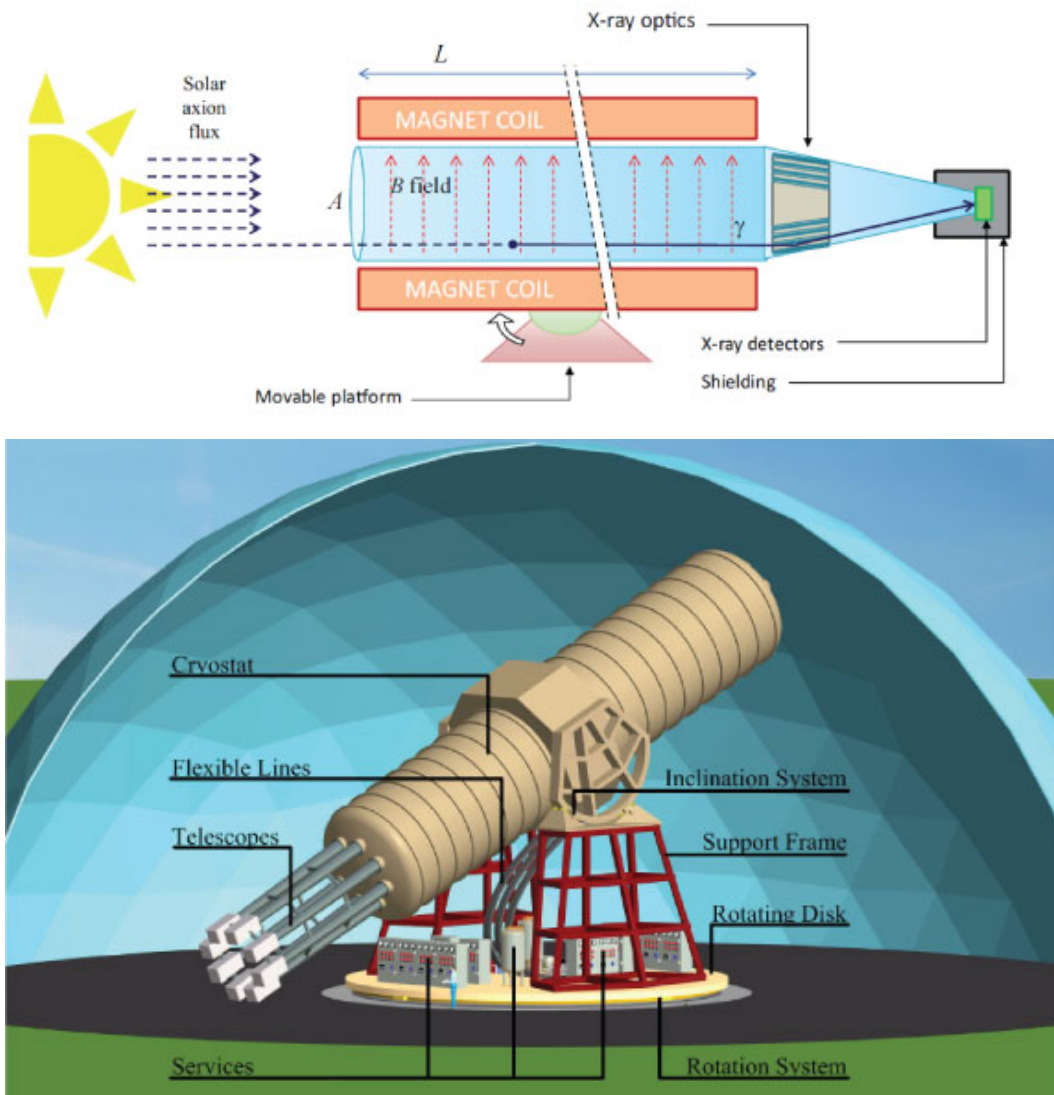
Figure 5.1: Top: Sketch of the IAXO principle. Bottom: Possible implementation of IAXO. The cryostat is shown with eight X-ray optics attached to X-ray detectors.
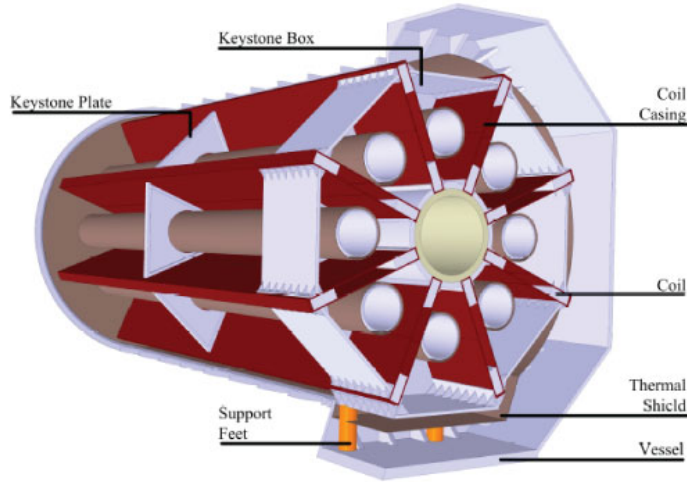
Figure 5.2: View of the IAXO cryostat showing the cold mass (eight coils with the central cylinder to support the magnetic force load) and its supports surrounded by the thermal shield and the vacuum vessel.

The toroidal magnet consists of eight coils and their casing within an inner cylindrical support for the magnetic forces as shown in figure 5.2. The operational current is of 12.3 kA with a stored energy of ∼500 MJ.

Safety margins have been taken into account in the operational current and temperature to allow proper operation. The operational temperature will be of 4.5 K. For safety it is also necessary to design a quench protection system to allow the release of the stored energy safely.

The magnet needs to follow the sun as long as possible requiring a horizontal and vertical movement. In order to track the time for a half day a horizontal movement of 360º will be required with a vertical movement of 25º. The rotation system can be seen in figure 5.1: the whole system is supported by the central post with an inclination system that allows the vertical movement sitting on a rotating platform allowing the full horizontal rotation.

In order to validate the design of the IAXO magnet it would be desirable to build and test a single short (2 m) prototype coil in the short term. The tests would demonstrate the feasibility of the IAXO toroid magnet.

5.2.2   The X-ray telescopes

The use of X-ray telescopes allow to enhance the signal to background ratio by concentrating the potential signal in a small spot. The main requirements of a helioscope optics are high efficiency in the 1–10 keV range and a pupil entrance that fits the area of the magnet bore with a solid angle acceptance that is greater than the 0.3 arcmin (extent of the solar core where axions are produced). Taking into account these requirements, using reflective X-ray optics seemed to be the most appropriate choice.

The parameters of the optics need to be optimised in order to have the smallest spot, a, and the highest reflectivity. To have a small spot, the optics should have a small focal length, f, since $a \propto f^2$. However the reflectivity increases with decreasing graze angle, α and since $f \propto \frac{1}{\alpha}$, to achieve the highest throughput (efficiency) the optics should have the maximum possible focal length. In addition, the design has to take into account that the performance
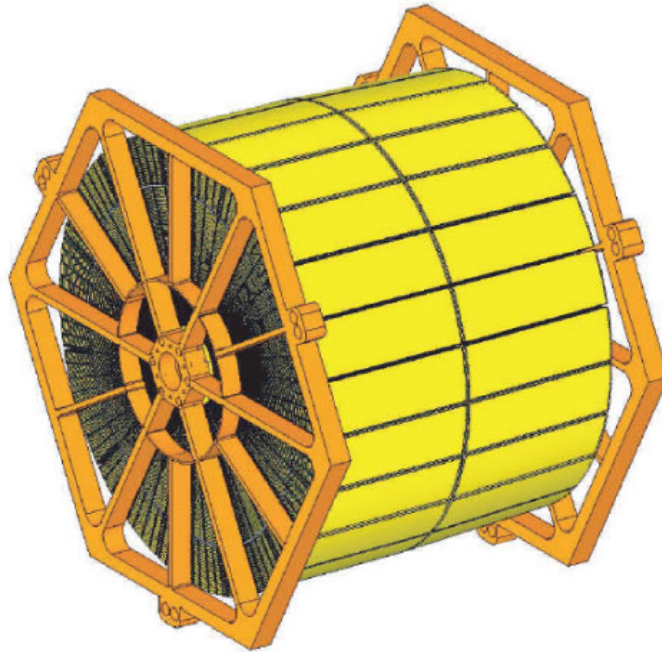
Figure 5.3: View of the IAXO optic with the hexagonal spider structure that will support the thousands of individual mirror segments.

of the optics have a complex dependence on the incident photon energy and α. Moreover the reflectivity depends also on the coating material and in the number of reflections.

The fabrication technology that has been chosen is a segmented, slumped glass optics were several individual pieces of substrate make a single layer. The reasons are that the technology is mature and not expensive, it has been developed by members of IAXO for the NuStar Satellite mission [94], it is easy to deposit a single layer or multi-layers reflective coatings and the imaging requirements can be satisfied.

The design studies have taken into account the axion spectrum and the detector efficiency in order to achieve the highest figure of merit, f_{DO} with the optimisation of the optics parameters (f, a, number of layers, single and multilayer coatings). An example of how this optimisation has been achieved is given in figure 5.4. The optimal figure of merit is found for 5 m focal length with 123 layers with W/B$_4$C multilayers coating and with a spot of ~ 4 mm.

5.2.3 The X-ray detectors

The Micromegas detectors developed for the CAST experiment are the baseline technology for the X-ray detectors of IAXO. The levels of background achieved during CAST operation have been described in detail in the previous chapter. As already mentioned, the levels achieved result from a global approach where the improvement have come from different fronts: from the manufacturing technique leading to highly intrinsically radiopure detectors with high performance, from the optimisation of the passive and active shielding thanks to understanding of the background and from the refinement of the selection algorithms.
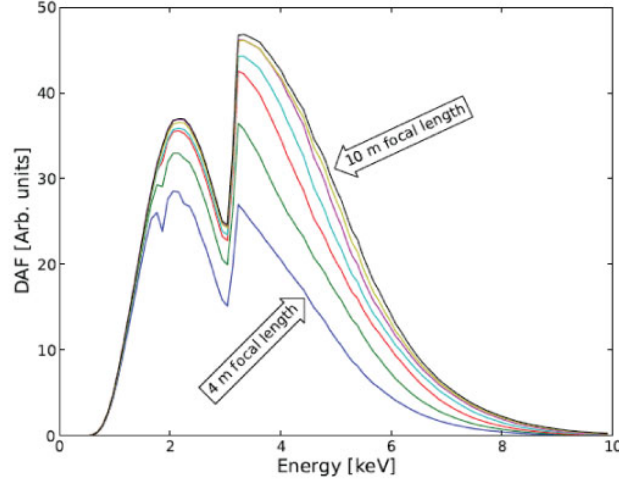
Figure 5.4: Detected axion flux (DAF) as a function of the photon energy for different focal lengths from $f = 4\,\mathrm{m}$ (lowest curve) up to $f = 10\,\mathrm{m}$ (highest curve). The shape of the curve with different edges is due to absorption lines in detector and coating materials and to the shape of the solar axion spectrum.

The lowest background achieved in CAST during the 2013 data taking campaign is below $10^{-6}\mathrm{counts\,keV^{-1}\,cm^{-2}s^{-1}}$ with the sunset detectors. IAXO aims to background levels of at least $10^{-7}\mathrm{counts\,keV^{-1}\,cm^{-2}s^{-1}}$. The detector to be installed in the 2014 CAST data taking campaign in the sunrise side coupled to the X-ray telescope should achieve easily levels below $10^{-7}\mathrm{counts\,keV^{-1}\,cm^{-2}s^{-1}}$. It can be considered as the first Micromegas prototype for IAXO. These activities have been largely supported by the T-REX R&D project [103, 69, 70] funded by the European Research Council (ERC). Further improvements are still expected:

- Use of segmented mesh microbulks (see next chapter) with auto-trigger electronics;

- more stringent selection on the radioactive requirements of the components of the detectors;

- upgrade of the active muon and gamma shielding;

- improvement of the selection algorithms.

5.2.4   Additional equipment

Additional equipment can be considered to enlarge the physics goals of the experiment. GridPix detectors [55], Transition Edge Sensors (TES) [105] and Charged Coupled Devices (CCD) [61] could be interesting to search for signatures requiring lower energy thresholds like hidden photons, chameleons or other ALPs. Furthermore possibilities to search for relic axions in IAXO with microwave cavities are also been explored [63]. In this way, the IAXO sensitivity would be extended to very low mass entering the interesting region for Dark Matter axions.

Parameter	Units	CAST	IAXO Nominal	IAXO Enhanced
Magnet				
B	T	9	2.5	2.5
L	m	9.26	20	20
A	m^2	2×0.0015	8×0.283	8×0.283
f_m^*		1	300	300
Detector and Optics				
b	$\frac{10^{-5}c}{\mathrm{keV\,cm^2\,s}}$	~ 4	5×10^{-3}	10^{-3}
ϵ_D		0.5-0.9	0.7	0.8
ϵ_O		0.3	0.5	0.7
a	cm^2	0.15	8×0.2	8×0.15
f_{DO}^*		1	17	60
Tracking time				
ϵ_t		0.12	0.5	0.5
t	year	~ 1	3	3
f_T^*		1	3.5	3.5
f^*		1	2×10^4	6×10^4

Table 5.1: Values of the relevant parameters for the IAXO experiment compared to those of CAST from [63]. The figure of merit relative to CAST is also indicated, i. e $f^* = f/f_{\mathrm{CAST}}$.

5.3 Expected Sensitivity

A summary table of the relevant experimental parameters is given in table 5.1 where it can be observed that in terms of detectable signal counts, IAXO is at least 10^4 better than CAST phase-I, resulting in sensitivity on $g_{a\gamma}$ one order of magnitude better. With these parameters, the expected sensitivity can be simulated and is given in figure 5.5. This exclusion plot is obtained by considering different scenarios of the expected performances of the different subsystems of IAXO (magnet, optics, X-ray detectors). To obtain this plot a vacuum run of 3 years effective data taking, IAXO run I, is considered with sensitivities to $m_a < 0.1\,\mathrm{eV}$ followed by IAXO run II that will use a buffer gas, ^{4}He, inside the magnet bores to reach higher masses up to $m_a \sim 0.25\,\mathrm{eV}$. In this way, a large unexplored region of the QCD axion phase space will be scanned reaching $g_{a\gamma} \sim$ few $10^{-12}\,\mathrm{GeV}^{-1}$ for masses up to $0.25\,\mathrm{eV}$. At high masses, the expected sensitivity will supersede the SN 1987 energy loss limit. This region is interesting because it is favoured for DM candidates.

In addition IAXO is also sensitive to non-hadronic models evoked to explain the anomalous cooling of white dwarfs with an increased sensitivity with respect to CAST [63]. Moreover IAXO will also be sensitive to hidden photons emitted from the sun and chameleons. For these searches, detectors with low energy threshold ($< 1\,\mathrm{keV}$), like ingrid, TES or CCD are needed.

The possibility to search for relic Dark Matter axions is also being considered by the coupling of microwave cavities to IAXO. The advantage with respect to ADMX is the fact that IAXO will be able to host larger cavities and to explore a fraction of the $g_{a\gamma} - m_a$ space complementary to that of ADMX.
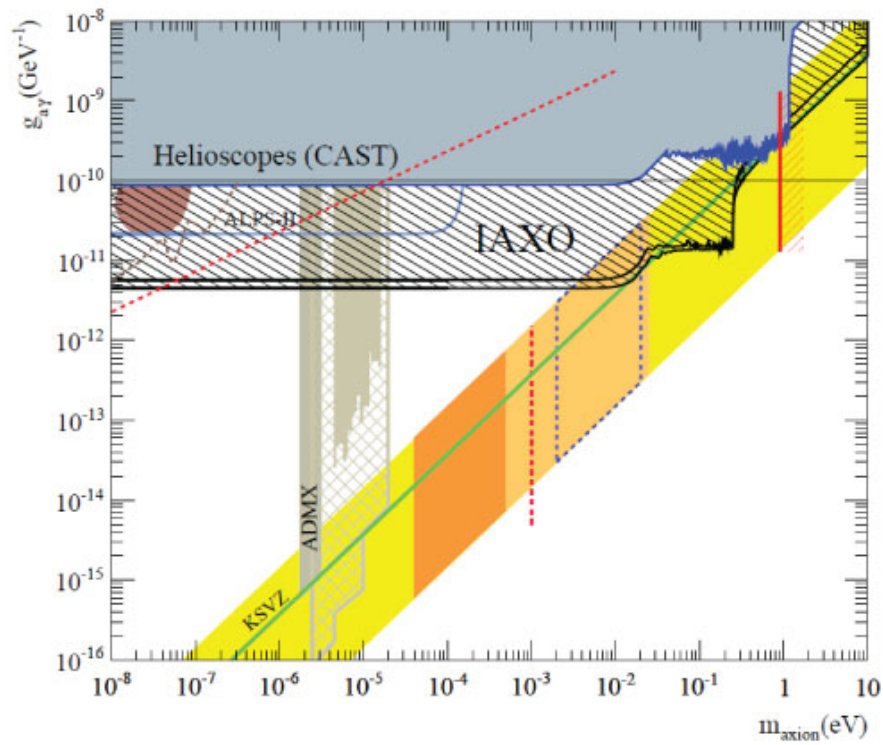
Figure 5.5: Expected IAXO sensitivity compared to CAST and ADMX limits. Future prospects of ADMX (dashed brown) and ALPS-II (light blue line) are shown. The nominal scenario takes into account the figures of merit described in the text while the enhanced scenario expects a lower background level (10^{-8} counts keV^{-1} cm^{-2}s^{-1} instead of 5×10^{-8}) for the Micromegas detector and an increased efficiency for the optics (70% instead of 50%) with a smaller spot size a (0.15 cm^2 instead of 0.2 cm^2).

.

Chapter 6

Related R&D

6.1 Introduction

This chapter is not directly related to the development of the Micromegas detectors for the CAST experiment. Nevertheless it might be of interest to consider the generic R&D that has been developed in parallel and to which I have actively contributed.

The first and second section describe recent developments on the microbulk technology. On the one hand, the first section concerns small gap microbulk detectors that are particularly suited for operation at high pressure, interesting for instance for double beta decay experiments. On the other hand, the second section is devoted to novel segmented microbulk detectors where 2D capabilities are achieved with an ultra low-mass microbulk. The third section is devoted to Piggyback Micromegas where the amplification structure and the detector volume are separated from the readout electronics. The signal is then transmitted by capacitive coupling. This way of reading the signal opens up avenues for the use of a wide range of electronics and for sealed detectors. Moreover by the use of resistive layers the signal can be spread in larger pitch strips while keeping a high spatial resolution. In this way the number of electronic channels can be decreased. This is specially interesting for large experiments where the electronics cost represent a high fraction of the total budget of the detector.

The last section of this chapter is devoted to the MIMAC experiment that considers the use of Micromegas detectors for WIMP Dark Matter search. Some of the issues are common to CAST in particular the strategies for background rejection (even if the signal events are very different) and the radiopurity of the construction materials of the detector. The readout planes that have been developed for the MIMAC experiment were based on the experience accumulated with the CAST Micromegas detectors.

6.2 Small gap microbulks

6.2.1 Motivations

The virtues of microbulk detectors have been discussed in chapter 3 and 4. The most commonly used microbulk detectors have an amplification gap of $50\,\mu$m. The manufacturing procedure developed at CERN has been optimised for this geometry since 2006. However smaller gap detectors are interesting for applications where high pressure operation is required. This

amplification gap (μm)	hole diameter (μm)	hole pitch (μm)
12.5	25	80
25	30	100
50	40	90

Table 6.1: Summary of the pattern of holes diameters and pitchs for the three different amplification gaps of the tested detectors.

property is important in the field of rare event searches in order to increase the sensitivity as for instance for the case of NEXT TPC [51, 67, 66] for the double beta decay search. In [99] characterization of microbulk detectors was investigated with different gas mixtures of Argon and Neon for 50 and 25 μm gaps. In the present work, the study is extended to 25 and 12.5 μm.

Indeed, in [87] it was shown that small gap Micromegas detectors would be optimum for operation at high pressure whilst larger gaps are more suited for low pressure applications. This is easily shown by writing the Townsend coefficient in the Rose-Korff's parametrisation [140]:

$$\alpha = PAe^{\frac{-BP}{E}} \tag{6.1}$$

where P is the gas pressure, A and B are parameters that depend on the gas and E is the electric field. The gain can be then written as:

$$G = \exp\left(PAe^{\frac{-BP}{E}}\right) = \exp\left(PAe^{\frac{-BPd}{V}}\right) \tag{6.2}$$

with V being the applied voltage on the mesh. We recall here that this expression can be differentiated in order to find a set of parameters (pressure and voltage) that optimises the stability operation:

$$\frac{\partial G}{\partial P} = G\alpha\left(1 - \frac{BPd}{V}\right) \tag{6.3}$$

In [54], this was done by testing various Micromegas detectors of the Ingrid type with gaps from 45 μm to 68 μm at fixed gas conditions to observe the evolution of the gain at a given voltage.

We chose to manufacture microbulks of 12.5 and 25 μm amplification gap and to compare their performances to the well known 50 μm amplification gap microbulks. Their characteristics are given in table 6.1. Usually in Micromegas detectors with a larger amplification gap, the geometry of the holes is designed as to have the diameter of the holes smaller than the amplification gap in order to favor the funnel electric field effect. In the case of the present detectors with gaps of 25 and 12.5 μm this is not possible. The limitation comes from the attainable precision on the mask films that define the minimum mesh holes diameter. This limitation could be exceeded by an alternative more expensive technique, using glass masks, where holes of 20 μm diameter could be achieved. Going further with the present techniques seems difficult.

The detectors have been installed in an aluminium vessel with an aluminized mylar window allowing calibration by X-ray from an ^{55}Fe source. The prototypes used in these tests are single anode round detectors with an active zone of a diameter of 3.5 cm. A picture of the detector and a zoom of the active area are shown in figure 6.3. The gas mixture is circulated
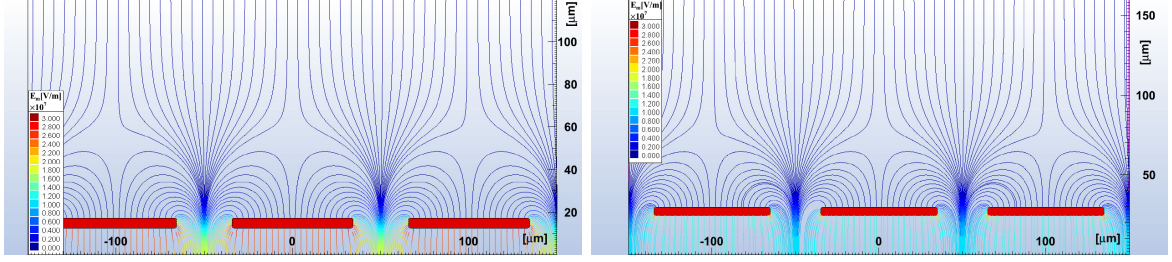
Figure 6.1: Field line simulation of a 12.5 (left) and 50 μm (right) amplification gap Micromegas detector with the hole and pitch dimensions described in table 6.1.

for several hours before each measurement and at every change of the gas mixture or the pressure. The drift gap is defined by a mesh frame layed on 5 mm pillars on top of the anode plane. The mesh signal is read out by the usual electronic chain charge preamplifier (ORTEC 142C) followed by a spectroscopy amplifier (ORTEC 472A). The pulse height distributions are recorded by a multi-channel analyzer (AMPTEK MCA-8000A) and each spectrum is fitted by two Gaussian functions, corresponding to the K_{α} (5.9 keV) and K_{β} (6.4 keV) lines of the ^{55}Fe source; the mean position and width of the main peak are obtained for each fit. Full characterisation of these detectors in terms of gain and resolution for different gas mixtures are shown as well as novel results exhibiting the relation gap versus gas pressure. Here we focus on the latter. We just show the gas gains obtained in an Argon-10% Isobutane mixture in figure 6.4 for comparison. The highest gain is obtained for the 50 μm gap achieving values greater than 10^4. The value for 12.5 μm is only of several thousands probably due to hole geometry limitations for this gap that affect the maximum field achieved near the hole. This effect has been shown with electrostatic field simulations. A field line simulation is shown in figure 6.1. The typical funnel shape of the field lines at the mesh hole entrance seems well preserved. However figure 6.2 shows the magnitude of the electric field at different heights within the amplification gaps across the hole as indicated in the sketch of figure 6.2. The depicted electric field ranges from 99% (black points) to 1% (pink points) of the amplification gap for the three different cases (12.5, 25 and 50 μm). The 99% correspond to heights at the level of the mesh while heights of 1% correspond to heights close to the anode, where the electric field is the strongest. The voltage applied is the same for the different gaps and only relative differences are pertinent here.

If we compare the ratio of the field at 99% and 1% of the amplification gap for the different gaps, we observe that for the 50 μm gap this ratio is 1.77 while for the 12.5 μm is 1.49. This means that the increase of the field near the anode for the small gaps is smaller than for the larger gaps with this hole geometry. This will probably lead to reduced gains for the small gaps. This effect would be corrected if the diameter of the holes could be reduced.

The second consideration is that for the small gaps there is a greater dispersion of the magnitude of the electric field close to the anode i.e for the 50 μm the magnitude of the electric field is nearly constant from heights greater than 50%.

Concerning the energy resolutions, the best values obtained are below 15% and achieving 11% (FWHM) for the 25 and 50 μm. These values are close to the theoretical limitations. This is observed by calculating the lower limit on the obtainable energy resolution in gas detectors taking into account primary and avalanche fluctuations. It can be written as follows:
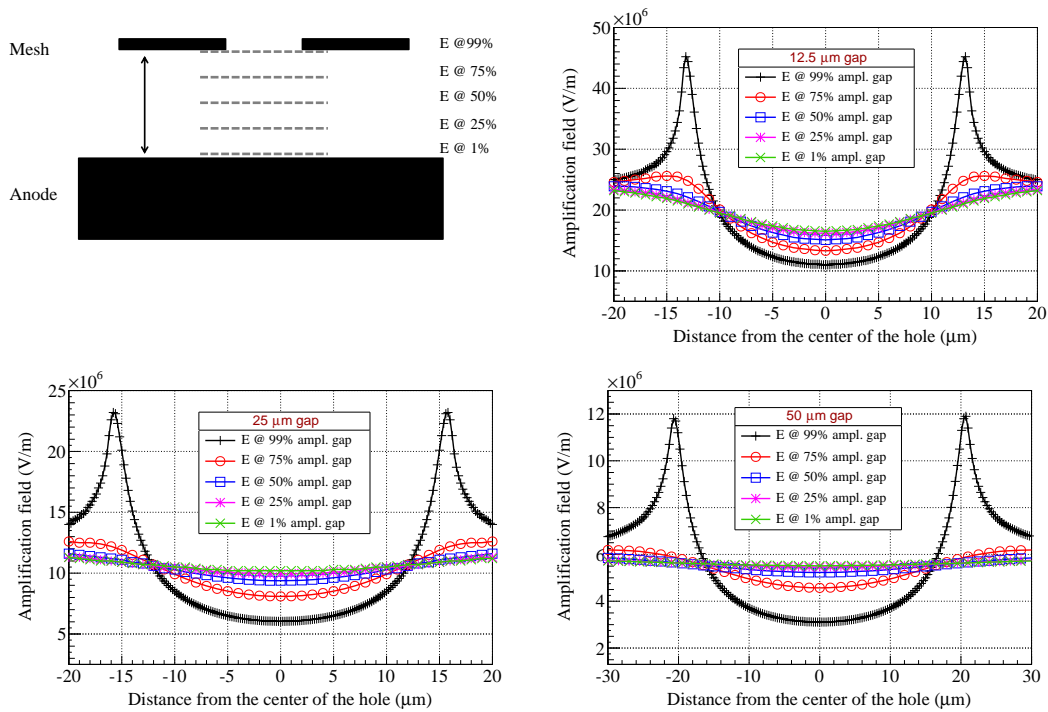
Figure 6.2: Sketch to illustrate the electrostatic simulation (top left). Magnitude of the eletric field at different heights within the amplification holes for the 12 (top right), 25 (bottom left) and 50 (bottom right) μm amplification gaps.
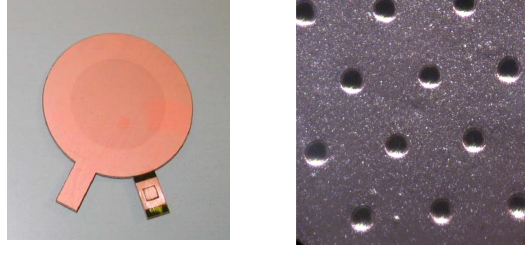
Figure 6.3: Left: Picture of a 3.5 cm diameter circular microbulk used in these tests. Right: Zoom of the active area. The hexagonal pattern of the 30 μm diameter mesh holes with a pitch of 100 μm can be observed.

$$\frac{\sigma_E}{E}(FWHM) = 2.35\sqrt{\frac{W}{E_0}(F + b)}, \tag{6.4}$$

where W is the mean energy per ion pair, E_0 is the initial total energy of the ionization particle, F is the Fano factor and b is the relative variance for the distribution of the number of electrons produced in a single avalanche. F reflects the fraction of the incident particle energy that is converted into information carriers within the detector. It is an intrinsic constant of the detecting medium, in our case of the gas. The values of F are less than 1 for gases and are in the range of 0.1-0.3 [54]. Using typical values for Argon of $F = 0.2$, $W = 25$ eV and $b = 0.5$, the minimum resolution at 5.9 keV is 10.8% (FWHM). The energy resolution of the 12.5 μm amplification gap is also degraded because of a larger dispersion of the maximum electric fields achieved along the gap, due to the limitations of the hole manufacturing.

6.2.2 Influence of pressure

The pressure has been scanned from 0.5 to 1.7 bar. The gains achieved in this range are larger than 5×10^4 for the 12.5 μm gap and 10^4 for the 25 μm gap. For the 50 μm gap the gains are as high as 3×10^4 and no degradation is seen with increasing pressure. The trend for the energy resolution as a function of electric field is shown in figure 6.5. The best minimum is between 11% and 13% for the three gaps. A summary of these results can be seen figure in 6.5 where the evolution of the gain and the energy resolution as a function of pressure is given for a fixed electric field.

The gain follows the expected bell shape with a shifting maximum with amplification gap. For the energy resolution the minimum is reached at the maximum of the gain [87]. The optimum of pressure is 0.4 bar for the 50 μm gap, 0.7 bar for the 25 μm gap while for the 12.5 μm is 0.9 bar. In figure 6.6 the best energy resolution at each pressure is shown independently of the electric field applied. The range of pressure where the behaviour is optimal is within ± 0.1 bar around the minimum.

6.2.3 Perspectives

Microbulk detectors of 25 and 12.5 μm amplification gaps have been manufactured and tested with success. Gains greater than 10^4 for the 25 μm detectors and 8×10^3 for the 12.5 μm have been obtained in Argon/Isobutanes mixtures. Energy resolutions as low as 11%–13%
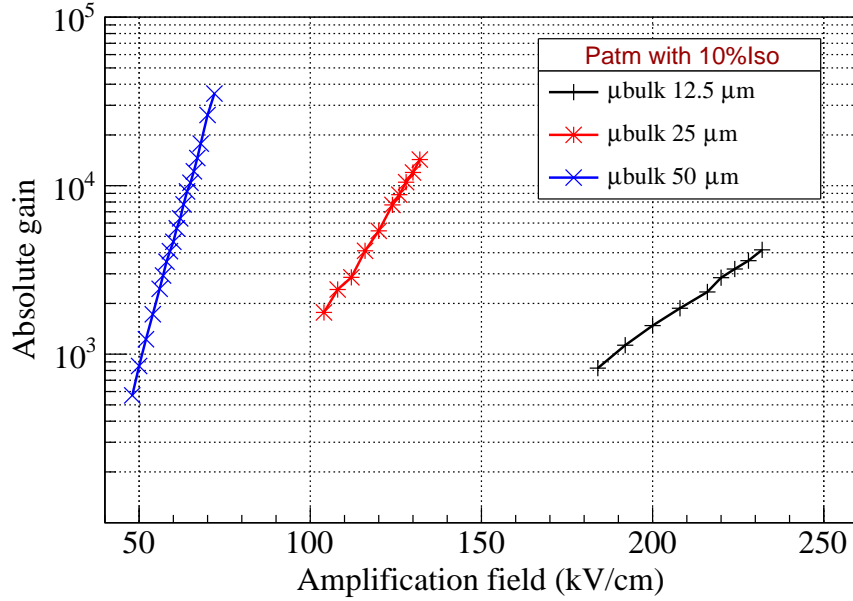
Figure 6.4: Comparison of gain for the different gaps at atmospheric pressure in Ar + 10% Isobutane.

(FWHM) at 5.9 keV have been obtained for the three different amplification gaps. These values are very close to the minimum energy resolution that can be achieved with gaseous detectors taking into account the fluctuations due to electron multiplication. The electric field simulation has helped us to understand qualitatively that the geometry of the hole pattern, due to manufacturing limitations for the smallest gap, leads to reduced gain and energy resolutions. These limitations could be partially overcome by using other type of mesh, as BOPP meshes [161], where the hole diameter can be as low as 15 μm. In this case, we would print the small gap pillars in the readout plane and have this deported mesh stretched on top of the pillars.

The behaviour of these detectors have also been studied as a function of pressure from 0.5 bar to 1.7 bar. The gain follows the expected bell shape with a shifting maximum with amplification gap: smaller gaps are more suitable for higher pressures. A summary of the performances is given in table 6.2. The full study is detailed in [19].

These tests confirm the appropriateness of small gap microbulk detectors for rare event detection in terms of good energy resolution, radiopurity, background discrimination and operation at high pressure.

6.3 Segmented mesh microbulks

6.3.1 Description

The localization of charge is an important parameter in background rejection especially in rare event experiments. Often the signal events have a different topology than background events. For instance in the CAST context, signal events have a localised energy deposition and background events often have a more dispersed distribution. This is the reason why 2D
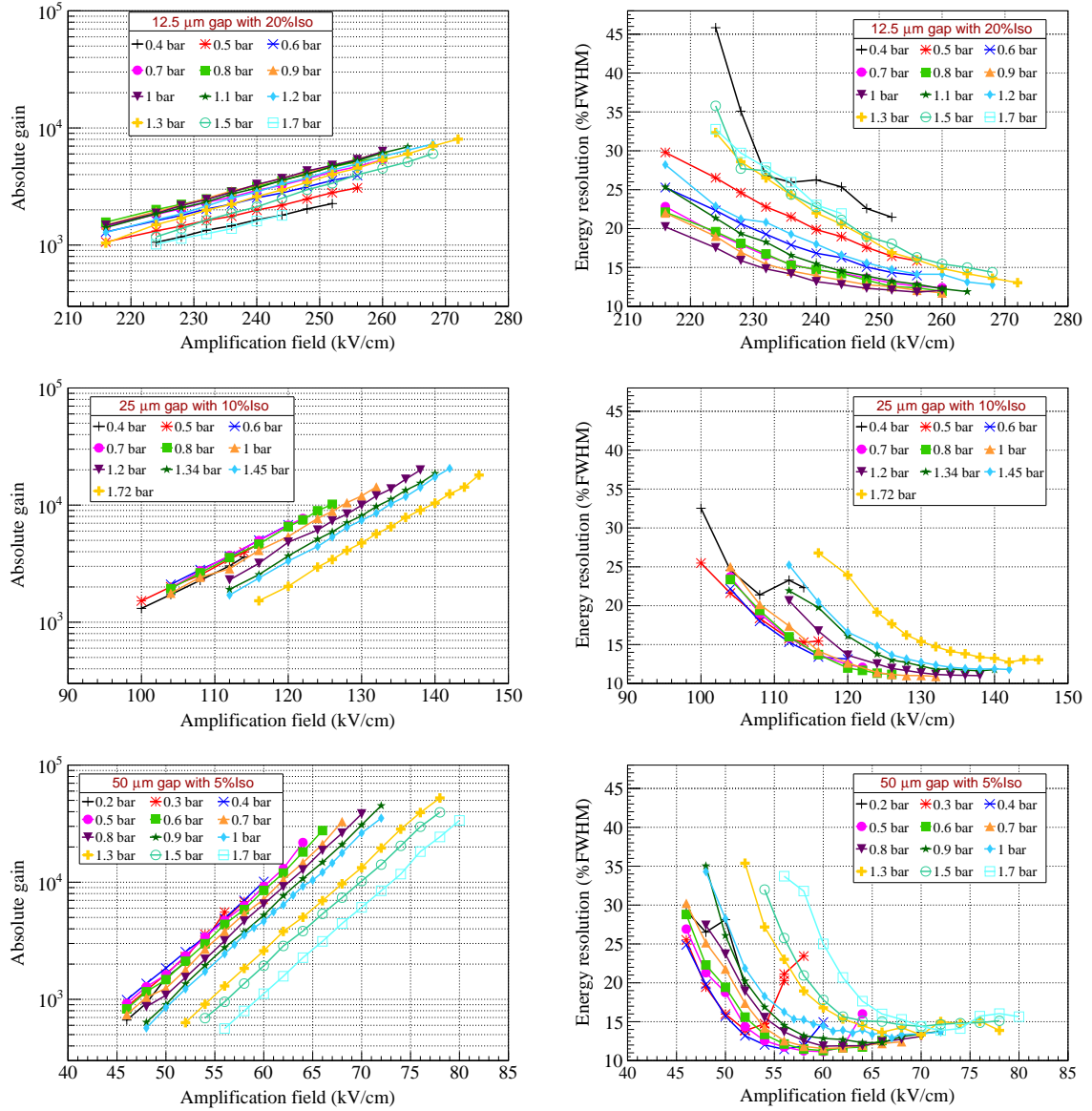
Figure 6.5: Gain measurements (left) and energy resolution (right) for various pressures in Argon-Isobutane mixtures: 20% for 12.5 μm, 10% for 25 μm and 5% for 50 μm amplification gaps.

amplification gap (μm)	Maximum gain $\times 10^4$ Ar+10%Iso.	Best energy resolution		
		(FWHM)	Pressure (bar)	Gas mixture
12.5	0.4	11.9	1.1	Ar+20%Iso.
25	1.4	11	1	Ar+10%Iso.
50	3.5	11	0.5	Ar+5%Iso.

Table 6.2: Summary of the maximum gains achieved in Argon+10%Isobutane and of the best energy resolutions for each amplification gap tested for different gas mixtures.

Figure 6.6: Gain (left) and resolution (right) versus pressure for $50\,\mu$m, $25\,\mu$m and $12.5\,\mu$m at a given amplification field for each detector gap.

Figure 6.7: Sketch of the 2D readout planes used up to now. Left: interconnected pixels in the two directions. Right: strips in the y direction and interconnected pixels in the x direction with metallised holes.
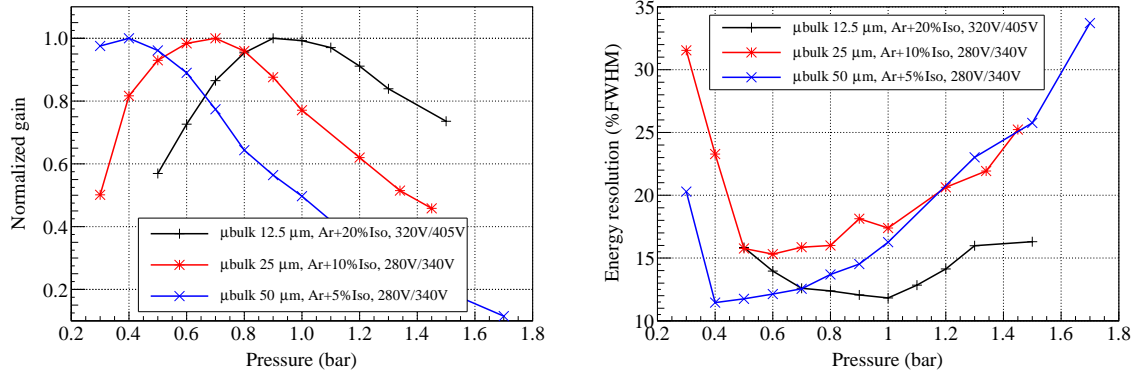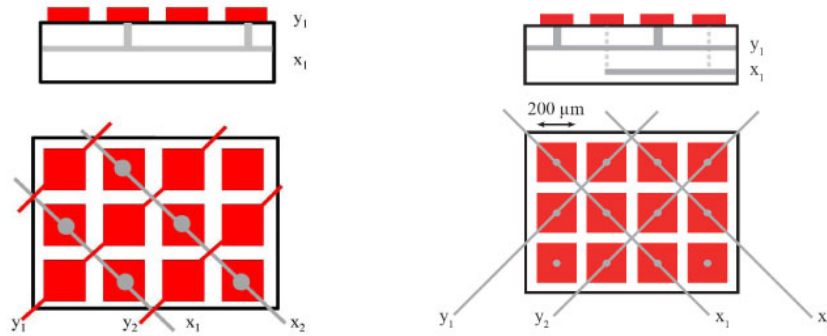
detectors have been developed since 2002 as described in previous chapters and have been used in a number of different applications like MIMAC and nTOF in a different context.

To cover medium or large surfaces with a 2D pattern, the developed strategy up to now is an $x - y$ structure out of electrically connected pads in the diagonal direction through metallised holes as shown in figure 6.7. This readout strategy reduces the number of channels with a fine granularity covering a large anode. In CAST, these anode signals are combined and are correlated to the integrated signal of the mesh in the discrimination algorithms. The mesh signal can also be used as a trigger signal. This strategy has been very successful and has allowed impressive background rejections as described in chapter 4. One of the issues of this structure is that in the theoretical limit of no gas diffusion, the charge would only be collected in one pixel and the 2D capabilities would be lost. Even if in practice this does not happen, the charge collection in the two directions is not completely equivalent. Another major disadvantage is the complexity of manufacturing of this multilayer stack. Moreover, when coupled to the microbulk technology, this readout structure complexifies the manufacturing of the detector and decreases the yield production.

We are developing a novel concept to have "intrinsic true 2D microbulks" detectors in the
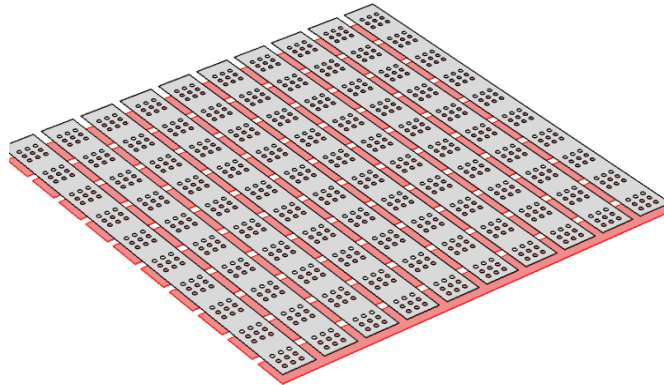
Figure 6.8: Sketch of the segmented mesh microbulk, the so called "intrinsic 2D microbulk".

context of an RD51[1] project in collaboration with the University of Zaragoza (Spain), NCSR Demokritos (Greece) and CERN. The idea is to manufacture a microbulk Micromegas detector with 1D strips in the readout plane and a stripped micromesh in the orthogonal direction. A sketch of the concept is shown in figure 6.8. We call it "intrinsic true 2D microbulks" because the two opposite fully correlated signals induced on the anode and on the mesh strips provide intrinsically spatial information in two directions. Furthermore this structure coupled to autotrigger electronics will be able to provide a very low threshold detector compaired for instance to the CAST detectors, where the trigger was provided by the whole mesh taking into account the total detector capacitance.

The manufacturing process is similar to that of the microbulk one and should be easier once it is mastered. At the moment the challenge is to maintain the top mesh $y-$strips intact while etching the kapton under the holes without completely removing the material in between the x–strips.

This concept, if successful, would open up large mass production of radiopure Micromegas detectors. It would be a big step forward for rare event searches communities especially directional dark matter and double beta decay searches where large surfaces detectors are needed. In addition this type of detectors would are also of interest for neutron beam imaging, as the detector has a very low material budget and interacts minimally with the beam.

6.3.2 First tests

In February 2012 the first batch of three segmented microbulks was delivered. The active area of the detector was of $38 \times 38\,\mathrm{mm}^2$ with Cu strips at a $1\,\mathrm{mm}$ pitch with a strip isolation of $100\,\mu\mathrm{m}$ and an amplification gap of $50\,\mu\mathrm{m}$. During manufacturing, the mesh holes were developed first and consequently the x and y strips. For the first batch trials, the detector design was kept very simple and the detectors were not equipped with lines for connectors.

---

[1]RD51 is a research collaboration based at Cern grouping around 90 universities and research laboratories around the world. All partners are already actively pursuing either basic or application oriented R&D involving a variety of MPGD concepts. http://rd51-public.web.cern.ch/RD51-Public/
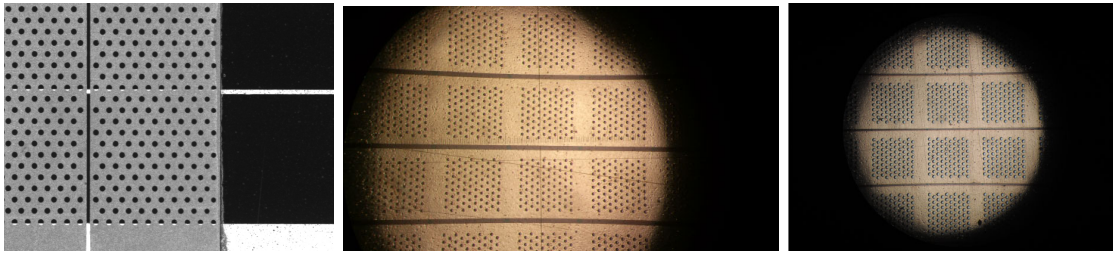
Figure 6.9: Pictures of the evolution of different batch of manufactured segmented mesh detectors. From the oldest to the present design (from left to right).

Their operation was problematic with many short circuits between strips. Pictures of the produced detectors are given in figure 6.9. One of the main problems was that the holes of the mesh were covering the interstrip kapton region of the x-strips favoring short circuits.

The second batch of these detectors was produced by the end of 2012. The geometry was changed slightly with an active area of 20×20 mm^2 with 20 $x-$strips and 20 $y-$strips with lines for external connection. The strip pitch and the strip isolation was the same as in the previous batch (1 mm and 100 μm respectively). Two different hole diameters were tested: 40 μm (3 detectors) and 60 μm (2 detectors). Despite a few strips in short circuits the detectors were tested in an Argon-5% Isobutane mixture with a ^{55}Fe source. As the detectors were not equipped with connectors, the test was performed by connecting all the y strips together and the x strips together. The detectors worked with a degraded energy resolution. Electric field simulations attributed this loss of performance to the perturbation of the electric field by the wide strip isolation (100 μm). This was corrected for the next batch of detectors.

The third batch of detectors was manufactured in September 2013 with the modified strip geometry. The detectors achieved reasonable gains (a few thousands) and energy resolution ranging from 13%-20% depending on the tested detectors. A summary of the performances is given in figure 6.10. The next step is to test the real 2D capability of the detectors by reading individual strips. Dedicated electronics have been developed in order to supply the bias high voltage and at the same time to provide the y signal information. We plan to test the detectors with autotrigger AGET electronics [31] to validate the 2D performance. In addition, a first fully operational prototype is being developed in the context of the NTOF experiment.

6.4   Piggyback Resistive Micromegas

In most of the Micromegas applications the design of the detector vessel and the readout plane are completely linked. A way of dissociating these two components would be by separating the amplification structure and detector volume from the readout plane and electronics. This is achieved with the so called "Piggyback" Micromegas detectors. The signal is then transmitted by capacitive coupling to the readout pads.

The operation principle is sketched in figure 6.11. The standard elements of a Micromegas detectors are shown: the drift plane, the amplification gap defined by a woven mesh connected to high voltage laying on pillars of around 100 μm height and a resistive layer.

The novelty is the way in which the resistive layer is deposited on an insulator substrate instead of being directly deposited on the anode plane. The insulator is then posed on the
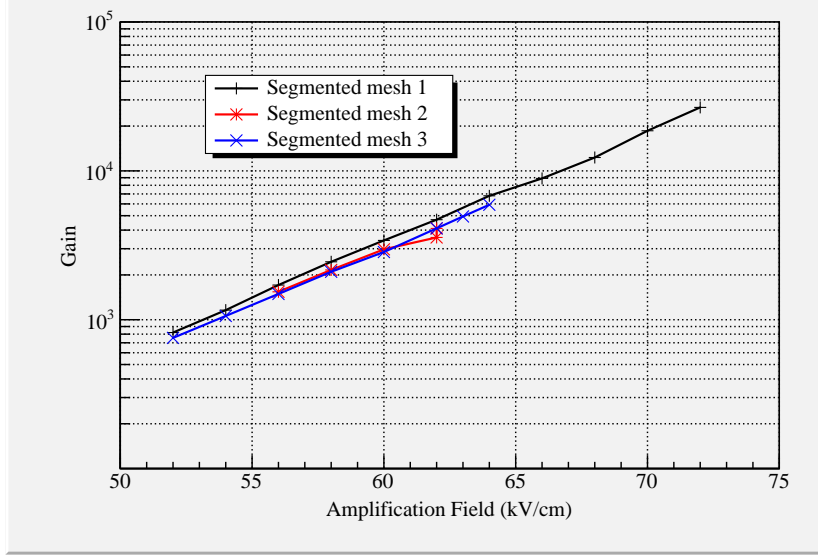
Figure 6.10: Gain as a function of amplification field for the last batch of manufactured segmented mesh detectors.

readout plane. The Micromegas detector operates as usual in the proportional avalanche mode inducing signals on the resistive anode plane. The structure needs to be optimised in such a way that the electronic signal is not lost through the resistive layer but is propagated to the readout plane i.e the capacitance of the insulator needs to be much larger than the capacitance of the amplification gap. In practice the optimisation consists in keeping the insulator thickness small compared to the product of the amplication gap and the dielectric constants ratio in the following way:

$$t_{\mathrm{insu}} \ll t_{\mathrm{amp}} \frac{\epsilon_{\mathrm{insu}}}{\epsilon_{\mathrm{gas}}} \tag{6.5}$$

where ϵ_{insu} is the dielectric constant of the insulator, ϵ_{gas} is the gas dielectric constant and t_{insu} and t_{amp} the thickness of the insulator layer and of the amplification gap respectively.

Materials with large dielectric constants are favoured ($\gg$10). The first experimental tests have been performed with a bulk Micromegas with an amplification gap, t_{amp}, of $128\,\mu\mathrm{m}$ and a ceramic layer with t_{insu} of $300\,\mu\mathrm{m}$. For the resistive layer, ruthenium oxide ($\mathrm{RuO_2}$) has been chosen for its robustness, stability and wide range of resistivity values available.

This new approach is described in [18] where characterisation measurements of gain, energy resolution, rate capability and coupling with a Medipix chip are shown. Here we only show the ongoing tests and the perspectives.

6.4.1 Current tests

Piggyback Micromegas is an adequate structure to build a low out-gassing detector. Tests in sealed mode have been performed and the stability of the performance of the detector has been studied with a standard detector in a Ne and 10% ethane mixture. The gain over 30 days has been monitored and is constant within less than 10% with a detector where no real particular precautions were taken for operation in sealed mode. The result is shown in figure
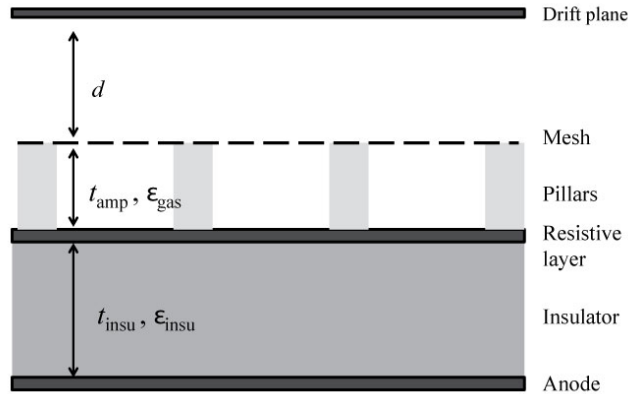
Figure 6.11: Sketch of the Piggyback structure.

6.12. The black points show the data recorded with the gas circulating while the the red points show the behaviour in sealed mode. The four high spikes observed in the "gas off" curve correspond exactly to the times that the source was removed and placed back due to charging up effects. The small repetitive fluctuations are probably correlated to day-nights effects and to the temperature of the laboratory. This effect will be verified in a future set-up where the pressure and temperature will be monitored. For the basic precautions taken, this result is very encouraging. On the contrary, the day-night effect is more prominent in the "gas on" mode where the behaviour of the detector is more subjected to these changes. The big spike present in the curve is attributed to this effect.

A new detector has been designed for this purpose. A sketch of this new design is shown in figure 6.13. The chamber is made out of stainless steel in order to minimise the outgassing and the ceramic is sandwiched between the two gaskets. In order to allow X-ray calibration from the outside of the detector, the piece constituting the body of the detector has been thinned in the central region down to $100\,\mu$m. Tests are on going to study the improved performance of this new design. Moreover we are currently studying how to optimise this mode of operation by means of the choice of construction materials, cycles of bake-out and choice of gas.

6.4.2 Perspectives

Piggyback resistive Micromegas detectors are a novel type of Micromegas detectors that are currently being developed. They open up new possibilities of application in terms of adaptability to new electronics. In particular, Piggyback resistive Micromegas can be easily coupled to modern pixel array electronic ASICs. First tests have been carried out with Medipix chips where the protection of the resistive layer has been proved. We are also investigating the possibility of coupling Piggyback Micromegas with the readout module of Caliste [122]. Caliste is a high performance spectro-imager with event time-tagging capability, able to detect photons between $2\,$keV and $250\,$keV in the context of a spatial micro spectro-imaging polarimetrer. It consists of the assembly of a 1 or $2\,$mm thick CdTe detector mounted on top of a readout module. In the current application we use the readout module only with the Piggyback Micromegas as the sensitive detector. We will benefit of the good spatial
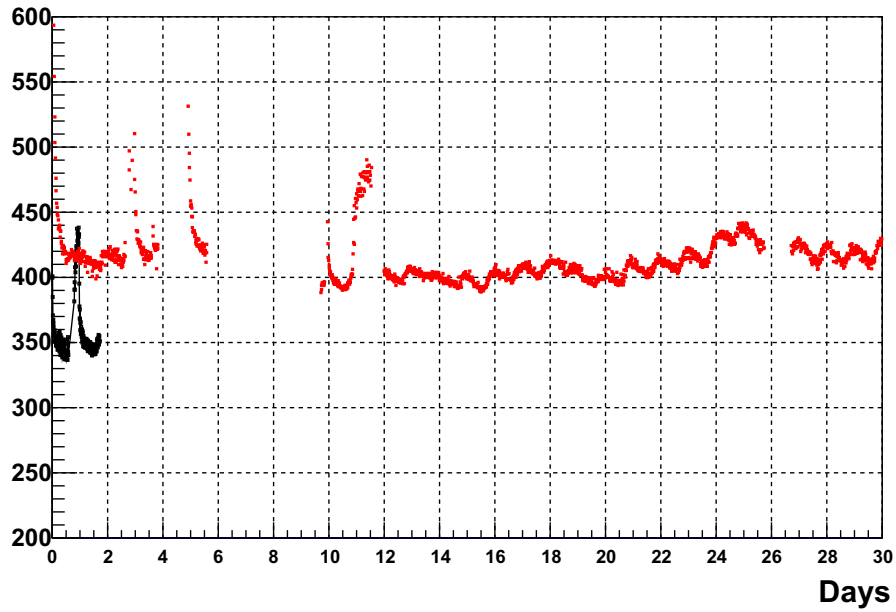
Figure 6.12: Gain in arbitrary units as a function of time. The black points represent data taken with circulating gas during 2 days and red points have been recorded in sealed mode for 30 days with a stability better than 10%.
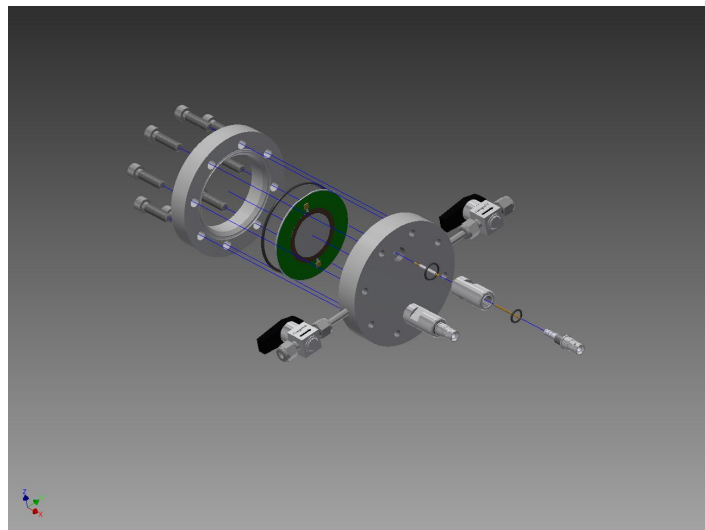

Figure 6.13: Sketch of the Piggyback structure.

resolution thanks to the high density readout pixels ($\sim$600 μm pixel pitch) and of the low noise, of the low power and of the radiation hard integrated front end IDEF-X electronics [124]. The advantage of such a device would be to have a high gain, low noise, low threshold, robust detector operated at room temperature. This would be very attractive for space applications, for instance X-ray polarisation.

6.5   R & D for the MIMAC experiment

The experimental signature of a Weakly Interacting Particle (WIMP) with matter is given by nuclear recoils produced by the elastic scattering of WIMPs with atomic nuclei. This signature has to be discriminated from neutrons that mimic the same signature. In the gas, an efficient way of achieving this discrimination is by correlating the elastic collisions in the detector with the relative motion of our solar system with respect to the galactic halo. Indeed it has been shown that most WIMPs would come from the direction of the Cygnus constellation showing a preferred direction [148]. This can be done if the direction of the recoil track of the events can be measured allowing to distinguish unambiguously the isotropical background from the anisotropical WIMP signal. The experimental challenges of the so-called directional dark matter experiment are the reconstruction of low energy (tens of keV) recoil tracks. In gaseous detectors operated at low pressure, the track extends a few mm needing a readout system with high spatial resolution. In solid detectors this is not possible as the recoils are of the order of 100 Å. MPGDs, and Micromegas in particular are specially suited thanks to their very good granularity, good spatial and energy resolutions and low threshold as already mentioned in the previous chapters. Moreover as discussed previously, the present manufacturing techniques, namely bulk [89] and microbulk [6], where the amplification region is produced as a single entity, allow production of large, robust inexpensive modules. In addition they can be made of very radiopure materials [48, 49, 50].

The MIcro-tpc MAtrix of Chambers (MIMAC) collaboration is developing a detector based on the direct coupling of large pixellized Micromegas with a specially developed fast self-triggered electronics showing the feasibility of a new generation of directional detectors. The R&D efforts devoted to the demonstration of the feasibility of the MIMAC experiment in which our group was involved, through an ANR funding, are discussed in detail in [98]. Here we outline the main points that we developed as well as the perspectives for the scaling up of the detector.

6.5.1   Design and operation of the MIMAC 10$\times$10 cm^2 prototype

The nuclear recoil produced by a WIMP in the TPC produces electron-ion pairs in the conversion gap of the Micromegas detector that drift towards the amplification gap (128 μm or 256 μm in this case) producing an avalanche that will induce signals in the pixelized $x - y$ anode and in the mesh. The third dimension z of the recoil is reconstructed by the drift time with dedicated self-triggered electronics specifically designed for this project [137, 138, 39, 38] that is able to perform a full anode sampling at a frequency of 50 MHz. The concept has been verified by the construction of a 10×10 cm^2 detector to validate the feasibility of a large TPC for directional detection with a realistic size prototype. The design of the bulk Micromegas was guided by the requirements on the granularity of the anode as well as by the operation conditions. Simulation studies showed that the granularity of the readout plane needed strips of 200 μm size. Moreover the end cap was designed to be versatile as the detector was first to

be validated by the T2K electronics [30] before the final conclusive test with the specifically designed MIMAC electronics.

The system consists of a leak-tight read-out plane on a 2 cm aluminium cap endplate. A general sketch of the mechanical assembly is given in figure 6.14. The system was designed to hold vacuum. The bulk Micromegas is fabricated on a Printed Circuit Board (PCB), called *Readout PCB*, of 1.6 mm thickness (*a* in figure 6.14).
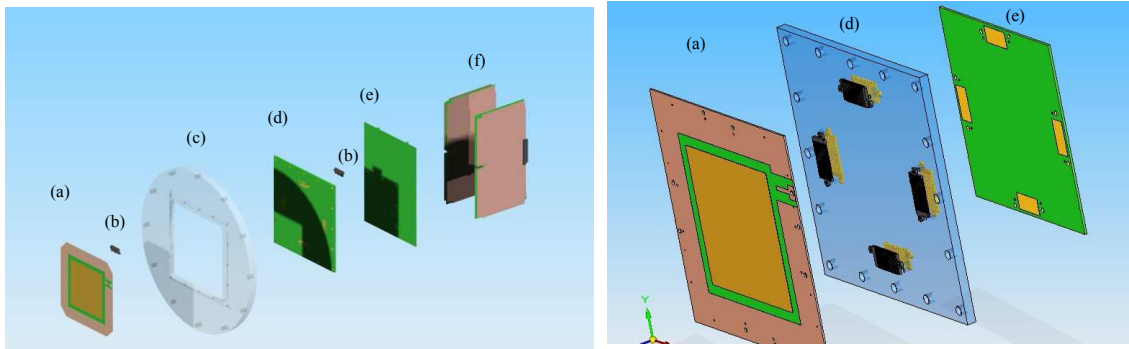

Figure 6.14: Left: Sketch of the mechanical assembly. Right: Zoom of the Readout PCB (*a* in the image), Leak tight PCB (*d*) and the Interface PCB (*e*).

The active surface is of $10.8 \times 10.8 \, \text{cm}^2$ with 256 strips per direction. The charge collection strips make-up an $x - y$ structure out of electrically connected pads in the diagonal direction through metallised holes as can be seen in figure 6.7 (right) similarly to the readout planes developed for the CAST experiment. The pads are $200 \, \mu\text{m}$ large with an isolation of $100 \, \mu\text{m}$ resulting into a strip pitch of $424 \, \mu\text{m}$. The quality of the surface of the readout plane can be observed in figure 6.15 (right). The $100 \, \mu\text{m}$ diameter metallised holes have been fully filled yielding a completely uniform surface. This fact is a prerequisite to obtain a uniform performance of a bulk Micromegas detector and not all printed circuit board companies are capable of achieving this surface finish. Another challenge was to extract in a compact way the electronic channels. This was done by using dense compact connectors shown in figure 6.14.

The readout planes were characterized in Saclay in Argon (95%)-Isobutane (5%) mixture at atmospheric pressure to validate the readout planes. In Grenoble, a prototype was mounted composed of two ($10 \times 10 \, \text{cm}^2$) readout planes with a common cathode with a 25 cm drift distance. The operation gas was a mixture of CF_4 (70%), CHF_3 (28%) and C_4H_{10} (2%) at 50 mbar. The standard gas for directional detection is CF_4 while CHF_3 has been added to lower the electron drift velocity and C_4H_{10} allows to reach higher gains.

The TPC was installed in the Modane underground laboratory in July 2012. It was calibrated with low energy X-rays demonstrating the capability of measuring low energy tracks [116]. The aim of the data campaign is to identify the main background sources. Moreover the detector has been used for neutron metrology of energies below 1 MeV proving the ability to measure nuclear recoils efficiently [120] and to obtain the directional sensitivity.
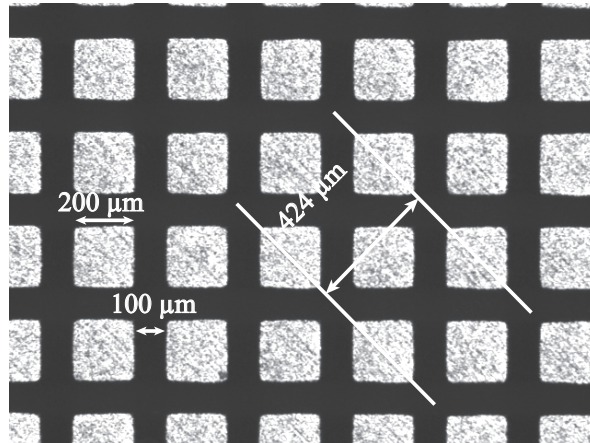
Figure 6.15: Microscope picture of the 2D readout for the MIMAC $10\times10\,\mathrm{cm}^2$ prototype.

6.5.2   Perspectives

The plans for the near future are to build a $1\,\mathrm{m}^3$ detector. The design is based on the concept of using dual TPC chambers but with an upgraded design to include larger Micromegas modules (35×35 cm^2). The readout planes developed for the previous prototypes could be extrapolated to larger surfaces, however at a high cost. It seems more reasonable to opt for a different readout technique. If the ceramic support of the Piggyback Micromegas can be made out of low radioactive materials, this might be a possible solution. Another challenge is to cope with the high channel density for large area detectors. The Piggyback Micromegas could also be an appropriate solution for this aspect. These options are being explored at the moment for the construction of a $1\,\mathrm{m}^3$ detector. The electronics will also be upgraded to include a fiber optical link to synchronise the chambers in order to be able to veto multiple events. Special care will be taken to select carefully the materials of the construction of the detector in order to improve the radiopurity of the system.

Conclusion and Perspectives

Axions were predicted more than 25 years ago to explain the absence of charge-parity symmetry violation in strong interactions. These neutral, very light particles (in the mass range 10^{-5}–$10\,\mathrm{eV}$) interact so weakly with ordinary matter that they are good candidates for Dark Matter. Besides, axions can also be created near the strong electric field inside the hot plasma core of the sun, where thermal X-rays can be efficiently converted into axions. These axions would stream out freely and arrive on Earth in quantities larger than solar neutrinos.

The CERN Axion Solar Telescope (CAST) is devoted to the search of QCD-inspired solar axions using an LHC dipole magnet. To cover the widest possible range of axion masses, spanning between cosmologically derived lower (cold Dark Matter) and upper (hot Dark Matter) limits, the operation of the CAST experiment was divided into two phases. During phase I (2003-2004) the experiment operated with vacuum inside the magnet bores and covered axion masses up to $0.02\,\mathrm{eV}$. In order to extend the CAST sensitivity to higher axion masses, the experimental setup was upgraded in 2005 to operate with magnet bores filled with a buffer gas. To equally cover a possible range of axion masses above $0.02\,\mathrm{eV}$, the gas density has been increased in appropriate steps. By the end of the 2011 the experiment scanned the range up to $1.16\,\mathrm{eV}$ achieving its original goal. CAST published results represent the best experimental limit on the photon couplings to axions and other similar exotic particles called WISPs (Weakly Interacting Slim particles) in the considered mass range, and for the first time the limit enters the region favored by QCD–axion models.

The CAST experiment has been a fertile ground for the development of Micromegas detectors as a competitive option for rare event detection experiments. The levels of background achieved by the present microbulk detectors, $<10^{-6}\,\mathrm{counts\,keV^{-1}\,cm^{-2}s^{-1}}$, are more than two orders of magnitude better than the levels obtained with the first Micromegas detectors installed in 2003. This accomplishment has been possible thanks to the development of the microbulk technology but also to the detailed study of the background and to the shielding optimisation as well as the refinement of the selection procedure. These achievements have enabled reconsidering some of the past data taking configurations with enhanced sensitivity to standard Peccei-Quinn axion models, the main objective of CAST. In particular in 2014-2015, the data taking will be devoted to reconsider the vacuum CAST phase I, with major upgraded configuration detector systems in particular Micromegas detectors with improved performances and the introduction of a new X-ray telescope. This can be considered as a preliminary step and a path finder for the Micromegas-X-ray systems required for the 4th generation of axion helioscope: the International Axion Observatory (IAXO).

IAXO aims at building and operating a new generation axion helioscope with a sensitivity much beyond current CAST limits. IAXO is based on the design and construction of a dedicated superconducting magnet, optimised to maximize the figure of merit of an axion helioscope. This will be accomplished with a magnet of toroidal geometry that will allow to

increase the magnetic volume by more than 2 orders of magnitude with respect to the CAST magnet. The design of the proposed magnet system is largely inspired of the toroidal magnet system of the ATLAS detector at the LHC. Moreover, IAXO will pursue and extend the originalities and innovations of CAST by the extensive use of X-ray optics in every magnet bore and the use of ultra-low background Micromegas detectors.

Following my participation to the CAST experiment, to the development of the microbulk technology and having contributed to the Letter of Intent I would like naturally to pursue in the optimisation of the Micromegas detectors for IAXO and in the effort that will lead to its construction.

Besides the detector developments for the CAST experiment, I have also taken part in an R&D effort to develop a large scale Dark Matter directional detector, MIMAC (MIcro TPC MAtrix of Chambers). The MIMAC collaboration aims at building a directional Dark Matter detector composed of a matrix of Micromegas detectors measuring both 3D track and ionization energy of recoiling nuclei, thus leading to the possibility to achieve directional Dark Matter detection. Prototypes using bulk Micromegas of $10 \times 10 \, cm^2$ have been designed and built. Characterisation tests in the laboratory have shown good performance in terms of gain, uniformity, energy resolution and track measurements. The detectors have been tested in a neutron beam facility with neutrons of few keV using the specifically designed MIMAC electronics demonstrating that the detector can efficiently reconstruct the nuclear recoils produced by neutrons. A bi-chamber module was installed in the Frejus underground laboratory running for long data periods (2×4 months) helping to define the project of the construction of a bigger competitive detector. The next step will be to build a detector at the $1 \, m^3$ scale. In the next few years, hopefully with the support of the French National Research Agency (ANR), I will participate to the design, manufacturing, tests and characterisation of such a detector.

To conclude, three aspects of generic R&D have been discussed in this manuscript. The first two concern the microbulk technology: small gap and segmented mesh microbulks. For the small gap, microbulks detectors of 25 and $12.5 \, \mu$m amplification gaps have been manufactured and tested with success obtaining high gains and energy resolutions as low as 11-13% (FWHM) at 5.9 keV. These values are very close to the minimum energy resolution that can be achieved with gaseous detectors taking into account the fluctuations due to electron multiplication. The behaviour of these detectors have also been studied as a function of pressure from 0.5 bar to 1.7 bar. Their performance follows the expected bell shape with pressure: smaller gaps exhibit the maximum of performance at higher pressures. These tests confirm the suitability of small gap microbulk detectors for rare event detection and represent an interesting option for the R&D efforts of Micromegas for the NEXT experiment.

The second aspect of development of the microbulk technology concerns the segmented microbulk. This is a novel concept to obtain $x - y$ low mass detectors that are under development. The idea is to have 1D strips in the readout plane and a stripped micromesh in the orthogonal direction. The manufacturing process becomes then very simple. A recent production of successful detectors have been achieved showing confortable gains (a few thousands) and reasonable energy resolutions (13%-20% FWHM at 5.9 keV). The 2D capability of the detectors is being tested at the moment. This concept opens up large mass production of low mass, flexible, radiopure Micromegas detectors. It will be a big step forward for the rare event

searches community especially double beta decay searches where large surfaces detectors are needed. In addition these segmented detectors are very attractive for measurements of flux and monitoring of neutron beams. In the context of the NTOF experiment, we will develop a segmented microbulk detector with the support of P2IO Labex funding.

The third area of generic R&D research that has been exposed is related to Piggyback Micromegas: this new concept consists in a Micromegas bulk detector manufactured on top of a resistive anode deposited on a thin ceramic substrate. One of the main advantages is that the active region is dissociated from the readout plane providing full spark protection by the resistive layer. Another relevant advantage is its excellent outgassing properties making it appropriate for sealed operation opening up new windows of applications. The first tests have proved the effectiveness of the protection of the resistive layer. Sealed detector operation is also being investigated for the first time. The radiopurity of this new structure has to be measured but it could be interesting for large rare event detection experiments in order to limit the number of electronic channels by the use of the resistive coating keeping a high spatial resolution with a large strip pitch. In addition the dissociation of the amplification structure from the readout plane gives versatility on the electronics to be used. We have started a collaboration to couple a Piggyback Micromegas with the readout module of Caliste (high performance spectro-imager with event time-tagging capability with a 2 keV and 250 keV sensibility). At present the first integration tests are taking place. The main advantages of such a device would be to have a high gain, low noise, low threshold, robust detector operated at room temperature. This would be very attractive for spatial applications, for instance for X-ray polarisation measurements.

To conclude this memoir, I can say that retracing my main activities in instrumentation in gaseous detectors for rare event search experiments over the last 12 years has been an interesting and useful exercise, at least at a personal level. I can only hope that the future will be as stimulating and exciting as these past years.

Appendix: Publications

The Micromegas detector of the CAST experiment

P Abbon[1], **S Andriamonje**[1], **S Aune**[1], **T Dafni**[1,2,3],
M Davenport[4], **E Delagnes**[1], **R de Oliveira**[4], **G Fanourakis**[5],
E Ferrer Ribas[1,9], **J Franz**[6], **T Geralis**[5], **A Giganon**[1], **M Gros**[1],
Y Giomataris[1], **I G Irastorza**[1], **K Kousouris**[5], **J Morales**[1],
T Papaevangelou[4], **J Ruz**[7], **K Zachariadou**[5] and **K Zioutas**[3,8]

[1] DAPNIA, Centre d'Études Nucléaires de Saclay (CEA-Saclay),
Gif sur Yvette, France
[2] Technische Universität Darmstadt, IKP, Schlossgartenstrasse, 9,
D-64289 Darmstadt Germany
[3] Gesellschaft für Schwerionenforschung, GSI-Darmstadt, Plasmaphysik,
Planckstr. 1, D-64291 Darmstadt
[4] European Organization for Nuclear Research (CERN), CH-1211 Genève 23,
Switzerland
[5] National Center for Scientific Research 'Demokritos', Athens, Greece
[6] Universität Freiburg, Physikalisches Institut, Herrman-Herder-Strasse 3,
D-79104 Freiburg, Germany
[7] Instituto de Física Nuclear y Altas Energías, Universidad de Zaragoza,
Zaragoza, Spain
[8] University of Patras, Patras, Greece
E-mail: eferrer@dapnia.cea.fr

Abstract. A low-background Micromegas detector has been operating in the CAST experiment at CERN for the search for solar axions during the first phase of the experiment (2002–2004). The detector, made out of low radioactivity materials, operated efficiently and achieved a very high level of background rejection (5×10^{-5} counts $keV^{-1} cm^{-2} s^{-1}$) without shielding.

[9] Author to whom any correspondence should be addressed.

IOP Institute of Physics Φ DEUTSCHE PHYSIKALISCHE GESELLSCHAFT

Contents

1. Introduction

The CAST experiment (Zioutas *et al* 2005, Andriamonje *et al* 2007a) uses three different types of detectors to detect the x-rays originating from the conversion of the axions inside a magnet: a time projection chamber (TPC, Autiero *et al* 2007), an x-ray telescope (Kuster *et al* 2007), and a Micromegas detector. The Micromegas detector of CAST is a gaseous detector optimized for the detection of low energy (1–10 keV) x-ray photons. It is based on the micropattern detector technology of MICROMEGAS (MICROMEsh GAseous Structure) developed in the mid 90s (Giomataris *et al* 1996, Giomataris *et al* 1998, Charpak *et al* 2002). Collar and Giomataris (2000) first suggested the advantages of using the Micromegas for low-threshold, low-background measurements such as those required by the CAST experiment. These advantages include sensitivity in the keV and sub-keV energy region where very good energy resolution can be achieved, excellent spatial resolution, one-dimensional or *X–Y* readout capability, stability, construction simplicity and low cost. In addition, the proper choice of construction materials would lead to a detector appropriate for low-background measurements.

The CAST Micromegas group designed and constructed a low-background detector, the very first made with an *X–Y* readout structure, optimized for the efficient detection of 1–10 keV photons. Several detectors have been developed during the course of the CAST running, each successive detector with increasingly improved characteristics replacing the older module during shutdown and maintenance periods. The detector is mounted on one of the two west superconducting magnet apertures looking for 'sunrise' axions converted into x-ray photons that will enter the detector active volume perpendicularly to the *X–Y*-strip plane.

2. Detector description

The principle of operation of the Micromegas detector designed for the CAST experiment is sketched in figure 1. A photon, after traversing a vacuum buffer space, enters the conversion-drift region, filled with a mixture of argon–isobutane (95–5%), where it generates a photoelectron
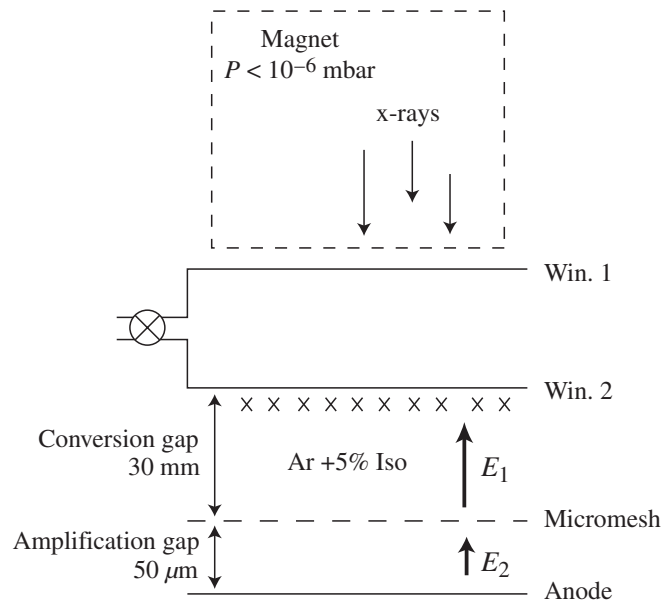
Figure 1. The Micromegas CAST detector.

via the photoelectric effect. The photoelectron travels a short distance during which it creates ionization electrons. The electrons drift in a field of about $250\,V\,cm^{-1}$, until they reach and funnel through the micromesh and into the amplification region where a strong field of about $40\,kV\,cm^{-1}$ causes an avalanche. The resulting electron cluster is collected on the *X–Y*-strips of the anode plane. The maximum achievable gain is about 10^5, but for CAST gains of 5×10^3 up to 10^4 are sufficient to achieve the required threshold (around $1\,keV$).

The main sources of background are cosmic rays and natural radioactivity. Special care has been taken in the materials used for the construction of this Micromegas detector in order to reduce the natural radioactivity: the body of the chamber is made out of Plexiglas, all the weldings inside the detector have been made with low radioactive soldering and the readout plane is made out of Kapton or Kevlar (FR4 epoxy has been avoided). Other developments have been necessary in order to optimize this detector, given the aim and the environment of the experiment. A description of the most important elements specific to the CAST Micromegas detector are given below.

2.1. Mechanical structure

The detector frame consists of Plexiglas cylinders held together via plastic bolts. The drift and multiplication electrodes are attached to these cylinders. Figure 2 shows the mechanical structure of the detector. The conversion region can be 2.5 or 3 cm thick and is formed between a 4 μm thick aluminized polypropylene window, glued on stainless steel or aluminium strongback, capable of holding vacuum at the magnet side, and the micromesh plane. The window of the conversion region also serves as the cathode for the drift field. The amplification region is only 50(100) μm thick and is formed between the micromesh plane and the charge collection plane with the help
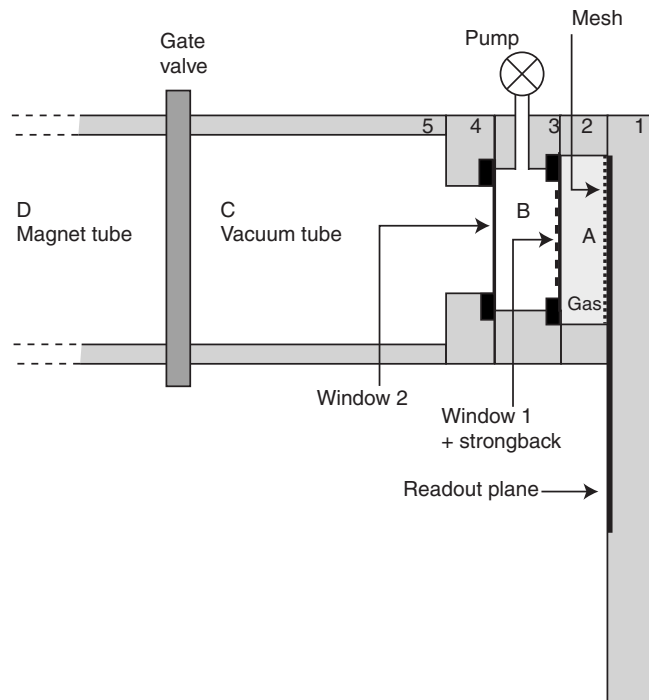
Figure 2. The mechanical design of the detector. The drift electrode is attached on disk 3. The micromesh on disks 2 and 4 is used to hold an extra vacuum window. The drawing is not made to scale.

of pillars spaced 1 mm apart with a diameter of $100\,\mu$m. The micromesh is made of $4\,\mu$m thick copper and is fabricated at CERN (Delbart *et al* 2001). The active zone of the detector is $45\,\text{cm}^2$.

2.2. Differential pumping

The detector is fastened to one of the magnet bores with the help of an aluminium tube and a flange. A gate valve separates the magnet volume from the tube volume. In order to couple a gaseous detector with a vacuum environment, keeping the maximum transparency to x-ray photons and a minimum vacuum leak, the solution of two $4\,\mu$m polypropylene windows with a differential pumping was adopted. The first window, that undergoes a pressure difference of 1 bar, is glued on a strongback with a 94.6% transparency. The two windows delimit 3 zones that can be seen in figure 2. Zone A is the gaseous detector at a pressure of 1 bar. Zone B is the vacuum gap at a pressure of 5×10^{-4} mbar obtained with the pumping group. Zone C is the vacuum tube at a pressure of 5×10^{-7} mbar in the magnet. The leak of the first window is proportional to the differential pressure between zone A and B, i.e., 1 bar. This differential pressure imposes the use of a strongback. The leak for this window due to its porosity, tested with zone A full of helium, is 4×10^{-5} mbar l s^{-1}. As the differential pressure between zones B and C is only 5×10^{-4} bar, a strongback is not needed. The net leak for this window when zone A is full of helium, has been measured to be 3×10^{-9} mbar l s^{-1}. The leak on the first window has
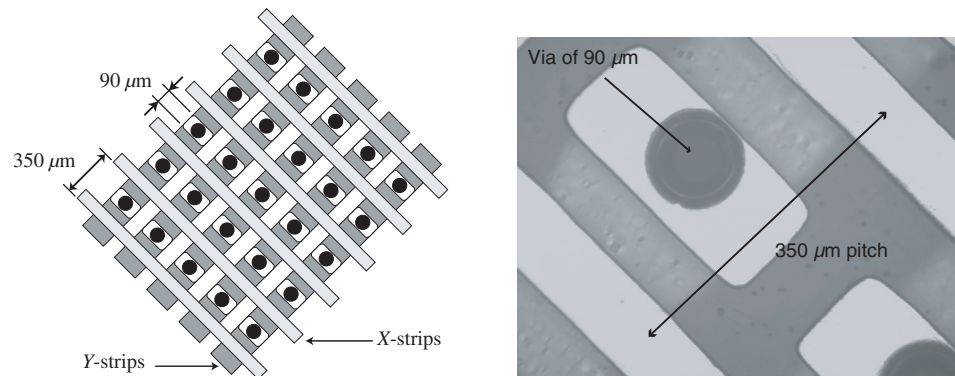
Figure 3. The X–Y-strip charge collection structure. The strip pitch is $350\,\mu$m. The X-srips are those in light grey and the Y-strips, in the underneath layer, in dark grey. The metalized holes of $90\,\mu$m diameter, allow the surface charge collection for the Y-strips.

been evacuated by the pump. The pump system used for this application is made of a small dry turbo pump (magnetic bearing) and of a dry primary pump. The convolution of the transmission of the two windows together with the conversion efficiency of photons in the detector gas (argon with 5% isobutane) over the energy spectrum of solar axions between 2 and 10 keV results in a combined efficiency of 85%. For sub-keV sensitivity a more efficient gas, like xenon, could be used as well as thinner polypropylene windows.

2.3. Charge collection in two dimensions

The charge collection strips make-up an X–Y structure out of electrically connected pads see figure 3. The connections for the formation of the X-strips are on one side of the doubly copper clad Kapton, while the connections for the Y-strips are made at the other side, with the help of metalized holes on the Y-pads. Each CAST detector has 192 X- and 192 Y-strips of $350\,\mu$m pitch making up an active area of about $45\,\mathrm{cm}^2$ as already mentioned. The Kapton with the X- and Y-strips and the readout lines is glued on a paddle shaped plexiglass piece of the Micromegas structure, where the readout connectors are also fastened. New improvements are underway combining an integrated Micromegas and a CMOS micro-pixel anode plane (Colas *et al* 2004, Giomataris *et al* 2006).

2.4. Readout electronics and data acquisition

The charge on the X- or Y-strips is read out with the help of four front end (FE) electronic cards based on the Gassiplex chip (Santiard *et al* 1994) controlled by a CAEN sequencer (V 551B) with two CRAM (V550) modules in a VME crate (Geralis *et al* 2003).

One FE card integrates 96 signals (96 strips) and operates at a maximum clock speed of 1 MHz. It provides a multilevel output where each level corresponds to the result of the integration of the signal from a particular strip. The cards are powered by a 6 V power supply (positive and negative). The sequencer provides the proper timing signals (clock, track and hold and reset) to the FE cards. The CRAM modules integrate and store the total charge of each channel indicated
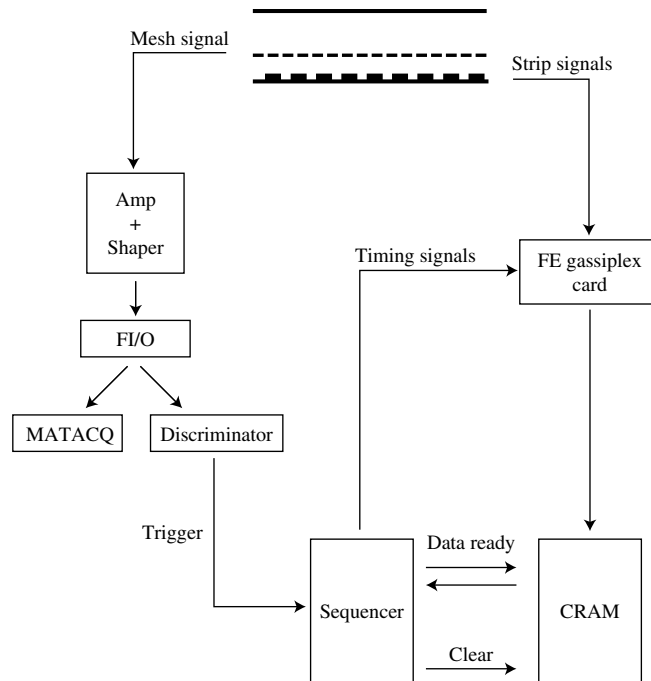
Figure 4. Trigger and readout logic.

by the signal provided by the FE cards until the software reads the data and transfers them to the PC for permanent storage and analysis. The signal for triggering the Micromegas device is obtained through the micromesh signal. The output of the preamplifier is subsequently shaped and amplified to produce the appropriate trigger signal. Because of the low rates involved (1 Hz) the zero suppression and pedestal subtraction capabilities of the CAEN modules are not used and all strip data are recorded.

The features of this Micromegas detector also include the recording of the mesh pulse via a high rate sampling VME digitizing board, the MATACQ (MATrix for ACQuisition) board (Breton *et al* 2005). This board, based on the MATACQ IC, can code 4 analogue channels of bandwidth up to 300 MHz over 12 bits dynamic range and a sampling frequency reaching up to 2 GHz and over 2520 usable points. One of these channels is used to record the time structure of the mesh pulse. Signal events have a characteristic mesh pulse that will be used in order to reject events with unexpected shapes as background events. Figure 4 shows a schematic of the Micromegas trigger and readout.

The data acquisition and monitoring system is based on the LabView software package, of National Instruments, running on a PC with either the Linux RedHat 7.3.1 (CERN release) or the Windows 2000 operating system. A dual boot PC is used to connect to the VME controller and run the data acquisition software. The connection is performed via a PCI-MXI2 card sitting on the PCI bus of the PC, a VME-MXI2 controller card sitting on the VME and a 20 m long MXI2 cable connecting these two cards. The DAQ system runs on Linux since it provides the facilities of the CASTOR (CERN Advanced STORage manager) automatic data archiving system and the xntp software for the synchronization of the PC clock to the GPS universal time. The online software is controlled by LabView virtual modules that initialize the run (allowing parameters
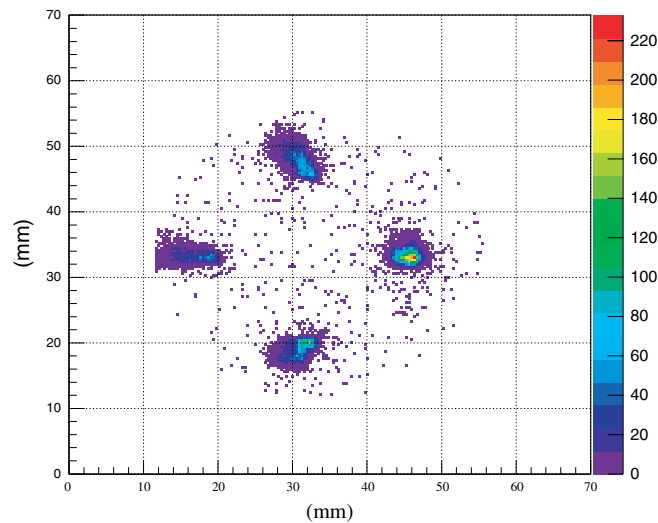
Figure 5. A two-dimensional plot showing the *X–Y*-strip image of the four holes where the 5.9 keV x-rays go through during a calibration run. The individual image of the holes is not identical due to the relative position of the source with respect to the detector plane. The units of the colour scale are counts.

to be changed) and monitor its status. An event display is used to view the strip charges and the mesh signal recorded by the MATACQ board. An online analysis is performed in order to give out plots that are used to monitor the detector performance.

2.5. Calibrator

The calibration of the detector is done by shining a ^{55}Fe source daily at the back of the detector. An automatic mechanism, controlled by the acquisition software is used; the ^{55}Fe source is moved in front of four blind holes drilled in the Plexiglass paddle piece to allow the passage of the 5.9 keV x-rays in the chamber (see figure 5). Once the calibration run is finished the source is parked inside a lead shielding.

3. Detector performance

3.1. Characterization

To characterize the detector a test was done at the PANTER x-ray facility of the Max-Planck-Institut für extraterrestrische Physik (MPE) in Munich (Freyberg *et al* 2005). A detector was mounted in the focal plane at the x-ray focusing telescope (now part of the CAST experiment) and tested with photon beams of varying energy. The detector, at the time, had a buffer space between the vacuum window and the detector drift electrode filled with helium gas at atmospheric pressure. The buffer of helium gas was used in order to couple the gaseous Micromegas volume at atmospheric pressure to the vacuum environment of the x-ray telescope (and of the CAST magnet bore) before the solution of the differential pumping was adopted. The drift space was
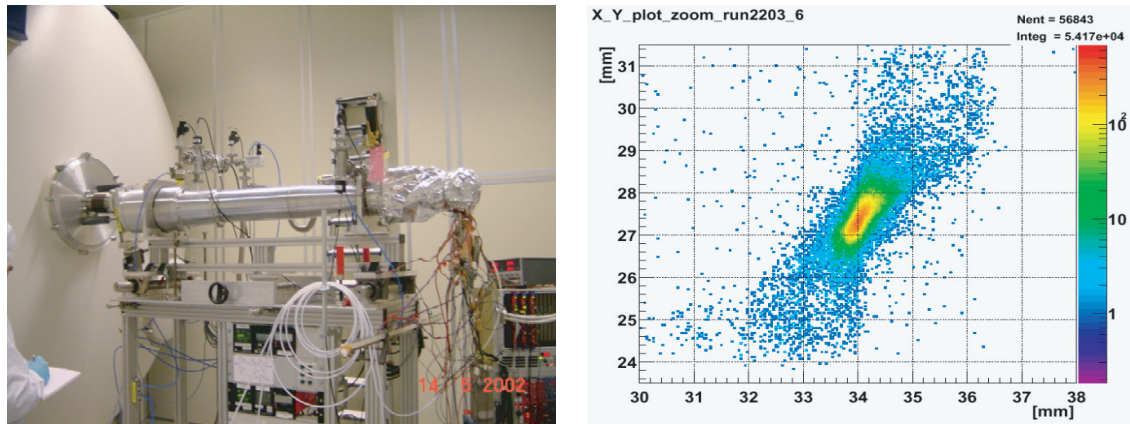
Figure 6. Left panel: photo of the Micromegas detector mounted in the focal plane of the x-ray telescope at the PANTER facility. Right panel: transverse position of the 4.5 keV focused photon beam at PANTER.
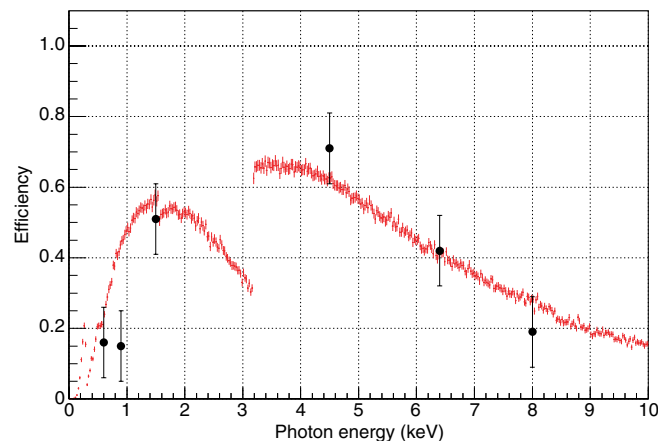

Figure 7. Simulated detector efficiency as a function of energy compared with the experimental points measured at PANTER. The agreement between the simulation and the experimental points shows that the behaviour of the detector is understood correctly.

18 mm wide and the amplification gap was 50 μm. The *X–Y* position determination capability was for the first time shown and the remarkable agreement with the beam shape expected from the focusing properties of the x-ray telescope exhibited (Andriamonje *et al* 2004). Figure 6 shows a photo of the experimental set-up as well as the logarithmic intensity plot of the *X–Y* position of 4.5 keV photons at the focus. The millimetre size core of the beam is clearly visible.

The efficiency of the detector was simulated using the GEANT4 package (Agostinelli *et al* 2003). The dimensions of the detector, the materials of the windows (drift and helium buffer), the gas mixture as well as the beam spot were taken into account. In figure 7 the simulated efficiency with the experimental measured points is shown. The agreement observed within experimental
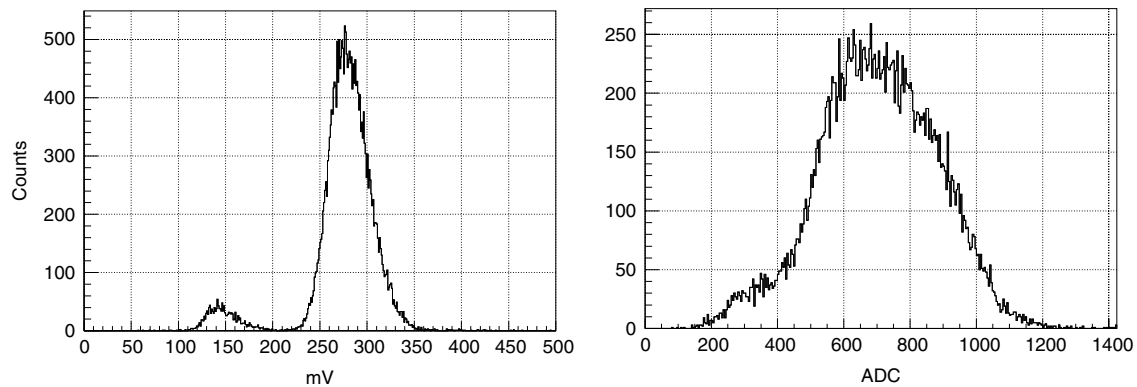
Figure 8. Energy spectrum for a calibration run using a ^{55}Fe source obtained with the mesh signal read by the MATACQ card (left panel) and with the strips (right panel). The energy resolution obtained with the strips is degraded due to residual crosstalk between the strips.

errors allow us to use this simulation with slightly different parameters (drift space or window thickness) for the detectors that were used in the data taking periods.

3.2. The 2003 detector

The Micromegas detector used for 2003 data taking was designed with a 25 mm drift space and 50 μm amplification gap, formed by the help of Kapton pillars on the micromesh plane. The detector accumulated data from May to mid-November without accidents. For the last three months of data taking, the MATACQ card was installed allowing the recording of the pulse structure of the mesh pulse. An example of a calibration run is given in figure 8 where an energy resolution of 16% (FWHM (full width at half maximum)) is obtained at 5.9 keV. The energy resolution obtained with the strips is about 30%. This degraded performance was due to some crosstalk between the strips caused by residual copper left on the Kapton pillars of the micromesh, which when in contact with the copper strips of the readout plane gave rise to this crosstalk. This effect can be removed by improving the etching process used to develop the micromesh. In principle this technique is now well mastered.

The detector's linearity was verified by using a ^{109}Cd source which produced fluorescence of the detector's material at different energies. Figure 9 shows the energy spectra as well as the linearity. The system was extremely stable: the time characteristics and energy response of the mesh pulses showed less than a 2% variation during the entire period.

The Micromegas detector records tracking data at sunrise, and during the rest of the day background data is taken. The detector is calibrated daily. Signal events (photons with energy of 1–8 keV) have a well defined signature giving a typical cluster in the read out strips and a typical pulse in the micromesh. Background events, coming from cosmic rays and natural radioactivity, give a bigger cluster in the strips, and the pulse shape in the micromesh is very different, favouring an efficient rejection based on the micromesh pulse shape and on the cluster topology.

In figure 10, two event display windows show the distribution of X- and Y-strip charges and the MATACQ pulse for a calibration and a background event. It can be observed that the pulse shape is very different in the two cases. The topology of the clusters is a discriminant element as
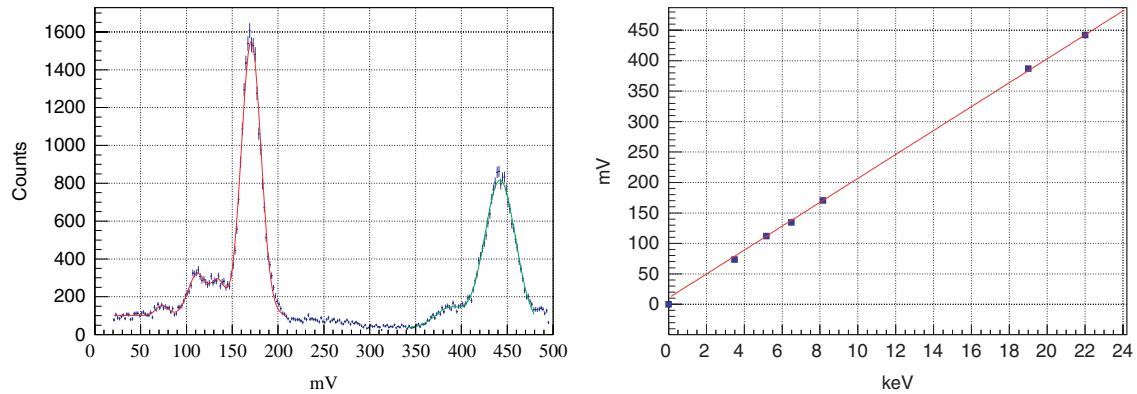
Figure 9. On the left panel energy spectra obtained with a Cd source. Peaks at 8 keV due to the fluorescence of the copper and the Cd 22 keV peak can be seen and their escape peaks at lower charge. On the right panel, the linearity plot showing the pulse height as a function of energy.
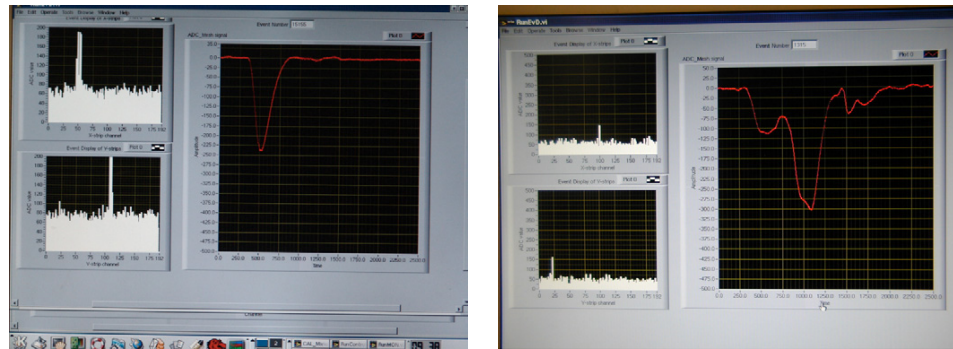

Figure 10. Event display showing the distribution of X- and Y-strip charges in the MATACQ pulse. Right panel: distributions obtained for a calibration event. Left panel: distributions for a background event.

well as the number of clusters in the event as can be seen in figures 11 and 12. In a background event there is a high probability of having more than one cluster whereas in a calibration event, most of the time, (more than 90%), the event has a single cluster.

The offline analysis was based on sequential cuts, mainly on the micromesh pulse observables and less on the clustering (due to the strip crosstalk). Figure 13 shows the energy spectra for background events after the sequential cuts where the average background rate is 1.4×10^{-4} counts cm^{-2} s^{-1} keV^{-1} region. The background is composed of events coming from cosmic rays, natural radioactivity and fluorescence from materials present in the detector. The most visible peak is at 8 keV due to the copper present in the anode plane as well as in the mesh cathode. The efficiency is defined as the ratio of the number of events that pass sequential cuts over the number of initial reconstructed events before cuts. This efficiency was calculated using daily calibration data runs giving 80 and 95% for 3 and 5.9 keV respectively.
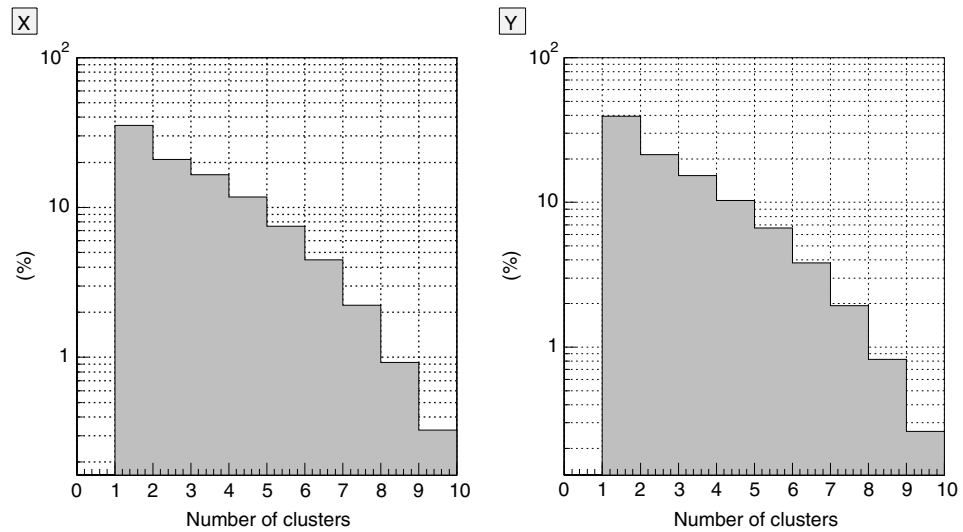
Figure 11. Percentage of events as a function of number of clusters in *X*- and *Y*-directions for background events.
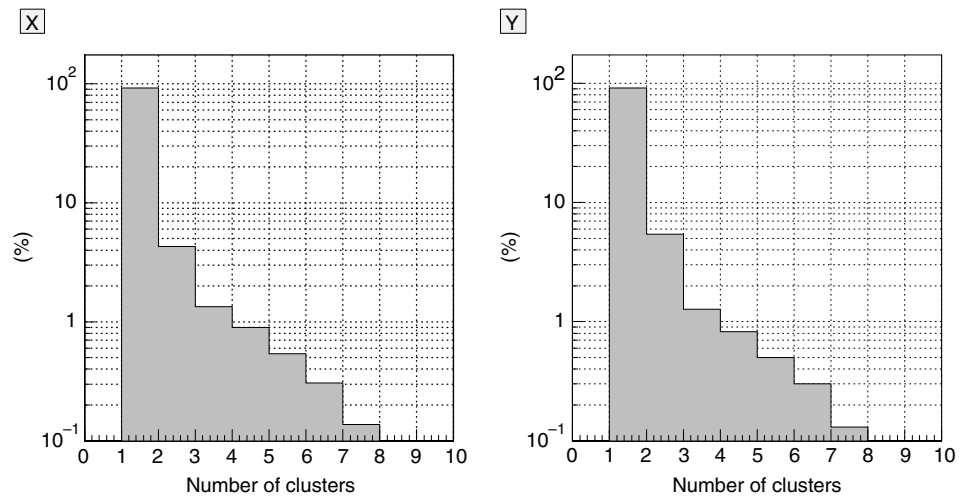
Figure 12. Percentage of events as a function of number of clusters in *X*- and *Y*-directions for calibration events.

3.3. The 2004 detector

The experience acquired during the 2003 run led to the development of the so called V4 model with 30 mm conversion gap and 100 μm amplification gap, which was designed to eliminate the 'crosstalk' effects present in the previous model and to improve the quality of the strips. Both goals were achieved and moreover a faster MATACQ board was installed, reducing the detector's dead time to 14 ms (less than 1.5% of the net data rate) while the energy resolution was 19% FWHM at 5.9 keV. The spectra obtained with the mesh signal recorded by the MATACQ card (left) and with the strips (right) are shown in figure 14. The energy resolution obtained with
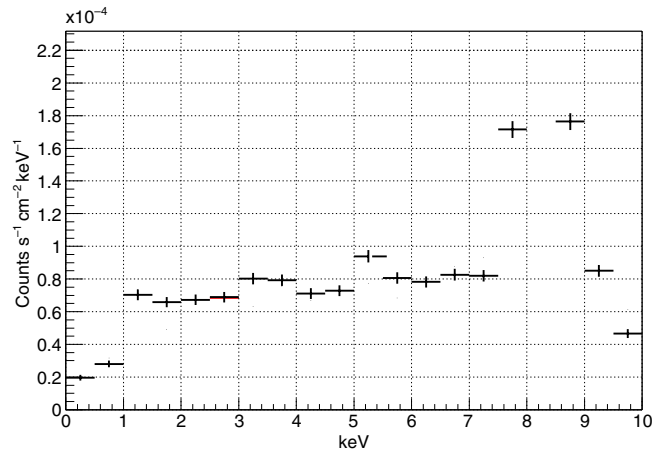
Figure 13. Background spectra after the filtering cuts for the 2003 data.
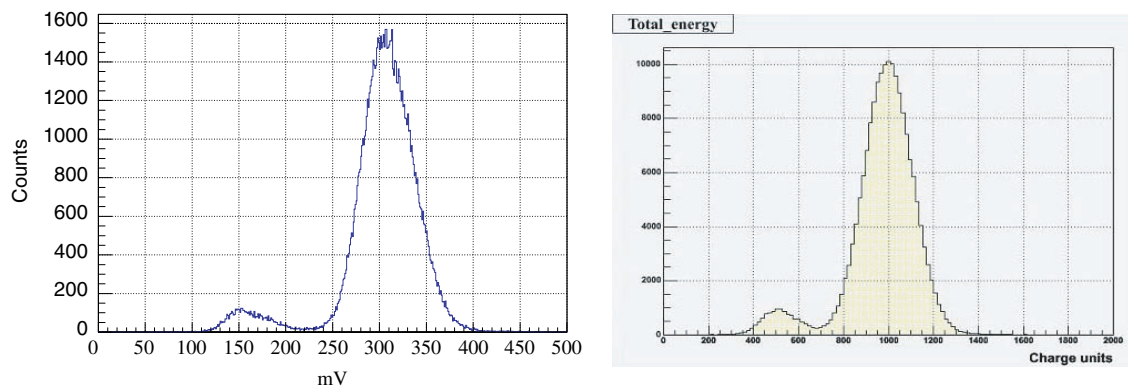

Figure 14. Energy spectrum for a calibration run using a ^{55}Fe source obtained with the mesh signal read by the MATACQ card (left panel) and with the strips (right panel). The good energy resolution (less than 20% (FWMH)) allows the identification of the argon escape peak (low charge peak) using both signals.

the mesh signal or with the strips is equally good for this detector due to the reduction of the strips crosstalk. In this model, the amplification gap is obtained by Kevlar pillars attached to the readout plane (instead of the Kapton pillars attached to the mesh for the detector used in 2003) so the crosstalk due to the copper left on the pillars was not present anymore.

The very accurate strip data allowed us to improve the offline analysis dramatically by combining the information from the spatial distribution of the charge collected during an event with the time structure of the mesh pulses. More specifically, six observables (pulse risetime, pulse width, pulse height versus pulse integral correlation, X- and Y-strip multiplicity balance, X- and Y-strip charge balance, pulse height versus total strip charge correlation) were used in a modified Fisher discriminant (Fisher 1936, Kendall 1975) method to distinguish more efficiently the proper x-ray events from other signals. This method is a standard method to obtain a single discriminant variable from a large number of variables which can be correlated, which is the
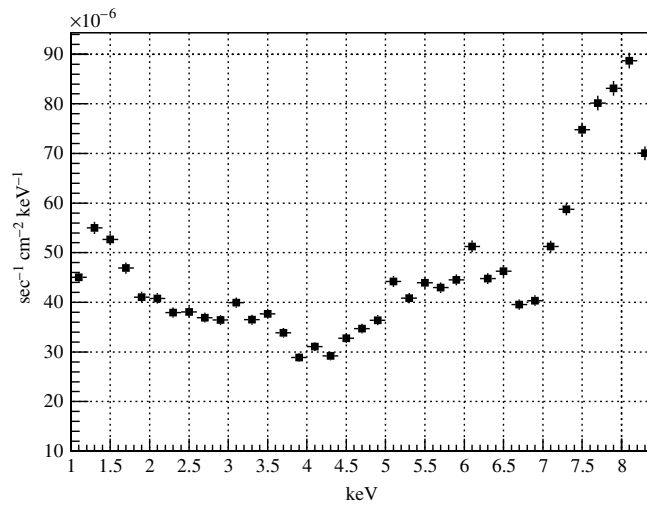
Figure 15. Background spectra after applying the Fisher discriminant method for analysis of the 2004 data (see Andriamonje *et al* 2007b).

case in our analysis. Fugure 15 shows the resulting background rejection to be at the level of 4.8×10^{-5} counts $cm^{-2}\,s^{-1}\,keV^{-1}$ region with 94% uniform software efficiency. The system's stability is demonstrated through the mesh pulses' time structure (0.5% variation of risetime and width during the six months of the run) and the moderate gain variation (10% on a weekly base) which was corrected with daily calibration.

The background spectra shown in figures 13 and 15 have the same rough shape: both are dominated by the copper peak. Small differences in the shape of the background are expected due to the fact that the two detectors were not identical: the 2003 detector used a plotted mesh and in the 2004 detector the amplification gap was formed by Kevlar pillars on the readout plane. Moreover the drift electrodes were made out of stainless steel in 2003 and of aluminium in 2004. Another important point already mentioned is that the two detectors did not have the same energy resolution so the overall level of background achieved is expected to be different. In addition two different filtering methods were used to analyse the data (sequential cuts for 2003 and Fisher discriminant method for the 2004) which can also explain the small differences observed in the two background plots.

4. Conclusion

A Micromegas detector with novel features, such as the *X–Y*-strip readout and the low-background materials (such as Plexiglas, Kapton, Kevlar), was designed and constructed for the detection of 1–10 keV x-ray photons for the solar axion search experiment CAST at CERN. The excellent stability, linearity, position determination capability, low threshold and good energy resolution are shown. The analysis of the events permits the rejection of a large fraction of cosmic ray related background using the observed properties of genuine photon events such as the rise time and width of the micromesh signal, the cluster size and the *X–Y* energy balance. The best background rejection obtained has been shown to be at the level of 5×10^{-5} counts $cm^{-2}\,s^{-1}\,keV^{-1}$ with an

efficiency of 92%. With appropriate shielding the rejection factor should easily be improved. This Micromegas design has produced a powerful device for the detection of x-rays from axions in the energy range of 1–10 keV. The achieved background rejection opens up the use of the Micromegas detector for other rare event searches.

Acknowledgments

References

Agostinelli S *et al* 2003 *Nucl. Instrum. Methods Phys. Res.* A **506** 250–303 online at http://www.cern.ch/geant4

Andriamonje S *et al* 2007a *New. J. Phys.* in preparation

Andriamonje S *et al* 2007b *J. Cosmol. Astropart. Phys.* JCAP04(2007)010

Andriamonje S *et al* 2004 *Nucl. Instrum. Methods Phys. Res.* A **518** 252–5

Autiero D *et al* 2007 *New. J. Phys.* **9** 171

Breton D, Delagnes E and Houry M 2005 *IEEE Trans. Nucl. Sci.* **52** 2853

Charpak G, Derré J, Giomataris Y and Rebourgeard P 2002 *Nucl. Instrum. Methods Phys. Res.* A **478** 26–36

Colas P, Colijn A P, Fornaini A, Giomataris Y, van der Graaf H, Heijne E H M, Llopart X, Schmitz J, Timmermans J and Visschers J L 2004 *Nucl. Instrum. Methods Phys. Res.* A **535** 506–10

Collar J and Giomataris Y 2000 *Nucl. Instrum. Methods Phys. Res.* A **471** 254

Delbart A, Oliveira R D, Derré J, Giomataris Y, Jeanneau F, Papadopoulos Y and Rebourgeard P 2001 *Nucl. Instrum. Methods Phys. Res.* A **461** 84–7

Fisher R A 1936 *Ann. Eugen.* **7** 179–88

Freyberg M J *et al* 2005 *Exp. Astron.* **20** 405–12

Geralis T, Fanourakis G, Giomataris Y and Zachariadou K 2003 *IEEE Nucl. Sci. Symp. Conf. Record* **5** 3455–99

Giomataris I *et al* 2006 *Nucl. Instrum. Methods Phys. Res.* A **560** 405–8

Giomataris Y 1998 *Nucl. Instrum. Methods Phys. Res.* A **419** 239–50

Giomataris Y, Rebourgeard P, Robert J P and Charpak G 1996 *Nucl. Instrum. Methods Phys. Res.* A **376** 29–35

Kendall M 1975 *Multivariate Analysis* 1st edn (London: Charles Erifin)

Kuster M *et al* 2007 *New J. Phys.* **9** 169

Santiard J C, Beusch W, Buytaert S, Enz C, Heijne E, Jarron P, Krummenacher F, Marent K and Piuz F 1994 Presented at the *6th Pisa Meeting on Advanced Detectors (La Biodola, Isola d'Elba, Italy, 22–28 May)* CERN-ECP-94-17

Zioutas K *et al* 2005 *Phys. Rev. Lett.* **94** 121301

Development and performance of Microbulk Micromegas detectors

S. Andriamonje,[a] **D. Attie,**[b] **E. Berthoumieux,**[b] **M. Calviani,**[a] **P. Colas,**[b] **T. Dafni,**[c]
G. Fanourakis,[d] **E. Ferrer-Ribas,**[b] **J. Galan,**[c] **T. Geralis,**[d] **A. Giganon,**[b] **I. Giomataris,**[b]
A. Gris,[a] **C. Guerrero Sanchez,**[a] **F. Gunsing,**[b] **F.J. Iguaz,**[c] **I. Irastorza,**[c]
R. De Oliveira,[a] **T. Papaevangelou,**[b,1] **J. Ruz,**[a] **I. Savvidis,**[e] **A. Teixera**[a] **and A. Tomás**[c]

[a]*CERN, European Organization for Particle Physics and Nuclear Research,*
 Geneva, Switzerland

[b]*IRFU, Centre d'Etudes Nucléaires de Saclay,*
 Gif sur Yvette, France

[c]*Laboratorio de Física Nuclear y Astropoartículas, Universidad de Zaragoza,*
 Zaragoza, Spain

[d]*Institute of Nuclear Physics, NCSR Demokritos,*
 Athens, Greece

[e]*Aristotle University,*
 Thessaloniki, Greece

 E-mail: Thomas.Papaevangelou@cern.ch

ABSTRACT: A new Micromegas manufacturing technique, based on kapton etching technology, has been developed recently, resulting in further improvement of the characteristics of the detector, such as uniformity and stability. Excellent energy resolution has been obtained, reaching 11% FWHM for the 5.9 keV photon peak of the ^{55}Fe X-ray source and 1.8% FWHM (with possible evidence of less than 1%) for the 5.5 MeV alpha peak of the ^{241}Am source. The new Microbulk detector shows several advantages like flexible structure, low material and high radio-purity, opening thus new possibilities for both accelerator and low counting-rate experiments. The detector has already been used in CAST and n-TOF, while it is being tested for future neutrinoless double-beta decay experiments like NEXT. Details of the production of several types of Microbulk detectors will be described. First benchmark results will be presented, demonstrating the enhanced performance of Microbulk detectors.

---

[1]Corresponding author.

Contents

1 Introduction

Gas proportional counters based on the Micromegas [1, 2] technology are an example of a new generation of detectors that exploit narrow anode-cathode gaps, rather than thin wires, to create gas gain. These detectors, called Micropattern Gaseous Detectors, are inherently pixel detectors that can be made at large size for reasonable costs. Because of their intrinsic gain and room-temperature operation, they can be instrumented at very low power per unit area, making them valuable for a variety of particle physics applications where large-area particle tracking is required. Micromegas is a Parallel Plate Detector (PPD) with three electrodes, cathode, micromesh and anode and a narrow amplification space, typically 50-100 microns, between the micromesh and the anode. The detector gain depends directly on the distance between the micromesh and anode, therefore controlling the geometry of the amplification region is crucial in order to achieve good energy resolution [2].

In its traditional form, Micromegas is built by use of a thin electroformed Nickel mesh as the Frisch grid for dividing the gas chamber into the drift and amplification gaps. The mesh is stretched and glued on a removable glass-fiber frame and placed above the anode plane [3]. To maintain a uniform gap, small cylindrical insulating spacers made of photo-imageable resin, 100 μm thick and 150 μm in diameter, are fixed to the anode strips by a standard printed circuit technique. Another type of mesh based on simple chemical-etching techniques on a single foil of kapton copper plated on both sides has been also developed. The manufacturing process relies on the high accuracy of the photolithography technique that allows to print on a 5 μm copper grid with 25 μm openings and a pitch of 50 μm; the kapton is partially removed, leaving kapton pillars that are used as spacers for the amplification gap of the detector [4].

Figure 1. Kapton pillars are created below the copper in each mesh step.

Efforts have been focused on producing the amplification region as a single piece using the newly developed "bulk" method [5]. A woven mesh is laminated on a PC board covered by a photo-imageable polyimide film, and the pillars are made by a photochemical technique with insulation through the grid. Such an 'all-in-one' detector, called 'bulk' Micromegas, is robust and will allow large areas to be made in one piece. This industrial assembly process allows the regular production of large, stable and inexpensive detector modules [5].

We present a novel fabrication technique using kapton thin-foil etching technology. We have used this technique to fabricate detectors, reading out anode and cathode strips, in a single integrated structure. We present gain and energy resolution measurements, detailed results stability and uniformity from these detectors, as well as several applications in high energy and nuclear physics.

2 Manufacturing process

The raw material is a thin flexible polyimide foil with a thin copper layer on each side. The foil is usually glued on top of a rigid substrate that provides the support of the micro-structure and most of the time carries anode strips or pixels. In some applications demanding low detector material the foil is stretched and glued on a suitable frame.

We have used two slightly different technologies that are described below. In both technologies (see figure 1–2) a standard lithography and kapton etching is used. This technology is inspired by the GEM detector fabrication process invented at CERN [6]. A thin photoresistive film is laminated on top of the kapton foil and it is insolated by UV light to produce the required mask. The copper is then removed by a standard lithographic process, the non-insulated places producing a pattern of a thin mesh. In our first prototype the holes are 30 μm in diameter and a pitch of 80 μm. The polyimide is then etched and partially removed in order to create tiny pillars in the shadow part of the mesh below the copper mesh.

In the second approach the polyimide is completely removed except the points where small pillars are created (about 100 μm in diameter) with a pitch of ∼1 mm. To achieve this, an additional insolating spot (about 200 μm) is formed during insolation process, leaving after the lithographic process a copper spot of 200 μm in diameter (see figure 2). By increasing the duration of the etching process, the polyimide under the mesh is removed completely except the points below the shadow of these copper spots.

Figure 2. Left: Kapton pillars are created with a step of about 500 microns; Right: photo of a mesh with copper spots used to protect the polyimide bellow during etching in order to form the pillars.
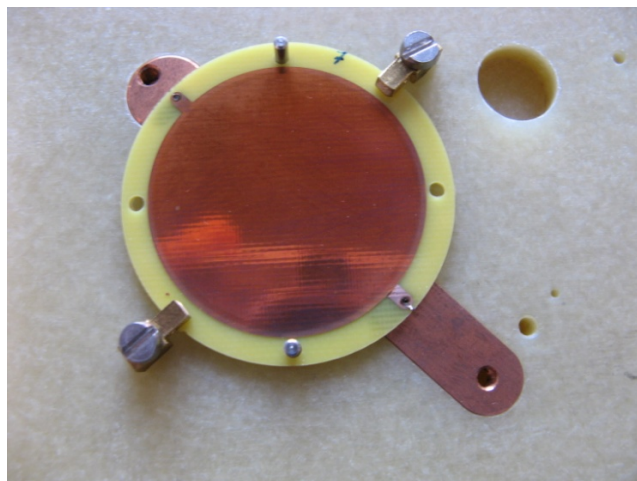

Figure 3. Photo of the 3.5 cm diameter circular Micromegas.

In both cases a structure of Micromegas is produced with two types of pillars that are maintaining flat the amplification gap between the mesh (cathode) and anode plane. Notice that the pillars are always on the shadow of copper pads therefore any dead space is avoided, as in the conventional structure. This is also an advantage in imaging applications with x-rays or neutrons. We have successfully built prototypes using polyimide foils of 25 and 50 micron thick providing amplification gaps of 25 and 50 micron respectively.

3 Characterization measurements

Different batches of 3.5 cm diameter circular Micromegas were produced at CERN. The amplification gap was 50 μm while the anode was non-segmented. A picture of the readout plane can be seen in figure 3. The hole diameters of the mesh are 30 μm with a pitch of 100 μm. These detectors were tested in a test chamber at atmospheric pressure with a gas mixture of argon with 5% isobutene, having a drift gap of 5 mm. The signal was read out from the Micromegas mesh using an ORTEC 142B preamplifier and fed into an ORTEC 572 shaper amplifier. A multi-channel analyzer AMPTEK MCA-8000A was used for spectra recording.

The energy resolution was measured by irradiating the detector with a ^{55}Fe collimated source. We obtain a result 11.2% FWHM at 5.9 keV, and a well separated escape peak at 3 keV as shown in
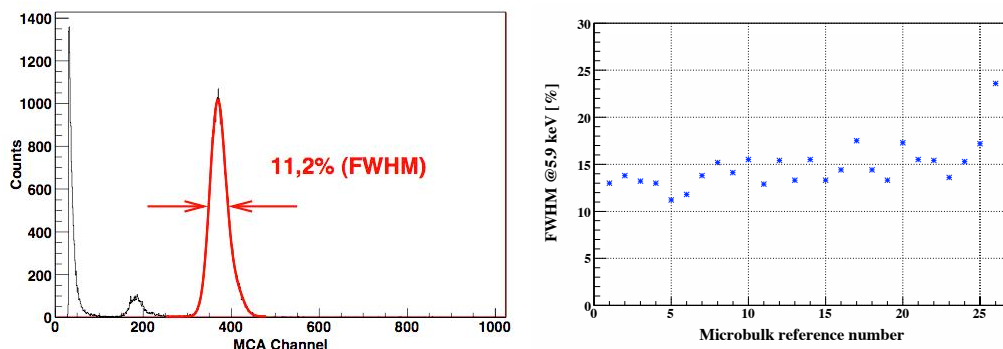
Figure 4. Left: Energy resolution with a ^{55}Fe source. Right: Energy resolution (FWHM) obtained for 26 Microbulk detectors at 5.9 keV.

Figure 5. Gain as a function of amplication field in an argon - 5% isobutane mixture at atmospheric pressure for 26 Microbulk detectors.

figure 4 (Left). Figure 4 (Right) shows the energy resolution for a bunch of 26 Microbulk detectors with a mean value of 15% FWHM. This value shows an improvement with respect to traditional Micromegas detectors thanks to the better controlled gap size.

Figure 5 shows the gain curve as a function of the amplification field for 26 Microbulks produced over more than 1 year. The gains obtained, reaching values higher than 10^4, are of the same order as in standard Micromegas detectors and the dispersion at a given field value is around 13%. This dispersion accounts, apart from the dispersion in performance, for a variation of environmental conditions as the measurements were realized over one year in a non-controlled pressure and temperature environment.

Microbulks of gap size of 25 μm have also been manufactured. Their performance in terms of gain and in comparison with standard Microbulk (50 μm gap size) is given in figure 6 at atmo-
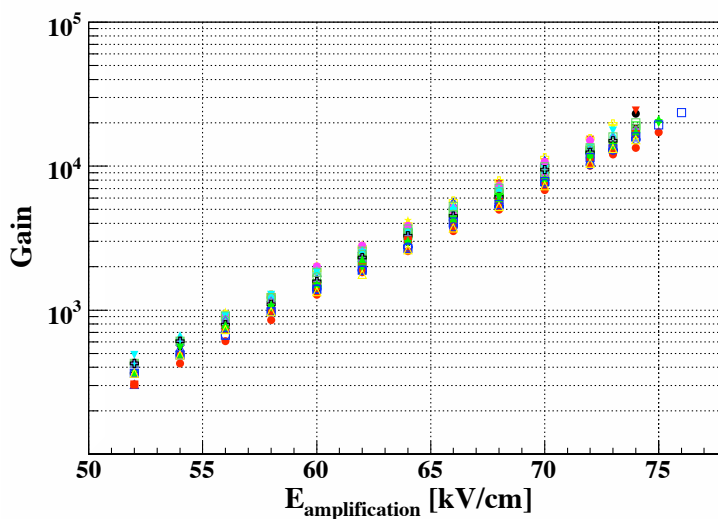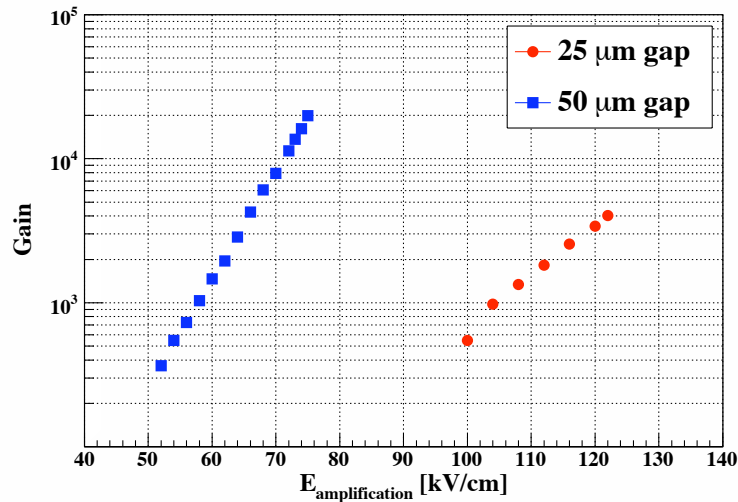
Figure 6. Gain as a function of amplication field in an argon - 5% isobutane mixture at atmospheric pressure for a Microbulk with a gap of 50 μm and 25 μm.

spheric pressure. The maximum gain obtained with the 25 μm gap is not optimized as it is known that smaller gap sizes are best suited for higher pressures. For the 25 μm gap size, the optimum is around 2 bar.

The resolution of Microbulk Micromegas detectors at high pressures with high energy particles has been largely studied in reference [7, 8] in regard to a high pressure TPC for a future double beta experiment. Here we will only stress two aspects. The first one is that energy resolutions down to 1.8% and 2% FWHM have been obtained at 5.5 MeV by using an ^{241}Am alpha source in 2% and 5% argon-isobutane mixtures. The second one is that, in pure xenon gas, energy resolutions of 2.8% and 4.5% FWHM have been obtained for 2 bar and 4 bar respectively although being limited by gas purity. These preliminary results in pure xenon are very encouraging in the prospects of using Microbulk Micromegas detectors for a double beta decay experiment.

4 Performance in physics experiments

Micromegas detectors constructed with Microbulk technology have several advantages like low material, high radiopurity and better energy resolution which makes them very attractive for rare event detection experiments. The detector has been already used for axion searches in CAST [9–12] and it is being tested for future experiments like NEXT [13]. Furthermore, the minimal amount of material, and the small neutron sensitivity makes these detectors suitable for neutron beam experiments, such as n_TOF where Microbulks are being used for beam monitoring.

4.1 Microbulk in CAST

The expected signal in CAST is an excess of X-rays of energy 1-10 keV during solar tracking, over the background. Thus, low background detectors are a key element for the experiment's sensitivity.
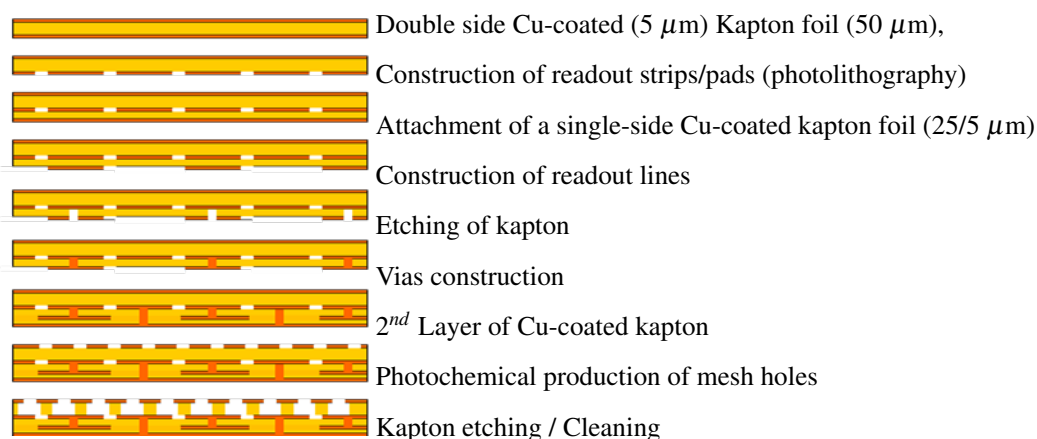
Double side Cu-coated (5 μm) Kapton foil (50 μm),

Construction of readout strips/pads (photolithography)

Attachment of a single-side Cu-coated kapton foil (25/5 μm)

Construction of readout lines

Etching of kapton

Vias construction

2nd Layer of Cu-coated kapton

Photochemical production of mesh holes

Kapton etching / Cleaning

Figure 7. Manufacturing process of a Microbulk with a 2D readout scheme.

Such detectors should show low intrinsic radioactivity, good energy and spatial resolution, time stability and particle discrimination capability. Since 2008 three Microbulk detectors are being used, replacing the conventional Micromegas and the TPC.

The manufacturing process of the CAST Microbulk with a 2D readout scheme is summarized in figure 7. The detector anode consists of square pads interconnected in the diagonal direction through vias in two extra back-layers. In a recent development, the connections in one direction were done at the pads level, so only a single extra layer was needed for the other direction, thus further reducing the detectors material (figure 8). The micromesh is formed by holes constructed on top of the pads, insuring in combination with the electron diffusion in the drift gas, that similar amount of charge is deposited on both X and Y pads. The strip pitch is 550 μm, while the spatial resolution is better than 100 μm due to the diffusion, which results on a mean multiplicity of $\sim$8 in each direction for 6 keV X-ray events.

The rest of the detector chamber consists of Plexiglas, while a thin (5 μm) aluminized mylar window with an aluminum strong back is used for the coupling with the magnet vacuum. The readout lines are constructed on the same kapton and the front-end electronics are placed well away from the sensitive area, so that they can be placed outside the shielding. All these result in having only very low radioactivity materials (kapton, copper, Plexiglas and aluminum) on the detector area, which in combination with appropriate shielding can lead to a minimal internal background level.

The main source of background in CAST conditions is cosmic muons which give a trigger rate of the order of 1 Hz in each Micromegas detector. However this background can be suppressed by applying a pattern recognition algorithm on the offline data, since muons have a completely different signature than X-rays of few keV. Another source is environmental radiation like gammas and neutrons, which can be reduced using a passive shielding. In CAST, we are using a shielding that consists of 2.5 cm of archaeological lead, surrounded by polyethylene of a thickness varying up to 25 cm, limited only by space constrains. Between the lead and the polyethylene there is a 2 mm thick cadmium foil to absorb thermal neutrons. Inside the lead there is a 5 mm thick copper layer, also serving as faraday cage. The front-end electronics are placed outside the shielding. The shielding interior is flushed with nitrogen in order to reduce radon radioactivity.
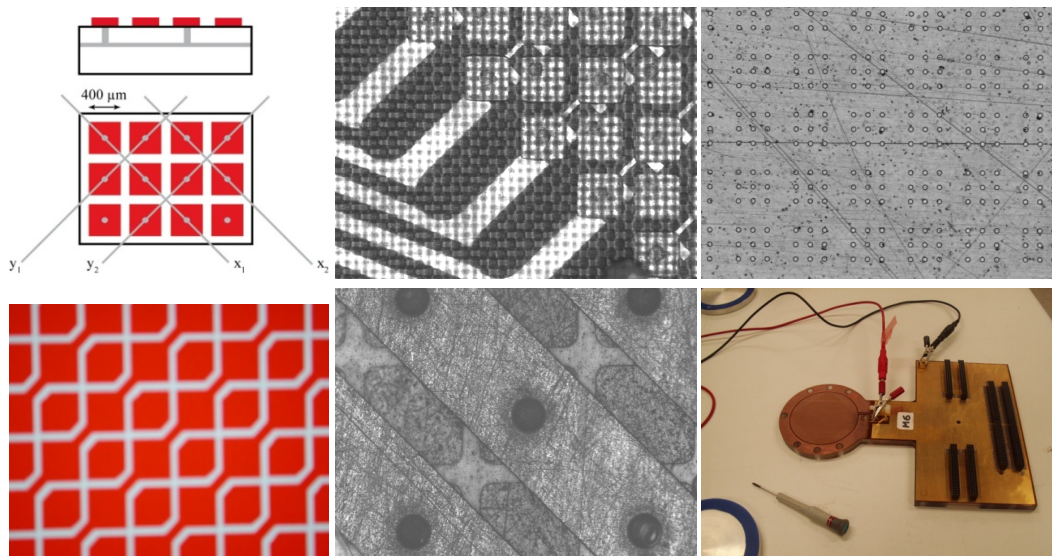
Figure 8. Left: schematic drawing of the 2D readout schemes, with two extra layer vias (top) and with one direction connected on the pad layer (bottom). Middle: corresponding photos from the front (top) and or the back side (bottom). Right (top): photo of the mesh. Right (bottom): photo of an open detector.
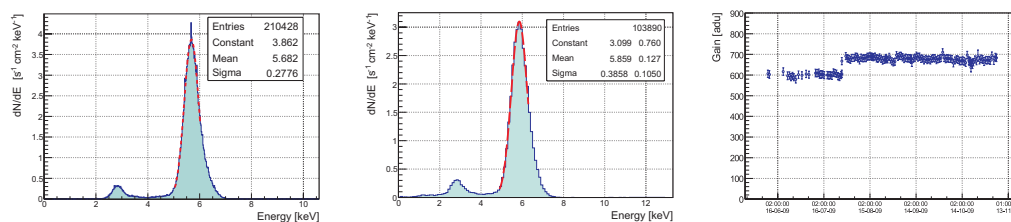

Figure 9. From left to right: 55 Fe energy spectrum with 5% isobutane collimated source; 2.3% isobutane non-collimated source; gain stability with time, the steep is due to the increase in the applied voltage by 1 Volt.

In such a configuration the achieved background level is determined by the detector's radiopurity and particle discrimination efficiency, for the same shielding quality. A Microbulk detector, besides its radiopurity, offers better energy resolution and time stability compared to conventional and bulk Micromegas, which lead to enhanced particle discrimination efficiency.

The energy resolution of the CAST Microbulk reaches 11.5% FWHM at 6 keV, for a gas mixture of argon 95% - isobutane 5% when the detector is irradiated with a collimated (∅ 15 mm) ^{55}Fe source (figure 9). In CAST, safety rules limit the isobutane fraction to less than 2.3%, so the resolution is relatively reduced, however it still reaches 15.5% for non-collimated total surface irradiation. This performance is comparable with the one achieved with the single-pad Microbulk detectors used in laboratory tests, showing that the 2D structure does not affect the energy resolution.

The stability of the detector with time is also crucial in a rare event detection experiment, where statistics are accumulated over long periods. The gain of Microbulk detectors is more stable

than traditional Micromegas due to the attachment of the mesh to the anode. Microbulks are also less sensitive to gas pressure variations than the bulk migromegas due to the smaller amplification gap. This stability has been observed, over 30 days, during the operation in CAST as shown in figure 9 (right).

The Microbulk detectors showed the lowest background level among all detectors used in CAST, reaching less than 10^{-6} s^{-1}cm^{-2}keV^{-1}. Beyond this nominal operation, there have been several periods where the background have been reduced to the extraordinary low level of $\sim 2 \times 10^{-7}$s^{-1}cm^{-2}keV^{-1} [14, 15], due to reasons which are under investigation, and which could be partially linked to variations in the radon concentration inside the shielding.

4.2 Microbulk for NEXT

NEXT [13] is a neutrinoless double beta decay experiment using a high pressure gas xenon TPC. Critical requirements for the detector in such an experiment is excellent energy resolution and background reduction from event topology, characteristics that has already been shown that the Microbulk meets.

In order to investigate the performance of Microbulks in high gas pressures, a series of experimental tests were performed and are still going on, at the Zaragoza University and at CEA Saclay. These tests have shown that there is no critical limitation for Micromegas to work up to 10 bar. No significant differences have been found in the response on low energy X-rays or high energy alpha particles, regarding the ionization yield or electronic transparency of Micromegas' mesh. Less than 1% FWHM is pointed out as the intrinsic energy resolution of Micromegas for 5.5 MeV alphas in argon-isobutane mixtures. There was no indication in these tests that these results have to be strongly dependent on pressure (probed up to 4.5 bar) or gas mixture (Microbulk have run in xenon without quencher). A detailed report on these results can be found at [8].

Another development towards a large scale TPC was the successful testing of the first 10x10 cm Microbulk with pixelised readout. The first medium area (30×30 cm) Microbulk is currently being built.

4.3 Microbulk in n_TOF

The n_TOF experiment [16]–[17] is performing high precision cross-section measurements of neutron-induced reactions, using a neutron beam of a very wide energy range (thermal up to GeV). A critical point in these measurements is the precise knowledge of the energy distribution of the neutron flux at the measured sample position, without the need to measure the absolute flux. In the ideal case the flux measurements should be performed in parallel with the cross-section ones. Therefore a very low mass detector is needed to minimize the beam distraction and the background induced to the other detectors. Furthermore, the detector should show high resistance to radiation and low gamma sensitivity. A system consisting of a ^{6}Li deposit on a mylar foil and 4 off-beam silicon detectors detecting the ^{6}Li(n,α)^{3}H reaction products has been used [18], Although the ^{6}Li(n,α)^{3}H total cross section is considered a standard, the angle differential cross section is not. Therefore the useable energy range of this detector is limited by the uncertainties in the angular distribution. In addition the angular efficiency of the detector is difficult to measure.

A detector system based on Microbulk Micromegas was designed (figure 10 left) in order to be placed in the neutron beam in a short distance in front of the measuring point. The system consists
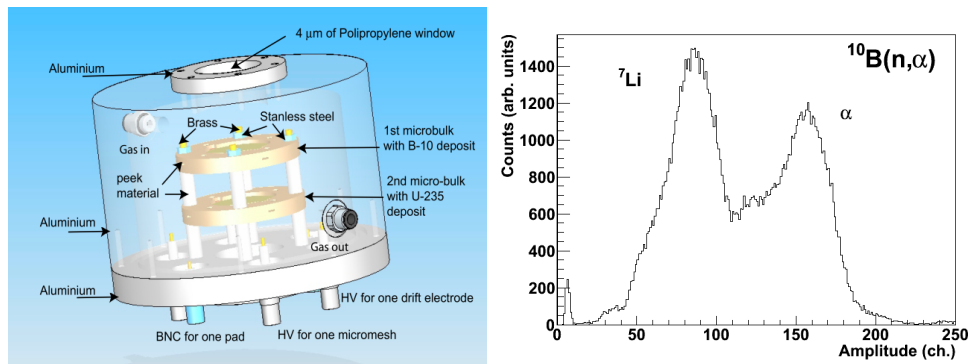
Figure 10. Left: schematic layout of the Microbulk based neutron flux monitor. Right: amplitude spectrum of $^{10}B(n,\alpha)$ reaction obtained at n_TOF facility.

of two Micromegas detectors placed inside a cylindrical chamber closed at the ends by kapton foils of 75 μm thick facing ^{10}B and ^{235}U neutron converters. In case the detector is placed in air the thickness of the kapton can be reduced to 10 μm. The detector consists of a drift cathode of 1.5 μm aluminized mylar with 1 mg of ^{10}B, and a second drift cathode of 1.5 μm aluminized mylar with 1 mg of ^{235}U. Each Microbulk has two 5 μm thick copper layers and 25 μm kapton forming the pillars. The pillars were constructed with a pitch of 500 μm, minimizing thus the material to the point that the main disturbance to the beam is caused by the neutron converters. In parallel, such a detector consisting of kapton and copper only shows very high radiation resistance.

The detector was used in laboratory and beam tests and was installed in n_TOF during the commissioning and start-up measurements in 2009. It showed the good energy resolution of all Microbulks, allowing the separation of the reaction fragments (alphas and ^{7}Li for ^{10}B, fission fragments and alphas for ^{235}U, figure 10 right), while it has been insensitive to the intense gamma-flash that accompanies every neutron pulse in n_TOF. Its performance was very stable, without major disturbance on the other measurements, and the system will be used for the rest of the campaign. Furthermore, the segmentation of the micromesh will allow the construction of a low mass detector with "real" 2D readout scheme for the first time, to be used as flux *and* beam profile monitor.

5 Future developments

The capacity of the detector is higher in the first fabrication mode described in section 2 because of the large quantity of kapton left in between the electrodes. We will push the etching process in order to remove as much kapton as possible and leave only tiny pillars. This improvement is necessary not only for lowering the electronic noise but also for decreasing the amount of charge released during an occasional discharge.

Up to now two-dimensional strip read-out in previous Micromegas detectors was possible by interconnecting pads in the anode plane as explained in the previous section. The new micro-Bulk technology offers the possibility to segment the cathode element, the copper mesh. Such X-Y read-out is suitable in some applications where a fully correlated anode-cathode signal is required.
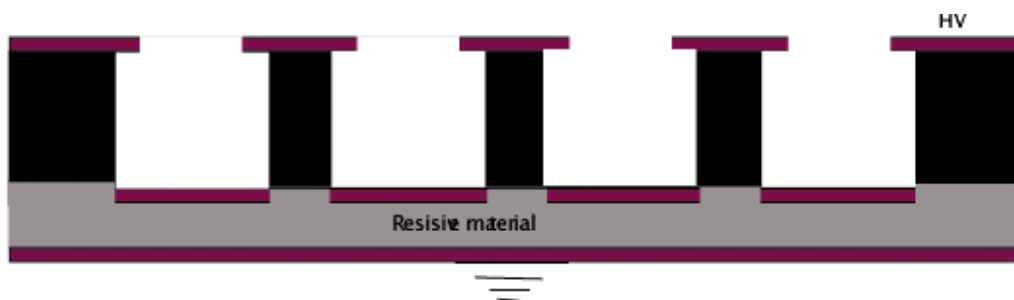
– 9 –

Figure 11. In red from top to bottom the copper mesh, the pillars, the bottom copper pads, the resistive layer, the bottom copper plane.

The size of the Microbulk will also be pushed as much as possible to tackle some applications requiring large detector area. To be able to produce larger size detectors we will follow also new developments going on at CERN through the RD51 collaboration. A study is going on to upgrade the equipment and the organization of the existing facility and contacts with industrial partners could also help to reach this goal.

For applications requiring operation at high pressures we are interested in decreasing the amplification gap. Present technology allows to fabricate 25 μm gap and our next goal is a 12.5 mm gap on a commercially available kapton foil. However such development requires a simultaneous decrease of the mesh openings and hole pitch. In order to achieve holes as low as 15 μm and pitches of 30 μm we need to change the mask technology for the photolithography process. A precise mask made out of glass, available in the industry, should be developed. Another idea is to interface the micro-Bulk structure to the read-out strip through a resistive thin layer as shown in figure 11. Using lithographic process the bottom copper is forming small circular pads facing the holes of the micromesh and then a resistive glue or resistive paste is used to interconnect the micro-Bulk to the read-out plane (presented by the copper layer in the drawing).

6   Conclusion

The new micro-Bulk Micromegas is a quite successful technique used already by some experiments. It provides excellent uniformity and energy resolution and could be manufactured by an industrial process. The detector has low material budget and could provide cylindrical or other curved shapes.Its low intrinsic radioactivity and stability make this detector quite attractive for low background rare event search. For high rate particle physics experiment the detector could be used as internal high-precision tracker. Its low material is a key point to achieve good momentum resolution in high energy physics spectrometers, usually limited by the effect of multiple scattering of charged particles in the detector material

References

[1] Y. Giomataris, P. Rebourgeard, J.P. Robert and G. Charpak, *MicrOMEGAs: a high-granularity position-sensitive gaseous detector for high particle-flux environments*, *Nucl. Instrum. Meth.* **A 376** (1996) 29.

[2] Y. Giomataris, *Development and prospects of the new gaseous detector 'MicrOMEGAs'*, *Nucl. Instrum. Meth.* **A 419** (1998) 239.

[3] G. Charpak, J. Derre, Y. Giomataris and P. Rebourgeard, *MicrOMEGAs, a multipurpose gaseous detector*, *Nucl. Instrum. Meth.* **A 478** (2002) 26.

[4] A. Delbart et al., *New developments of MicrOMEGAs detector*, *Nucl. Instrum. Meth.* **A 461** (2001) 84.

[5] I. Giomataris et al., *MicrOMEGAs in a bulk*, *Nucl. Instrum. Meth.* **A 560** (2006) 405 [physics/0501003].

[6] F. Sauli, *GEM: a new concept for electron amplification in gas detectors*, *Nucl. Instrum. Meth.* **A 386** (1997) 531.

[7] T. Dafni et al., *Energy resolution of alpha particles in a microbulk MicrOMEGAs detector at high pressure Argon and Xenon mixtures*, *Nucl. Instrum. Meth.* **A 608** (2009) 259.

[8] A. Tomas et al, *Development of Micromegas towards Double Beta Neutrinoless Decay Searches*, 1st International Conference on Micro Pattern Gaseous Detectors, June 12–15, 2009, Kolympari, Crete, Greece.

[9] CAST collaboration, K. Zioutas et al., *First results from the CERN Axion Solar Telescope (CAST)*, *Phys. Rev. Lett.* **94** (2005) 121301 [hep-ex/0411033].

[10] CAST collaboration, S. Andriamonje et al., *An improved limit on the axion-photon coupling from the CAST experiment*, *JCAP* **04** (2007) 010 [hep-ex/0702006].

[11] CAST collaboration, E. Arik et al., *Probing eV-scale axions with CAST*, *JCAP* **02** (2009) 008 [arXiv:0810.4482].

[12] P. Abbon et al., *The Micromegas detector of the CAST experiment*, *New J. Phys.* **9** (2007) 170.

[13] THE NEXT collaboration, . F. Granena et al., *NEXT, a HPGXe TPC for neutrinoless double beta decay searches*, arXiv:0907.4054.

[14] S. Aune et al., *An ultra-low-background detector for axion searches*, *J. Phys. Conf. Ser.* **179** (2009) 012015.

[15] J. Galan et al, *Micromegas Detectors in the CAST Experiment*, 1st International Conference on Micro Pattern Gaseous Detectors, June 12–15, 2009, Kolympari, Crete, Greece.

[16] C. Rubbia et al., *A High Resolution Spallation Driven Facility at the CERN-PS to Measure Neutron Cross Sections in the Interval from 1 eV to 250 MeV: a Relative Performance Assessment*, CERN-LHC-98-002-EET-Add.1 (1998).

[17] n_TOF collaboration F. Gunsing et al., *Status and outlook of the neutron time-of-flight facility n_TOF at CERN*, *Nucl. Instrum. Meth.* **B 261** (2007) 925.

[18] S. Marrone et al., *A low background neutron flux monitor for the n_TOF facility at CERN*, *Nucl. Instrum. Meth.* **A 517** (2004) 389.

Micromegas detector developments for Dark Matter directional detection with MIMAC

F.J. Iguaz,[a] **D. Attié,**[a] **D. Calvet,**[a] **P. Colas,**[a] **F. Druillole,**[a] **E. Ferrer-Ribas,**[a,1]
I. Giomataris,[a] **J.P. Mols,**[a] **J. Pancin,**[b] **T. Papaevangelou,**[a] **J. Billard,**[c] **G. Bosson,**[c]
J.L. Bouly,[c] **O. Bourrion,**[c] **Ch. Fourel,**[c] **C. Grignon,**[c] **O. Guillaudin,**[c] **F. Mayet,**[c]
J.P. Richer,[c] **D. Santos,**[c] **C. Golabek**[d] **and L. Lebreton**[d]

[a]*CEA/DSM/IRFU,*
CEA, 91191 Gif sur Yvette, France

[b]*GANIL,*
Bvd H. Becquerel, Caen, France

[c]*LPSC, Universite Joseph Fourier Grenoble 1,*
CNRS/IN2P3, Institut Polytechnique de Grenoble, France

[d]*LMDN, IRSN Cadarache,*
13115 Saint-Paul-Lez-Durance, France

E-mail: esther.ferrer.ribas@cea.fr

ABSTRACT: The aim of the MIMAC project is to detect non-baryonic Dark Matter with a directional TPC using a high precision Micromegas readout plane. We will describe in detail the recent developments done with bulk Micromegas detectors as well as the characterisation measurements performed in an Argon(95%)-Isobutane(5%) mixture. Track measurements with alpha particles will be shown.

----

[1]Corresponding author.

Contents

1 Introduction

The MIMAC (MIcro TPC MAtrix of Chambers) collaboration [1] aims at building a directional Dark Matter detector composed of a matrix of Micromegas [2] detectors. The MIMAC project is designed to measure both 3D track and ionization energy of recoiling nuclei, thus leading to the possibility to achieve directional dark Matter detection [3]. It is indeed a promising search strategy of galactic Weakly Interacting Massive Particles (WIMPs) and several projects of detector are being developed for this goal [4]. Recent studies have shown that a low exposure CF_4 directional detector could lead either to a competitive exclusion [5], a high significance discovery [6], or even an identification of Dark Matter [7], depending on the value of the WIMP-nucleon axial cross section.

Gaseous detectors present the advantage of being able to reconstruct the track of the nuclear recoil and to access both the energy and the track properties. Micropattern gaseous detectors are particularly suited to reconstruct low energy (few keV) recoil tracks of a few mm length due to their very good granularity, good spatial and energy resolution and low threshold. Micromegas detectors have shown these qualities in different environments [8–11]. In particular thanks to the new manufacturing techniques, namely bulk [12] and microbulk [13], where the amplification region is produced as a single entity. In bulk Micromegas a woven mesh is laminated on a printed circuit board covered by a photoimageable film and the pillars are made by a photochemical technique with insulation through a grid. This technique can be transfered to industry allowing the production of large, robust inexpensive detector modules.

This paper describes the developments done with bulk Micromegas detectors in order to show the feasability of a large TPC (Time Projection Chamber) for directional detection. Section 2 describes briefly the strategy of the MIMAC project. In section 3 we discuss in detail the design of the first prototype detector of $10 \times 10 \, \text{cm}^2$. The experimental set-up used for the characterisation in the laboratory is presented in section 4 and the results are given in section 5. Section 6 is devoted to the the results obtained for the reconstruction of tracks with alpha particles. Finally, the conclusions and the perspectives are discussed in section 7.

2 The MIMAC concept

The nuclear recoil produced by a WIMP in the TPC produces electron-ion pairs in the conversion gap of the Micromegas detector that drift towards the amplification gap ($128\,\mu$m or $256\,\mu$m in this case) producing an avalanche that will induce signals in the x-y anode and in the mesh. The track of the recoil is thus projected on the anode, providing 2D information. The third dimension z of the recoil is reconstructed by dedicated electronics specifically designed for this project [14, 15] which is able to perform anode sampling at a frequency of 40 MHz. The triggering is done by asking coincidence of at least one signal in x and y above threshold.The event recording is performed as long as the trigger firing is continuous, which is equivalent to have a constant flow of electrons arriving on the anode. Once the trigger becomes inactive, the event recording is stopped. Knowing the electron drift velocity, information on the third coordinated can be obtained. The concept had already been tested with a prototype detector of small size 3×3 cm^2 and with the first version of the electronics [1, 16].

The aim of building a detector of 10×10 cm^2 was to validate the feasability of a large TPC for directional detection with a realistic size prototype. The design of the bulk Micromegas was guided by the requirements on the granularity of the anode as well as by the operation conditions. Simulation studies showed that the granularity of the readout plane needed strips of $200\,\mu$m size. The MIMAC project will be optimised to get the directionality information of the WIMPs so low pressures down to 50 mbar in CF$_4$ and an adapted micromegas are needed. From the beginning of the design, it was known that the detector would be first validated in the laboratory with the T2K electronics [17, 18] before the final conclusive test with the specifically designed MIMAC electronics [14, 15]. Special care was taken in the design to have a portable system.

3 Design of the Bulk Micromegas detector: 10×10 cm^2

In order to have a detector that can stand operation at low and high pressure the design relies on the idea of assembling a leak-tight read-out plane on a 2 cm aluminium cap. A general sketch of the mechanical assembly is given in figure 1.

The bulk Micromegas is on a Printed Circuit Board (PCB), called *Readout PCB*, of 1.6 mm thickness (*a* in figure 1). The active surface is of 10.8×10.8 cm^2 with 256 strips per direction. The charge collection strips make-up an x-y structure out of electrically connected pads in the diagonal direction through metallized holes as can be seen in figures 2 and 3. This readout strategy reduces the number of channels with a fine granularity covering a large anode surface. The pads are $200\,\mu$m large with an isolation of $100\,\mu$m resulting into a strip pitch of $424\,\mu$m. The quality of the surface of the readout plane can be observed in figure 2. The $100\,\mu$m diameter metallized holes have been fully filled yielding a completely uniform surface. This fact is a prerequisite to obtain a uniform performance of a bulk Micromegas detector.

The strips signals are rooted into 4 connectors prints at the sides of the Readout PCB . The Readout PCB is screwed on a thick 0.5 cm PCB, called *Leak Tight PCB* (*b* in figure 1), that will ensure the leak tightness of the system. The Leak Tight PCB is constituted of various layers of FR4 with blind metallized vias in the inner layer. This piece is then screwed on a 2 cm thick aluminium cap that constitutes the bottom of the TPC. The signal connections from one board to another are
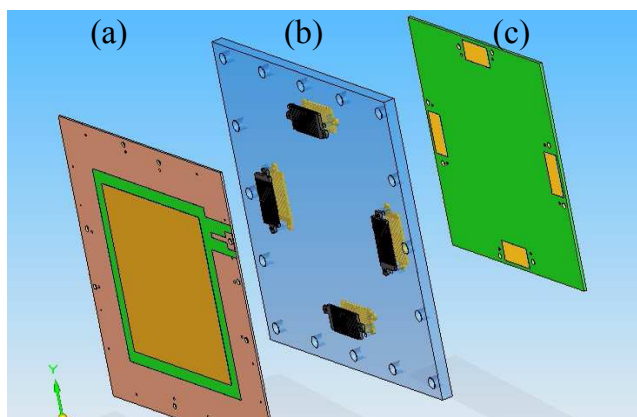
Figure 1. Sketch of the general assembly constituting the readout plane and the interface to electronics: Readout PCB (*a* in the image), Leak tight PCB (*b*) and the Interface PCB (*c*).
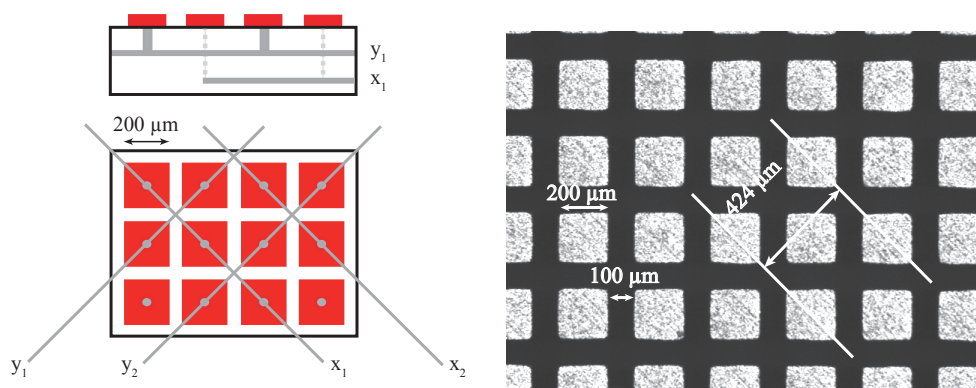

Figure 2. Left: sketch of the 2D readout used. Right: microscope photograph of the 2D readout.

done by means of SAMTEC connectors (GFZ 200 points) that are placed and screwed between the two boards (*b* in figure 1). On the outside of the vessel an *Interface card* distributes the signals to the desired electronics (*c* in figure 1). Two versions of this card exists: one dedicated to the laboratory set-up and a second one for the final MIMAC electronics.

This design offers several advantages: a simple, compact and leak-tight way for the signal connections and a versatility for two different types of electronics. Bulk Micromegas with two different amplification gaps were produced in order to choose the best gap for different running pressure conditions. Characterisations tests described in section 5 concern three readout planes with a gap of 128 μm and two with a gap of 256 μm.

4 Experimental set up

A dedicated vessel was built as shown in figure 4. It consists of two aluminium caps screwed to create the TPC. In the top cap, an iso-KF25 valve is used for pumping in order to reduce the outgassing from the inner walls. This cap is also equipped with two outlets for gas circulation and
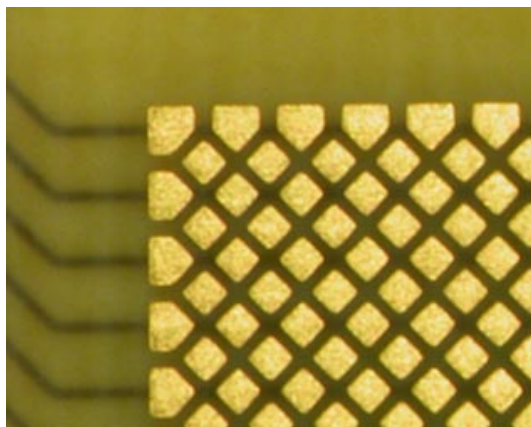
Figure 3. In this picture the pixel and the readout strips can be seen. The pixels are at 45º with respect to the readout strips (observed by transparency).
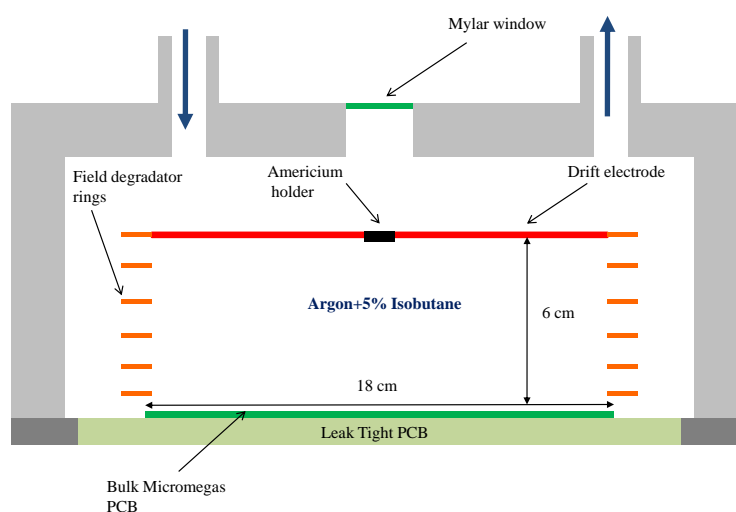
Figure 4. Schematic drawing of the set-up.

four SHV electrical connections. The bottom cap with the bulk Micromegas has been described in section 3.

To uniformise the drift field in the conversion volume of 6 cm of height, the vessel is equipped with a field shape degrador. It consists of 5 copper squared rings and a copper plate, separated by a distance of 1 cm by four peek columns. The plate and the rings are electrically connected via resistors of 33 MΩ. The voltage of the last ring is fixed with a variable resistor located outside the vessel. The drift electrode has been designed to accommodate an ^{241}Am source. The source in its holder is screwed to the cathode plate. For illumination with X-ray and gamma sources a thin mylar window has been placed at the top of the vessel.

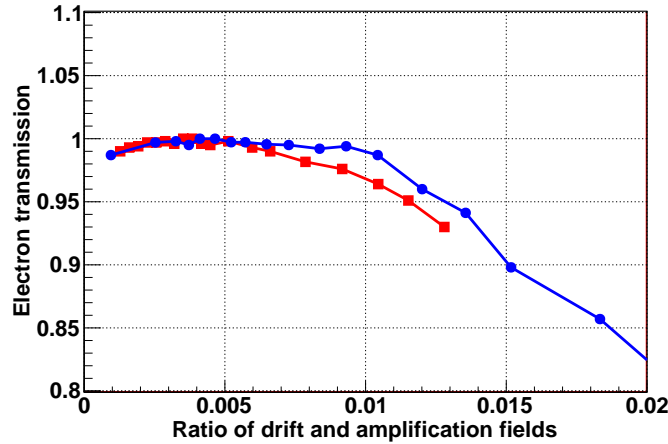**Figure 5**. Dependence of the electron mesh relative maximum transmission with the ratio of the drift and amplification fields for the readouts with a 128 μm (red squared line) and a 256 μm-thick amplification gap (blue circled line).

5   Characterisation measurements and results

After the installation of the detector in the dedicated vessel, the TPC was closed and pumped to reduce the outgassing of the walls. A flow of 10 l/h of an Argon(95%)-Isobutane(5%) mixture was circulated for some hours before starting the measurements. This gas was used for the characterisation measurements eventhough the chosen gas for dark matter search will be CF_4. Indeed most of Micromegas detectors are first characterised in Argon mixtures where their performance can be compared easily.

The strips were connected to ground and the readout was illuminated by an iron [55]Fe source (X-rays of 5.9 keV) located on the TPC window. The mesh voltage was typically varied from 300 to 450 V for detectors with a gap of 128 μm and between 470 to 600 V for those with a gap of 256 μm. The drift voltage was changed from 300 to 3000 V. Mesh and drift voltages were powered independently by CAEN N126 and CAEN N471A modules respectively. The signal induced in the mesh was read out by an ORTEC 142C preamplifier, whose output was fed into an ORTEC 472A Spectroscopy amplifier and subsequently into a multi-channel analyzer AMPTEK MCA-8000A for spectra building. Each spectrum contained at least 5×10^4 events and was fitted to get the peak position and the energy resolution.

In order to obtain the electron transmission curve, the drift voltage was varied for a fixed mesh voltage. Figure 5 shows the typical plateau for Micromegas readout planes where the maximum electron transmission is obtained for a ratio of drift and amplification fields lower than 0.01. For ratios over this value, the mesh stops being transparent for the primary electrons generated in the conversion volume and both the gain and the energy resolution deteriorate for high drift fields. As shown in figure 5, readouts with a 256 μm-thick gap have a slightly larger plateau than those with a 128 μm-thick gap. No other significant difference was observed among the tested readouts.

After this first test, the ratio of drift and amplification fields was fixed in the region where the
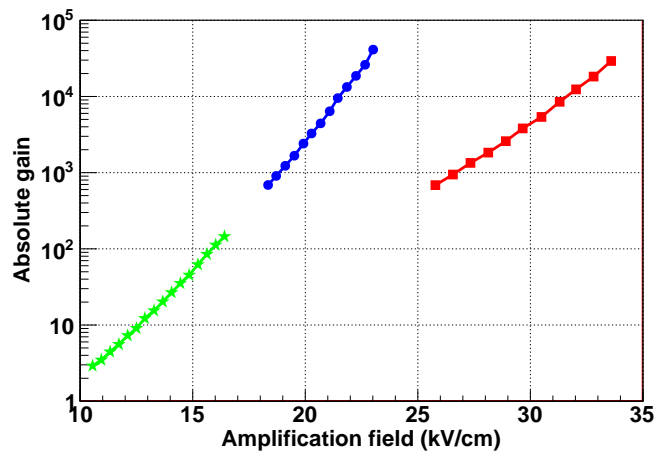
Figure 6. The absolute gain as a function of the amplification field is shown for the readouts with a 128 μm (red squared line) and 256 μm-thick amplification gap (blue circled line) obtained with a iron ^{55}Fe source using an Argon(95%)-Isobutane(5%) mixture at 1 bar. The extension at low gain (green star line) for the 256 μm readout was obtained with an alpha source. The maximum gain was obtained before the spark limit.

Table 1. Energy resolutions measured at 5.9 keV for the 3 different readouts of 128 μm and for 2 at 256 μm-thick amplification gap.

Detector	Num	Energy Resolution
		(% FWHM)
128 μm	1	21.0 $\pm$ 0.3
	2	23.4 $\pm$ 0.4
	3	23.2 $\pm$ 0.4
256 μm	1	16.0 $\pm$ 0.1
	2	17.8 $\pm$ 0.3

mesh showed the maximum electron transmission and the mesh voltage was varied to obtain the gain curves, shown in figure 6. The tested readouts reach gains greater than 2×10^4 before the spark limit for both amplification gaps.

As shown in figure 7 for the best cases, the energy resolution stays constant for a wide range of amplification fields. At low fields, the resolution worsens due to the noise level that is comparable to the signal height. At high fields, it deteriorates due to the gain fluctuations. The values measured for each detector are shown in table 1. We note that the readouts with a gap of 256 μm show a better energy resolution than those with a gap of 128 μm. This effect is possibly due to the thickness of the bulk mesh. Indeed for both amplification gaps the same mesh thickness (30 μm) was used. Therefore the non-uniformity of the gap will have a bigger effect on the electric field of smaller gaps.
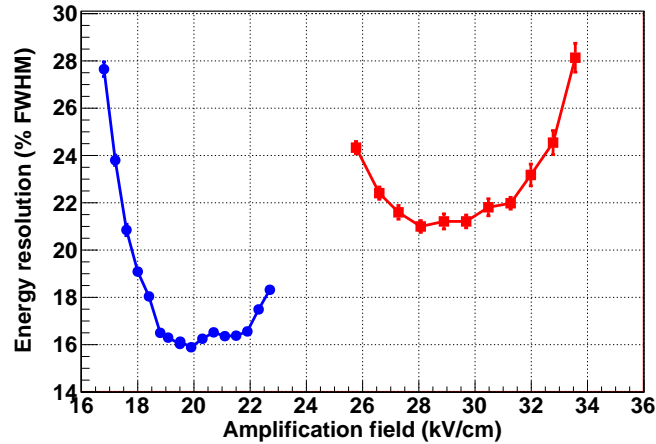
Figure 7. Dependence of the energy resolution at 5.9 keV with the amplification field for the readouts of 128μm (red squared line) and 256 μm-thick amplification gaps (blue circle line).

6 Track measurements with alpha particles

The T2K electronics [17, 18] has been used to read the signals induced in the strips to fully validate the concept of MIMAC readouts for the reconstruction of tracks. Eight flat cables connect the strips signals to two *Front End Cards*. Each card is equipped with four ASIC chips, called AFTER, which digitize in 511 samples the signals of 72 channels, which are previously amplified and shaped. Finally, the data of each AFTER is sent by a *Front End Mezzanine* (FEM) card to a DAQ card and subsequently to the computer for recording. As the external trigger mode of the T2K DAQ has been used, a trigger signal has been created feeding the bipolar output of the ORTEC VT120 amplifier/shaper into a FAN IN/OUT Lecroy 428F and subsequently into a NIM-TTL converter. Strips pulses have been sampled every 20 ns and the peaking time has been fixed to 100 ns. The dynamic range is of 120 fC.

In order to reconstruct the two 2D projection of each event, an offline analysis software has been developed. It extracts the strips pulses by using the amplitude of each pulse sample and the readout decoding. An example of the strips pulses and the XZ reconstruction of one event is shown in figure 9.

During three weeks of data-taking, a constant flow of 5 l/h of Ar+5%iC$_4$H$_{10}$ was circulated in the dedicated vessel. The detector (with 256 μm of amplification gap) was maintained in voltage (E$_{amp}$ = 21.9 kV/cm, E$_{drift}$ = 88 V/cm) acquiring events in a continous way. The detector was calibrated with an iron ^{55}Fe source twice per day to monitor the evolution of the gain and of the energy resolution. The gain fluctuations observed were below 10% due to the variations of pressure and temperature inside the vessel. It must be stressed that the pressure and the temperature were not controlled. The energy resolution varied between 18 and 20% FWHM during the same period as can be seen in figure 10.

In the two spatial projections (x and y) of the event, different parameters characterising the charge were calculated like mean position, width and number of activated strips. The analysis was
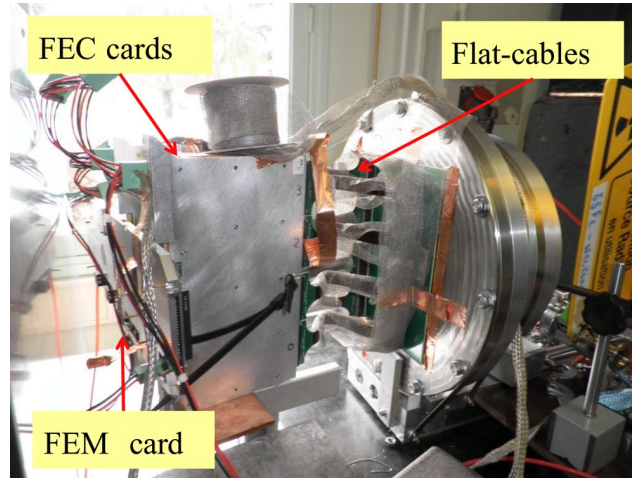
Figure 8. A view of the dedicated vessel used to test MIMAC readouts when reading the strips with the T2K electronics. A detailed description is made in text.
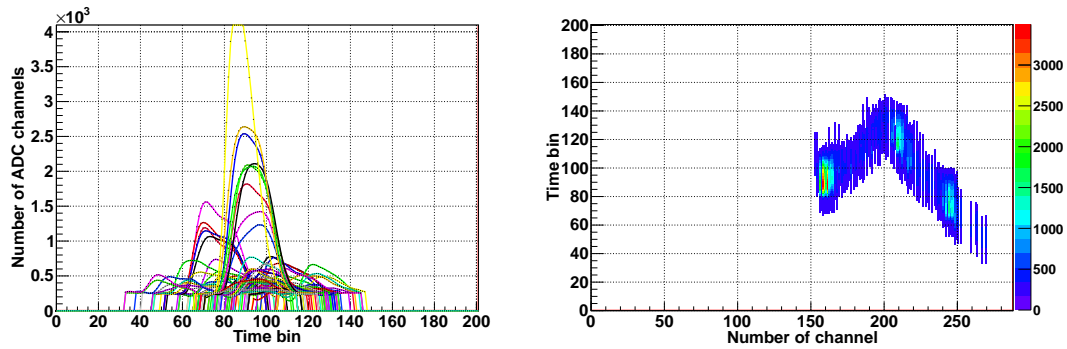

Figure 9. Left: example of pulses induced in the strips acquired with the T2K electronics. Right: the re-construction of the XZ projection of the same event. The physical event is an electron candidate of 44.4 keV with a final charge accumulation (or blob).

then extended to the perpendicular direction using the amplitudes of strips pulse in each temporal bin. Finally, the total charge of each event was obtained summing the charge of both projections. After having tested the readout with low energy events, we evaluated its performance at low gain with high energy events. For this purpose, an ^{241}Am alpha source was installed in the source keeper screwed at the center of the drift plate. The source consists of a metallic circular substrate of 25 mm diameter where the radioactive material has been deposited on its center in a circular region of about 8 mm of diameter. The alpha particles are emitted isotropically. The 5.5 MeV alphas were used to characterize the readout as it was done with the iron source in section 5, generating the electron transmission and gain curves. The electron transmission curve, taken at an absolute gain of 85, matched with the one showed in figure 5. Meanwhile, the gain curve was produced varying the mesh voltage between 270 and 420 V, as shown in figure 6, and follows the tendency of the one generated by photons.
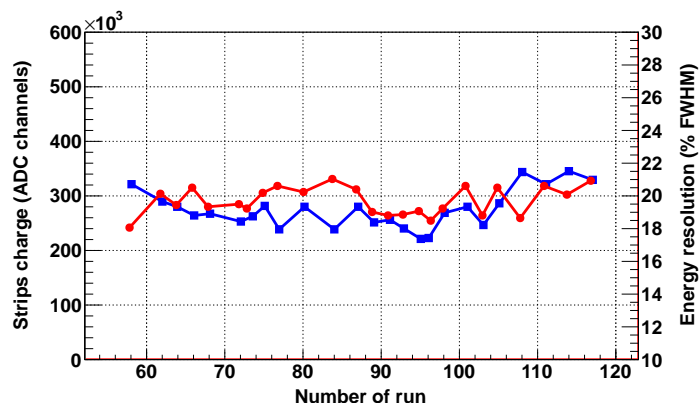
Figure 10. Evolution of the strips charge (red squared line) and the energy resolution at 5.9 keV (blue circled line) during the successive calibration runs with a source of ^{55}Fe. The temporal distance between each calibration run is half day.
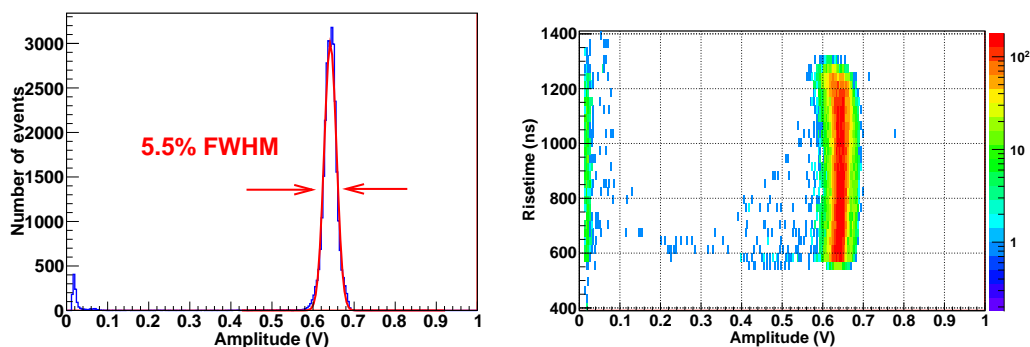

Figure 11. Left: spectrum generated by the mesh pulses induced by the ^{241}Am alphas, showing an energy resolution of 5.5% FWHM. Right: distribution of the risetime versus the amplitude of the mesh pulses induced by the ^{241}Am alphas.

The spectra generated by the ^{241}Am source showed an energy resolution of 5.5% FWHM, as the one shown in figure 11. This value was independent of the drift voltage and the readout gain. To check the possible presence of attachment effects in the gas, mesh pulses were acquired by a LeCroy WR6050 oscilloscope. In an offline analysis, the amplitude and risetime of the pulses were calculated and the 2D distribution of these parameters was generated to look for correlations. Alpha events showed the same amplitude, independently of their risetime, i.e., their spatial direction. Therefore attachement effects are not observed. An example of these 2D distribution is shown in figure 11 (right).

Several alpha tracks were also acquired with the T2K electronics, as shown in figure 12 (left). The mesh and drift voltages were respectively set to 400 and 820 V, which correspond to a gain of 85 and a drift field of 70 V/cm. For each event, the length of the track projection on the XY plane was calculated and the distribution of this variable was generated and is shown in figure 12 (right). The maximum value obtained (54 mm) matches the theoretical length expected for a 5.5 MeV alpha particles in an argon-based mixture [20].
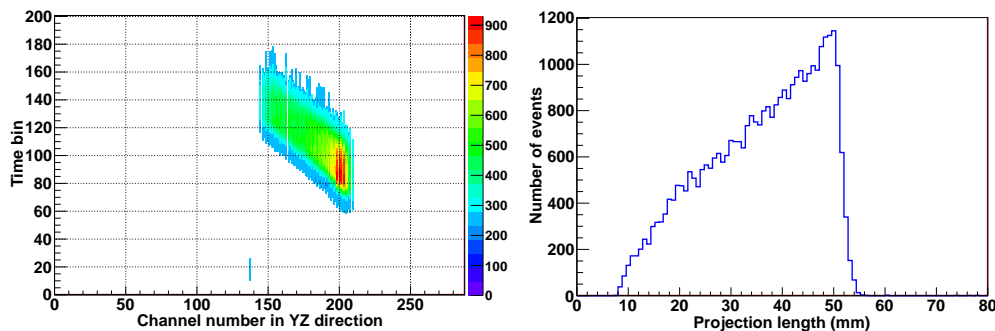
Figure 12. Left: an alpha event acquired by the T2K electronics. The track shows a final charge accumulation. Right: distribution of the length of the track projection on the XY plane, calculated by the number of strips activated in each direction. The maximum length of the distribution matches the Geant4 simulation value (54 mm).

7   Conclusions and perspectives

The readout plane of the Bulk $10 \times 10 \, \text{cm}^2$ Micromegas designed and built for the MIMAC project has been described. The first characterisation tests in the laboratory show good performance in terms of gain, uniformity, energy resolution and track measurements. The following steps are to test this detector in a neutron beam facility with neutrons of few keV using the specifically designed MIMAC electronics to reach the ultimate performance of the detector for the detection of Dark Matter. Plans for a test in the Frejus underground laboratory with a module containing two $10 \times 10 \, \text{cm}^2$ detectors are envisaged in the next coming months. This measurement, in a realistic environment for a Dark Matter experiment, will give crucial information (background rejection as well as intrinsic contamination of the used materials) before the construction of a $1 \, \text{m}^3$ experiment. In any case the results obtained up to now validate the MIMAC concept for the construction of a large TPC for directional detection of Dark Matter.

Acknowledgments

References

[1] D. Santos et al., *MIMAC: a micro-tpc matrix for directional detection of dark matter*, in the proceedings of the 5th *international symposium on large TPCs for low energy rare event detection*, December 14–17, Paris, France (2010), to appear in *J. Phys.* [arXiv:1102.3265].

[2] Y. Giomataris et al., *Micromegas: a high granularity position sensitive gaseous detector for high particle flux environments*, *Nucl. Instrum. Meth.* **A 376** (1996) 29.

[3] D. N. Spergel, *The motion of the earth and the detection of WIMPs*, *Phys. Rev.* **D 37** (1988) 1353.

[4] S. Ahlen et al., *The case for a directional dark matter detector and the status of current experimental efforts*, *Int. J. Mod. Phys.* **A 25** (2010) 1 [`arXiv:0911.0323`].

[5] J. Billard et al., *Exclusion limits from data of directional Dark Matter detectors*, *Phys. Rev.* **D 82** (2010) 055011 [`arXiv:1006.3513`].

[6] J. Billard et al., *Directional detection as a strategy to discover galactic Dark Matter*, *Phys. Lett.* **B 691** (2010) 156 [`arXiv:0911.4086`].

[7] J. Billard et al., *Markov Chain Monte Carlo analysis to constrain Dark Matter properties with directional detection*, *Phys. Rev.* **D 83** (2011) 075002 [`arXiv:1012.3960`].

[8] S. Aune et al., *An ultra-low-background detector for axion searches*, *J. Phys. Conf. Ser.* **179** (2009) 012015.

[9] T. Dafni et al., *New Micromegas for axion searches in CAST*, *Nucl. Instrum. Meth.* **A 628** (2011) 172.

[10] T. Dafni et al., *Energy resolution of alpha particles in a microbulk Micromegas detector at high pressure Argon and Xenon mixtures*, *Nucl. Instrum. Meth.* **A 60** (2009) 259 [`arXiv:0906.0534`].

[11] A. Delbart et al., *Production and calibration of* $9\,m^2$ *of bulk-Micromegas detectors for the readout of the ND280/TPCs of the T2K experiment*, *Nucl. Instrum. Meth.* **A 623** (2010) 105.

[12] I. Giomataris et al., *Micromegas in a bulk*, *Nucl. Instrum. Meth.* **A 560** (2006) 405 [`physics/0501003`].

[13] S. Andriamonje et al, *Development and performance of Microbulk Micromegas detectors*, 2010 *JINST* **5** P02001.

[14] J. P. Richer et al., *Development of a front end ASIC for Dark Matter directional detection with MIMAC*, *Nucl. Instrum. Meth.* **A 620** (2010) 470 [`arXiv:0912.0186`].

[15] O. Bourrion et al., *Data acquisition electronics and reconstruction software for directional detection of Dark Matter with MIMAC*, *Nucl. Instrum. Meth. A* **662** (2010) 207 [`arXiv:1006.1335`].

[16] D. Santos et al., *Ionization quenching factor measurement of* ^4He, `arXiv:0810.1137`.

[17] P. Baron et al., *Architecture and implementation of the front-end electronics of the time projection chambers in the T2K experiment*, *IEEE Trans. Nucl. Sci.* **NS-57** (2010).

[18] P. Baron et al., *AFTER, the front end ASIC of the T2K time projection chambers*, talk presented at the *Topical Workshop on Elctronics for Particle Physics*, September 21–25, Paris, France (2009).

[19] A. Allaoua et al, *Novel recoil nuclei detectors to qualify the AMANDE facility as a standard for mono-energetic neutron fields*, *Radiat. Meas.* **44** (2009) 755 [`arXiv:0812.0336`].

[20] F. J. Iguaz Gutiérrez, *Development of a time projection chamber prototype with technology for the search of the double beta decay of* ^{136}Xe, Ph.D. thesis, Universidad de Zaragoza, Zaragoza, Spain (2010), http://zaguan.unizar.es/record/5731.

World Scientific
www.worldscientific.com

MICROMEGAS IN THE RARE EVENT SEARCHES FIELD

IGOR G. IRASTORZA[*,‡], ESTHER FERRER-RIBAS[†] and THEOPISTI DAFNI[*]

[*]*Laboratorio de Física Nuclear y de Astropartículas, Departamento de Física Teórica,
Facultad de Ciencias, Universidad de Zaragoza, C/P. Cerbuna 12, Zaragoza, 50009, Spain*
[†]*IRFU, Centre d' Études Nucléaires de Saclay (CEA-Saclay), 91191, Gif-sur-Yvette, France*
[‡]*igor.irastorza@cern.ch*

The Micromegas detectors have been gaining importance as reliable options in their implementation to Time Projection Chambers (TPCs) in experiments searching for Rare Events mainly due to their demonstrated good performance regarding low background levels, energy and time resolution, gain and stability of operation. In the present paper, we will briefly review the latest developments carried out within the T-REX project of detector R&D, and the performance achieved in the context of several experiments: the CAST solar axion search experiment, the NEXT experiment of double beta decay and the MIMAC dark matter directional search.

Keywords: Micromegas; dark matter; axions; neutrinos; WIMPs.

1. Micromegas Readouts for Rare Event Searches

The common characteristic of the so-called rare event searches, like axion, dark matter or double-beta decay ($\beta\beta$) searches, is the extremely low signal rate expected. The ultra-low backgrounds required are achieved by the use of active and passive shielding, operation in underground sites, event discrimination and a careful selection of the detector materials from the radiopurity point of view.

Gaseous Time Projection Chambers (TPCs) can offer features of particular interest for rare event detection. The topological information of the event in gas, precisely registered by an appropriately patterned readout, is a powerful tool for signal identification and background rejection. The advent of micropattern gas detectors (MPGD) is allowing the competitive proposal of gas TPCs in different rare event applications. Their simplicity, robustness and mechanical precision are much higher than those of MWPCs. Micromegas readouts[1] have turned out to be a particularly attractive type of MPGD for application in rare events due to — apart from reasons common to other MPGDs — their particularly good energy resolution, the

stability and homogeneity of the gain and the possibility of manufacturing them with radiopure materials.

These particular features of Micromegas are being thoroughly studied within the T-REX project,[2,3] funded by a Starting Grant of the European Research Council. The main component of these studies is exploring the latest gas TPC readout concepts from the viewpoint of low background know-how, and focuses on the latest generation Micromegas *microbulk* readout planes[4] and their further development in order to meet requirements from axion, dark matter and $\beta\beta$ searches. The most relevant T-REX results up to now regard advances in the low background X-ray detectors being used in the CAST experiment,[5–7] as well as the studies of Micromegas readouts for the double beta decay of ^{136}Xe within the NEXT project.[8] In addition, Micromegas readouts are being used to measure the WIMP-induced nuclear recoil direction in the MIMAC experiment. A short description of these developments is given in the following.

1.1. *Micromegas in the search for solar axions*

The CERN Axion Solar Telescope (CAST) is the most powerful implementation of the "helioscope concept", searching for hypothetical axions coming from the Sun. The experiment is counting with a powerful dipole magnet that triggers the conversion of the axions into photons of energy 1–10 keV. Low background X-ray detectors are therefore necessary for high sensitivity. Recently, a much improved version of the helioscope concept has been proposed[9] exploiting the innovations introduced by CAST and improves its sensitivity substantially. One of the necessary elements of this new generation axion helioscope are X-ray detectors with even lower background levels, and is the main motivation of the development presented here.

Micromegas detectors are being used in CAST since the beginning of the experiment in 2003. CAST has been a test ground for these detectors, where they have been combined with low background techniques like the use of shielding, radiopurity screening of detector components or advanced event discrimination techniques based on the detailed topological information offered by the readout. The CAST detectors were the first Micromegas with a 2D pattern, with a pitch of 300 μm.[10]

Since the upgrade in 2007, the number of Micromegas detectors installed in the experiment was increased from one to three, being now all three of them of the microbulk type.[4] During the upgrade there were improvements in the shielding of all detectors, which in combination with the better characteristics of the microbulks, has lead to an improvement of the detector performance. The effect on the background levels can be appreciated in the plot of Fig. 1(a): they have been reduced by at least a factor of 20, with the current detectors showing levels of 6–9 $\times 10^{-6}$ s^{-1} cm^{-2} keV^{-1}.

Current efforts are focused on understanding the sources of the present background level and design strategies to further reduce it in subsequent designs of the detectors setup. A copy of one of the CAST detector systems was prepared
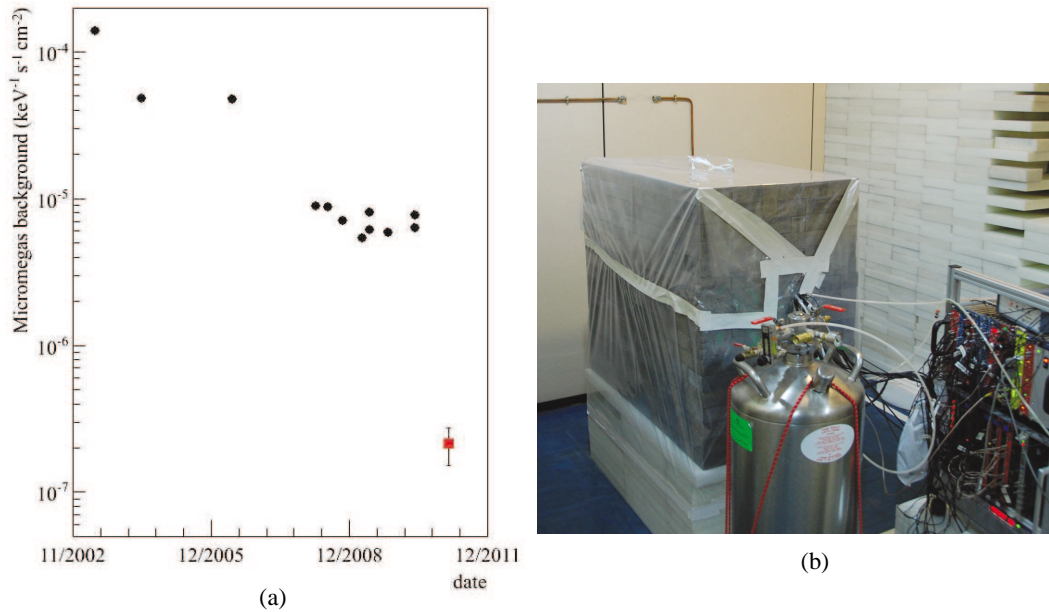
Fig. 1.   (a) A history of the background levels of the Micromegas detectors registered in different periods of data taking in the CAST experiment. The last point on the right represents the background level recorded at the LSC under special shielding conditions (see text). (b) A photo of the setup in the LSC: The Faraday cage that houses the detector is placed inside a 4π lead shielding. The dewar placed in front of the shielding provides the nitrogen flux.

and installed to take data in the Zaragoza laboratory. The setup is housed inside a Faraday cage, with an inner shielding of copper and lead, an outer shielding of polyethylene and it has been completed with a nitrogen flux in the vicinity of the chamber, reproducing the setup of the CAST detectors.[11,12]

After a short period of data-taking, the system was moved underground, in the Canfranc Underground Laboratory (LSC) in the Spanish Pyrenees. In this environment, data have been taken in different shielding configurations and in well known conditions regarding the external gamma background to assure a reliable comparison with simulation data. A continuous nitrogen flux is provided to purge the radon that could stay close to the detector (Fig. 1(b)). A detailed account of the tests performed is presented elsewhere.[14–16]

Although the studies are still ongoing, levels as low as 2×10^{-7} s^{-1} cm^{-2} keV^{-1} have already been reached in the underground configuration with the largest lead thickness (20 cm), a level much lower than the one at CAST (Fig. 1(a)). The preliminary conclusions are that this is the intrinsic level of the radiopurity of the detector components, while the level obtained at CAST is still dominated by external gammas, probably from the poorly shielded solid angle due to the detector's connection to the magnet. These studies have provided the needed information in order to design improvements on the CAST shieldings that are being implemented for the next data taking phase. An intermediate milestone was achieved in CAST, already in 2012, with the realization of several improvements in the shielding that

led to an improved $\sim 2 \times 10^{-6}$ s^{-1} cm^{-2} keV^{-1} background in two of the CAST Micromegas,[13] result which is under preparation for publication. As a subsequent step a new design of the detector is being carried out to better incorporate these findings. The work at LSC is now focused on studying and identifying internal sources of background, whose removal could eventually lead to improvements beyond the 10^{-7} and approaching the 10^{-8} s^{-1} cm^{-2} keV^{-1} level, as required for the future helioscope.[9]

In addition to this work, a detailed simulation of the detector setup has been prepared. Apart from a GEANT4-based geometry description for particle transport of the detector and its shielding, a complete modelization of the detector physics has been implemented. It includes most aspects of the response of the detector and the electronics chain currently used in CAST: electron diffusion along the drift path, signal generation and pixelization in the readout, and temporal pulse shaping by the front-end electronics. The simulated signals reproduce remarkably well the experimental data, in detector-specific aspects like multiplicity (number of strips typically triggered by an event) or the temporal information of the mesh signal.[14,15] The offline criteria used on the real data are equally well applied to the simulated data, reproducing the background rejection factors obtained experimentally. This simulation will reveal the relevant background population after the rejection mechanisms and is being used to create a detailed background model of the detector in order to eventually identify and reduce effective sources of background.

1.2. *Micromegas for double beta decay*

The neutrinoless double beta decay of ^{136}Xe could be searched for by a calorimetric gaseous TPC. This approach was pioneered by the Gothard TPC in the 1990s, although only recently a competitive implementation of a gaseous TPC is considered feasible thanks to the latest advances in TPC readouts. The Neutrino Xenon TPC (NEXT) experiment is considering a 100 kg gas Xe TPC for this goal, to be operated at the LSC.[8] Here we describe the latest results performed in the context of the NEXT project to develop Micromegas readouts for $\beta\beta$ searches.[17] Although the decided baseline for the NEXT100 detector is an electroluminescent photosensor readout, the development of Micromegas is still motivated as a backup option or for eventual future extension to larger masses, due to the promising prospects for large areas offered by MPGDs. Another collaboration, EXO-gas, also develops a gas TPC to search for the double beta decay of ^{136}Xe, and considers Micromegas as an option for its readout.[18]

The strong points of using a gas TPC with respect to competing technologies reside in the potentially very good energy resolution which can be achieved, while taking advantage of the background rejection power provided by the topological information of the electron tracks. The requirements on the readout include ability to operate at high pressure, sufficient granularity, good energy resolution and low radioactivity. Microbulk Micromegas are promising options because of the best en-

ergy resolutions obtained among MPGDs, the well proven capability for a granular design and the fact that they are manufactured out of kapton and copper foils, two materials of known radiopurity. Indeed, the radioactivity of several samples (from raw materials to fully manufactured detectors) were studied with a high purity Ge detector at the LSC. The results obtained are comparable[19] to the cleanest detector components of the most stringent low background experiments at present, despite the fact that these detectors were manufactured without any special care from the radiopurity point of view. In any case, work is ongoing to increase the sensitivity of the measurements and further reduce any possible remaining radioactivity.

The studies performed up to now has been focused on establishing the capability of microbulk readouts to work in high pressure Xe and more specifically to measure their energy resolution in those conditions. For that task, two prototypes have been built. The first one, known as NEXT-0-MM, is a stainless steel vessel of 2 L, with a diameter of approx. 14 cm and a drift region of 6 cm and is devoted to measurements with small scale readouts, to study gain, operation point and energy resolution with low energy gammas or alphas. The second prototype, of much larger size (drift of 35 cm and a readout area of 30 cm in diameter), NEXT-MM, is capable of fully confining a high energy electron track and will therefore probe the detection principle in realistic conditions. A picture of this detector is shown in Fig. 2.

Working with high pressure and high purity Xe implies very stringent restrictions on leak-tightness and outgassing in the chambers, as well as special gas distribution system with recirculation and filtering stages. Both prototypes have been built keeping combined specifications on ultra high vacuum and high pressure, and keeping a strict control of the materials to be installed inside. A description of both

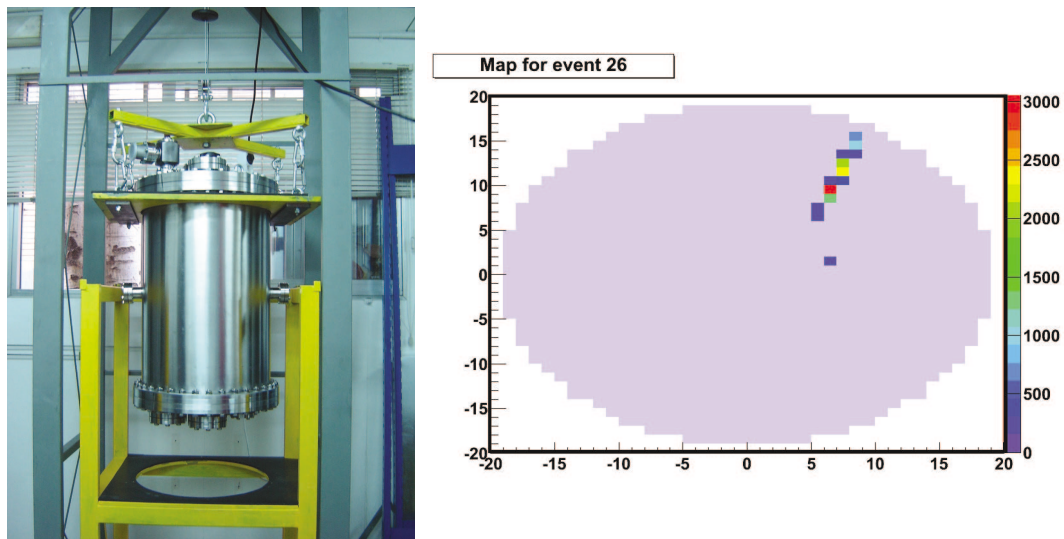
Fig. 2.   Left: a photo of the NEXT-1-MM prototype and its supporting structure. Right: an alpha track of approximately 4cm obtained with the ^{222}Rn source in NEXT-1-MM. The shaded area corresponds to the active surface of the bulk detector.

I. G. Irastorza, E. Ferrer-Ribas & T. Dafni

prototypes can be found elsewhere,[20,21] as well as the various tests performed in NEXT-0-MM with small (~ 3 cm diameter) readouts, and with a first pixelized 10×10 cm^2 (the largest at the time) microbulk readout that allowed to register the first alpha tracks. Only a summary of the latest results will be given here.

First tests were performed in Argon-iC$_4$H$_{10}$ mixtures, and later on in pure Ar and in pure Xe. Data have been taken in pressures up to ~ 8 bar. The results prove that microbulk Micromegas work well in pure, high pressure Xe reaching gains above 100. This is noteworthy because in absence of a quencher early break-down occurs in all other MPGDs.[22] For the 5.5 MeV alpha peak of the ^{241}Am, energy resolutions down to $\sim 2\%$ FWHM in pure Ar or Xe, roughly independent of pressure, have been measured (to be compared with 0.7% FWHM in Ar-2%iC$_4$H$_{10}$ at 4.75 bar.[23]) For the low energy (59.5 keV) photon peak of the ^{241}Am (visible when blocking the alpha emission) energy resolutions of 7.8% FWHM at 2 bar and 9.3% FWHM at 3.5 bar have been achieved. Data taken in a different setup[22] are consistent with these values.

Although the operation in pure Xe is a remarkable achievement for a MPGD readout, the possibility of adding a quencher to the Xe may bring further advantages. Several mixtures have been tested, being the most promising Xe+TMA. TMA (trimethilamine) forms a Penning mixture with Xe and indeed much higher gains are observed for the same voltage with respect to pure Xe. Systematic study of this mixture in microbulk Micromegas point to remarkable results, with stable high-gain operation in all the pressure range from 1 to 10 bar, and energy resolutions below 1% at $Q_{\beta\beta}$.[24]

The larger prototype NEXT-1-MM was first equipped with a more conventional bulk Micromegas readout, shown in Fig. 3 with 1252 pixels independently read. Electronics based on the AFTER chip were used for the data acquisition. First alpha tracks were recorded with NEXT-1-MM using this readout (Fig. 2). Recently, the definitive microbulk version of this readout (Fig. 3) have been mounted and tested.
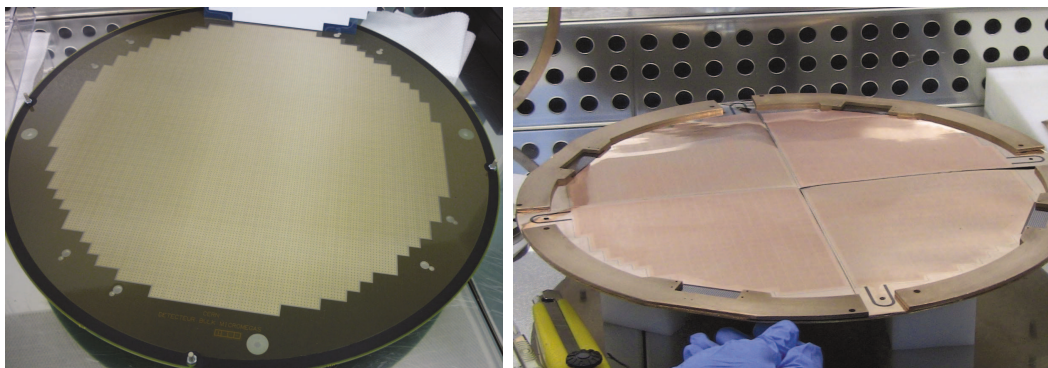

Fig. 3. On the left a photo of the bulk Micromegas detector first installed in the NEXT-1-MM. It has a diameter of 30 cm and its anode is segmented to ~ 1200 pixels. On the right the new microbulk version of the same readout, recently installed in the detector. It is divided in 4 circular segments and constitutes the largest surface built up to now of this type of readout.

It is composed of four circular segments covering the 30 cm diameter circular area. Together, they are the largest readout manufactured to date using the microbulk technique. The detector with the new readout is being commissioned at the moment and first preliminary results show promising tracking capabilities.[25]

1.3. *Directional WIMP dark matter detection: MIMAC*

The purpose of the MIMAC (MIcro TPC MAtrix of Chambers) Collaboration[26] is to build a large directional Dark Matter detector composed of a matrix of Micromegas detectors. The MIMAC detector will be designed to measure both the 3D track and the ionization energy of recoiling nuclei, allowing the possibility to achieve directional Dark Matter detection. This is proposed to be accomplished by the use of a Bulk Micromegas detector[27] operated in low pressure (50 mbar) CF_4.

The concept is based on the detection of the nuclear recoil produced by a WIMP in the TPC which produces electron-ion pairs in the conversion gap of the Micromegas detector that drift towards the amplification gap. In the amplification gap, thanks to the high electric field, an avalanche will be produced inducing signals in the x-y anode and in the mesh. The track of the recoil is thus projected on the anode, providing 2D information[28] (Fig. 4). The z dimension of the recoil is reconstructed by dedicated electronics[29,30] reaching an anode sampling frequency of 40 MHz.

One critical aspect of WIMP search is to know precisely the ionization quenching factor (IQF). Especially because at low energies, in the range of a few keV, the ionization produced in a medium falls rapidly and systematic measurements are not available. The IQF of ^{4}He has been measured in order to be able to evaluate the total recoil energy with a dedicated set-up[31] down to 1 keV recoil energies. The IQF dependence on the pressure and percentage of the isobutane has been studied for four different pressures ranging from 350 mbar to 1300 mbar.
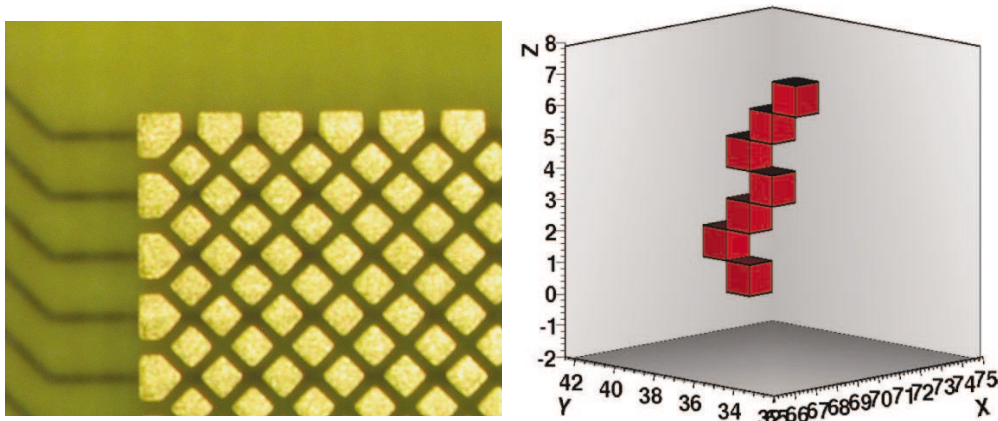

Fig. 4.   Left: A photo of the 2D readout plane of the MIMAC detector. The pixels and the strips can be seen. Right: An example of a recorded track of 8 keV hydrogen nucleus in 350 mbar of ^{4}He with 5% of C_4H_{10}.

I. G. Irastorza, E. Ferrer-Ribas & T. Dafni

A bi-chamber has been installed in the underground laboratory of Modane[32] consisting of two detectors of a readout plane of 10×10 cm^2 with a drift of 25 cm equipped with 1024 electronic channels. The gas used is a mixture of 70%CF$_4$ + 28%CHF$_3$ + 2%C$_4$H$_{10}$ at 50 mbar. This set-up will allow background rejection measurements in a realistic environment for a dark matter experiment and will allow to identify main sources of background before scaling the detector to the m^3 scale.

Moreover, the detector conditions (gas, pressure and voltages) have been optimized to be able to perform energy and flux measurements for metrological purposes in the Amande facility.[33] A comparison of experimental measurements with simulation showed good agreement of energy spread after reconstruction of neutron fields from 50 keV to 250 keV using pure C$_4$H$_{10}$.[34]

The next steps are to move forward to new and bigger anode readout structures of 20 cm $\times$ 20 cm in order to achieve 1 m^3. These anodes will use the piggyback[35] technology, already tested in smaller detectors, in order to simplify the readout plane design. An upgraded version of the dedicated electronics will be designed for 1024 channels. Two big chambers, composed of 25 bi-chambers each, will be constructed. This should allow the validation of a new generation of Dark Matter detector including directionality.

2. Conclusion

In the last decade, Micromegas detectors have been confirmed as a competitive option for rare event detection. We have presented here the performances of the Micromegas used in the CAST experiment as well as for the studies carried out within the NEXT and MIMAC projects. These applications have benefited from two aspects: on one hand, the strengths of the Micromegas technology, such as are the good energy resolution, the homogeneity of the gain, the stability in operation and the radiopurity; on the other, the ultra-low background techniques, like the use of an appropriate shielding, the exploitation of the event topology provided by the detector readout and the use of radiopure construction materials.

References

1. Y. Giomataris *et al.*, *Nucl. Instrum. Meth. A* **376**, 29 (1996).
2. I. G. Irastorza *et al.*, *EAS Publications* **53**, 147 (2012).
3. T. Dafni *et al.*, *J. Phys. Conf. Ser.* **347**, 012030 (2012).
4. S. Andriamonje *et al.*, *J. Instrum.* **5**, P02001 (2010).
5. CAST Collab. (K. Zioutas *et al.*), *Phys. Rev. Lett.* **94**, 121301 (2005).
6. CAST Collab. (S. Adriamonje *et al.*), *J. Cosmol. Astropart. Phys.* **04**, 01 (2007).
7. CAST Collab. (E. Arik *et al.*), *J. Cosmol. Astropart. Phys.* **0902**, 008 (2009).
8. V. Álvarez *et al.*, *J. Instrum.* **7**, T06001 (2012).
9. I. G. Irastorza *et al.*, *J. Cosmol. Astropart. Phys.* **06**, 013 (2011).
10. P. Abbon *et al.*, *New J. Phys.* **9**, 170 (2007).
11. J. Galán *et al.*, *J. Instrum.* **5**, P01009 (2010).
12. T. Dafni *et al.*, *Nucl. Instrum. Meth. A* **628**, 172 (2011).
13. J. García *et al.*, talk given at the *6th Symposium on Large TPCs for Low Energy Rare Event Detection*, Paris (2012).
14. A. Tomás *et al.*, *X-ray Spectrometry* **40**, 240 (2011).
15. A. Tomás *et al.*, *Phys. Procedia* **37**, 478 (2012).
16. J. Galán *et al.*, *EAS Publications* **53**, 155 (2012).
17. S. Cebrián *et al.*, *J. Cosmol. Astropart. Phys.* **10**, 010 (2010).
18. EXO-Bern Collab. (D. Franco *et al.*), *J. Phys. Conf. Ser.* **309**, 012004 (2011).
19. S. Cebrián *et al.*, *Astropart. Phys.* **34**, 354 (2011).
20. H. Gómez *et al.*, PoS(IDM2010)10 (2010).
21. NEXT Collab. (T. Dafni *et al.*), *J. Phys. Conf. Ser.* **309**, 012009 (2011).
22. C. Balan *et al.*, *J. Instrum.* **6**, P02006 (2011).
23. T. Dafni *et al.*, *Nucl. Instrum. Meth. A* **608**, 259 (2009).
24. S. Cebrián *et al.*, accepted for publication in *J. Instrum.*, arXiv:1210.3287v3.
25. D. C. Herrera *et al.*, talk given at the *6th Symposium on Large TPCs for Low Energy Rare Event Detection*, Paris (2012).
26. S. Santos *et al.*, *J. Phys. Conf. Ser.* **309**, 012014 (2011).
27. Y. Giomataris *et al.*, *Nucl. Instrum. Meth. A* **560**, 405 (2006).
28. F. J. Iguaz *et al.*, *J. Instrum.* **6**, P07002 (2011).
29. J. P. Richer *et al.*, *Nucl. Instrum. Meth. A* **620**, 470 (2006).
30. O. Bourrion *et al.*, *Nucl. Instrum. Meth. A* **662**, 207 (2006).
31. O. Guillaudin *et al.*, *Eur. Phys. J. Plus* **127**, 119 (2012).
32. F. Piquemal *et al.*, *Eur. Phys. J. Plus* **127**, 110 (2012).
33. V. Gressier *et al.*, *Radiat. Prot. Dosim.* **110**, 49 (2004).
34. C. Golabek *et al.*, *Nucl. Instrum. Meth. A* **678**, 33 (2012).
35. D. Attié *et al.*, arXiv:1208.6525.

Towards smaller gap microbulks

D. Attié,[a] **L. Boilevin-Kayl,**[a] **T. Dafni,**[b] **E. Ferrer-Ribas,**[a,*] **S. Ferry,**[c] **Y. Giomataris,**[a] **D.C. Herrera,**[b] **F.J. Iguaz,**[a,†] **I.G. Irastorza,**[b] **M. Kebbiri,**[a] **T. Papaevangelou,**[a] **R. de Oliveira,**[c] **L. Seguí**[b,‡] **and A. Tomás**[b,§]

[a]*IRFU, Centre d'Études Nucleaires de Saclay,*
(CEA-Saclay), Gif-sur-Yvette, France

[b]*Instituto de Física Nuclear y Altas Energías,*
Universidad de Zaragoza, Zaragoza, Spain

[c]*European Organization for Nuclear Research (CERN),*
Genève, Switzerland

E-mail: esther.ferrer-ribas@cea.fr

ABSTRACT: Small gap Micromegas detectors ($< 50\,\mu$m) are expected to be optimal for high pressure applications. Combining the microbulk manufacturing technique with a small gap can result in attractive detectors for rare event detection, in particular double beta decay or dark matter searches. We present novel results obtained with small gap microbulks (25 and $12.5\,\mu$m) that have been manufactured recently. For the first time for this type of detectors, we show experimentally that for each amplification gap there is an optimal pressure and that smaller gaps are more suitable for higher pressures.

---

*Corresponding author.

†Present address: Instituto de Física Nuclear y Altas Energías, Universidad de Zaragoza, Zaragoza, Spain.

‡Present address: University of Oxford, Oxford, United Kingdom.

§Present address: Brackett Laboratory, Imperial College, United Kingdom.

Contents

1 Introduction

Exploring new physics in particle or nuclear physics needs high performance detectors. The microbulk [1] is a new gaseous detector based on the Micromegas structure [2], which is now a mature technology used in different experiments such as CAST, NEXT, NTOF. The Micromegas gap is fabricated by etching of a polyimide layer, usually 50 μm thick, sandwitched between two thin metallic layers. The high accuracy of this process provides a high precision avalanche gap and it reduces gain fluctuations with improved energy resolution and detector stability. The outcome is a low-mass detector, a key element in many applications while at the same time the use of clean raw-materials provides a unique feature of an intrinsically radiopure detector [4, 5].

In solar axion search (CAST experiment at CERN [6]) the microbulk is used as a low background X-ray detector since 2008. It has shown remarkable operation stability and an extremely low background level at low energy. In neutrinoless double beta decay experiments using a high pressure Xenon TPC the microbulk could be a precious tool due to its low background and enhanced energy resolution capability; developments are in progress in the context of the NEXT experiment [7–9]. In nuclear physics investigations (NTOF experiment) the low material is of paramount importance in order to provide a "neutron transparent" detector for measuring on-line neutron flux and neutron beam profile [10–12].

In previous investigations [3], it was shown that small gap Micromegas detectors would be optimum for operation at high pressure where the gain could be maximised and fluctuations due to geometrical factors or environmental ones would be cancelled. This property is important in the field of rare event searches in order to increase the sensitivity and, in the case of Xenon gas, to enhance detection efficiency of gamma rays. In [13] characterization of microbulk detectors was investigated with different gas mixtures in Argon and neon for 50 and 25 μm gaps. In the present work the study is extended down to 12.5 μm.

Table 1. Summary of the pattern of holes diameters and pitchs for the three different amplification gaps of the tested detectors.

amplification gap (μm)	hole diameter (μm)	hole pitch (μm)
12.5	25	80
25	30	100
50	40	90

The paper is organised as follows: section 2 describes briefly the microbulk fabrication process and the mesh geometry of the studied detectors. In addition electric field simulations are presented to understand experimental results obtained with various avalanche gaps indicating the technological roadmap for future optimization of the microbulk detector. Section 3 is devoted to the performance of 25 and 12.5 μm gap microbulks compared to 50 μm including gain and energy resolution. Novel results are shown exhibiting the relation of amplification gap versus gas pressure. Finally conclusions and perspectives are discussed in section 4.

2 Fabrication process and mesh geometry considerations

The manufacturing process of a microbulk detector was described in detail in [1]. Here we only remind the main three steps in figure 1. The raw material is a thin flexible kapton foil (of 25 μm or 12.5 μm) with a 5 μm copper layer on each side (figure 1 step 1). A thin photoresistive film is laminated on top of the kapton foil and it is illuminated by UV light to produce the required mask (figure 1 step 2). The copper is then removed by a standard lithographic process and the non-illuminated regions produce a pattern of a thin mesh. The polyimide is then etched and partially removed in order to create tiny pillars in the shadow part of the mesh below the copper mesh. In the prototypes used here the holes are 30 (25) μm in diameter with a pitch of 100 (80)μm for the 25 (12.5) μm amplification gaps in a hexagonal pattern to optimise electron transmission. A summary of the geometry of the holes diameters and pitch for the different amplifications gaps is given in table 1.

In 50 μm gap Micromegas detectors, the holes diameter is usually conceived smaller than the amplification gap to favor the funnel electric field effect. In the case of the present detectors with gaps of 25 and 12 .5 μm this is not possible. The limitation comes from the attainable precision on the mask films that define the minimum mesh holes diameter. This limitation could be exceeded by an alternative more expensive technique, using glass masks, where holes of 20 μm diameter could be achieved. Going further with the present techniques seems difficult.

In order to verify that the thickness of the mesh as well as the diameter of the holes will not perturb the shape of the electric field lines, a field simulation was effectuated using the Lorentz software package [14]. In figure 2 the field line configuration is shown for the 12.5 and 25 μm amplification gap with a simplified geometry. The insulating kapton pillars have not been considered for these simulations. The typical funnel shape of the field lines at the mesh hole entrances seems well preserved. However figure 3 shows the magnitude of the electric field at different heights within the amplification gaps across the hole as indicated in the sketch of figure 3. The depicted
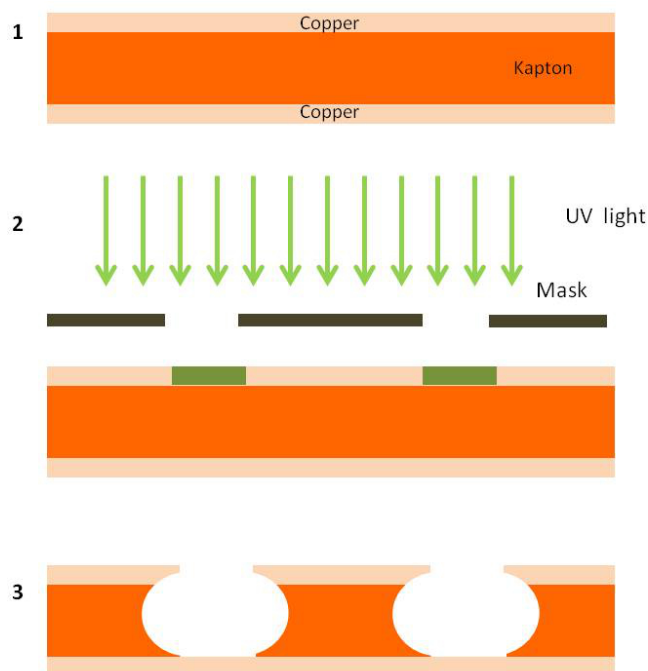
Figure 1. Summary of the manufacturing process of a single anode microbulk, described in the text.

electric field ranges from 99% (black points) to 1% (pink points) of the amplification gap for the three different cases (12.5, 25 and 50 μm). The 99% correspond to heights at the level of the mesh while heights of 1% correspond to heights close to the anode, where the electric field is the strongest. The voltage applied is the same for the different gaps and only relative differences are pertinent here.

If we compare the ratio of the field at 99% and 1% of the amplification gap for the different gaps, we observe that for the 50 μm gap this ratio is 1.77 while for the 12.5 μm is 1.49. This means that the increase of the field near the anode for the small gaps is smaller than for the larger gaps with this hole geometry. This will probably lead to reduced gains for the small gaps. This effect would be corrected if the diameter of the holes could be reduced.

The second consideration is that for the small gaps there is greater dispersion of the magnitude of the electric field close to the anode i.e for the 50 μm the magnitude of the electric field is nearly constant from heights greater than 50%. Another way of seeing this effect, is by looking at the integration of the electric field across the amplification gap. Figure 4 shows the integrated electric field across the amplification gap at two different positions: at the middle of the hole and a position shifted of 15% to one side as shown in the sketch. The difference between the two curves is greater for the small gaps than for the 50 μm. In particular the difference between the integration of the two positions at the level of the anode at the maximum of the electric field is only of 1% while for the 12.5 μm amplification gap the difference reaches 8%. In addition, the averaged integrated field ratio between the two positions is of 12% for the 12.5 μm amplification gap and only of 5% for the 50 μm amplification gap meaning that the avalanche will take place in a similar manner regardless
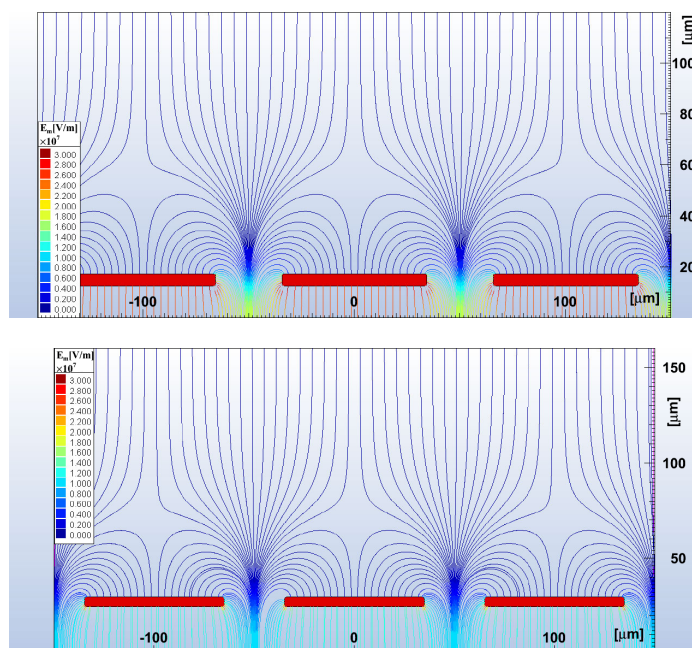
Figure 2. Field line simulation of a 12.5 and 25 μm amplification gap Micromegas detector with the hole and pitch dimensions described in table 1.

of position within the hole for the 50 μm amplification gap. This fact will probably have an effect on the energy resolution.

3   Performances of 12.5 and 25 μm gap microbulks compared to 50 μm

The microbulks of 50 μm are relatively well-known. They have been well characterised [1, 7, 13] and are being used in the CAST experiment [1], in the R&D for the NEXT experiment [8] and in the NTOF [10]. In the next section we will compare the performance of the novel small gap microbulk with respect to the well known 50 μm amplification gap ones. In particular, it is the first time that the behaviour of smaller gap microbulks as a function of pressure (from 0.4 bar to 1.7 bar) is studied in Argon-Isobutane mixtures.

3.1   Set-up description

The detectors were installed in an aluminium vessel with an aluminized mylar window allowing calibration by X-rays from an ^{55}Fe source. The prototypes used in these tests are single anode round detectors with an active zone of a diameter of 35 mm. A picture of the detector and a zoom of the active area are shown in figure 5. The gas mixture was allowed to circulate for several hours before each measurement and at every change of the gas mixture or the pressure. To maintain the drift gap, a mesh frame is layed on 10 mm pillars. The mesh signal was read out by an ORTEC 142B preamplifier followed by a CANBERRA 2022 Spectroscopy amplifier. The pulse height distributions are recorded by a multi-channel analyzer AMPTEK MCA-8000A. Each spectrum
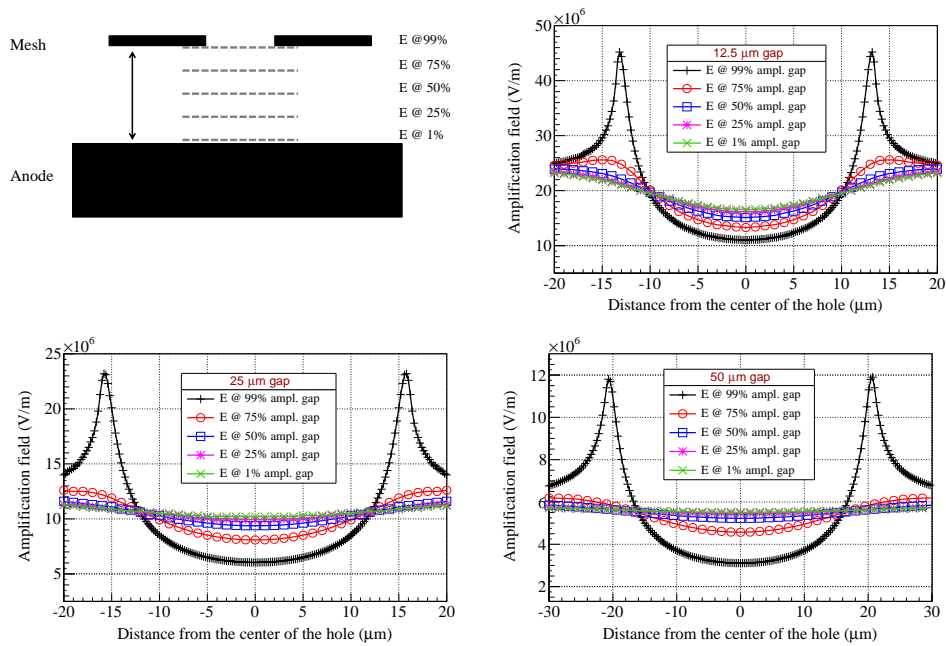
Figure 3. Sketch to illustrate the electrostatic simulation (top left). Magnitude of the electric field at different heights within the amplification holes for the 12 (top right), 25 (bottom left) and 50 (bottom right) μm amplification gaps.

was fitted by two Gaussian functions, corresponding to the K_α (5.9 keV) and K_β (6.4 keV) lines of the ^{55}Fe source; the mean position and width of the main peak were obtained for each fit.

3.2 Measurements at atmospheric pressure

3.2.1 Gain

The 25 and 12.5 μm detectors were tested at atmospheric pressure with different percentages of Isobutane. A scan of the drift field was done at fixed amplification field in order to obtain the electron transmission and to find the range of optimal operation. The result is shown in figure 6 exhibiting a similar behaviour for the two different gaps. It is noteworthy that there is a wide range of ratios of drift and amplification fields, where the relative electron transmission is greater than 90%. The region where the electron transmission is constant, called the plateau, is extended when the percentage of Isobutane is increased [15]. This effect is correlated with the diffusion coefficient and was already verified in [7, 13, 20]. On the other hand, there is a steady increase of the gain with the drift field that is more prominent at high Isobutane concentrations and for the 12.5 μm gap. This effect was already observed in [13] and has been simulated with the neBEM and Garfield [16, 17]. At high drift fields, the mesh stops being transparent as some of the field lines stop at the mesh and part of the electrons are lost.

In order to obtain the gain of the detector as a function of amplification field, the ratio of drift and amplification field is set at the maximum of transmission. Figure 7 shows the gain versus
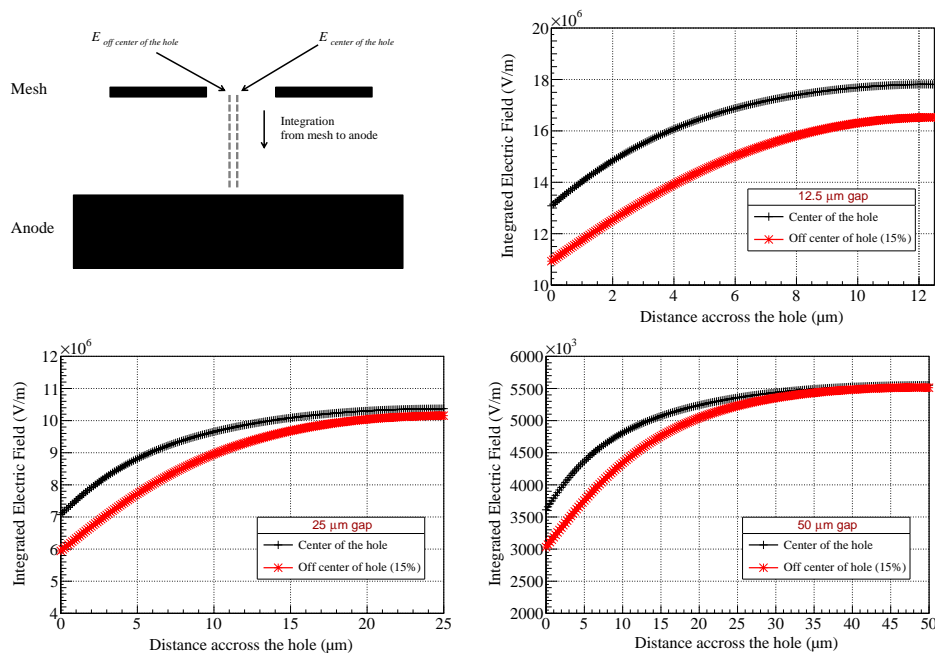
Figure 4. Integrated electric field across the amplification gap for the 12 (a), 25 (b) and 50 (c) μm amplification gaps. The full line corresponds to the integrated electric field at the center of the hole whilst the dashed line corresponds to the integrated field shifted of 15% from the center of the hole.
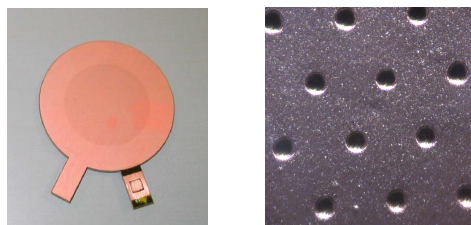
Figure 5. Left: picture of a 3.5 cm diameter circular microbulk used in these tests. Right: zoom of the active area. The hexagonal pattern of the 30 μm diameter mesh holes with a pitch of 100 μm can be observed.

amplification fields for different gas mixtures for 12.5 μm (left) and 25 μm (right) amplification gaps. Gains greater than 7×10^3 are obtained for the 12.5 μm gap. For the 25 μm, the maximum gains reach 10^4 for concentrations of 15% and 20%. The maximum gains observed are below the sparking point of the detector, i.e the detectors have not been pushed to the limit. The results for the 25 μm detectors corroborate the previous measurements in [13]. In order to have a common point of comparison, figure 8 shows the gain for the three different gaps in the same conditions, at atmospheric pressure in an Ar + 10% Isobutane mixture showing that the highest gains are obtained for the 50 μm gap despite the lowest electric field applied as the distance for the avalanche to develop is larger.

– 6 –

Figure 6. Electron transmission versus ratio of drift and amplification fields for different gas mixtures for 12.5 μm (left) and 25 μm (right) amplification gaps.
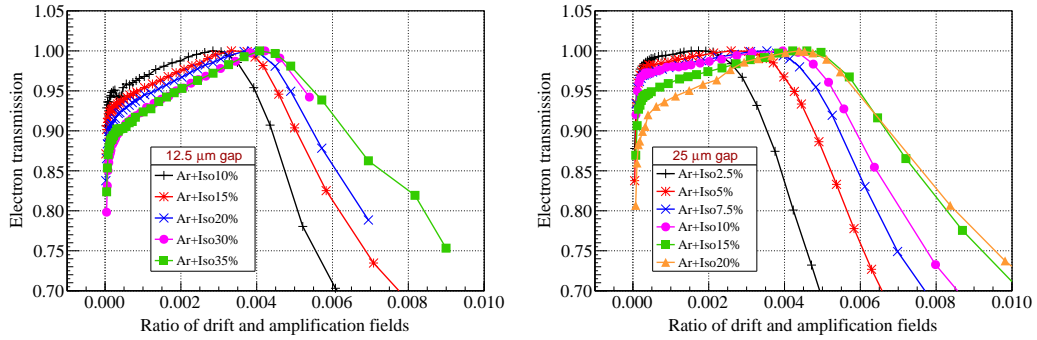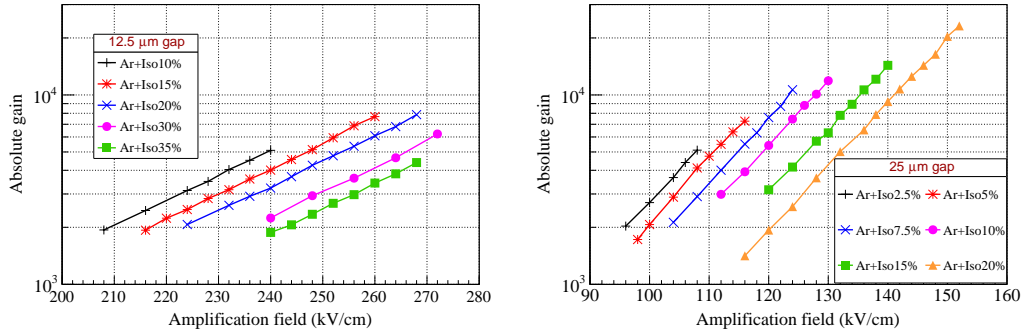

Figure 7. Gain versus amplification fields for different gas mixtures for 12.5 μm and 25 μm amplification gaps.

3.2.2 Energy resolution measurements

The energy resolution has been studied for different concentrations of Isobutane. The results are shown in figure 9. For a given gas mixture the energy resolution increases with gain as the signal to noise ratio is increased. Normally a minimum is reached and at high gain a degradation can be observed due to the extra fluctuations [18]. This degradation is not observed neither for the 12.5 μm nor for the 25 μm. As in the gains studies, detectors have not been pushed to the sparking limit.

Regarding the percentage of quencher, at low concentrations the energy resolution is worse as not all the UV photons in the avalanche are absorbed. The best energy resolution is obtained at Ar + 10% Isobutane and Ar + 20% mixtures for the 25 μm and 12.5 μm respectively. These concentrations, that seem optimum for the energy resolution, will be the reference ones to study the performance as a function of pressure in the next section.

In order to obtained the ultimate energy resolution we have repeated the measurement using a chrome foil in order to select the K$_\alpha$ (5.9 keV) line of the ^{55}Fe. This is shown in figure 10. We can see that these values, 12% and 11% for the 25 and 50 μm gaps respectively are close to the theoretical limitations and do not depend on our fitting procedure.

– 7 –
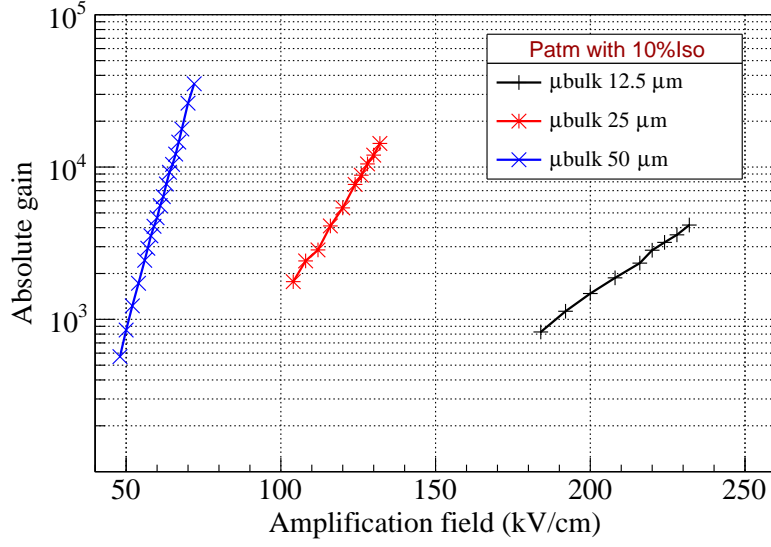
Figure 8. Comparison of gain for the different gaps at atmospheric pressure in Ar + 10% Isobutane.
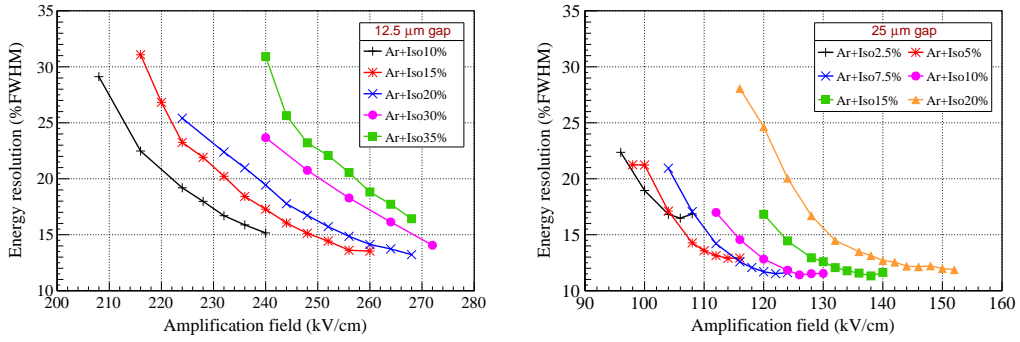
Figure 9. Resolution versus amplification fields for different gas mixtures for 12.5 μm and 25 μm amplification gaps.

This is observed by calculating the lower limit on the obtainable energy resolution in gas detectors taking into account primary and avalanche fluctuations. It can be written as follows:

$$\frac{\sigma_E}{E}(FWHM) = 2.35\sqrt{\frac{W}{E_0}(F+b)}, \tag{3.1}$$

where W is the mean energy per ion pair, E_0 is the initial total energy of the ionization particle, F is the Fano factor and b is the relative variance for the distribution of the number of electrons produced in a single avalanche. Using typical values of $F = 0.2$, $W = 25$ eV and $b = 0.5$ [19], the minimum resolution at 5.9 keV is 10.8% (FWHM).
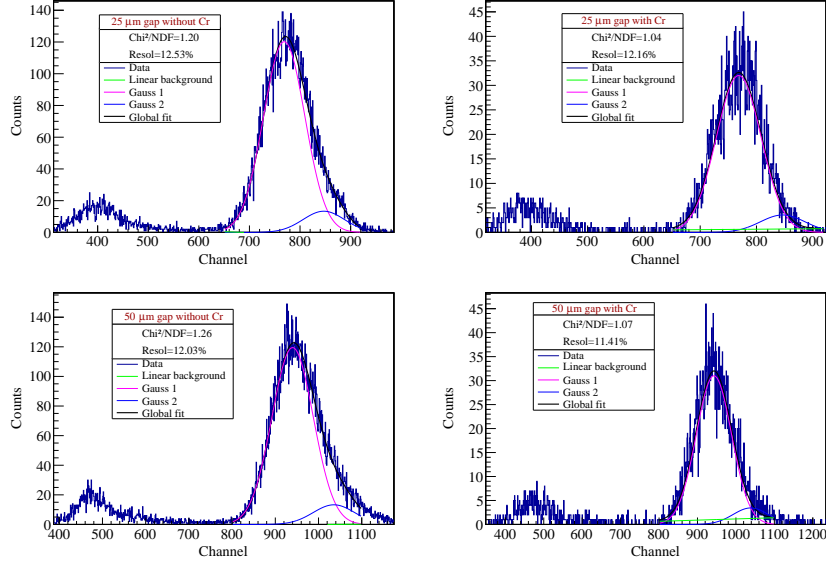
Figure 10. Comparison of the energy resolution for the 25 and 50 μm amplification gaps without (left) and with (right) a chrome foil. The chrome foil selects the K_α (5.9 keV) line.

3.3 Performance versus pressure

The motivation for this study is to show experimentally that there is an optimal range of pressures for operation for every amplification gap. This theory was shown in [3] by the Townsend coefficient in the Rose-Korff's parametrisation [22]:

$$\alpha = PAe^{\frac{-BP}{E}} \tag{3.2}$$

where P is the gas pressure, A and B are parameters that depend on the gas and E is the electric field. The gain can be then written as:

$$G = \exp\left(PAe^{\frac{-BPd}{E}}\right) = \exp\left(PAe^{\frac{-BPd}{V}}\right) \tag{3.3}$$

with V being the applied voltage. We recall here that this expression can be differentiated in order to find a set of parameters (pressure and voltage) that will optimise the stability operation:

$$\frac{\partial G}{\partial P} = G\alpha\left(1 - \frac{BPd}{V}\right) \tag{3.4}$$

We can then deduce, by setting 3.4 equal to 0, that for each gap there is an optimal pressure that can be written as:

$$P = \frac{V}{Bd} \tag{3.5}$$

From this relation, we can see that the pressure is inversely proportional to the amplification gap, so it is expected that small amplification gaps will be more suitable for operation at higher pressures. In [20] this idea was done by testing different Micromegas detectors of the Ingrid [21] type with gaps from 45 μm to 68 μm at fixed gas conditions to observe the evolution of the gain at a given voltage. Here the gain for the three different gaps has been measured at different pressure conditions. The gas mixture that optimises the behaviour for each gap in terms of energy resolution

and gain have been chosen. The curves are shown in figure 11 for various pressures and Isobutane percentages: 20%, 10% and 5% for 12.5, 25 and 50 μm amplification gaps.

The pressure has been scanned from 0.5 to 1.7 bar. The gains achieved in this range are greater than 5×10^4 for the 12.5 μm gap and 10^4 for the 25 μm gap. For the 50 μm gap the gains are as high as 3×10^4 and no degradation is seen with the pressure. The trend for the energy resolution as a function of electric field is shown in figure 12. The best minimum is between 11 and 13% for the three gaps. A summary of these results can be seen figure 12 where the evolution of the gain and the energy resolution as a function of pressure is given for a fixed electric field. The gain follows the expected bell shape with a shifting maximum with amplification gap. The best value of energy resolution is reached at the maximum of the gain [3]. The optimum range of pressures is 0.4 bar for the 50 μm gap, 0.7 bar for the 25 μm gap while for the 12.5 bar is 0.9 bar confirming that smaller gaps are optimum for higer pressures. As these measurements have been performed in different Argon-Isobutane mixtures (5% Isobutane, 10% Isobutane and 20% for the 50 μm, 25 μm and 12.5 μm respectively) in order to optimise the energy resolution, we have verified that at fixed gas mixture (with B of equation (3.4) fixed) the trend is the same. Figure 13 shows the evolution of the gain and the energy resolution as a function of pressure for a gas mixture of Argon+10%Isobutane. The general trend is the same as in figure 12. However the maximum for the 12.5 μm amplification gap is slightly shifted to a higher pressure and the resolution is $\sim 14\%$ instead of $\sim 12\%$. Concerning the 50 μm amplification gap the maximum has not been reached, as lower pressures were needed that were not reachable but the resolution reamins unchanged ($\sim 11\%$).

In figure 14 the best energy resolution at each pressure is shown independently of the electric field applied. The range of pressure where the behaviour is optimal is within ± 0.1 bar around the minimum and is broader for the 12.5 and 25 μm gaps. In addition, this figure indicates that the optimum gap in an Argon-Isobutane mixture at atmospheric pressure is probably 25 μm.

4 Conclusion and perspectives

Microbulk detectors of 25 and 12.5 μm amplification gap have been manufactured and tested with success. Gains greater than 10^4 for the 25 μm detectors and 8×10^3 for the 12.5 μm have been obtained in Argon-Isobutane mixtures. Energy resolutions as low as 12% (FWHM) for the 12.5 μm while for the 25 μm values of 11.5% have been reached at 5.9 keV. These values are very close to the minimum energy resolution that can be achieved with gaseous detectors taking into account the fluctuations due to electron multiplication. The electric field simulations qualitatively indicate that the differences in the gain and resolution of the two detector types could be due to the holes pattern and the manufacturing limitations of the smallest gaps.

The behaviour of these detectors has also been studied as a function of pressure from 0.5 bar to 1.7 bar. The gain follows the expected bell shape with the maximum shifted with the pressure: smaller gaps are more suitable for higher pressures.

These tests confirm the suitability of small gap microbulk for rare event detection that would require operation pressures above the atmospheric.

Acknowledgments
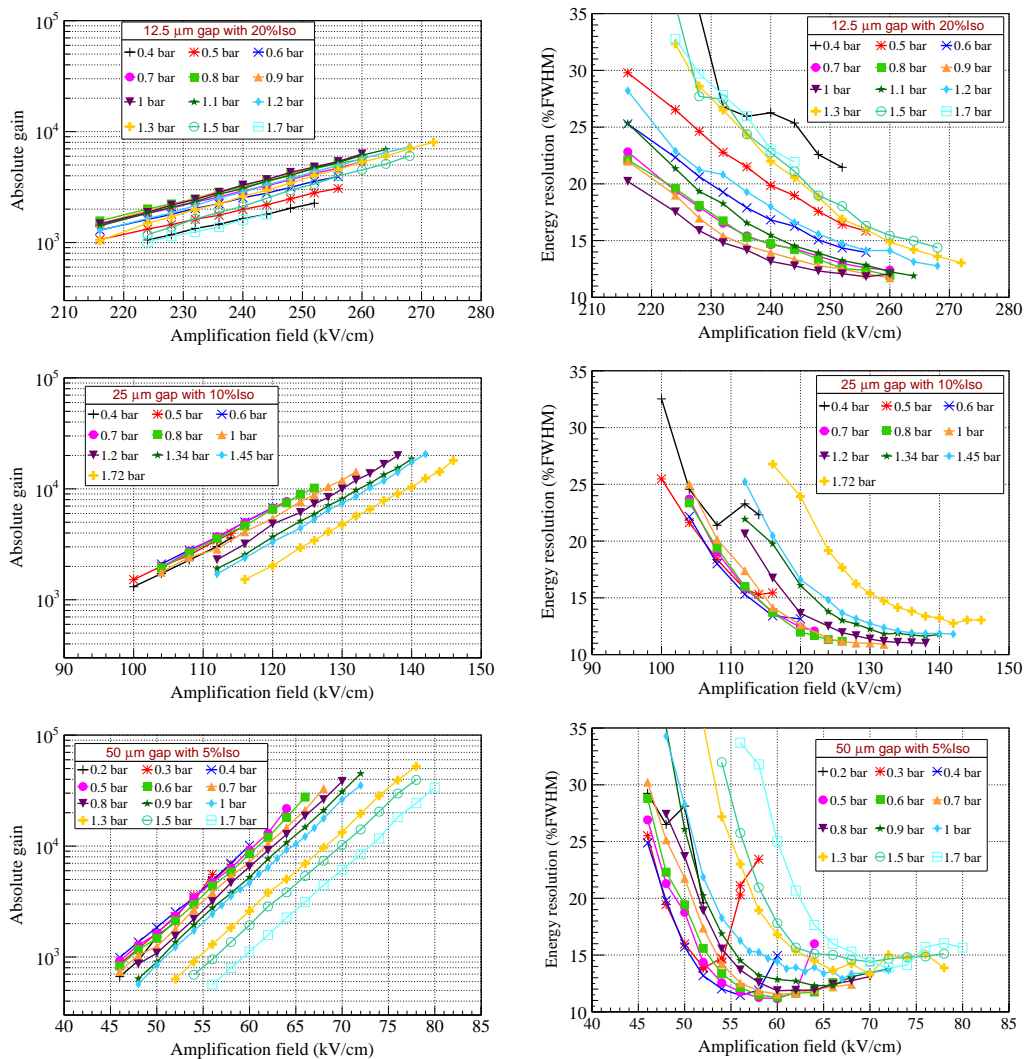
Figure 11. Gain measurements (left) and energy resolution (right) for different pressures in Argon-Isobutane mixtures: 20% for 12.5 μm , 10% for 25 μm and 5% for 50 μm amplification gaps.
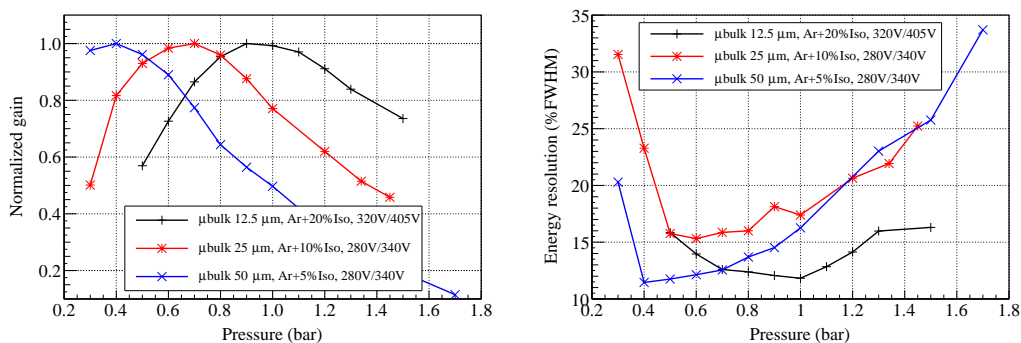
Figure 12. Gain (left) and resolution (right) versus pressure at a given amplification field for each detector gap in Argon-Isobutane mixtures: 20% for 12.5 μm , 10% for 25 μm and 5% for 50 μm amplification gaps.
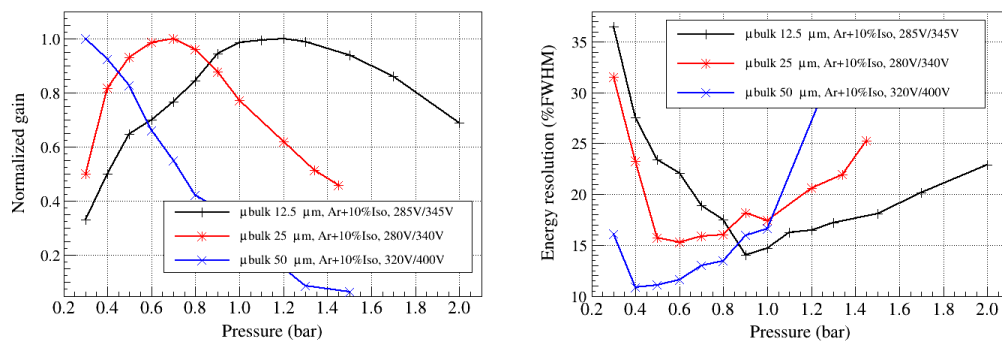
Figure 13. Gain (left) and resolution (right) versus pressure for 50 μm, 25 μm and 12.5 μm at a given amplification field for each detector gap for an Argon-10% Isobutane mixture.
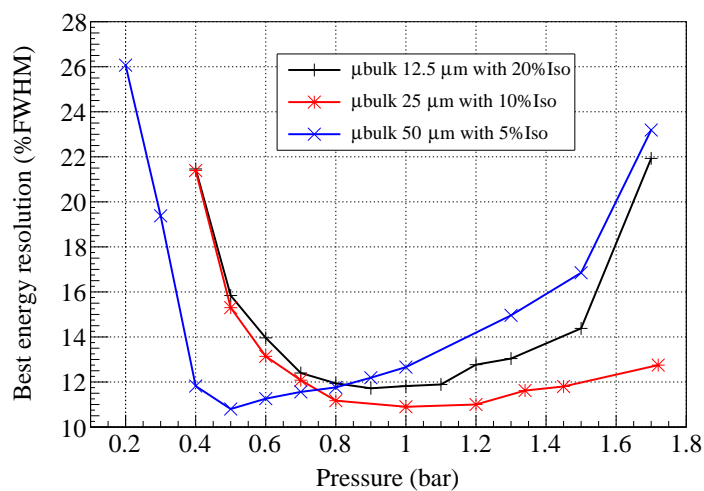
Figure 14. Best energy resolution versus pressure for 50 μm, 25 μm and 12.5 μm amplification gaps at a given amplification field for each detector gap.

References

[1] S. Andriamonje et al., *Development and performance of Microbulk Micromegas detectors*, 2010 *JINST* **5** P02001

[2] Y. Giomataris, P. Rebourgeard, J.P. Robert and G. Charpak, *MicrOMEGAs: A High granularity position sensitive gaseous detector for high particle flux environments*, *Nucl. Instrum. Meth.* **A 376** (1996) 29 [INSPIRE].

[3] Y. Giomataris, *Development and prospects of the new gaseous detector 'MicrOMEGAs'*, *Nucl. Instrum. Meth.* **A 419** (1998) 239 [INSPIRE].

[4] I.G. Irastorza, E. Ferrer Ribas and T. Dafni, *Micromegas in the rare event searches*, *Mod. Phys. Lett.* **A 28** (2013) 1340026.

[5] S. Cebrián, T. Dafni, E. Ferrer-Ribas, J. Galan, I. Giomataris et al., *Radiopurity of MicrOMEGAs readout planes*, *Astropart. Phys.* **34** (2011) 354 [arXiv:1005.2022].

[6] S. Aune, J.F. Castel, T. Dafni, M. Davenport, G. Fanourakis et al., *Low background x-ray detection with MicrOMEGAs for axion research*, 2014 *JINST* **9** P01001 [arXiv:1310.3391].

[7] T. Dafni, E. Ferrer-Ribas, I. Giomataris, P. Gorodetzky, F. Iguaz et al., *Energy resolution of alpha particles in a microbulk MicrOMEGAs detector at high pressure Argon and Xenon mixtures*, *Nucl. Instrum. Meth.* **A 608** (2009) 259 [arXiv:0906.0534].

[8] S. Cebrián et al., *Micromegas-TPC operation at high pressure in xenon-trimethylamine mixtures*, 2013 *JINST* **8** P01012.

[9] THE NEXT collaboration, V. Alvarez et al., *Characterization of a medium size Xe/TMA TPC instrumented with microbulk MicrOMEGAs, using low-energy γ-rays*, arXiv:1311.3535 [INSPIRE].

[10] F. Belloni et al., *Micromegas for neutron detection and imaging* , *Mod. Phys. Lett.* **A 28** (2013) 1340023.

[11] S. Andriamonje et al., *A Transparent Detector for n TOF Neutron Beam Monitoring J. Korean Phys. Soc.* **59** (2011) 1597.

[12] C. Guerrero et al., *Simultaneous measurement of neutron-induced capture and fission reactions at CERN*, *Eur. Phys. J.* **A** (2012) 48: 29.

[13] F.J. Iguaz, E. Ferrer Ribas and Y. Giomataris, *Characterization of microbulk detectors in Argon- and neon-based mixtures*, 2012 *JINST* **7** P04007.

[14] Integrated Engineering Software, http://www.integratedsoft.com/.

[15] A. Tomás Alquezar, *Development of Time Projection Chambers with Micromegas for Rare Event Searches.*, Ph.D. Thesis, 2013 JINST TH 001, Laboratorio de Física Nuclear y Astropartículas, Departemento de Física Teórica, Universidad de Zaragoza (2013).

[16] P. Bhattacharya et al., *Performance Studies of BULK Micromegas with Different Amplification Gaps*, in proceeding of *3rd International Conference on Micro Pattern Gaseous Detectors*, 1–6 July, 2013, Zaragoza, Spain.

[17] P. Bhattacharya et al.,*Characteristic Studies of Micromegas*, presentation at the RD51 meeting 14-17 October 2013.

[18] I.K Bronic and B. Grosswendt, *Gas amplification and ionization coefficients in Isobutane and Argon-Isobutane mixtures at low gas pressures*, *Nucl. Instrum. Meth.* **B 142** (1998) 219.

[19] W. Blum and L. Rolandi, *Particle detection with drift chambers*, Springer-Verlag (1993).

[20] M. Chefdeville, *Development of Micromegas-like gaseous detectors using a pixel readout chip as collecting anode*, Ph.D. Thesis, University of Amsterdam (2009).

[21] M. Chefdeville, H. van der Graaf, S. van der Putten, J. Timmermans, J.L. Visschers et al., *An electron-multiplying 'MicrOMEGAs' grid made in silicon wafer post-processing technology*, *Nucl. Instrum. Meth.* **A 556** (2006) 490.

[22] M.E. Rose and S.A. Korff, *An Investigation of the Properties of Proportional Counters*, *P*hys. Rev. **59** (1941) 850.

Bibliography

[1] C. E. Aalseth *et al.* Proposal to the SPSC : A solar axion search using a decommissioned LHC test magnet. *CERN-SPSC-99-21 ; SPSC-P-312*, 1999.

[2] P. Abbon *et al.* The Micromegas detector of the CAST experiment. *New J. Phys.*, 9:170, 2007.

[3] T. Alexopoulos, G. Iakovidis, and G. Tsipolitis. Study of resistive micromegas detectors in a mixed neutron and photon radiation environment. *JINST*, 7:C05001, 2012.

[4] M. Alfonsi *et al.* Status of triple GEM muon chambers for the LHCb experiment. *Nucl. Instr. Meth. A*, 581:283–286, 2007.

[5] S. Andriamonje *et al.* A Micromegas detector for the CAST experiment . *Nuclear Instruments and Methods in Physics Research Section A: Accelerators, Spectrometers, Detectors and Associated Equipment*, 518(1-2):252 – 255, 2004.

[6] S. Andriamonje *et al.* Development and performance of microbulk micromegas detectors. *JINST*, 5:P02001, 2010.

[7] S. Andriamonje *et al.* A Transparent Detector for nTOF Neutron Beam Monitoring. *J. Korean Phys. Soc.*, 59:1597–1600, 2011.

[8] S. Andriamonje *et al.* [CAST Collaboration]. An improved limit on the axion-photon coupling from the CAST experiment. *J. Cosmol. Astropart. P.*, 10:[arXiv:hep–ex/0702006], 2007.

[9] S. Andriamonje *et al.* [CAST Collaboration]. Search for 14.4 keV solar axions emitted in the M1-transition of 57Fe nuclei with CAST. *J. Cosmol. Astropart. P.*, 12:002, 2009.

[10] S. Andriamonje *et al.* [CAST Collaboration]. Search for solar axion emission from ^{7}Li and D(p,gamma)^{3}He nuclear decays with the CAST gamma-ray calorimeter . *J. Cosmol. Astropart. P.*, 03:032, 2010.

[11] M. Archidiacono, S. Hannestad, A. Mirizzi, G. G. Raffelt, and Y. Y. Y. Wong Wong. Axion hot dark matter bounds after planck. *J. Cosmo. and Astro. Phys.*, 010:020, 2013.

[12] E. Arik *et al.* [CAST Collaboration]. Probing eV-scale axions with CAST. *J. Cosmol. Astropart. P.*, 008:[arXiv:hep–ex/0810.4482], 2009.

[13] E. Arik *et al.* [CAST Collaboration]. Search for Sub-eV Mass Solar Axions by the CERN axion Solar Telescope with ^{3}He Buffer Gas. *J. Cosmol. Astropart. P.*, 107:261302 [arXiv:hep–ex/0810.4482], 2011.

[14] M. Arik *et al.* [CAST Collaboration]. CAST solar axion search with ^{3}He Buffer gas: Closing the hot dark matter gas . *J. Cosmol. Astropart. P.*, Accepted, 2014.

[15] S. J. Asztalos and G. Carosi *et al.* SQUID-Based Microwave Cavity Search for Dark-Matter Axions. *Phys. Rev. Lett.*, 104:041301, 2010.

[16] D. Attié *et al.* Gas pixel detector for X-ray observation. *EAS Publications Series*, 37:181–188, 2009.

[17] D. Attié *et al.* A piggyback resistive micromegas. *JINST*, 8:P05019, 2013.

[18] D. Attié *et al.* Piggyback resistive micromegas. *JINST*, 8:C11007, 2013.

[19] D. Attié *et al.* Towards small gap microbulks. *JINST*, 9:C04013, 2014.

[20] S. Aune *et al.* Low background x-ray detection with micromegas for axion search. *JINST*, 2013.

[21] S. Aune *et al.* X-ray detection with micromegas with background levels below 10^{-6}counts keV^{-1} cm^{-2}s^{-1} . *JINST*, 9:P01001, 2014.

[22] D. Autiero *et al.* The CAST time projection chamber. *New J. of Phys.*, 9:171, 2007.

[23] K. J. Bae, H. Baer, and A. Lessa. Implications of mixed axion/neutralino dark matter for the cosmic frontuer: a snowmass whitepaper. page [arXiv:1306.2986].

[24] J. Baechler *et al.* Status of the TOTEM experiment at LHCb. *Nucl. Instr. Meth. A*, 718:21–25, 2013.

[25] J. Baechler *et al.* The cylindrical GEM detector for the KLOE-2 Inner Tracker. *JINST*, 9:C01014, 2014.

[26] H. Baer, A. Lessa, and W. Sreethawong. Coupled boltzmann calculation of mixed axion/neutralino cold dark matter production in the early universe. *J. Cosmo. and Astro. Phys.*, 1201:036, 2012.

[27] R. Bähre *et al.* Any Light Particle Search II- Technical Design Report. *JINST*, 8:T09001, 2013.

[28] C. A. Baker *et a.l.* An improved experimental limit on the electric dipole moment of the neutron. *Phys. Rev. Lett.*, 97:131801 [arXiv:hep–ex/0602020], 2006.

[29] K. Baker *et al.* The quest for axions and other new light particles. *Annalen der Physik*, 525:A93–A99, 2013.

[30] P. Baron *et al.* Architecture and Implementation of the Front-End Electronics of the Time Projection Chambers in the T2K Experiment. *IEEE Trans. Nucl. Sci.*, NS-57, 2010.

[31] P. Baron *et al.* AGET, the Get Front-End ASIC, for the readout of the Time Projection Chambers used in Nuclear Physic Experiments. *NSS/MIC/RTSD IEEE*, 2011.

[32] K. Barth *et al.* [CAST Collaboration]. CAST constraints on the axion-electron coupling. *J. Cosmol. Astropart. P.*, 05:010, 2013.

[33] A. Bay *et al.* Study of sparking in Micromegas chambers. *Nucl. Instr. Meth. A*, 488:162–174, 2002.

[34] F. Belloni *et al.* Micromegas for neutron detection and imaging. *Mod. Phys. Lett. A*, 28:340023, 2013.

[35] B. Beltran. *A TPC for axion searches at CERN* . PhD thesis, Laboratorio de Física Nuclear y Astropartículas, Departemento de Física Teórica, Universidad de Zaragoza, 2006.

[36] B.D. Blout, E. J. Daw, M.P. Decowski, T.P. Ho Paul, L.J. Rosenberg, and D.B Yu. A radio telescope search for axions. *Astrophys. J.*, 546:825–828, 2001.

[37] P. Borgeaud *et al.* The LArg Tower Builder Board: calculation, simulation, measurements. ATL-LARG-2002-001, 2002.

[38] O. Bourrion *et al.* Data acquisition electronics and reconstruction software for real time 3D track reconstruction within the MIMAC project. *JINST*, 6:C11003, 2011.

[39] O. Bourrion *et al.* Dedicated front-end and readout electronics developments for real time 3D directional detection of dark matter with MIMAC. *EAS Publ. Ser.*, 53:129, 2012.

[40] P. Brax, A. Lindner, and K. Zioutas. Detection prospects for solar and terrestrial chameleons. *Phys. Rev.*, D85:043014, 2012.

[41] P. Brax and K. Zioutas. Solar chameleons. *Phys. Rev*, D82:043007, 2010.

[42] A. Breskin, R. Alon, M. Cortesi, R. Chechik, J. Miyamoto, et al. A Concise review on THGEM detectors. *Nucl.Instrum.Meth.*, A598:107–111, 2009.

[43] D. Breton and E. Delagnes. *IEEE Trans. Nucl. Sci.*, 52:2853, 2005.

[44] D. Calvet *et al.* A new Versatile and Cost effective Readout System for Small to Medium Scale Gaseous and Silicon Detectors. *NSS/MIC/RTSD IEEE*, 2013.

[45] G. Cantatore *et al.* [CAST Collaboration]. pages arXiv:0809.4581 [hep–ex], 2008.

[46] G. Carosi *et al.* Report of the Workhsop Vistas on Axion Physics, Seattle. *Mod. Phys*, To be published, 2013.

[47] S. Cebrián *et al.* Background study for the pn-CCD detector of CERN Axion Solar Telescope. *Astro. Phys.*, 9:163, 2009.

[48] S. Cebrián *et al.* Micromegas readouts for double beta decay searches. *JCAP*, 1010:010, 2010.

[49] S. Cebrián *et al.* Radiopurity of Micromegas readout planes. *Astropart. Phys.*, 34:354–359, 2011.

[50] S. Cebrián *et al.* Assesment of material radiopurity for rare event experiments using micromegas. *JINST.*, 8:C11012, 2013.

[51] S. Cebrián *et al.* Micromegas-TPC operation at high pressure in xenon-trimethylamine mixtures. *JINST*, 8:P01012, 2013.

[52] G. Charles. *Development of Micromegas detectors for the CLAS12 experiment at Jefferson Laboratory.* PhD thesis, Université Paris-Sud, 2013.

[53] G. Charpak *et al.* First beam test results with micromegas, a high rate, high resolution detector. *Nucl. Instr. Meth. A*, 412:47–60, 1998.

[54] M. Chefdeville. *Development of Micromegas-like gaseous detectors using a pixel readout chip as a collecting anode.* PhD thesis, Paris Sud University and Amsterdam University, 2009.

[55] M. Chefdeville *et al.* An electron-multiplying micromegas grid made in silicon wafer post-processing technology. *Nucl. Instr. Meth. A*, 556:490–494, 2006.

[56] A. S. Chou, W. Wester, A. Baumbaugh, H. R. Gustafson, Y. Irizarry-Valle, P. O. Mazur, J. H. Steffen, R. Tomlin, X. Yang, and J. Yoo. Search for axionlike particles using a variable-baseline photon-regeneration technique. *Phys. Rev. Lett.*, 100:080402, 2008.

[57] P. Colas, I. Giomataris, and V. Lepeltier. Ion backflow in the Micromegas TPC for the future linear collider. *Nucl. Instr. Meth. A*, 535(1-2):226 – 230, 2004.

[58] ATLAS Collaboration. New Small Wheel Technical Design Report. Technical report, CERN-LHCC-2013-006, ATLAS-TDR-020.

[59] CAST Collaboration. Status report of the CAST Experiment, planning and requests for 2013-2014. Technical report, CERN-SPSC-2013-027, SPSC-SR-123.

[60] CAST collaboration. 2011.

[61] DAMIC Collaboration. Direct Search for Low MAss Dark Matter Particles with CCDs. *Phys. Lett. B*, 711:264–269, 2012.

[62] HESS Collaboration. Constraints on axion-like particles with H.E.S.S from the irregularity of the PKS 2155-304 energy spectrum. *Phys. Rev. D*, 88:102003, 2013.

[63] IAXO Collaboration. Letter of Intent to the CERN SPSC,The International Axion Observatory IAXO. Technical report, CERN-SPSC-2013-022, SPSC-I-242.

[64] IAXO Collaboration. Conceptual design of the international axion observatory (IAXO). *JINST*, pages arXiv:1401.3233 [physics.ins–det], 2014.

[65] NEXT Collaboration. The NEXT-100 experiment for neutrinoless double beta decay searches (conceptual design report). pages arXiv:1106.3630 [physics.ins–det], 2011.

[66] The NEXT Collaboration. Characterization of a medium size Xe/TMA TPC instrumented with microbulk micromegas, using low-energy γ-rays. *JINST*, page arXiv:1311.3535, 2013.

[67] The NEXT Collaboration. Description and commissioning of next-mm prototype: first results from operation in a xenon-trimethylamine gas mixture. *JINST*, page arXiv:1311.3242, 2013.

[68] J. Collar and Y. Giomataris. Possible low-background applications of micromegas detector technology. *Nucl. Inst.. Meth. A*, 471:254, 2000.

[69] T. Dafni, S. Aune, J. Castel, S. Cebrián, G. Fanourakis, et al. The T-REX project: Micromegas for rare event searches. *J.Phys.Conf.Ser.*, 347:012030, 2012.

[70] T. Dafni, S. Aune, S. Cebrian, G. Fanourakis, E. Ferrer-Ribas, et al. Rare event searches based on micromegas detectors: The T-REX project. *J.Phys.Conf.Ser.*, 375:022003, 2012.

[71] T. Dafni *et al.* Energy resolution of alpha particles in amicrobulk micromegas detector at high pressure argon and xenon mixtures. *Nucl. Instr. Meth. A*, A 608:259–266, 2009.

[72] S. Dalla Torre. MPGD developments: historical roadmap and recent progresses in consolidating MPGDs. *JINST*, 8:C10020, 2013.

[73] R. de Oliveira. Fabrication techniques and industrialization of mpgds. *Presentation at the MPGD conference, Zaragoza*, 2013.

[74] J. Derré and Y. Giomataris. Recent experimental results with Micromegas. *Nucl. Instr. Meth. A*, 477:23–28, 2002.

[75] J. Derré, Y. Giomataris, Ph. Rebourgeard, H. Zaccone, J.P. Perroud, and G. Charpak. Fast signals and single electron detection with a MICROMEGAS photodetector. *Nucl. Instr. Meth. A*, 449(1-2):314 – 321, 2000.

[76] Gas detectors development group. http://gdd.web.cern.ch/GDD/.

[77] M. Dine, W. Fischler, and M. Srednicki. A simple solution to the strong CP problem with a harmless axion. *Phys. Lett. B.*, 104:199, 1981.

[78] M. S. Dixit and A. Rankin. Simulating the charge dispersion phenomena in micro pattern gas detectors with a resistive anode. *Nucl. Instrum. Meth. A*, 566:281–285, 2006.

[79] B. Döbrich *et al.* The quest for axions and other new light particles, input to the open call to the european strategy for particle physics. *Fundamental Physics at low energies.*, 2012.

[80] W. J. Egle *et al.* Mirror system for the German X-ray satellite ABRIXAS:II. Design and mirror development. *Proc. SPIE*, 3444:359–68, 1998.

[81] K. Ehret *et al.* New ALPS results on hidden-sector lightweights. *Phys. Lett.*, B689:149–155, 2010.

[82] N. Abgrall *et al.* Time projection chambers for the {T2K} near detectors. *Nuclear Instruments and Methods in Physics Research Section A: Accelerators, Spectrometers, Detectors and Associated Equipment*, 637(1):25 – 46, 2011.

[83] E. Ferrer Ribas. *Etude des états finals contenant deux jets de particules et de l'énergie manquante avec le détecteur DELPHI à LEP*. PhD thesis, Laboratoire de l'Accélerateur Linéaire, Université Paris-Sud, 2000.

[84] P. Friedrich *et al.* X-ray tests and calibrations of the ABRIXAS mirror systems X-Ray Optics. *Proc. SPIE*, 3444:369, 1998.

[85] J. Galán *et al.* An ageing study of resistive micromegas for the HL-LHC environment. *JINST*, 8:P04028, 2012.

[86] J. Galán Lacarra. *Probing eV-mass scale Axions with a Micromegas Detector in the CAST experiment.* PhD thesis, Laboratorio de Física Nuclear y Astropartículas, Departemento de Física Teórica, Universidad de Zaragoza, 2011.

[87] Y. Giomataris. Development and prospects of the new gaseous detector Micromegas. *Nucl. Instr. Meth. A*, 419:239–250, 1998.

[88] Y. Giomataris, P. Rebougeard, Robert J. P., and G. Charpak. Micromegas: A high granularity position sensitive gaseous detector for high particle flux environments. *Nucl. Instr. Meth. A*, 376:29–35, 1996.

[89] Y. Giomataris *et al.* Micromegas in a bulk. *Nucl. Instr. Meth. A*, 560:405–408, 2006.

[90] J. Gracia *et al.* X-ray detection with micromegas with background levels below 10^{-6} counts keV^{-1} cm^{-2}s^{-1} . *JINST*, page 010001, 2013.

[91] Particle Data Group. Particle physics booklet. *Phys. ReV.*, D86:010001, 2012.

[92] C. Guerrero *et al.* Simultaneous measurement of neutron-induced capture and fission reactions at cern. *Eur. Phys. J.*, A:48: 29, 2012.

[93] S. Hannestad, A. Mirizzi, G. G. Raffelt, and Y. Y. Y. Wong Wong. Cosmological constraints on neutrino plus axion hot dark matter: Update after wmap-5. *J. Cosmo. and Astro. Phys.*, 001:1008, 2010.

[94] F. A. Harrison *et al.* (NuSTAR Collaboration). The Nuclear Spectroscopic Telescope Array (NuSTAR) Mission . *ApJ*, 770, 2013.

[95] M. P. HertzBerg *et al.* Axion cosmology and the energy scale of inflation. D78:083507, 2008.

[96] J. Hewett *et al.* Fundamental Physics at the Intensity Frontier. *Report of the Workshop on the Intensity Frontier, Rockville* , page arXiv:1205.2671, 2011.

[97] M. Houry, E. Delagnes, D. Riz, B. Canaud, L. Disdier, F. Garaude, Y. Giomataris, V.Yu. Glebov, Ph. Legou, Ph. Rebourgeard, and C. Sangster. DEMIN: A neutron spectrometer, Micromegas-type, for inertial confinement fusion experiments. *Nucl. Instr. Meth. A*, 557(2):648 – 656, 2006.

[98] F. J. Iguaz *et al.* Micromegas detector developments for dark matter directional detection with MIMAC. *JINST*, 6:P07002, 2011.

[99] F. J. Iguaz *et al.* Characterization of microbulk detectors in argon- and neon-based mixtures. *JINST*, 7:P04007, 2012.

[100] Y. Inoue, Y. Akimoto, R. Ohta, T. Mizumoto, A. Yamamoto, and M. Minowa. Search for solar axions with mass around 1 eV using coherent conversion of axions into photons. *Phys. Lett. B*, 668:93, 2008.

[101] Y. Inoue, T. Namba, S. Moriyama, M. Minowa, Y. Takasu, T. Horiuch, and A. Yamamoto. Search for sub-electronvolt solar axions using coherent conversion of axions into photons in magnetic field and gas helium. *Phys. Lett. B*, 536:18, 2002.

[102] I. G. Irastorza, E. Ferrer Ribas, and T. Dafni. Micromegas in the rare event searches. *Mod. Phys. Lett. A*, 28:1340026, 2013.

[103] I.G. Irastorza, J. Castel, S. Cebrián, T. Dafni, G. Fanourakis, et al. Status of R&D on Micromegas for Rare Event Searches : The T-REX project. *EAS Publ.Ser.*, 53:147–154, 2012.

[104] I. G. Irastorza *et al.* Towards a new generation axion helioscope. *J. Cosmo. and Astro. P.*, 06:013, 2011.

[105] K. Irwin *et al. Transition-edge sensors.* Springer-Verlag Berlin, 2005.

[106] J. Isern, S. Catalan, E. Garcia-Berro, and S. Torres. Axions and the white dwarf luminosity function. *J. Phys. Conf . Ser.*, 172:012005, 2009.

[107] J. Isern, E. Garcia-Berro, S. Torres, and Catalan S. Axions and the coouling of white dwarfs stars. *Astrophys. J.*, 682:L109, 2008.

[108] F. Jeanneau. La Saga Micromegas. *Presentation at the Assamblée Générale de l'IRFU*, 2013.

[109] Fabien Jeanneau, Mariam Kebbiri, and Vincent Lepeltier. Ion back-flow gating in a micromegas device. *Nucl.Instrum.Meth*, 623(1):94 – 96, 2010. 1st International Conference on Technology and Instrumentation in Particle Physics.

[110] J. Kaminski, C. Krieger, Y. Bilevych, T. Krautscheid, and K. Desch. Gridpix as a candidate for the future of cast. *Journal of Phys.*, 263:351, 2013.

[111] J. E. Kim. Weak interaction singlet and strong CP invariance. *Phys. Rev. Lett.*, 43:103, 1979.

[112] C. Krieger *et al.* Gridpix as a candidate for the future of CAST. *J. Phys. Conf. Ser.*, 460:012004, 2012.

[113] C. Krieger *et al.* Ingrid-based x-ray detector for low background searches. *Nucl. Instr. Meth. A*, A729:905–909, 2013.

[114] F. Kune *et al.* The gaseous microstrip detector Micromegas for the COMPASS experiment at CERN. *Nucl. Phy. A*, 721:1087–1090, 2003.

[115] M Kuster *et al.* The x-ray telescope of CAST. *New J. Phys.*, 9:169, 2007.

[116] J. Lamblin. *Xenon100 et MIMAC, des détecteurs à la recherche de matière noire.* PhD thesis, University of Grenoble, 2013.

[117] D. M. Lazarus *et al.* Search for solar axions. *Phys. Rev. Lett.*, 69:2333, 1992.

[118] A. D. Linde. Inflation and axion cosmology. *Phys. Lett*, B201:437, 1988.

[119] G. Luzón *et al.* Background studies and shielding effects for the TPC detector of the CAST experiment. *New J. of Phys.*, 9:163, 2007.

[120] D. Maire *et al.* Development of a microtpc detector as a standard instrument for low energy neutron field characterization. *arXiv:1310.5923 [physics.ins-det]*, 2013.

[121] J. Manjarres *et al.* Performances of anode-resistive micromegas for hl-lhc. *JINST*, 7:C03040, 2012.

[122] A. Meuris *et al.* A new fine pitch Cd(Zn)Te Imaging spectrometer from 2 keV up to 1 MeV. *NSS/MIC/RTSD IEEE*, 2011.

[123] M. Meyer *et al.* First lower limits on the photon-axion-like particle coupling from very high energy gamma-ray observation. *Phys. Rev.*, D87:035027, 2013.

[124] A. Michalowska *et al.* A low power multi-gain CMOS ASIC for the readout of Cd(Zn)Te detectors. *NSS/MIC/RTSD IEEE*, 2011.

[125] S. Moriyama, M. Minowa, Y. Inoue, T. Namba, Y. Takasu, and A. Yamamoto. Direct search for solar axions by using strong magnetic field and X-ray detectors. *Phys. Lett. B*, 434:147, 1998.

[126] A. Obertelli *et al.* MINOS: A vertex tracker coupled to a thick liquid-hydrogen target for in-beam spectroscopy of exotic nuclei. *Eur. Phys. Jour. A*, 50:8, 2014.

[127] A. Oed. Position-sensitive detector with microstrip anode for electron multiplication in gases. *Nucl. Instr. Meth. A*, 263:351, 1988.

[128] J. Pancin. *Détection de neutrons avec un détecteur de type Micromegas: de la physique nucléaire à l'imagerie.* PhD thesis, Université Bordeaux 1, 2004.

[129] H. Peng and S. Asztalos *et al.* Cryogenic cavity detector for a large-scale cold dark-matter axion search. *Nucl. Instr. Meth. A*, 444:569–583, 2000.

[130] Planck Collaboration, P. A. R. Ade, N. Aghanim, C. Armitage-Caplan, M. Arnaud, M. Ashdown, F. Atrio-Barandela, J. Aumont, C. Baccigalupi, A. J. Banday, and et al. Planck 2013 results. XVI. Cosmological parameters. *ArXiv e-prints*, 2013.

[131] S. Procureur. Micromegas trackers for hadronic physics. *Mod. Phys. Lett. A*, 28:1340024, 2013.

[132] S. Procureur. Private communication. 2014.

[133] G. G. Raffelt. *Phys. Lett.*, B166:402, 1986.

[134] G. G. Raffelt. Astrophysical axion bounds diminished by screening effects. *Phys. Rev. D*, 33:897, 1986.

[135] G. G. Raffelt. Photon-axion conversion in intergalactic magnetic fields and cosmological consequences. *Lect. Notes Phys.*, 741:51, 2008.

[136] G. G. Raffelt and D. S. P. Dearborn. Bounds on hadronic axions from stellar evolution. *Phys. Rev. D*, 36:2211, 1987.

[137] J. P. Richer *et al.* Development of a front end ASIC for Dark Matter directional detection with MIMAC. *Nucl. Instrum. Meth. A*, 470, 2010.

[138] J. P. Richer *et al.* Development and validation of a 64 channel front end ASIC for 3D directional detection for MIMAC. *JINST*, 6:C11016, 2011.

[139] C. Robilliard, R. Battesti, M. Fouche, J. Mauchain, A. M. Sautivet, et al. No light shining through a wall. *Phys.Rev.Lett.*, 99:190403, 2007.

[140] M. E. Rose and S. A. Korff. An investigation of the properties of proportional counters. *Phys. Rev.*, 59:850, 1941.

[141] J. Ruz. *Search for solar axions with the Time Projection Chamber of the CERN Axion Solar Telescope with 4-Helium as buffer gas* . PhD thesis, Laboratorio de Física Nuclear y Astropartículas, Departemento de Física Teórica, Universidad de Zaragoza, 2008.

[142] J. Santiard *et al. Proceedings of the 6th Pisa Meeting on Advanced Detectors*, 1994.

[143] F. Sauli. GEM: A new concept for electron multiplication in gas detectors. *Nucl. Instr. Meth. A*, 386:531, 1997.

[144] H. W. Schnopper *et al.* X-ray optics made from thin plastic foils. *Proc. SPIE*, 3766, 1999.

[145] M. A. Shifman, A. I. Vainshtein, and V. I. Zakharov. Can confinment ensure natural cp invariance of strong interactions? *Nucl. Phys. B*, 166:493, 1980.

[146] P. Sikivie. Experimental test of the invisible axion. *Phys. Lett.*, 51:1415, 1983.

[147] M. Simet *et a.l.* The milky way as a kiloparsec-scale axionscope. *Phys. Rev.*, D77:063001, 2008.

[148] D. N. Spergel. Motion of the earth and the detection of weakly interacting massive particles. *Physical Review D*, 37:1353–1355, 1988.

[149] T. Tavernier. *Experimental Techniques in Nuclear and Particle Physics*. Springer, 2010.

[150] D. Thers *et al.* Micromegas as a large microstrip detector for the COMPASS experiment. *Nucl. Instr. Meth. A*, 469:133–146, 2001.

[151] M. Titov. New developments and future perspectives of gaseous detectors. *Nucl. Instr. Meth. A*, 581:25–37, 2007.

[152] M. Titov and L. Ropelewski. Micro-Pattern Gaseous detector technologies and RD51 collaboration. *Mod. Phys. Lett. A*, 28:1340022, 2013.

[153] A. Tomás Alquezar. *Study on Time Projection Chambers with Micromegas for Rare Event Searches*. PhD thesis, Laboratorio de Física Nuclear y Astropartículas, Departemento de Física Teórica, Universidad de Zaragoza, 2013.

[154] A. Tomás *et al.* The new micromegas X-ray detectors in CAST. *X-Ray Spectrometry*, 40:240–246, 2011.

[155] T. Vafeaidis. *Contribution to the search for solar axions in the CAST experiment.* PhD thesis, Aristotle University of Thessaloniki, 2012.

[156] K. van Bibber. Private communication. 2014.

[157] K. van Bibber, D. Morris, P. McIntyre, and G. Raffelt. Design for a practical laboratory detector for solar axions. *Phys. Rev. D*, 39:2089–2099, 1989.

[158] H. van der Graaf. The gridpix detector: history and perspective. *Mod. Phys. Lett. A*, 28:1340026, 2013.

[159] M. Vandenbroucke. Private communication. 2014.

[160] O. Wantz and E. P. S. Shellard. Axion cosmology revisited. *Phys. Rev.*, D82:123508, 2010.

[161] BOPP web site. http://www.bopp.com/.

[162] S. Weinberg. A new light boson? *Phys. Rev. Lett.*, 40:223, 1978.

[163] F. Wilczeck. Problem of strong p and t invariance in the presence of instantons. *Phys. Rev. Lett.*, 40:279, 1978.

[164] J. Wotschack. The development of large-area micromegas detectors for the atlas upgrade,. *Mod. Phys. Lett. A*, 28:1340020, 2013.

[165] E. Zavattini and G. Zavattini *et al.* Experimental observation of optical rotation generated in vaccuum by a magnetic field. *Phys. Rev. Lett.*, 96:110406, 2006.

[166] E. Zavattini and G. Zavattini *et al.* Editorial note: Experimental observation of optical rotation generated in vaccuum by a magnetic field. *Phys. Rev. Lett.*, 99:129901, 2007.

[167] A. R. Zhitnitsky. On possible supression of the axion hadron interactions. *Sov. J. Nucl. Phys.*, 31:260, 1980.

[168] K. Zioutas *et al.* [CAST Collaboration]. First results from the CERN Axion Solar Telescope. *Phys. Rev. Lett.*, 94:121301 [arXiv:hep–ex/0411033], 2005.